Adamantyl-Group Containing Mixed-Mode Acrylamide-Based Continuous Beds for Capillary Electrochromatography: Synthesis, Characterization, Optimization and Investigation of the Chromatographic Efficiency

Kumulative Dissertation

zur

Erlangung des Doktorgrades

der Naturwissenschaften

(Dr. rer. nat.)

dem

Fachbereich Chemie der Philipps-Universität Marburg

vorgelegt von

M.Sc. "Ayat Allah" Turki Al-Massaedh

Aus

Jordanien

Marburg an der Lahn 2014

Vom Fachbereich Chemie der Philipps-Universität Marburg
als Dissertation angenommen am: .....

Erstgutachter: Prof. Dr. Ute Pyell

Zweitgutachter: Prof. Dr. Andreas Greiner (University of Bayreuth)

Tag der mündlichen Prüfung: 16.05.2014

(Hochschulkennziffer: 1180)

Die vorliegende Dissertation wurde in der Zeit von Januray 2011 bis April 2014 am Fachbereich Chemie der Philipps-Univerofrsität Marburg unter der Leitung von Prof. Dr. Ute Pyell angefertigt.

In den folgenden Artikeln wurden Teile dieser Kumulativen Dissertation bereits veröffentlicht:

A. A. Al-Massaedh, U. Pyell, *J. Chromatogr. A* 1286 (**2013**) 183-191. "Adamantyl-group containing mixed-mode acrylamide-based continuous beds for capillary electrochromatography. Part I: Study of a synthesis procedure including solubilization of N-adamantyl-acrylamide via complex formation with a water-soluble cyclodextrin".

A. A. Al-Massaedh, U. Pyell, *J. Chromatogr. A* 1325 (**2014**) 247-255. "Adamantyl-group containing mixed-mode acrylamide-based continuous beds for capillary electrochromatography. Part II. Characterization of the synthesized monoliths by inverse size exclusion chromatography and scanning electron microscopy".

A. A. Al-Massaedh, U. Pyell, *J. Chromatogr. A* 1325 (**2014**) 186-194. "Adamantyl-group containing mixed-mode acrylamide-based continuous beds for capillary electrochromatography. Part III. Optimization of the chromatographic efficiency".

A. A. Al-Massaedh, U. Pyell, *J. Chromatogr. A* 1349 (**2014**) 80-89. "Adamantyl-group containing mixed-mode acrylamide-based continuous beds for capillary electrochromatography. Part IV: Investigation of the chromatographic efficiency dependent on the retention mode".

Erklärung

Ich erkläre, dass eine Promotion noch an keiner anderen Hochschule als der Philipps-Universität Marburg, Fachbereich Chemie, versucht wurde.

Ich versichere, dass ich meine vorgelegte Dissertation

"Adamantyl-Group Containing Mixed-Mode Acrylamide-Based Continuous Beds for Capillary Electrochromatography: Synthesis, Characterization, Optimization and Investigation of the Chromatographic Efficiency"

selbst und ohne fremde Hilfe verfasst, nicht andere als die in ihr angegebenen Quellen oder Hilfsmittel benutzt, alle vollständig oder sinngemäß übernommenen Zitate als solche gekennzeichnet sowie die Dissertation in der vorliegenden oder einer ähnlichen Form noch bei keiner anderen in- oder ausländischen Hochschule anlässlich eines Promotionsgesuchs oder zu anderen Prüfungszwecken eingereicht habe.

Marburg, April 2014

Unterschrift

("Ayat Allah" Al-Massaedh)

Dedication

This thesis is dedicated to my father, my mother, my brothers, and my sisters who have supported me all the way since the beginning of my studies and who have been a source of encouragement and inspiration to me throughout my life.

Also, this thesis is dedicated to my wife, my daughter (Wjdan), and my son (Mohammed).

Acknowledgement

My praise, gratitude and thanks to God, the Almighty, for guiding and helping me to achieve this work.

I am very grateful to my supervisor, Prof. Dr. Ute Pyell, for her kind supervision, for her patience, for her insightful criticism, and for helpful scientific instructions and comments that she always offered to me during this project. My sincere thanks and acknowledgement to her for providing all the facilities that helped me to complete this project. Also, I am very grateful to her for providing me the possibility to attend the course of "Electromigration Separation Techniques" given by her.

Thanks are also due to Prof. Dr. Seema Agarwal (University of Bayreuth, Germany) for giving me samples of the polystyrene standards. Also my thanks extended to *Mr. M. Hellwig* (Electron Microscopy and Microanalysis Laboratory, University of Marburg, Marburg, Germany) who provided me the technical assistance needed for carrying out the SEM measurements.

I would like also to express my thanks to my colleagues in the research group of Prof. Dr. Ute Pyell and my colleagues at Philipps Universität Marburg for providing a friendly and supportive environment. I thank also my short-practical student Dominic Urban.

Special thanks go to my family (my father, my mother, my brothers, my sisters, my wife, my daughter, and my son) for their unlimited encouragement, love, support, and continuous advices during my stay at Philipps Universität Marburg.

I am grateful to Al albayt University (Mafraq, Jordan) for funding my PhD project throughout my stay in Germany.

Finally, I can't end without thanking Prof. Dr. Nabil Shawagfeh (the president of Al-Balq'a Applied University, Jordan), Prof. Dr. Hasan Tashtoush (Chemistry Department , Yarmouk University, Jordan), Prof. Dr. Adnan Massadeh (Faculty of Pharmacy, Jordan University of Science and Technology, Jordan), and Prof. Dr. Eqab Rabei (Physics Department, Al albayt University, Jordan) for their help in getting my PhD scholarship.

Ayat Allah Al -Massaedh

List of abbreviations and symbols

Abbreviations

EOD	1,2-Epoxyoctadecane
AMPS	2-acrylamido-2-methyl-2-propanesulfonic acid
HEMA	2-Hydroxyethyl methacrylate
2-HP-γ-CD	2-Hydroxypropyl-γ-cyclodextrin
ACN	Acetonitrile
AA	Acrylamide or acetic acid
AGE	Allyl glycidyl ether
APS	Ammonium persulfate
AS	Ammonium sulfate
ANOVA	Analysis of variance
APCI	Atmospheric pressure chemical ionization
AFM	Atomic force microscopy
ABN	Azobisisobutyronitrile
BGE	Background electrolyte
BET	Brunauer, Emmett, and Teller nitrogen adsorption isotherm
CEC	Capillary electrochromatography
CE	Capillary electrophoresis
CLC	Capillary liquid chromatography
CMC	Critical micellar concentration
CD	Cyclodextrin
DNA	Deoxyribonucleic acid
$CDCl_3$	Deuterated chloroform-d_1
MeOD	Deuterated methanol
D_2O	Deuterated water
EOF	Electroosmotic flow
ESI	Electrospray ionization
GC	Gas chromatography

HETP	Height equivalent of a theoretical plate
HeA	Hexylacrylate
HPLC	High performance liquid chromatography
HILIC	Hydrophilic interaction liquid chromatography
ICD	In-column detection
I.D	Inner diameter
IUPAC	International union of pure and applied chemistry
ISEC	Inverse size exclusion chromatography
LC	Liquid chromatography
MS	Mass spectrometry
MIP	Mercury intrusion porosimetry
MA	Methacrylamide
Me-β-CD	Methylated-β-cyclodextrin
MEKC	Micellar electrokientic chromatography
TEMED	N,N,N',N'-tetramethylethylenediamine
DAA	N,N'-Ethylenedianilinediacrylamide
BIS	N,N'-methylenebisacrylamide
DMF	N,N-dimethyl formamide
DMAA	N,N-dimethylacrylamide
NIP	N-Isopropylacrylamide
^{1}H NMR	Nuclear magnetic resonance
^{13}C NMR	Nuclear magnetic resonance spectroscopy to carbon
^{1}H-NOESY	Nuclear Overhauser Enhancement Spectroscopy
ODS	Octadecylsilane
OCD	On-column detection
OTCs	Open-tubular columns
O.D	Outer diameter
OHP	Outer Helmholtz plane
PCs	Particulate columns
PDA	Piperazinediacrylamide
PEG	Poly(ethylene glycol)

RSD	Relative standard deviation
RP	Reversed-phase
ROMP	Ring-opening metathesis polymerization
SEM	Scanning electron microscopy
S/N	Signal-to-noise ratio
SEC	Size exclusion chromatography
SDS	Sodium dodecyl sulfate
TEOS	Tetraethoxy silane
THF	Tetrahydrofuran
TMSO	Tetramethoxy silane
TEM	Transition electron microscopy
TEA	Triethylamine
UV	Ultraviolet
VSA	Vinylsulfonic acid

Symbols

t_R'	Adjusted retention time
K*	Apparent partitioning coefficient
pH*	Apparent pH
U	Applied voltage
$\overline{M}_{w,n}$	Average molar mass of a polystyrene standard
N_A	Avogadro number
d	Capillary diameter
$\Delta\delta$	Change in the chemical shift
q	Charge
$\rho_{(x)}$	Charge density distribution
A	Coefficient of eddy diffusion
B	Coefficient of longitudinal diffusion or complex formation constant
C_m	Coefficient of resistance to mass transfer in the mobile phase

C_s	Coefficient of resistance to mass transfer in the stationary phase
d_c	Coil diameter of a polystyrene standard
c	Concentration
%C	Crosslinker concentration
t_0	Dead time or hold-up time
κ	Debye-Hueckel parameter (reciprocal of the double layer thickness) or electric conductivity
D_m	Diffusion coefficient
D_s	Diffusion coefficient of a solute in the stationary phase
K_{dis} or K_D	Distribution coefficient
d_f	Effective film thickness of the stationary phase
L_{eff} or L_D	Effective length of a capillary (from inlet to detection window)
E	Electric field strength
ε_o	Electric permittivity of vacuum
μ_{eo}	Electroosmotic mobility
v_{ep}	Electrophoertic migration velocity
μ_{ep}	Electrophoertic mobility
e	Elementary electric charge
t_s	Elution time of a polystyrene standard
t_T	Elution time of a t_0 marker
V_s	Elution volume of a polystyrene standard
V_T	Elution volume of a t_0 marker or total pore volume
K_c	Equilibrium constant
ϕ_n	Exclusion pore diameter
ε_F	Flow through porosity
V_n	Fractional volume of pores
R	Gas constant
λ	Inhomogenity factor

ε_I	Internal porosity
I	Ionic strength
L	length of a capillary
u	Linear velocity
v_{eo} or u_{eo}	Linear velocity of electroosmotic flow
t_{max}	Maximum elution time
V_{max}	Maximum elution volume
u_{max}	Maximum mobile phase velocity
$\bar{k}$	Mean of two peak retention factors
α_{meth}	Methylene selectivity
t_{min}	Minimum elution time
V_{min}	Minimum elution volume
H_{min}	Minimum plate height
c_m	Molar concentration of a solute in the mobile phase
c_s	Molar concentration of a solute in the stationary phase
c_{com}	Molar concentration of the complexed solute in the mobile phase
c_{aq}	Molar concentration of the free solute in the mobile phase
$M_{w,min}$	Molar mass of a t_0 marker
$\overline{M}_{w,max}$	Molar mass of the largest polystyrene standard
X	Mole fraction
n_{CH2}	Number of methylene group
n_m	Number of moles of a solute in the mobile phase
n_s	Number of moles of a solute in the stationary phase
k_{obs}	Observed retention factor
k*	Observed retention factor
γ	Obstruction factor
u_{opt}	Optimum mobile phase velocity

K	Partitioning coefficient
AF	Peak asymmetry factor
σ_L^2	Peak variance in length units
K_p	Permeability
φ	Phase ratio
H	Plate height
$H_{B,opt}$	Plate height due to axial molecular diffusion at u_{opt}
H_F or H_A	Plate height due to flow inhomogeneity
H_D	Plate height due to longitudinal diffusion
$H_{D\,M}$	Plate height due to longitudinal diffusion in the mobile phase
$H_{D\,S}$	Plate height due to longitudinal diffusion in the stationary phase
H_T	Plate height due to radial temperature gradient
H_R	Plate height due to resistance to mass transfer
N	Plate number or number of replicates
d_p	Pore diameter
p	pressure
ΔP	Pressure difference
r	Radius
τ	Relative elution time
ε_r	Relative permittivity of the medium (dielectric constant)
R_s	Resolution
k	Retention factor
t_R	Retention time
α	Selectivity factor
K°	Specific permeability
d_m	Spherical molecule diameter
s_b	Standard deviation of the slope

s_a	Standard deviation of the y-intercept
σ	Standard deviation or surface charge density
ΔB	Standard error of the complex formation constant
T	Temperature
μ_1	The first moment about the origin
C	The overall resistance to mass transfer in the stationary and mobile phases
μ'_2	The second moment about the mean
m_0	The zeroth moment
δ	Thickness of the electrical double layer or chemical shift
t	time
V_G	Total geometrical volume
L_{total}	Total length of a capillary
%T	Total monomer concentration
ε_p or ε	Total porosity
V_p	Total volume of pores accessible to the mobile phase
σ^2 or S^2	Variance
σ_D^2	Variance due to detection
σ_I^2	Variance due to injection
σ_{sep}^2	Variance due to separation process
η	Viscosity
dV	Volume element
F	Volume flow rate
$\phi_{(methanol)}$	Volume fraction of methanol in the mobile phase
V_F	Volume of flow through pores
V_I	Volume of inter-globular and intra-globular pores
V_m	Volume of the mobile phase
V_s	Volume of the stationary phase

V_m	Volume of the stationary phase (monolith, polymer)
$w^{0.5}$	Width at half the maximum height of a peak
w	Width at the base line of a peak
ζ	Zeta potential

Table of Contents

1. Introduction

1.1 Fundamentals of chromatography

Chromatography is a physical separation method in which the analytes to be separated are distributed between two immiscible phases, a mobile phase passing through a stationary phase. The mobile phase is either a liquid, a gas, or a supercritical fluid, while the stationary phase is either a solid or a thin film of a liquid or a liquid-crystalline phase coated on surface of a solid support. Analytes are separated as result of differences in the distribution coefficient. The equilibrium constant K (the partitioning coefficient) is defined as the molar concentration of an analyte in the stationary phase c_s divided by the molar concentration of the analyte in the mobile phase c_m:

$$K = \frac{c_s}{c_m} \tag{1}$$

The time between sample injection and analyte detection by a detector at the end of the column is called the retention time t_R, whereas the time taken for the mobile phase to pass through the column (the time it would take an unretained analyte) is called the dead time t_0. The retention factor k which is used to describe the retention behaviour of an analyte on a column is defined as the amount of analyte in the stationary phase n_s divided by the amount in the mobile phase n_m:

$$k = \frac{n_s}{n_m} = \frac{c_s\, V_s}{c_m\, V_m} = K\,\frac{V_s}{V_m} \tag{2}$$

where V_s and V_m are the volumes of stationary and mobile phase in the column, n_s and n_m are the amount of substance of an analyte in these phases, and V_s/V_m is the phase ratio φ.

The retention factor k is independent of the length of the column, the velocity of the mobile phase, or the analyte concentration. It can be determined from the retention time of the analyte t_R and from the dead time t_0:

$$k = \frac{t_R - t_0}{t_0} = \frac{t'_R}{t_0} \tag{3}$$

where t'_R is the adjusted retention time ($t'_R = t_R - t_0$).

The selectivity factor (separation factor) α is a thermodynamic quantity that is a measure of the relative retention of analytes, and is given by:

$$\alpha = \frac{t'_{RB}}{t'_{RA}} = \frac{k_B}{k_A} \qquad (k_B > k_A) \tag{4}$$

where t'_{RB} *and* t'_{RA} are the adjusted retention time of the analytes B and A, and k_B and k_A are the retention factors of the analytes B and A, respectively. The selectivity factor α is ≥ 1.

The resolution R_s provides a quantitative measure of the quality of a separation. It is defined as:

$$R_s = \frac{2\,[(t_R)_B - (t_R)_A]}{w_A + w_B} = 1.18\,\frac{(t_R)_B - (t_R)_A}{w_A^{0.5} + w_B^{0.5}} \tag{5}$$

where $(t_R)_A$ and $(t_R)_B$ are the retention times of analyte A and B, respectively, w_A and w_B are the width at the base line of Peak A and Peak B, respectively, and $w_A^{0.5}$ and $w_B^{0.5}$ are the width at half maximum height of Peaks A and B, respectively.

It is useful to correlate the resolution to the number of theoretical plates N in the column, the selectivity factor α and the mean of the two peak retention factors $\bar{k}$ via the Purnell equation:

$$R_s = \frac{\sqrt{N}}{4}\left(\frac{\alpha - 1}{\alpha}\right)\left(\frac{\bar{k}}{1 + \bar{k}}\right) \tag{6}$$

According to the Purnell equation, high resolution can be obtained by increasing the number of theoretical plates, increasing the selectivity, or by adjustment of the retention factor.

The theoretical plate model, which was developed by Martin and Synge [1] assumes that the column is containing a large number of discrete zones called theoretical plates, and that in each zone, equilibration of the distribution of the analyte between mobile and stationary phase takes place. According to this model, the analyte zone passes through the column by a step-wise movement of equilibrated mobile phase from one plate to the next. Also it is assumed that the partitioning coefficient K of an analyte is the same in each plate and that it is independent of the concentration of the analyte.

In chromatography, the efficiency of a separation is expressed by two related terms, the height equivalent of a theoretical plate (*HETP, H*) and the number of theoretical plates *N*. The two terms are related to each other by the following equation:

$$H = \frac{L_{eff}}{N} \tag{7}$$

where L_{eff} (form inlet to detection window) is the effective length of the column.

The efficiency of a chromatographic column increases with increasing number of theoretical plates and decreasing plate height. It is mainly influenced by the homogeneity of the flow through the packing, the kinetics of adsorption/desorption, and the mass transport in the stationary and mobile phases. The number of theoretical plates can be calculated directly from the chromatographic peak (elution chromatography) as follows:

$$N = 5.54\left(\frac{t_R}{w^{0.5}}\right)^2 \tag{8}$$

An alternative way to estimate the number of theoretical plates is from its retention time t_R and the peak width w measured at the base:

$$N = 16\left(\frac{t_R}{w}\right)^2 \tag{9}$$

However, the plate number is usually normalized on the effective length of the column in order to compare the efficiency independent of the column length.

According to the theoretical plate model the chromatographic band must be Gaussian in shape. Gaussian curves are obtained when replicate values of measurements are plotted as a function of the frequency of their occurrence. Experimentally, the plate height is the effective length of the column divided by the number of theoretical plates (Eq. 7). It is defined as the peak variance of the chromatographic band in length units σ_L^2 normalized on (divided by) the migrated distance L_{eff} [2,3]:

$$H = \frac{\sigma_L^2}{L_{eff}} \tag{10}$$

In 1956 Van Deemter *et al.* derived an equation that included various independent mechanisms contributing to column band broadening. For LC, the Van Deemter equation is [4]:

$$H = A + \frac{B}{u} + C_s u \tag{11}$$

where u is the linear mobile phase velocity (the velocity with which an unretained marker t_0 is transported with the mobile phase along the effective length of the column ($u = L_{eff}/t_0$)), A is the eddy diffusion term, B is the longitudinal diffusion constant, and C_s is the resistance to mass transfer in the stationary phase constant. As the Van Deemter equation (Eq. 11), was developed for gas chromatography, Van Deemter *et al.* considered the resistance to mass transfer in the mobile phase C_m to be negligible. As result, they did not derive an expression for this term in their equation and it was left to Purnell and Quinn [5] who suggested that the term of the resistance to mass transfer in the mobile

phase employed by Golay [6] in his rate equation for capillary columns (see Eq. 21), would also be appropriate for a packed column in LC. As result, a simplified form of the Van Deemter equation for LC becomes [4]:

$$H = A + \frac{B}{u} + C\,u \tag{12}$$

where C is the overall resistance to mass transfer in the stationary and mobile phases. However, Eq. 12 is written nowadays in the form of:

$$H = A + \frac{B}{u} + C_s\,u + C_m\,u \tag{13}$$

1.1.1 Band broadening processes

In the chromatographic process, contributions to band broadening can be divided into two major classes. One is the contribution from the injection and detection processes, which is referred to extra-column band broadening. The second source of band broadening is the contribution from the separation process itself. In this section we will focus on the second type which occurs within the column.

1.1.1.1 Eddy Diffusion term (the multipath process)

The velocity independent A-term arises in packed beds because the stationary phase packing material (particles) has irregular shape, size, and distribution along the column. The presence of tortuous paths through a chromatographic bed has the consequence that analyte molecules take different paths with variable lengths through the chromatographic bed, so that the molecules with the shortest path length would move through the column more quickly than those that take the longest path length. The smaller the particles and the narrower their size distribution the smaller is the contribution of the A term to the overall band broadening. H_A is given by [4]:

$$H_A = 2\lambda d_p \tag{14}$$

where λ is the inhomogeneity factor, d_p is the particle diameter.

1.1.1.2 Longitudinal diffusion

The overall variance of the Gaussian distribution arising from diffusion process in an empty column σ^2 is given by the Einstein equation:

$$\sigma^2 = 2\,D_m\,t \tag{15}$$

where D_m is diffusion coefficient of an analyte in the mobile phase, and t is the time period over which the diffusion process occurs.

For a column packed with a solid stationary phase, the rate at which diffusion occurs is given by:

$$\sigma^2 = 2\gamma D_m\,t \tag{16}$$

where γ is the obstruction factor, which is identical to the inverse tortuosity factor.

If the analyte molecules diffuse only when they are in the mobile phase and remain stationary when they are in or on the stationary phase, the time in Eq. 16 can be replaced by the time that the analyte spends in the mobile phase. For a packed column, the contribution of the longitudinal diffusion in the mobile phase H_{DM} to the overall H per unit length is given by:

$$H_{DM} = \frac{2\gamma D_m}{u} \tag{17}$$

Furthermore, a second longitudinal diffusion takes place in the stationary phase. H_{DS} is given by [4]:

$$H_{DS} = \frac{2\gamma_2\,k\,D_s}{u} \tag{18}$$

where D_s is the diffusion coefficient of an analyte in the stationary phase, and k is the retention factor of the analyte.

By summing Eqs. 17 and 18, the total contribution from longitudinal diffusion processes in the stationary and mobile phases is given by:

$$H_D = \frac{2\gamma D_m}{u} + \frac{2\gamma_2\,k\,D_s}{u} \tag{19}$$

1.1.1.3 The resistance to mass transfer in the mobile phase

During passage through a chromatographic column, the solute molecules are continually transferred from the mobile phase into the stationary phase and back from the stationary phase into the mobile phase. This transfer is not instantaneous; time is required for the molecules to pass through the mobile phase to reach the interface and enter the stationary phase. However, since the mobile phase is continually moving through the column, during this time interval, those molecules that remain in the mobile phase will be swept along the column. The contribution of the resistance to mass transfer in the mobile phase H_{RM} to the overall H is given by [4]:

$$H_{RM} = C_m u = \frac{f_1(k) d_p^2}{D_m} u \quad (20)$$

The form of $f_1(k)$ derived by Golay [6] is given by:

$$f_1(k) = \frac{1 + 6k + 11k^2}{24(1+k)^2} \quad (21)$$

1.1.1.4 The resistance to mass transfer in the stationary phase

The band broadening resulting from the resistance to mass transfer in the stationary phase is analogues to that in the mobile phase. The contribution of C_s to the overall H can be reduced by decreasing the diffusion path length needed for solute molecules to diffuse from the stationary phase to the mobile phase. This can be achieved by decreasing the thickness of the stationary phase (using smaller diameter stationary phase particles). On the other hand, it was found that increasing column temperature has an influence on reducing this effect by speeding up the diffusion of analyte molecules into and out of the stationary phase (increasing D_m). The contribution of the resistance to mass transfer in the stationary phase H_{RS} to the overall H is given by [4]:

$$H_{RS} = C_s u = \frac{f_2(k) d_f^2}{D_S} u \quad (22)$$

where d_f is the effective film thickness of the stationary phase. The form taken by $f_2(k)$ was considered by Van Deemter to be:

$$f_2(k) = \frac{8}{\pi^2} \frac{k}{(1+k)^2} \quad (23)$$

The contributions to the HETP by the resistance to mass transfer depend linearly on the linear velocity, and the different contributions are additive:

$$H_R = C_s u + C_m u \quad (24)$$

1.1.2 Type of chromatography

In chromatography, different modes of interaction are existing according to the type of interaction of the analyte with the stationary phase involved, which is controlled by the type of the stationary phase [3]:

- **Adsorption Chromatography:** the stationary phase is a solid and the mobile phase is a liquid, a supercritical fluid, or a gas. Interaction of the analyte molecules with the stationary phase is via adsorption.

- **Partitioning Chromatography:** the stationary phase is a liquid supported on an inert solid, the mobile phase is either a liquid, a supercritical fluid, or a gas. In the normal-phase mode of liquid-liquid partitioning chromatography, a polar stationary phase is used with a non polar mobile phase. In another type of liquid-liquid partitioning mode a non-polar stationary phase is used, with a polar mobile phase. This mode is called reversed-phase liquid chromatography, which is the most widely used chromatography elution mode.

- **Ion Exchange Chromatography (IEC)**: the stationary phase is an ion exchange resin having positively, negatively, or zwitterionic charged groups. Retention in IEC is governed by a competition between sample ions and mobile phase counter ions for electrostatic interaction with stationary phase ionic groups of opposite charge. IEC is mainly used for the separation of inorganic ions, acids, bases, and large bio molecules such as proteins and peptides.

- **Size Exclusion Chromatography:** this type of chromatography is also known as gel permeation or gel filtration chromatography. In size exclusion chromatography a porous stationary phase is used. This mode provides separation on the basis of size parameters and is used mainly for the separation of synthetic polymers and large bio-molecules. Sample components should not interact with the stationary phase.

- **Affinity Chromatography:** this is the most selective type of chromatography employed. It utilizes very specific interactions. For example, if there is a structural feature of an enzyme that will attach to a specific structural feature of a protein, affinity chromatography exploits this feature by binding a ligand with the desired interactive capability to a support. The ligand retards a solute with the compatible structural feature and lets all other solutes pass. The solute is then eluted by a mobile-phase change such as incorporating a competing solute, changing the acidity, or changing the ionic strength of the eluent.

1.2 Capillary electromigration separation techniques

All separation techniques in which a high electric field is used to propagate the mobile phase and the analyte molecules through a separation capillary are referred to capillary electromigration separation techniques. Generally, these techniques are used for the separation of different classes of analyte molecules based on different separation principles while using (i) an empty capillary filled with a buffered mobile phase or (ii) a capillary filled with a chromatographic stationary phase. Both techniques have proven to be effective separation tools for the separation of small organic and inorganic ions,

drugs, pharmaceuticals, synthetic polymers, proteins, peptides, amino acids, and nanoparticles. Electromigration separation techniques are characterized by high analysis speed, high separation efficiency, fine-tuneable selectivity, high selective separation, high detection sensitivity, requirement of a small sample amount, and low consumption of organic solvents compared to conventional pressure driven liquid chromatography.

1.2.1 Capillary electrophoresis

Electrophoresis is the migration of charged analytes under the influence of an electric field. Cations migrate toward the cathode and anions migrate toward the anode. In 1937 Tiselius [7] reported for the first time the technique of moving boundary electrophoresis for the separation of different serum proteins in free solution. In 1967 Hjerten [8] was the first who introduced the use of a high voltage using rotating glass tubes with an internal diameter around 3 mm coated with methyl cellulose (free zone electrophoresis). In 1981 Jorgenson and Lukacs [9] published a paper which demonstrated the use of fused silica capillaries with a 75 µm i.d. and voltage up to 30 kV (capillary zone electrophoresis) for efficient CE separation of proteins and dansylated amino acids. Employing a capillary in electrophoresis provides a possibility for the separation of minute quantities of substances in a short time with high resolution and on-line detection. The heat generated inside the capillary is then effectively dissipated through the wall, which allows using very high electric field strengths.

The principle of separation by capillary electrophoresis (CE) is based on the fact that charged species are separated according to differences in their effective electrophoertic mobility. The electrophoretic velocity of a charged species v_{ep} is given by:

$$v_{ep} = \mu_{ep} E = \mu_e \left(\frac{U}{L_{total}} \right) \tag{25}$$

where μ_{ep} is the electrophoretic mobility (= v_{ep}/E), E is the electric field strength (= L_{total}/U), U is the voltage applied across the capillary, and L_{total} is the total length of the capillary.

The most simple approach assumes that in the steady state the electrostatic force is balanced by the oppositely directed frictional force:

$$v_{ep} = \frac{q E}{6 \pi \eta r} \tag{26}$$

where q is the charge of charged ion, r is the hydrodynamic radius of the charged ion, η is the bulk solution viscosity. Substitution of v_{ep} in Eq. (26) by Eq. (25) gives:

$$\mu_{ep} = \frac{1}{6\pi\eta}\frac{q}{r} \tag{27}$$

It is clear from Eq. (27) that the charge and size of the ion and the viscosity of the medium have a strong influence on the electrophoretic mobility.

1.2.1.1 Electroosmosis

Electroosmosis refers to the movement of a liquid inside the capillary as a consequence of the application of an electric field across the capillary. The linear velocity of the electroosmotic flow (EOF) can be determined from the effective length of the capillary L_{eff} and the hold up time t_0 as follows:

$$v_{eo} = \frac{L_{eff}}{t_0} \tag{28}$$

Formally, v_{eo} in an electrolyte solution depends on the electroosmotic mobility μ_{eo} and on the electric field strength E [10,11]:

$$v_{eo} = \mu_{eo} E \tag{29}$$

By substitution of the value of v_{eo} in Eq. 29 and replacing E with U/L_{total}, where L_{total} is the total length of the capillary (from inlet to the outlet), the electroosmotic mobility μ_{eo} becomes:

$$\mu_{eo} = \frac{v_{eo}}{E} = \frac{L_{eff}\ L_{total}}{t_0\ U} \tag{30}$$

In a fused silica capillary filled with a buffer, the silanol groups (Si-OH) on the surface of the interior wall dissociate into negatively charges silanol groups ($Si\text{-}O^-$). Two distinct layers are formed (Fig. 1); the first one consists of positively charged cations that are strongly attracted to the negatively charged capillary wall, resulting in a fixed compact layer called Stern layer [12]. The second layer next to the Stern layer is the diffuse layer or Gouy-Chapman layer. Several models have been reported in the literature for describing the structure of the electric double layer like Helmholtz layer model, Gouy-Chapman model, and Stern model [12]. In the Helmholtz layer model, the solvated ions arrange themselves along the charged surface but are held away from it by their hydration spheres. The location of the sheet of ionic charge, which is called the outer Helmholtz plane (OHP), is identified as the plane running through the solvated ions. This model assumes that the electric potential changes linearly within the layer confined by the charged surface on one side and the OHP on the other. Since this model assumes the presence of two rigid planes of charge, one plane is the outer Helmholtz plane (OHP) and the other plane is the charged capillary wall, it ignores the effect of thermal motion, which tends to

break up and disperse the rigid outer plane of charge. In the Gouy-Chapman model of the diffuse double layer, the disordering effect of thermal motion is taken into account in the same way as the Debye–Hückel model describes the ionic atmosphere of an ion with the latter's single central ion replaced by an infinite plane charged surface. The local concentrations of cations and anions differ in the Gouy–Chapman model from their bulk concentrations. Ions of opposite charge cluster close to the charged surface and ions of the same charge are repelled from it. Neither the Helmholtz nor the Gouy–Chapman model is a very good representation of the structure of the double layer. The former overemphasizes the rigidity of the local solution; the latter underemphasizes its structure. The two models are combined in the Stern model, in which the ions closest to the charged surface forming the Stern layer (which is the same of a rigid Helmholtz plane suggested by the Helmholtz layer model), while ions located outside that layer are diffused into the bulk solution as in the Gouy–Chapman model [12].

There is a charge density distribution $\rho_{(x)}$ near the charged wall. The electrostatic force exerted on a volume element *dV* is given by ρ(x) dV E.

The electroosmotic flow (EOF) may be produced either in open or in packed or in monolithic capillary columns, as well as in planar electrophoertic systems employing a variety of supports, such as paper or hydrophilic polymers. As it is seen from Fig. 1 the electric potential is assumed to decrease with distance linearly across the Stern layer, while across the diffuse region and into the bulk solution, the decrease in electric potential is assumed to be exponential (according to the linearized Poisson-Boltzmann equation). The inverse thickness of the diffuse layer κ depends inversely on the square root of the ionic strength of the mobile phase *I*, the temperature *T*, and on the electric permittivity ε of the mobile phase:

$$\kappa = \sqrt{\frac{N_A\, e^2 \sum (z_i^2\, c_i)}{\varepsilon_0\, \varepsilon_r\, k\, T}} \qquad (31)$$

where z_i is the charge of ion i, c_i is the molar concentration of ion i, *R* is the gas constant, *k* is Boltzmann constant, *T* is the absolute temperature, N_A is Avogadro number, ε_o is the electric permittivity of vacuum, ε_r is the dielectric constant, and e is elementary electric charge = 1.6021 x10^{-19} C.

The electric potential at the plane of shear (the interface between the compact and the diffuse layer) is known as the zeta potential ζ. The zeta potential depends on the surface charge density σ and the ionic strength. In case of r >> δ, where r is the radius of the capillary and δ is the double layer thickness (Debye length), the electroosmotic mobility μ_{eo} and the EOF linear velocity v_{eo} are given by the Smoluchowski equation [10,11]:

$$\mu_{eo} = \frac{\varepsilon_0 \, \varepsilon_r \, \zeta}{\eta} \tag{32}$$

$$v_{eo} = \frac{\varepsilon_o \varepsilon_r \zeta E}{\eta} \tag{33}$$

The electroosmotic mobility μ_{eo} depends on the zeta potential ζ and the viscosity η of the mobile phase (background electrolyte (BGE)), and the dielectric constant ε_r which are influenced by the following factors:

- pH: via change in the surface charge density σ.
- Temperature: via variation of the viscosity of the mobile phase.
- Ionic strength: via variation of the zeta potential.
- Content of organic solvent: via change in the dielectric constant to viscosity ratio ε_r/η and change in the zeta potential.

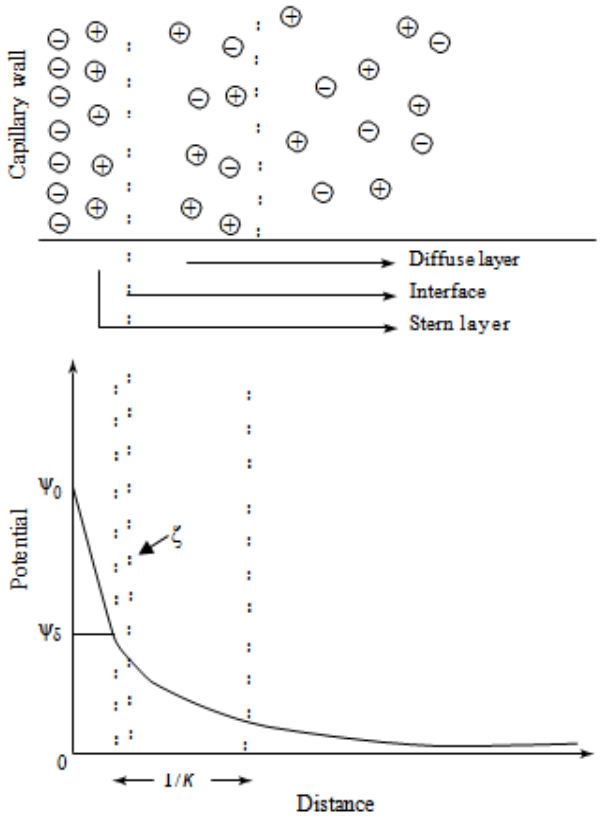

Figure 1: Graphical representation of the electric double layer at the solid–liquid interface within a capillary and diagram of the decrease of the electric potential with distance from the capillary wall [13].

1.2.2 Capillary electrochromatography (CEC)

In capillary electrochromatography (CEC), separation is possible by the partitioning of an analyte between a fixed stationary phase and a mobile phase. The driving force of the propagation of the mobile phase in capillary electrochromatography is the electroosmotic flow (EOF). Strain [14] was the first who reported the use of the EOF for the propulsion of the mobile phase in the separation of several dyes on alumina stationary phase. In 1952 Mould and Synge [15] demonstrated the use of the EOF in a thin-layer chromatographic system for the separation of polysaccharides in colloidal membrane strips. After that, Pretorius et al. [16] reported that using the EOF to propagate the mobile phase though a 1 mm i.d. glass tube packed with particles of 75 to 125 µm results in substantially smaller band broadening and thus better separation efficiency compared to the parabolic flow profile of pressure driven flow in liquid chromatography. In 1980s CEC experienced significant progress. Jorgenson and Lukacs [17] confirmed the feasibility of using the EOF for obtaining low reduced plate heights by using glass capillaries of 170 µm I.D packed with ODS packing.

The flat flow profile of the electroosmotic flow (compared to a parabolic flow profile) gives CEC advantages over HPLC regarding the separation efficiency. Analytes are separated in CEC according to differences in the partitioning coefficient between the stationary phase and the mobile phase, and to differences in their electrophoretic mobility. As in CE, small inner diameter 50-100 µm capillaries are employed to minimize a radial thermal gradient resulting from Joule heating, which would have an adverse effect on the efficiency gained.

The bulk EOF linear velocity is independent of the channel diameter (in the case of no double layer overlap). Thus variations in the flow velocity between regions of the column differing in the packing structure will be small in an electrically driven system [10]. Another important feature of the electroosmotic flow (compared to the pressure difference-induced laminar flow) is the reduction of band broadening due to mass transfer resistance in the mobile phase C_m. The reduction in the contribution of A and C_m terms to the band broadening results in an increase in efficiency in CEC compared to HPLC. A study by Tallarek *et al.* [18] showed the importance of the A term in defining the advantage of CEC over microHPLC using pulsed magnetic field gradient nuclear magnetic resonance to study flow field dynamics. The authors found that the A term is smaller by a factor of 2.5 in CEC than in microHPLC on the same column. A similar conclusion was obtained by Wen *et al.* [19] using chromatographic measurements. Moreover, the same authors observed a reduction in the C term. A further study by Jiang *et al.* [20] confirmed that with CEC a nearly flat van Deemter curve is obtained (Fig. 2), whereas in HPLC (with identical column) a typical minimum is found. This result is in accordance with the assumption of a reduced A term and C term in CEC. In addition, because the EOF velocity is independent of the mean channel width between the particles in the column, longer columns containing particles of very low diameter (< 0.5 mm) can be used. Consequently, efficiencies up to 500 000 m^{-1} can be achieved [11]. With such a high efficiency, also a higher column peak capacity is reached.

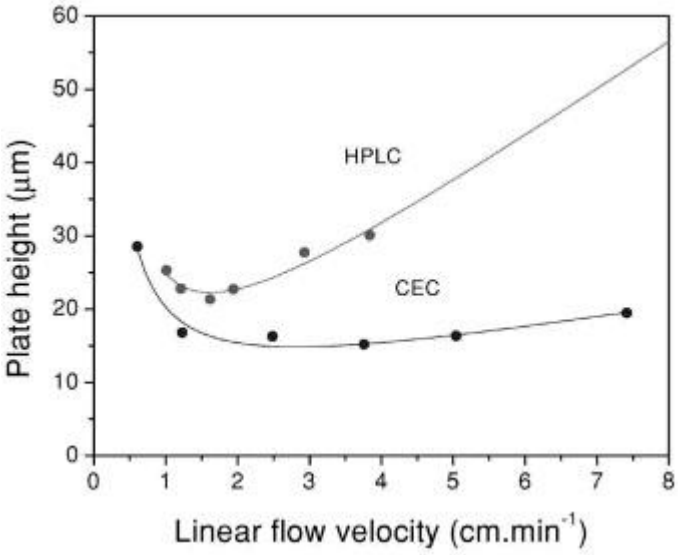

Figure 2: Comparison of Van Deemter curves under electro and pressure driven conditions. Column: Poly(alkylmethacrylate) monolith containing sulfonic acid functionalities, 41.5 cm (8.5 cm from detection window to outlet). Mobile phase: 20%, v/v sodium phosphate buffer (5 mmol L^{-1}, pH = 7) and 80% ACN, analyte: thiourea [20].

Because of the small internal diameter of the capillary columns used in CEC, both solvent flow and sample size are dramatically reduced compared to conventional HPLC. This results in a reduction of the consumption of solvent, which makes CEC economically attractive and environmentally friendly. In addition, CEC is easily compatible with mass spectrometry, which makes it to be a versatile analytical separation technique for biochemical analysis (amines and amino acids, peptides, proteins, nucleosides, nucleotides, and carbohydrates), environmentally and industrial applications (inorganic anions and cations, pesticides, insecticides, herbicides, synthetic polymer, and explosives), and chiral separations.

1.2.2.1 Instrumentation

In general, the instrument used in CEC is a slightly modified instrument designed for CE with the ability to pressurize both inlet and outlet ends of the separation capillary to prevent bubble formation inside the capillary. Smith and Evans [21] described the use of a modified CZE instrument that allowed electrochromatography to be performed at ±30 kV and 40 °C avoiding bubble formation. At the beginning, Knox and Grant indicated that Joule heating is the primary cause of bubble formation inside the packed column [22], but subsequent investigations made by Rebscher and Pyell [23] observed that the formation of bubbles invariably started at the border between the packed and the unpacked segment of the capillary. They explained this observation by the assumption that a change in the

electroosmotic velocity occurs when the mobile phase passes from the packed segment into the unpacked segment, whereas it can be assumed that the following segment has a higher electroosmotic velocity than the proceeding segment.

The schematic representation of a typical CEC instrument is demonstrated in Fig. 3. In general, there are five main parts: the separation capillary, a high voltage power supply, a detector, a data processor, and sample/buffer reservoirs. The CEC capillaries are with inner diameter between 50 and 100 µm filled with packing material (modified silica gel particles, a monolith, or coating with a thin film of a stationary phase like in an open-tubular column). The electric field is generated by a high voltage power supply that provides up to ±30 kV connected to the inlet platinum electrode. The outlet electrode is connected to the ground in order to complete the electric circuit.

Detection in CEC can be performed either by on-column (OCD) or by in-column (ICD) detection. In case of OCD, the capillary is composed of two segments, one filled with the stationary phase and another one empty (open segment used for detection). A second type of detection is ICD. In this case the capillary is completely filled with either packing material or a thin layer of stationary phase or a monolith. Detection with this mode has to be performed in the chromatographic bed itself [24]. Banholczer and Pyell [25] made a comparison between OCD and ICD photometric detection (UV detection) performed with fused silica capillaries of 180 µm i.d. packed with 3.0 µm octadecyl silica gel. They found that the baseline noise for ICD is about twice that for OCD. However, other detection techniques were used also in CEC, such as fluorimetric detection, and amperometric detection. In addition coupling with mass spectrometry (MS) has also been used by employing electrospray ionization (ESI) [26,27], and atmospheric pressure chemical ionization (APCI) modes [28], which are currently widely used in proteomics analysis. Moreover, coupling of CEC with NMR spectroscopy gives additional structural information of the analyte [29]. The output of the detector is connected to the data acquisition system. The inlet of the separation capillary is immersed into the inlet reservoir, while the outlet side is immersed into the outlet reservoir. The inlet reservoir is replaced with the sample reservoir during the injection step.

In CEC there are two types of injection: hydrodynamic and electrokinetic injection. Hydrodynamic injection is carried out by applying a pressure difference between the two ends of a capillary. This is the most used injection mode in CE, while it is of limited use in CEC due to the high pressure needed to propagate the mobile phase through the column. Another injection mode is electrokinetic injection, which is the most popular injection mode used in CEC. The instrumental realization of this mode makes it possible to inject reproducibly few nanoliters of a sample. In addition, it is relatively simple to be

implemented [30]. In order to introduce a small amount of the sample into the separation capillary, the vessel with mobile phase is replaced by a vessel containing the sample and applying a voltage ramp during a defined time period. With electrokinetic injection the sample containing neutral analytes is injected as a very narrow zone into the capillary by the effect of electroosmosis without discrimination between the sample constituents.

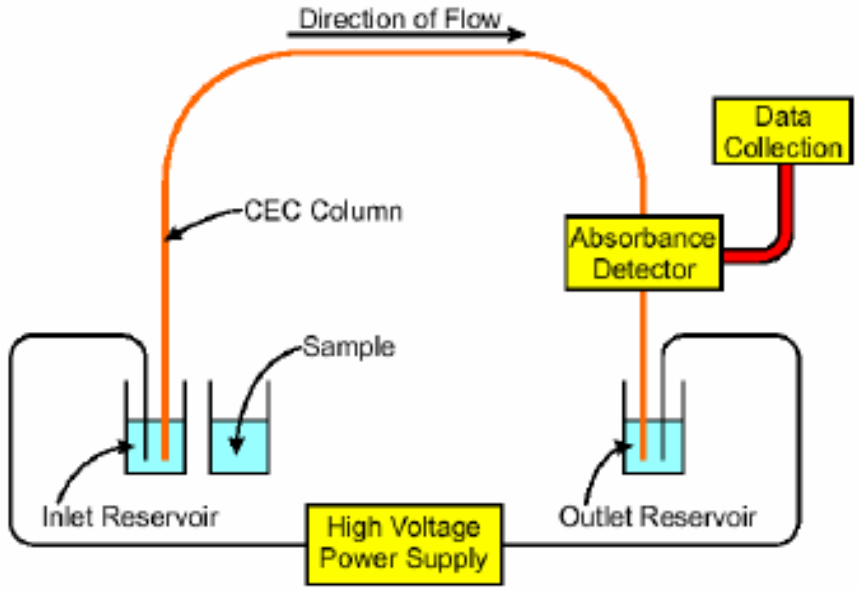

Figure 3: Schematic representation of the components of a CEC instrument [11].

1.2.2.2 Mobile phases for CEC

Typically, all mobile phases used in CEC have to be buffered in order to produce a constant electroosmotic flow needed to propagate the mobile phase through the capillary. Therefore most of the mobile phases used in CEC consist of an aqueous buffer mixed with an organic solvent like methanol or acetonitrile. In some rare cases, non-aqueous mobile phases are used.

In CEC the selection of the mobile phase plays a crucial role, since the composition and the bulk properties of the mobile phase like ε/η ratio, ionic strength, electric conductivity, and viscosity have a strong influence on the velocity and stability of the electroosmotic flow and thus on the reproducibility of the results obtained. In CEC, the optimization of the mobile phase composition must consider not only the retention of the analytes and the selectivity of the chromatographic system but also the electroosmotic mobility and the chromatographic efficiency [31].

1.3 Host-guest complexation using cyclodextrins

Cyclodextrins (CDs) are cyclic oligosaccharides built up of six (α-cyclodextrin), seven (β-cyclodextrin), and eight (γ-cyclodextrin) glucopyranose unites, which are joined by α-(1,4)-glycosidic linkages forming a torus-shaped ring (truncated cone) with a hydrophilic exterior and a hydrophobic interior (cavity). They are produced by bacterial digestion of starch. Different CDs have different cavity sizes depending on the number of glucopyranose unites. Their ability to form inclusion complexes makes them widely used as solubilizing agents in a large number of applications like food chemistry, textiles, agricultural, pharmaceuticals, cosmetics, polymer synthesis, and separation science. Generally, the aqueous solubility of the natural cyclodextrins, in particular β-CD, is much lower than that of comparable acyclic saccharides. This is because of a strong intramolecular hydrogen bonding between the neighbouring glucose units. Substitution of any of the hydrogen bond forming hydroxyl groups of cyclodextrins by, for example, methoxy or hydroxypropyl groups results in a dramatic improvement in their aqueous solubility. In this context, randomly (statistically) methylated-β-cyclodextrin is the most useful and accessible CD because of its high water solubility and low price.

The ability of cyclodextrins to form inclusion complexes with guest molecules depends on two main factors. The first factor is the steric effect. It depends on the matching of size between the relative size of the cyclodextrin cavity to the size of the guest molecule. Therefore the stability of a host-guest complex generally increases with the degree of geometrical fit of the guest molecule in the cyclodextrin cavity. In addition, the charge and polarity of the guest molecule also play an important role in the formation and the stability of the inclusion complex, so that highly water soluble guests are not suitable for complex formation. The second factor is the interaction between the different components of the system (cyclodextrin, guest, solvent). During the formation of an inclusion complex no covalent bonds are broken or formed and the main driving force of complex formation is the release of water molecules from the cavity (entropic effect), which are replaced by the more hydrophobic guest molecule present in solution [32]. In general, the driving forces for the complex formation include also electrostatic interactions, van der Waals interactions, hydrophobic interactions, hydrogen bonding, release of conformational strain, and charge-transfer interactions [33,34].

Each individual glucose ring has one primary and two secondary hydroxyl groups. The secondary glucopyranose hydroxyl groups (C_2 and C_3) are located at the wider edge of the truncated cone-like cyclodextrin and the primary hydroxyl groups (C_6) are located at the narrow edge (Fig. 4). Polar groups are not at inside of the truncated cone-like cyclodextrin, which results in a molecular structure with a hydrophilic outside (being able to form hydrogen bonding with water molecules), and a hydrophobic cavity,

which provides a hydrophobic microenvironment for a hydrophobic guest [32]. As a result of the unique structure of this cavity, cyclodextrins are able to form inclusion complexes with a wide variety of hydrophobic guest molecules like aldehydes, ketones, alcohols, organic acids, fatty acid, aromatics, halogen compounds, acrylic monomers, dyes, drugs, and amine derivatives [35]. One or two guest molecules can be entrapped by one, two or three cyclodextrins. Moreover, the ability of cyclodextrins to from inclusion complexes with organic hosts offers the possibility to build supramolecular structures, such as rotaxanes, polyrotaxanes, and catenanes [36].

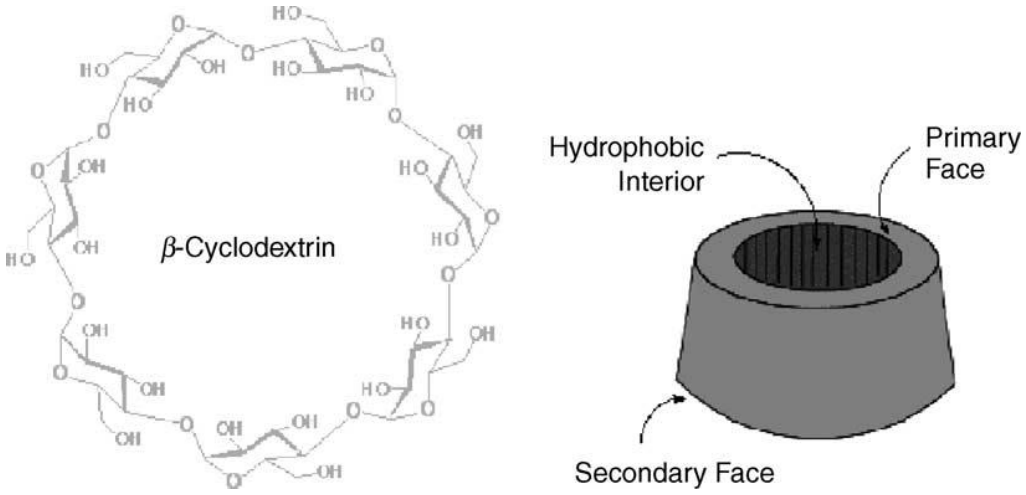

Figure 4: Chemical structure of β-cyclodextrin [32].

The formation of a host-guest complex can be described by the mass action law [37]:

$$[CD] + [G] \rightleftharpoons [CD\text{-}G] \tag{34}$$

Measurements of the stability constant or equilibrium constant (K_c or B) of the formed host-guest complex are important (especially for drug compounds). The formation of the inclusion complex can be verified by FTIR, ^{1}H NMR, 2D-NOESY, or ROESY spectroscopy. According to the mass action law, the complex formation constant (stability constant) B is defined as [37]:

$$B = \frac{[CD-G]}{[CD]\,[G]} \tag{35}$$

The use of purely aqueous polymerization media for the preparation of organic polymer monolithic stationary phases has a limitation regarding the incorporation of hydrophobic monomers into the polymerization mixture which is required for achieving the necessary hydrophobicity for reversed-phase separations. This problem has been overcome by either applying high-power ultrasonication to the

polymerization mixture containing a hydrophobic monomer or making polymerization in the presence of an organic solvent(s) (or mixture of aqueous buffer and organic solvent) or making polymerization in the presence of ionic liquid solvent(s), or adding a surfactant to the aqueous reaction medium at a concentration that exceeds the critical micellar concentration (CMC). An alternative to the use of an organic solvent, surfactant, or ionic liquid solvent is the solubilization of the hydrophobic monomer by host-guest complexation using a water soluble cyclodextrin (CD).

The procedure of solubilization of hydrophobic monomers by complex formation with water-soluble cyclodextrins and subsequent reaction of the formed host-guest complex by free radical polymerization or copolymerization in aqueous solution has been introduced in 1997 by Ritter and co-workers [38-47]. These authors reported free radical (co)polymerization of different hydrophobic monomers, such as acrylate (n-butyl, n-hexyl, and cyclohexyl acrylates) [38], isobornyl acrylate and butyl acrylate [39]. In addition, the same authors reported free radical homopolymerization of cyclohexyl and phenyl methacrylate [41], N-methacryloyl-11-aminoundecanoic acid [42], *tert*-butyl methacrylate [43], vinylferrocene [44], and N-adamantylacrylamide [45]. Ritter and co-workers have found that in nearly all cases the resulting polymer precipitates rapidly in a high yield. In order to achieve prolongation of the growing polymer chain during polymerization, the CD host has to slip off from the growing polymeric chain and thus remains dissolved in the aqueous phase and can be recycled [46,47] (Fig. 5).

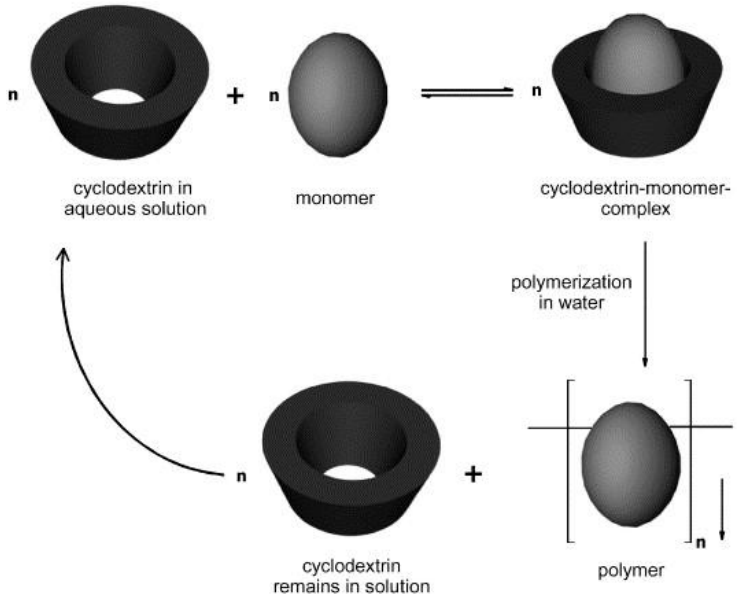

Figure 5: Solubilization of hydrophobic monomer by formation of inclusion complex with water- soluble cyclodextrin in aqueous medium followed by free radical polymerization of the formed inclusion complex [47].

1.4 Polymer-based monolithic stationary phases

In CEC, the selection of the stationary phase plays a crucial role since it provides interaction sites for the solutes and ionizable charged groups that play the dominant role in the generation of the EOF. The capillary columns used in CEC can be grouped into three types: packed columns (PCs), open-tubular columns (OTCs), and continuous beds/monoliths. In the first years of the development of CEC, silica particles have been used as packing materials for PCs [16,17]. In this context, several methods have been used for producing the packed capillary such as the slurry and electrokinetic methods. The silica matrix of such particles provides several advantages like the generation of a substantial EOF due to enough surface charge, a high loading capacity, and the possibility to use small particle sizes. However, several problems impair the development of this type of stationary phase like the need of using strong and reproducible two end frits that should stabilize the stationary phases inside the column, high pack pressures generated as results of using smaller particles, bubble formation generated inside the column, non-homogeneity of particles packing along the column, non-reproducibility of column packing, Joule heating, and the need for post column detection which might results in increasing the band broadening. These restrictions give the researchers working in the field of separation science the motivation to develop a new type of stationary phase which is called open-tubular columns (OTCs). With this type of column format, the inner wall surface of the confinement is coated with a thin layer of stationary phase. Despite of their lower loading capacity and insufficient sensitivity, OTCs provide a better efficiency and resolving power over PCs. In addition, OTCs provide other technical advantageous making them an alternative to PCs like the ease of their preparation, less prone to bubble formation, versatility in the chemistry of surface modification, and compatibility with small inner diameter confinements [48-51].

In 1950s Mould and Synge [15] suggested to fill the separation column with a continuous beds of porous gel structure with uniform porosity that enhances size exclusion separation of large molecules *"An alternative possibility, suggested in discussions between Dr. A. J. P. Martin, Prof. A. Tiselius and one of us (R.L.M.S.) is to use electro-endosmosis to move a solution through a continuous block of porous gel structure".* This idea was ignored by researchers till the end of 1980s, when Hjerten *et al.* [52], Svec and Tennikova [53], and Svec and Frechet [54] developed a new generation of stationary phase as a large single piece of highly porous organic polymer material that fills the interior volume of a confinement. This type of stationary phase is called in the literature [55] (i) continuous polymer bed, (ii) polymer rod column,(iii) continuous column support, (v) monolithic column, (vi) compressed gel column, and (vii) polymeric gel column. In the 1990s another type of monolithic stationary phase was developed by Tanaka's group [56] called inorganic silica-based monolithic stationary phase. In general, monolithic

stationary phases are classified into organic polymer-based monoliths (highly crosslinked macroporous copolymers), inorganic silica-based monoliths (silica rods), and hybrid monoliths.

According to the type of the mechanism of pore formation (phase separation process), two main types of organic polymer monoliths are produced: (i) highly crosslinked macroporous amphiphilic copolymers synthesized from acrylic monomers (mainly acrylate and acrylamide) dissolved in aqueous, aqueous-organic, or organic medium in the presence of a lyotropic salt used for adjusting the morphology and the porous properties of the synthesized monolith, and (ii) macroporous hydrophobic polymers synthesized from hydrophobic monomers dissolved in an organic solvent [57].

More than 20 years ago, a large number of polymer-based monolithic stationary phases have been synthesized. They can be classified according to the type of monomer used in the polymerization reaction such as polymethacrylate, polystyrene, or polyacrylamide. In a few cases polynorbornene-based monoliths were synthesized by ring-opening metathesis polymerization (ROMP). Polymer-based monoliths are usually synthesized within different confinements such as fused silica capillaries, borosilicate columns, or microfluidic chips. As an essential prerequisite for monolith preparation by polymerization in a confinement the inner wall has to be pre-treated prior to polymerization with a chemical reagent such as (3-trimethacryloyloxypropyl)tri-methoxysilane (bind silane)) in order to attach the formed polymer covalently to the inner wall of the housing confinement. The importance of this step is to prevent the mobile phase filling a gap between the wall of the confinement and the formed polymer and to prevent the formed polymer from shrinking and removing out of the confinement when applying high pressures. The vinylic group of the covalently attached acrylate reacts with other polymerization mixture constitutes during the free radical polymerization reaction resulting in the covalent attachment of the formed polymer to the inner wall of the housing confinement.

The most frequently used polymerization technique for the preparation of a polymer-based monolith is free-radical *in situ* polymerization. This process implies that a mixture of a monovinyl monomer(s), a divinyl monomer (crosslinker), and a free-radical initiator is dissolved in (a) solvent(s) (for a monolith prepared for CEC, a charged monomer has to be incorporated in the polymerization mixture in order to generate a sufficiently high and constant EOF). Free-radical polymerization is initiated either by heat (for thermally initiated polymerization and heat-induced polycondensation), light (for photochemically initiated polymerization), or addition of chemical reagents (accelerators, redox system). Other polymerization techniques like, heat-induced polyaddition, γ-irradiation-derived polymerization, UV initiation, and ring-opening metathesis polymerization (ROMP) have been rarely used. After the

completion of the polymerization, the capillary has to be rinsed with an appropriate solvent to remove the solvent and unreacted monomers form the pores of the formed monolith.

Polymer-based monolithic stationary phases offer the possibility to tailor the chemical structure, the morphology, the porous properties, and thus the chromatographic properties of the formed monolith. Practically, this can be achieved by adjusting the composition of the polymerization mixture and the reaction conditions. In this context, several factors affect the morphology, the mechanical properties (hydrodynamic permeability), the chemical stability, and the chromatographic properties of the produced organic polymer monolith like type(s) and molar fraction(s) of monomer(s), type and molar fraction of crosslinker (%C), total monomer concentration (%T), type(s) and concentration(s) of porogen(s), type of polymerization solvent, type, concentration and activation of initiator, polymerization time, and polymerization temperature. The influence of these parameters on morphology, porous properties, and chromatographic performance of polymer-based monolithic stationary phases is well explained in the literature [57-71].

1.5 Polyacrylamide-based monolithic stationary phases

The first monolith prepared by Hjerten *et al.* in 1989 [52] is based on a copolymer of acrylic acid and *N,N'*-methylenebisacrylamide (BIS). This monolith has been used as a cation-exchange stationary phase for the separation of proteins by HPLC. In 1992, the article published by Baba and Tsuhako [72] has shown the preparation of hydrophilic polyacrylamide-based gel-filled fused silica capillaries by copolymerization of a monovinyl monomer such as acrylamide (AA) and a divinyl monomer (crosslinker) such as N,N'-methylenebisacrylamide (BIS) in the presence of the redox initiator system peroxydisulfate-*N,N,N',N'*-tetramethylethylendiamine. Initiation of the polymerization process begins immediately upon mixing of all the components at room temperature. The resulting gel is very soft, a highly swollen material that contains no more than 5% solid polymer, which is similar to those gels used for capillary gel electrophoresis. In 1995 Fujimoto *et al.* [73] prepared a crosslinked acrylamide-based gel for CEC by copolymerization acrylamide (AA)/2-acrylamido-2-methyl-2-propanesulfonic acid (AMPS) and acrylamide (AA)/N,N'-methylenebisacrylamide (BIS)/2-acrylamido-2-methylpropanesulfonic acid (AMPS) inside a capillary. The formed gel shows a good physical stability although it has no chemical attachment to the inner wall of the capillary.

In 1996, Hjerten et al. [74] used a simple one-step procedure for the preparation of polyacrylamide-based monolithic capillaries for CEC. The polymerization mixture consisted of an aqueous solution of acrylamide (AA), piperazinediacrylamide (PDA), and vinylsulfonic acid (VSA). The desired

hydrophobicity of the resultant gel was achieved by adding stearoyl methacrylate or butyl methacryalte. Since both of these monomers are water insoluble, a surfactant (Triton X-100) was added to the mixture, followed by sonication to form an emulsion. Once the reaction was initiated by the addition of the redox initiator system peroxydisulfate-*N,N,N′,N′*-tetramethylethylendiamine, the polymerization mixture was immediately drawn into an acryloylsilanized capillary where the polymerization was completed. In the same year, the same working group [75] reported the synthesise of derivatized polyacrylamide-based monolithic stationary phases for reversed-phase chromatography using a two step reaction. The first step includes the synthesis of a continuous bed by copolymerization of piperazinediacrylamide (PDA), methacrylamide (MA), allyl glycidyl ether (AGE), and 2-hydroxyethyl methacrylate (HEMA). The second step includes the linking of C_{18} ligands to the formed matrix by reacting 1,2-epoxyoctadecane (EOD) with the epoxy and hydroxy groups in the matrix in the presence of BF_3 as catalyst. The polymerization reaction was initiated by adding the redox initiator system peroxydisulfate-*N,N,N′,N′*-tetramethylethylendiamine to the polymerization mixture. These monoliths showed high performance in the separation of standard proteins and peptides. In 1997 the same working group [76] synthesized highly crosslinked polyacrylamide monolithic stationary phases. The preparation procedures consist of several steps including the pre-treatment of the inner wall of the capillary with 3-(trimethoxysilyl)propyl methacrylate, two polymerization steps, and a chemical functionalization. The initial polymer matrix was synthesized by copolymerization of a dilute aqueous solution of 2-hydroxyethyl methacrylate (HEMA) and piperazinediacrylate initiated using the redox initiator system peroxydisulfate-*N,N,N′,N′*-tetramethylethylendiamine in the presence of a high concentration of ammonium sulfate (AS) as porogenic salt, which is added to obtain a porous structure with desired permeability. The formed pores of this matrix were then filled with another polymerization mixture containing allyl glycidyl ether (AGE) (20%), 2-hydroxyethyl methacrylate (HEMA) (50%), and piperazinediacrylate (30%) to which dextran sulfate was added. The polymerization mixture was initiated again using the same redox system. The second polymerization proceeded inside the pores of the skeleton of the initial formed polymer and leads to the immobilization of the charged dextran within the network of the newly formed matrix. Eventually, the reaction between both epoxide and hydroxyl functional groups of the resulting matrix with 1,2-epoxyoctadecane (EOD) catalyzed by BF_3 leads to the covalent functionalization of the matrix with an unquantified number of octadecyl chains.

In 1996 Fujimoto *et al.* [77] prepared crosslinked polyacrylamide-based continuous beds for CEC. The continuous beds were synthesized by free radical copolymerization of *N*-isopropylacrylamide (NIP), 2-acrylamido-2-methylpropanesulfonic acid (AMPS), and *N,N′*-methylenebisacrylamide (BIS) in the presence of the redox initiator system peroxydisulfate-*N,N,N′,N′*-tetramethylethylendiamine in aqueous

solution. These beds were successfully used for CEC separations of mixtures of steroids and polyaromatic hydrocarbons. In the same year, Svec et al. [60] synthesized a hydrophilic macroporous polyacrylamide-based monolith by free radical copolymerization of acrylamide (AA), N,N′-methylenebisacrylamide (BIS), and free radical initiator azobisisobutyronitrile (ABN) in the presence of a porogen. A combination of dimethylsulfoxide and 2-heptanol was selected from a broad spectrum of solvents and water soluble polymers to achieve the optimum composition of the porogenic mixture. In addition to the composition of the porogen, the authors optimized the porous properties of the synthesized stationary phases through changes in the percentage of the crosslinker and free radical initiator in the polymerization mixture, and the polymerization temperature. A major conclusion was that the polymerization temperature has a minor effect on the pore size distribution of the resultant monolith, and that increasing the content of crosslinker in the polymerization mixture results in smaller pores, whereas decreasing the content of initiator results in the formation of large microglobules.

Palm and Novotny [78] simplified the incorporation of hydrophobic monomers into an acrylamide-based matrix by using a mixture of aqueous buffer and/or organic solvent. They synthesized macroporous polyacrylamide-based monoliths for CEC from acrylamide (partly replaced by butyl, hexyl or lauryl acrylate and acrylic acid or vinylsulfonic acid (VSA)) and bisacrylamide in the presence of poly(oxyethylene) as porogenic polymer in formamide or N-methylformamide/aqueous buffer. For this type of stationary phase efficiencies up to ca. 400.000 plates m^{-1} were reported in the CEC mode (e.g. for phenones k = 0.1-0.4; H_{min} = 3.0 µm). The same type of stationary phase was synthesized by Zhang and El-Rassi [79]. In this case the authors prepared a monolithic stationary phase for CEC with sulfonic groups needed for the promotion of the EOF and non-polar dodecyl ligands for chromatographic interaction by using *N*-methylformamide/aqueous buffer solution as polymerization mixture. The authors observed that the synthesized monolithic stationary phase showed a reversed-phase retention behavior towards non-polar solutes (*e.g.*, long alkyl chains phenyl ketones) and a mixed-mode (reversed-phase/normal phase) retention behavior towards more polar solutes (polar pesticides). However, high separation efficiencies were achieved using the synthesized monoliths for alkylphenones and pesticides (H_{min} = ca. 2.5 µm).

In 1999 Ericson and Hjerten [80] described another method for the preparation of a monolithic capillary column that was used for gradient CEC separation of proteins using either co-EOF or counter-EOF modes. The synthetic route involves polymerization initiated by using the redox initiator system peroxydisulfate-*N,N,N′,N′*-tetramethylethylendiamine in a system consisting of two phases, an aqueous solution of acrylamide (AA) and piperazinediacrylamide (PDA) in a mixture of buffer and

dimethylformamide, and an immiscible highly hydrophobic octadecyl methacrylate phase. Continuous sonication for 45 minutes was needed in order to emulsify the octadecyl methacrylate and to form a dispersion of fine polymer particles. In the remaining steps of these procedures, another portion of initiator was added to the system to restart the polymerization of two newly added monomers, dimethyldiallylammonium chloride and piperazinediacrylamide (PDA). The resulting partly polymerized dispersion was drawn into a methacryloylated capillary using pressure and finally, the polymerization process was left to completion.

In 2001 Hoegger and Freitag [67] prepared macroporous polyacrylamide monolithic stationary phases for the CEC separation of a series of neutral aromatic compounds. The polymerization mixture consisted of *N,N*-dimethylacrylamide (DMAA), methacrylamide (MA), piperazinediacrylamide (PDA), and vinylsulfonic acid (VSA) in the presence of ammonium sulfate (AS) as porogen. Butyl acrylate or hexyl acrylate were added to the polymerization mixture for adjusting the hydrophobicty of the resulting stationary phase. The pore size of the synthesized monoliths was adjusted by adding varying amounts of ammonium sulfate (AS) to the reaction mixture. The authors observed that the retention mechanism for a series of neutral aromatic compounds is neither pure reversed-phase interaction nor pure normal-phase interaction, even when a high content of hydrophobic C_6 ligand was included in the preparation of the monolithic stationary phase. In 2003, the same authors [69] have prepared a similar monolith by copolymerization of piperazinediacrylamide (PDA), vinylsulfonic acid (VSA), and *N,N*-dimethylacrylamide (DMAA) for the separation of charged biomolecules by CEC using a mixed mode retention mechanism. Additionally, these authors investigated the influence of the concentration of ammonium sulfate (AS) in the polymerization mixture on the pore size of the resultant monoliths. They observed that an increase in the concentration of AS in the polymerization mixture leads to an increase in the mean pore diameter of the formed monolith. In a further study, the same authors [68] investigated the influence of various factors affecting the morphology and the chromatographic properties of hydrophilic polyacrylamide-based continuous beds polymerized form the water soluble co-monomers N,N-dimethylacrylamide (DMAA), piperazinediacrylamide (PDA), and vinylsulfonic acid (VSA). They observed that the mass fraction of crosslinker (%C), the type and the concentration of the pore forming agent, the type of solvent, and the type and molar fraction of the monomers in the polymerization mixture have a significant influence on the morphology and the chromatographic properties of the produced monolith. In a similar study, Ratautaite *et al*. [61] investigated the effect of buffer concentration and pH (buffer used as polymerization medium), and the total monomer concentration (%T) on the morphology and the chromatographic properties of amphiphilic polyacrylamide-based monoliths polymerized from the water soluble co-monomers methacrylamide (MA),

piperazinediacrylamide (PDA), N-isopropylacrylamide (IPA), and vinylsulfonic acid (VSA). The authors confirmed that the hydrodynamic permeability is dependent on the concentration of the buffer. There is an increase in the volume fraction of flow-through pores in the monolithic scaffold with increasing buffer concentration.

In 2002 Kornyšova *et al.* [81,82] demonstrated the one-step synthesis of an acrylamide-based continuous bed for CEC, which was prepared in the presence of native β-CD, sulphated β-CD, or 6-amino-β-CD. The authors concluded that a small fraction of cyclodextrin is trapped during the synthesis process via polyrotaxane formation. A rotaxane is a supramolecular unit in which a threaded cyclic molecule is irreversibly connected to a linear molecular unit simply by steric hindrance. Although there is no spectroscopic evidence for polyrotaxane formation, the authors have concluded the presence of immobilized CD in the formed continuous beds from two experimental observations: (i) The direction of electroosmotic flow is determined by the type of derivatized β-CD present in the polymerization mixture. (ii) The prepared continuous beds in the presence of β-CD could be employed for the enantioselective separation of metoprolol and ibuprofen enantiomers.

In 2004 Wahl et al. [70] were the first who used the principle of solubilization of hydrophobic monomers by complexation with water-soluble cyclodextrin (Section 1.3) in the synthesis of amphiphilic polyacrylamide-based monolithic stationary phases for CEC. These capillaries were synthesized by free radical copolymerization of N,N'-alkylenebisacrylamides (with different alkylene chain length) solubilized by the formation of an inclusion complex with statistically methylated β-CD (Me-β-CD), methacrylamide (MA), piperazinediacrylamide (PDA), and vinylsulfonic acid (VSA) in the presence of ammonium sulfate (AS) in the aqueous medium. Polymerization was achieved by using the redox initiator system peroxydisulfate-*N,N,N′,N′*-tetramethylethylendiamine and yielded monolithic stationary phases with embedded hydrophobic alkylene group unites. The authors observed a reversed-phase retention behaviour towards non-polar solutes (alkyl benzoates) and normal-phase retention behaviour towards polar analytes (phenols). In addition, the reversed-phase retention behaviour of the synthesized beds was confirmed from the direct proportionality between the retention factors of alkyl benzoates and the molar fraction of N,N-octamethylenebisacrylamide presents in the polymerization mixture.

In a different approach, Wahl et al. [71] have shown that the complex formation of the sterically adapted water-insoluble crosslinker N,N'-ethylenedianilinediacrylamide (DAA) with Me-β-CD and subsequent free radical copolymerization of the formed complex (pseudorotaxane) in aqueous solution is a viable route to synthesize polyacrylamide-based monolithic stationary phases for CEC with rotaxane-type

sterically immobilized derivatized β-CD. Amphiphilic mixed-mode monolithic stationary phases were synthesized by free radical copolymerization of the DAA-CD host-guest complex with N-isopropyl acrylamide (N-IPA), piperazinediacrylamide (PDA), and vinylsulfonic acid (VSA) in the presence of ammonium sulfate (AS) in aqueous medium. With help of ^{1}H-NMR chemical shift analysis, CD modified micellar EKC (CD-MEKC), 2D-NOESY spectroscopy, and solid state ^{13}C-NMR spectroscopy, the authors confirmed the formation of an inclusion complex between DAA and Me-β-CD in solution and the inclusion of the formed pseudorotaxane into the polymeric network. With this type of stationary phases, a reversed-phase retention behaviour was observed for the non-polar alkylphenones using an aqueous-organic mobile phase, while retention of the phenolic analytes with non-aqueous mobile phase corresponds to a normal-phase behaviour. With phenolic solutes eluted with an aqueous-organic mobile phase, it is observed that the elution order of solutes corresponds to the normal-phase mode, while the decrease in the retention factor with increasing the volume fraction of organic modifier corresponds to retention in the reversed-phase mode. This observation was explained by the authors with the presence of mixed-mode hydrophobic-hydrophilic interactions (combined reversed-phase-normal-phase retention behaviour).

1.6 References

[1] A. J. P. Martin, R. L. M. Synge, Biochem. J. 35 (1941) 1358.

[2] D. A. Skoog, F. J. Holler, S. R. Grouch, *Principles of Instrumental Analysis*, Thomson Higher Education, CA, USA, 2007.

[3] G. D. Christian, *Analytical Chemistry*, John Wiley and Sons, Inc., Hoboken, 2004.

[4] R. P. W. Scott., *Liquid Chromatography Column Theory*, John Wiley & Sons Ltd, West Sussex, England, 1992.

[5] J. H. Purnell, C. P. Quinn, *Gas Chromatography*, Butterworths London (1960) 184, 1960.

[6] M. J. E. Golay, *Gas Chromatography*, Butterworths, London, (1958) 36, 1958.

[7] A. Tiselius, Trans. Faraday Soc. 33 (1937) 524.

[8] S. Hjerten, Chromatogr. Rev. 9 (1967) 122.

[9] J. W. Jorgenson, K. D. Lukacs, Anal. Chem. 53 (1981) 1298.

[10] P.M. K. D. Bartle, *Capillary Electrochromatography*, The Royal Society of Chemistry, Cambridge, 2001.

[11] I. S. Krull, R. L. Stevenson, K. Mistry, M. E. Swartz, *Capillary electrochromatography and* pressurized *flow capillary electrochromatography*, HNB publishing, New Yourk, 2000.

[12] P. Atkins, J. De Paula, *Physical Chemistry*, 9th Edition, Oxford University Press, Oxford, UK, 2010.

[13] D. Corradini (Ed.), T. M. Phillips (consulting editor), *Handbook of HPLC*, 2th Edition, Taylor and Francis Group, LLC, Boca Raton, USA, 2011.

[14] H. H. Strain, J. Am. Chem. Soc. 61 (1939) 1292.

[15] D. L. Mould, R. L. M. Synge, Analyst. 77 (1952) 964.

[16] V. Pretorius, B. J. Hopkins, J.D. Schieke, J. Chromatogr. 99 (1974) 23.

[17] J. W. Jorgenson, K. Lukacs, J. Chromatogr. 218 (1981) 209.

[18] U. Tallarek, E. Rapp, T. Scheenen, E. Bayer, H. Van As, Anal. Chem. 72 (2000) 2292.

[19] E. Wen, R. Asiaie, C. Horvath, J. Chromatogr. A 855 (1999) 349.

[20] T. Jiang, J. Jiskra, H.A. Claessens, C. A. Cramers, J. Chromatogr. A 923 (2001) 215.

[21] N. W. Smith, M. B. Evans, Chromatographia 38 (1994) 649.

[22] J. H. Knox, I. H. Grant, Chromatographia 32 (1991) 317.

[23] H. Rebscher, U. Pyell, Chromatographia 38 (1994) 737.

[24] M. Verzele, C. Dewaele, HRC CC, J. High Resolut. Chromatogr. Chromatogr. Commun. 10 (1987) 280.

[25] A. Banholczer, U. Pyell, J. Microcolumn. Sep. 10 (1998) 321.

[26] E. R. Verheij, U.R. Tjaden, W.M.A. Niessen, Jan, van der Greef, J. Chromatogr. 554 (1991) 339.

[27] A. Apffel, H. Yin, W.S. Hancock, D. McManigill, J. Frenz, S.L. Wu, J. Chromatogr. A 832 (1999) 149.

[28] C. Gu, S. A. Shamsi, Electrophoresis 31 (2010) 1162.

[29] K. Pusecker, J. Schewitz, P. Gfroerer, L. H. Tseng, K. Albert, E. Bayer, Anal. Chem. 70 (1998) 3280.

[30] U. Pyell, J. Chromatogr. A 892 (2000) 257.

[31] A. Banholczer, U. Pyell, J. Chromatogr. A 869 (2000) 363.

[32] V. Del, Process Biochem. 39 (2004) 1033.

[33] T. Loftsson, P. Jarho, M. Masson, T. Jaervinen, Expert Opin. Drug Delivery 2 (2005) 335.

[34] L. Liu, Q.X. Guo, J. Inclusion Phenom. Macrocyclic Chem. 42 (2002) 1.

[35] G. Schmid, Trends Biotechnol. 7 (1989) 244.

[36] S. A. Nepogodiev, J. F. Stoddart, Chem. Rev. 98 (1998) 1959.

[37] J. Szejtli, Chem. Rev. 98 (1998) 1743.

[38] S. Bernhardt, P. Glockner, H. Ritter, Polym. Bull. 46 (2001) 153.

[39] P. Glockner, H. Ritter, Macromol. Rapid Commun. 20 (1999) 602.

[40] P. Casper, P. Gloeckner, H. Ritter, Macromolecules 33 (2000) 4361.

[41] J. Jeromin, H. Ritter, Macromol. Rapid Commun. 19 (1998) 377.

[42] J. Jeromin, O. Noll, H. Ritter, Macromol. Chem. Phys. 199 (1998) 2641.

[43] S. Schwarz-Barac, H. Ritter, J. Macromol. Sci. Pure Appl. Chem. A40 (2003) 437.

[44] H. Ritter, B.E. Mondrzik, M. Rehahn, M. Gallei, Beilstein J. Org. Chem. 6 (2010).

[45] C. Steffens, O. Kretschmann, H. Ritter, Macromol. Rapid Commun. 28 (2007) 623.

[46] S. Bernhardt, P. Gloeckner, A. Theis, H. Ritter, Macromolecules 34 (2001) 1647.

[47] H. Ritter, M. Tabatabai, Prog. Polym. Sci. 27 (2002) 1713.

[48] T. Tsuda, K. Nomura, G. Nakagawa, J. Chromatogr. 248 (1982) 241.

[49] G. J. M. Bruin, P. P. H. Tock, J. C. Kraak, H. Poppe, J. Chromatogr. 517 (1990) 557.

[50] J. J. Pesek, M. T. Matyska, S. Cho, J. Chromatogr. A 845 (1999) 237.

[51] A. Malik, Electrophoresis 23 (2002) 3973.

[52] S. Hjerten, J.L. Liao, R. Zhang, J. Chromatogr. 473 (1989) 273.

[53] T. B. Tennikova, B.G. Belenkii, F. Svec, J. Liq. Chromatogr. 13 (1990) 63.

[54] F. Svec, J.M.J. Frechet, Anal. Chem. 64 (1992) 820.

[55] G. Guiochon, J. Chromatogr. A 1168 (2007) 101.

[56] H. Minakuchi, K. Nakanishi, N. Soga, N. Ishizuka, N. Tanaka, Anal. Chem. 68 (1996) 3498.

[57] P. G. Wang (Ed.), *Monolithic Chromatography and its Modern Applications*, ILM Publications, 2010.

[58] F. Svec, J. Chromatogr. A 1217 (2010) 902.

[59] F. Svec, J. M. J. Frechet, Chem. Mater. 7 (1995) 707.

[60] S. Xie, F. Svec, J. M. J. Frechet, J. Polym. Sci. Part A: Polym. Chem. 35 (1997) 1013.

[61] V. Ratautaite, A. Maruska, M. Erickson, O. Kornysova, J. Sep. Sci. 32 (2009) 2582.

[62] S. Eeltink, J. M. Herrero-Martinez, G. P. Rozing, P. J. Schoenmakers, W. T. Kok, Anal. Chem. 77 (2005) 7342.

[63] O. Kornysova, A. Maruska, P.K. Owens, M. Erickson, J. Chromatogr. A 1071 (2005) 171.

[64] A. A. Al-Massaedh, U. Pyell, J. Chromatogr. A 1286 (2013) 183.

[65] A. A. Al-Massaedh, U. Pyell, J. Chromatogr. A 1325 (2014) 247.

[66] A. A. Al-Massaedh, U. Pyell, J. Chromatogr. A 1325 (2014) 186.

[67] D. Hoegger, R. Freitag, J. Chromatogr. A 914 (2001) 211.

[68] D. Hoegger, R. Freitag, Electrophoresis 24 (2003) 2958.

[69] D. Hoegger, R. Freitag, J. Chromatogr. A 1004 (2003) 195.

[70] A. Wahl, I. Schnell, U. Pyell, J. Chromatogr. A 1044 (2004) 211.

[71] A. Wahl, F. Al-Rimawi, I. Schnell, O. Kornysova, A. Maruska, U. Pyell, J. Sep. Sci. 31 (2008) 1519.

[72] Y. Baba, M. Tsuhako, Trends Anal. Chem. 11 (1992) 280.

[73] C. Fujimoto, J. Kino, H. Sawada, J. Chromatogr. A 716 (1995) 107.

[74] J. L. Liao, N. Chen, C. Ericson, S. Hjerten, Anal. Chem. 68 (1996) 3468.

[75] J. L. Liao, Y. M. Li, S. Hjerten, Anal. Biochem. 234 (1996) 27.

[76] C. Ericson, J. L. Liao, K. Nakazato, S. Hjerten, J. Chromatogr. A 767 (1997) 33.

[77] C. Fujimoto, Y. Fujise, E. Matsuzawa, Anal. Chem. 68 (1996) 2753.

[78] A. Palm, M. V. Novotny, Anal. Chem. 69 (1997) 4499.

[79] M. Zhang, Z. El Rassi, Electrophoresis 22 (2001) 2593.

[80] C. Ericson, S. Hjerten, Anal. Chem. 71 (1999) 1621.

[81] O. Kornysova, E. Machtejevas, V. Kudirkaite, U. Pyell, A. Maruska, J. Biochem. Biophys. Methods 50 (2002) 217.

[82] O. Kornysova, R. Surna, V. Snitka, U. Pyell, A. Maruska, J. Chromatogr. A 971 (2002) 225.

2. Objectives

It is investigated whether solubilization of the hydrophobic monomer N-(1-adamantyl)acrylamide via 1:1 complex formation with statistically methylated β-cyclodextrin can be used as a synthetic route to highly crosslinked macroporous amphiphilic adamantyl-group containing amphiphilic acrylamide-based monolithic stationary phases. The impact of the concentration of the lyotropic salt ammonium sulfate in the polymerization mixture is studied by synthesizing a series of macroporous adamantyl-group containing amphiphilic acrylamide-based monolithic stationary phases under variation of the concentration of ammonium sulfate in the polymerization mixture. These monoliths are to be characterized by scanning electron microscopy (SEM) and inverse size exclusion chromatography (ISEC) to study the impact of this varied synthesis parameter on the morphology, homogeneity, pore size distribution, and fractional volumes of mesopores and macropores of the synthesized monoliths.

The chromatographic efficiency of a series of N-adamantyl-group containing amphiphilic acrylamide-based monolithic stationary phases synthesized under variation of several synthetic parameters which can be regarded to be decisive for the morphology (and chromatographic efficiency) of the formed monolith will be investigated. These parameters are (i) concentration of ammonium sulfate in the polymerization mixture, (ii) concentration of the charge-bearing monomer vinylsulfonic acid, and (iii) concentration of the initiator ammonium persulfate in the polymerization mixture. With the monolithic capillary synthesized with optimized synthesis parameters, we aimed to investigate the impact of the type of retention mode (influenced by the type of analyte and the mobile phase composition) and the impact of the analyte functionality on the chromatographic efficiency and peak symmetry using different types of solutes with varied hydrophobicity.

3. Summary

The present work reports the synthesis, characterization, and optimization of the chromatographic efficiency of a highly crosslinked amphiphilic macroporous N-adamantyl-group containing mixed-mode acrylamide-based continuous bed synthesized for capillary electrochromatography (CEC) employing solubilization of the hydrophobic monomer by complexation with statistically methylated β-CD. The work includes the investigation of the chromatographic efficiency of the synthesized monoliths dependent on the retention mode and analyte functionality.

In the first part of the thesis a new synthesis procedure for amphiphilic macroporous N-adamantyl-group containing mixed-mode acrylamide-based continuous beds for capillary electrochromatography (CEC) is investigated employing solubilization of the hydrophobic monomer via 1:1 complex formation with Me-β-CD. For this purpose, N-(1-adamantyl)acrylamide was synthesized and characterized as a hydrophobic monomer forming a water soluble-inclusion complex with statistically Me-β-CD. Mixed-mode monolithic stationary phases were synthesized by *in situ* free radical copolymerization of cyclodextrin-solubilized N-adamantyl acrylamide, methacrylamide (MA), piperazinediacrylamide (PDA), and vinylsulfonic acid (VSA) in aqueous medium. Due to the amphiphilic nature of the synthesized capillaries, separations in the reversed-phase, in the normal-phase, and in a mixed-retention mode (depending on the composition of the mobile phase) are achieved for polar and non-polar neutral analytes. The stoichiometry, the complex formation constant, and the spatial arrangement of the formed inclusion complex are determined by CD modified capillary electrochromatography (CD-CEC), CD modified micellar EKC (CD-MEKC), and the application of ^{1}H NMR and 2D-^{1}H NOESY spectroscopy. The influence of the total monomer concentration (%T) on the chromatographic properties of the synthesized monoliths is also investigated.

In the second part of the thesis the morphology and the pore size distribution of a series of amphiphilic macroporous N-adamantyl-group containing mixed-mode acrylamide-based continuous beds synthesized under variation of the concentration of the lyotropic salt ammonium sulfate (AS) in the polymerization mixture are investigated by scanning electron microscopy (SEM) and inverse size exclusion chromatography (ISEC). The impact of the concentration of the lyotropic salt AS in the polymerization mixture on the formed morphology and pore size distribution is determined. SEM photographs demonstrate the homogeneity and uniformity of the formed monolith over the length of the capillary and the covalent attachment of the formed polymer to the confining wall. Additionally, SEM

photographs demonstrate a clear increase in the domain size (average size of globules + average flow through pore diameter) with increasing concentration of AS in the polymerization mixture. The pore size distribution determined with ISEC using the retention data of a series of polystyrene standards reveals the presence of two different types of pores for the synthesized capillaries: (i) pores located inside the microglobules (internal pores) and (ii) pores which are located between the microglobules (external pores). The presence of a trimodal pore size distribution is confirmed by ISEC for those monoliths which are synthesized with lower concentration of AS in the polymerization mixture, and a bimodal pore size distribution for those synthesized with higher content of AS in the polymerization mixture.

In the third part of the thesis, efficiency data are gained for a series of amphiphilic macroporous N-adamantyl-group containing mixed-mode acrylamide-based continuous beds synthesized under variation of different synthesis parameters. The studied synthesis parameters are (i) concentration of ammonium sulfate, (ii) concentration of the initiator ammonium persulfate, and (iii) concentration of the negatively charged monomer vinylsulfonic acid (VSA) in the polymerization mixture. The optimization of different synthesis parameters with regard to the chromatographic efficiency under isocratic conditions for alkylphenones in the reversed-phase mode is studied employing CEC. The major conclusion was that with varied concentration of AS or varied concentration of ammonium persulfate in the polymerization mixture, a strong impact on the chromatographic efficiency is observed, while there is only a minor influence when varying the molar fraction of VSA. In addition, the absence of a significant influence by heating (Joule heating) and via extra-column band broadening effects on the determined efficiency is confirmed.

In the fourth part of the thesis we studied with different classes of neutral analytes (with varied hydrophobicity) the impact of the type of retention mode (influenced by the type of analyte and the mobile phase composition) and the impact of the analyte functionality on the chromatographic efficiency and peak symmetry with a monolith synthesized with optimized parameters. With this monolithic capillary, high separation efficiencies (up to ca. 220,000 m^{-1}) were obtained for separations of different analyte classes (alkylphenones, nitrotoluenes, and phenolic compounds with $k = 0.2\text{-}0.55$) in the reversed-phase mode, in the normal-phase mode, and in mixed retention-mode. For neutral alkylanilines ($k < 0.25$) separated in the reversed-phase elution mode, high plate numbers exceeding 300,000 m^{-1} were routinely obtained. For phenolic analytes, it is shown that analyte functionality and mobile phase composition have a strong influence on peak symmetry and chromatographic efficiency.

4. Zusammenfassung

Berichtet wird in vorliegender Arbeit die Synthese, Charakterisierung und Optimierung der chromatographischen Effizienz eines hoch-quervernetzten mixed-mode Acrylamid-basierten makroporösen N-Adamantyl-Gruppen-haltigen Monolithen, der speziell für die Kapillar-Elektrochromatographie (CEC) unter Solubilisierung des hydrophoben Monomers durch Komplexierung mit statistisch methyliertem β-CD synthetisiert worden war. Eingeschlossen ist die Untersuchung der chromatographischen Effizienz abhängig vom Retentionsmodus und der Funktionalität des Analyten.

Im ersten Teil der Arbeitwird ein neues Synthese-Verfahren für amphiphile makroporöse N-Adamantyl-Gruppen-haltige mixed-mode Acrylamid-basierte Monolithe für die Kapillar-Elektrochromatographie (CEC) entwickelt und untersucht. Dieses Verfahren nutzt die Solubilisierung des hydrophoben Monomers über 1:1-Komplexierung mit Me-β-CD. N-(1-Adamantyl)acrylamidwurde synthetisiert und als hydrophobes Monomer hinsichtlich seines Komplexbildungsverhaltens (Bildung wasserlöslicher Einschlusskomplexe) mit statistisch methyliertemMe-β-CD untersucht. Gemischtmodige monolithische stationäre Phasen wurden durch *in situ*freieradikalische Co-Polymerisation von Cyclodextrin-solubilisiertemN-Adamantylacrylamid, Methacrylamid (MA), Piperazindiacrylamid (PDA), andVinylsulfonsäure (VSA) in wässrigemMedium hergestellt. Aufgrund des amphiphilen Charakters der hergestellten Kapillar-Säulen sind für Analyte unterschiedlicher Polarität Trennungen im Umkehrphasen-Modus, im Normalphasen-Modus und in einem gemischten Retentions-Modus möglich, abhängig von der Zusammensetzung der mobilen Phase. Die Stöchiometrie, die Komplexbildungskonstante und die räumliche Anordnung im gebildeten Einschlusskomplex werden durch CD-modifizierte Kapillar-Elektrochromatographie (CD-CEC), CD-modifizierte mizellareEKC (CD-MEKC) und die Anwendung von ^{1}H-NMR-und 2D-^{1}H-NOESY-Spektroskopie bestimmt. Ebenfalls untersucht wird der Einfluss der Gesamt-Monomerkonzentration(%T) auf die chromatographischenEigenschaften des synthetisierten Monolithen.

Im zweiten Teil der Arbeit wird die Morphologie und die Porengrößenverteilung einer Reihe von amphiphilen makroporösen N-Adamantyl-Gruppen-haltigen gemischtmodigen Acrylamid-basierten Monolithen(synthetisiert unter Variation der Konzentration des lyotropen Salzes Ammoniumsulfat (AS)) mittels Rasterelektronenmikroskopie (REM) und inverser Größenausschlusschromatographie (ISEC) untersucht. Bestimmt wird ebenfalls der Einfluss der Konzentration des lyotropen Salzes AP in der Polymerisationsmischung auf die gebildete Morphologie und Porengrößenverteilung. REM-Aufnahmen

zeigen die Homogenität und Einheitlichkeit des gebildeten Monolithen über die gesamte Länge derKapillare und die kovalente Anbindung des gebildeten Polymers an die begrenzende Wand. Zusätzlich weisen die REM-Aufnahmen eindeutig eine Abhängigkeit der Domänengröße (mittlerer Durchmesser der Globuli + mittlerer Durchmesser der Durchfluss-Poren) von der Konzentration des Salzes AS in der Polymerisationsmischung nach (Zunahme der Domänengröße mit erhöhter Konzentration des Salzes). Die Bestimmung der Porengrößenverteilung mittels ISEC zeigt das Vorhandensein zweier unterschiedlicher Porenklassen: (i) Poren innerhalb der Globuli (interne Poren) und (ii) Poren zwischen den Globuli (externe Poren). Das Auftreten einer trimodalen Porengrößenverteilung wird durch ISEC für diejenigen Monolithe bestätigt, die mit niedriger Konzentration AS hergestellt worden waren, während eine bimodale Porengrößenverteilung für diejenigen Monolithe ermittelt wird, die mit höherem Gehalt an AS in der Polymerisationsmischung synthetisiert worden waren.

Im dritten Teil der Arbeitwerden Effizienz-Daten für eine Reihe von amphiphilen makroporösen N-Adamantyl-Gruppen-haltigen gemischtmodigen Acrylamid-basierten Monolithenbestimmt, die unter Variation unterschiedlicher Synthese-Parameter hergestellt worden waren. Die untersuchten Synthese-Parameter sind (i) Konzentation von Ammoniumsulfat, (ii) Konzentration des Starters Ammonium-peroxodisulfat und (iii) Konzentration des Monomers Vinylsulfonsäure (VSA) in der Polymerisations-mischung. Die Optimierung der unterschiedlichen Syntheseparameter erfolgt durch Ermittlung der chro-matographischen Effizienz für Alkylphenoneunter isokratischen Bedingungen im Umkehrphasenmodus unter Verwendung der CEC. Während mit variiertem Gehalt an AS oder variierter Konzentration von Ammoniumperoxodisulfat ein erheblicher Einfluss auf die chromatographische Effizienz beobachtet wird, gibt es nur einen geringfügigen Einfluss bei Änderung des Stoffmengenanteils VSA. Zusätzlich wird bestätigt, dass Temperaturerhöhung durch elektrischen Leistungseintrag (Joule heating) und Bandenverbreiterung außerhalb der Säule vernachlässigt werden können.

Im vierten Teil der Arbeit werden mit einem Monolithen, der mit optimierten Syntheseparametern her-gestellt worden war, der Einfluss des Retentions-Modus (abhängig vomAnalyten und der Zusammen-setzung der mobilen Phase) und der Einfluss der funktionellen Gruppe des Analytenauf die chromato-graphische Effizienz und Peak-Symmetrie mit unterschiedlichen Klassenneutraler Analyte variierter Hydrophobizitätuntersucht. Sehr hohe Effizienzen (bis zu 220.000 m^{-1}) werden im Umkehrphasen-Modus, im Normalphasen-Modus und im gemischten Retentions-Modus für unterschiedliche Analyt-Klassen erzielt (Alkylphenone, Nitrotoluole und phenolischeVerbindungenmitk = 0,2-0,55). Für neutraleAlkylaniline ($k < 0.25$), getrennt im Umkehrphasen-Modus, werden unter Routinebedingungen

Bodenzahlen höher 300.000 m^{-1} erreicht. Für phenolische Verbindungen wird gezeigt, dass die funktionelle Gruppe des Analyten und die Zusammensetzung der mobilen Phase maßgeblichen Einfluss auf Peak-Symmetrie und chromatographische Effizienz ausüben.

5. Cumulative Part (Publications)

5.1. Publication I

Adamantyl-group containing mixed-mode acrylamide-based continuous beds for capillary electrochromatography. Part I: Study of a synthesis procedure including solubilization of N-adamantyl-acrylamide via complex formation with a water-soluble cyclodextrin

"Ayat Allah" Al-Massaedh, Ute Pyell

Journal of Chromatography A, 1286 (2013) 183–191

doi: 10.1016/j.chroma.2013.02.046

5.1.1. Summary and discussion

In this publication, a new synthesis procedure for amphiphilic macroporous N-adamantyl-group containing mixed-mode acrylamide-based continuous beds for capillary electrochromatography (CEC) is investigated employing solubilization of the hydrophobic monomer by complexation with a water soluble cyclodextrin. For this purpose, N-(1-adamantyl)acrylamide was synthesized and characterized as a hydrophobic monomer forming a water soluble-inclusion complex with a water soluble cyclodextrin. To this end, its solublization in aqueous solution was studied with different types of derivatized and non-derivatized cyclodextrins as potential complex forming agents. Statistically methylated-β-CD was found to solubilize N-(1-adamantyl)acrylamide with 1:1 molar ratio, and therefore, it is selected for the synthesis procedure. The stoichiometry, the complex formation constant, and the spatial arrangement of the formed inclusion complex (N-(1-adamantyl)acrylamide/Me-β-CD) are determined by CD modified capillary electrochromatography (CD-CEC), CD modified micellar electrokinetic chromatography (CD-MEKC), and the application of ^{1}H NMR and 2D-^{1}H NOESY spectroscopy. The results obtained show that Me-β-CD forms a strong inclusion complex with N-(1-adamantyl)acrylamide. Consequently, a very high value of the formation constant of the formed complex was determined (5896 $\pm$ 247). This reflects the good size matching between the size of the adamantyl group and the cavity of Me-β-CD. Mixed-mode monolithic stationary phases were synthesized by *in situ* free radical copolymerization of cyclodextrin-solubilized N-adamantyl acrylamide, methacrylamide (MA), piperazinediacrylamide (PDA), and vinylsulfonic acid (VSA) in aqueous medium in bind silane-pretreated fused silica capillaries.

The influence of the total monomer concentration (%T) on the chromatographic properties, electroosmotic mobility, and on specific permeability is investigated. The results obtained show that increasing %T in the polymerization mixture results in an increase in the phase ratio of the resultant monolith (V(stationary phase)/V(mobile phase)), which in turn leads to an increase in the retention factors of the analytes. Additionally, it is observed that increasing %T in the polymerization mixture leads to a decrease in the specific permeability, the electroosmotic mobility μ_{eo}, and the mean diameter of flow through pores of the formed monolith. With a homologues series of alkylphenones with different alkyl chain length it is confirmed that retention factors increase with increasing mass fraction of N-(1-adamantyl) acrylamide in the polymerization mixture. This confirms that the solubilised adamantyl group takes part in the polymerization mixture and that the composition of the formed polymeric monolith reflects the composition of the polymerization mixture.

The synthesized monolithic stationary phases have both hydrophilic and hydrophobic character (amphiphilic). Therefore, (depending on the composition of the mobile phase) they can be used to separate analytes in the reversed- and in the normal-phase mode, which was confirmed with polar and non-polar analytes. Observations made with polar analytes and polar mobile phase are explained by a mixed-mode retention mechanism (hydrophobic, hydrophilic, and ion exchange interactions). With this elution mode, it is observed that the elution order of solutes corresponds to the normal-phase mode, while the decrease in the retention factor with increasing the volume fraction of organic modifier corresponds to retention according to the reversed-phase mode.

5.1.2. Author contribution

The experimental part of this publication was carried out by me. For SEM photographs Mr. M. Hellwig (Electron Microscopy and Microanalysis Laboratory, University of Marburg, Marburg, Germany) provided the technical assistance needed in this regard. The draft of the manuscript was written by me and corrected by Prof. Dr. Ute Pyell. The final revision of the manuscript was conducted by me and Prof. Pyell before submission to the journal. Prof. Dr. Ute Pyell was responsible for the supervision of this work.

Journal of Chromatography A, 1286 (2013) 183–191

Contents lists available at SciVerse ScienceDirect

Journal of Chromatography A

journal homepage: www.elsevier.com/locate/chroma

Adamantyl-group containing mixed-mode acrylamide-based continuous beds for capillary electrochromatography. Part I: Study of a synthesis procedure including solubilization of N-adamantyl-acrylamide via complex formation with a water-soluble cyclodextrin

Ayat Allah Al-Massaedh, Ute Pyell*

University of Marburg, Department of Chemistry, Hans-Meerwein-Straße, D-35032 Marburg, Germany

ARTICLE INFO

Article history:
Received 14 November 2012
Received in revised form 12 February 2013
Accepted 15 February 2013
Available online 21 February 2013

Keywords:
Capillary electrochromatography
Monolithic stationary phase
Continuous bed
Cyclodextrin
Mixed-mode retention

ABSTRACT

A new synthesis procedure for highly crosslinked macroporous amphiphilic N-adamantyl-functionalized mixed-mode acrylamide-based monolithic stationary phases for capillary electrochromatography (CEC) is investigated employing solubilization of the hydrophobic monomer by complexation with a cyclodextrin. N-(1-adamantyl)acrylamide is synthesized and characterized as a hydrophobic monomer forming a water soluble-inclusion complex with statistically methylated-β-cyclodextrin. The stoichiometry, the complex formation constant and the spatial arrangement of the formed complex are determined. Mixed-mode monolithic stationary phases are synthesized by *in situ* free radical copolymerization of cyclodextrin-solubilized N-adamantyl acrylamide, a water soluble crosslinker (piperazinediacrylamide), a hydrophilic monomer (methacrylamide), and a negatively charged monomer (vinylsulfonic acid) in aqueous medium in bind silane-pretreated fused silica capillaries. The synthesized monolithic stationary phases are amphiphilic and can be employed in the reversed- and in the normal-phase mode (depending on the composition of the mobile phase), which is demonstrated with polar and non-polar analytes. Observations made with polar analytes and polar mobile phase can only be explained by a mixed-mode retention mechanism. The influence of the total monomer concentration (%*T*) on the chromatographic properties, the electroosmotic mobility, and on the specific permeability is investigated. With a homologues series of alkylphenones it is confirmed that the hydrophobicity (methylene selectivity) of the stationary phase increases with increasing mass fraction of N-(1-adamantyl)acrylamide in the synthesis mixture.

1. Introduction

Capillary electrochromatography (CEC) is a capillary electromigration separation method in which a high electric field is applied in a capillary containing a stationary phase (often an organic monolith) and a liquid mobile phase. Several organic polymer-based monoliths have been successfully used in CEC [1–8]. They are an attractive alternative to capillaries packed with particulate material because of the availability of a wide variety of suitable monomers, ease of their *in situ* preparation by single-step copolymerization, good reproducibility of the synthesis procedure, chemical stability within a broad pH range, and the possibility to fine-tune the selectivity of the separation system as well as the direction and velocity of the EOF [1,2]. Typically, organic polymer-based monoliths are prepared by *in situ* free radical copolymerization of a mixture of monomers dissolved in a porogenic solvent in the presence of an initiator (system) inside the capillary. The pore structure and pore size distribution of the resulting monolith result from phase separation of the growing solid polymer from the porogenic solvent during the polymerization process.

The use of purely aqueous polymerization systems for the preparation of monolithic stationary phases has a limitation regarding the incorporation of hydrophobic monomers into the polymerization mixture which is required for achieving the necessary hydrophobicity for reversed-phase CEC. One solution of this problem is sonication of the polymerization mixture containing a hydrophobic monomer [9,10]. Another solution is polymerization in the presence of an organic solvent [11–13]. An alternative to the use of an organic solvent is the solubilization of the hydrophobic monomer in aqueous medium by host–guest complexation using

* Corresponding author. Tel.: +49 6421 2822192; fax: +49 6421 2822124.
E-mail address: pyellu@staff.uni-marburg.de (U. Pyell).

0021-9673/$ – see front matter © 2013 Elsevier B.V. All rights reserved.
http://dx.doi.org/10.1016/j.chroma.2013.02.046

a cyclodextrin (CD) [1,3,14–16]. The principle of solubilization of hydrophobic monomers by complex formation with a water-soluble CD and subsequent reaction of the formed host–guest complex by free radical copolymerization in aqueous solution has been introduced into polymer chemistry by Ritter and co-workers [17,18].

Following types of organic monoliths have been synthesized and investigated as continuous beds for CEC: polymethacrylate-based monoliths [1,2,8,19], polystyrene-based monoliths [20,21], and polyacrylamide-based monoliths [5–7,22–24]. This list is not exhaustive. The first continuous phase based on co-polymerized acrylamides was introduced by Hjerten et al. in 1989 [25], who prepared compressed continuous polyacrylamide gels as cation-exchangers for the separation of proteins. In 1996, the same group developed polyacrylamide-based micro-columns for the RP-HPLC analysis of standard proteins and peptides [22].

According to the best of our knowledge the preparation of macroporous acrylamide-based continuous beds by co-polymerization of N-adamantyl-acrylamide with other acrylamides in aqueous solution has not been reported so far. Ohyama et al. [8] reported the synthesis of a different type of adamantyl-functionalized macroporous polymeric monolith for CEC. They employed the thermally initiated free-radical co-polymerization of 1-adamantyl-(α-trifluoromethyl)acrylate with ethylene dimethacrylate and 2-acrylamido-2-methyl-1-propanesulfonic acid with the main idea that the bulky adamantyl group will improve the peak symmetry for basic solutes by shielding the negatively charged sulfonic acid groups.

In our current study, amphiphilic macroporous N-adamantyl-functionalized mixed-mode acrylamide monolithic stationary phases were synthesized for capillary electrochromatography employing solubilization of the hydrophobic monomer by host–guest complexation with water-soluble statistically methylated-β-cyclodextrin. Stoichiometry, complex formation constant and spatial arrangement of the formed complex were studied by a combination of electrophoretic, chromatographic and NMR-spectroscopic methods. We have selected N-adamantyl-acrylamide as hydrophobic monomer, because the adamantyl group is known to form very stable inclusion complexes with β-CDs [26].

Free radical copolymerization of the water-soluble N-adamantyl–acrylamide–CD complex was performed in aqueous solution in the presence of the hydrophilic crosslinker piperazinediacrylamide, the charged monomer vinylsulfonic acid, the hydrophilic monomer methacryamide and the lyotropic salt ammonium sulfate. Different monoliths were prepared and tested under variation of the content of the hydrophobic monomer in the polymerization mixture and/or the total monomer concentration. The chromatographic properties of the resulting monoliths regarding polar and nonpolar solutes were investigated by employing CEC with aqueous and nonaqueous mobile phase.

2. Experimental

2.1. Chemicals and instruments

All chemicals were used without further purification. N,N,N′,N′-tetramethylethylendiamine (TEMED), 3-(trimethoxysilyl) propyl methacrylate (bind silane), di-sodium hydrogenphosphate dihydrate, N,N-dimethylformamide (DMF), ammonium sulfate (AS), sodium dodecyl sulfate (SDS), quinine hydrochloride dihydrate and hydrochloric acid (37%, v/v) were from Fluka (Buchs, Switzerland). Hydroxypropyl-β-CD, vinyl sulfonic acid (VSA, 25%, w/v in aqueous solution), N-isopropylacrylamide and alkylphenones were from Sigma–Aldrich (Steinheim, Germany). Methacrylamide

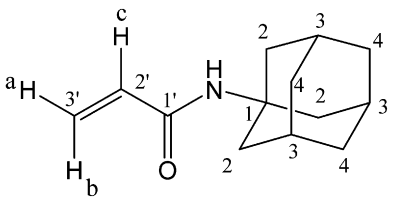

Fig. 1. Proton assignment N-(1-adamantyl)acrylamide.

(MA), ammonium peroxodisulfate (APS), acetic acid (AA), α-CD, acryloyl chloride, sodium dihydrogen phosphate monohydrate, 3-methoxybenzaldehyde, 3-methoxy-4-hydroxybenzaldehyde, 4-hydroxybenzaldehyde, 3,4-dihydroxybenzaldehyde and triethylamine (TEA) were from Merck (Darmstadt, Germany). Deuterated chloroform-d_1, deuterated water, and deuterated methanol-d_4 were from Deutero (Kastellaun, Germany). Thiourea and acetophenone were from Riedel-de Haen (Seelze, Germany). 1,4-Bis(acryloyl)piperazine (piperazinediacrylamide, PDA) was either from Alfa-Aesar (Karlsruhe, Germany) or from Molekula (Dorset, UK). Statistically methylated β-CD (Me-β-CD) was either from ABCR (Karlsruhe, Germany) or from Sigma–Aldrich (Steinheim, Germany). 2-Hydroxypropyl-γ-CD (2-HP-γ-CD) was either from Fluka (Buchs, Switzerland) or from Sigma–Aldrich (Steinheim, Germany). Dimethyl-β-CD was from Beckman Instruments (Fullerton, USA). 1-Adamantylamine was either from Alfa-Aesar (Karlsruhe, Germany) or from ICN Biochemicals (Cleveland, USA). Fused silica capillaries (100 μm I.D. × 360 μm O.D.) were from Polymicro Technologies (Phoenix, USA).

With all mobile phases the specific electric conductivity and the pH* value were controlled. The pH* value is the pH in the presence of organic solvent with a pH meter calibrated with aqueous buffer. The pH* was determined with the mobile phase after addition of the organic solvent to the aqueous buffer. The pH meter Inolan pH 720 (WTW instruments, Weinheim, Germany), and the conductometer LF 191 (WTW, Weinheim, Germany) were used to measure the pH* and the electric conductivity of the prepared mobile phases. Mobile phases were prepared by buffering 100 mL distilled water with 2–3 mL of a mixture of 0.2 mol L^{-1} TEA with 0.2 mol L^{-1} AA (1:1, v/v). Subsequently, the required volume of this solution is taken and mixed with the corresponding volume of organic solvent. The pH* and the electric conductivity of the final mixture were adjusted with 0.20 mol L^{-1} TEA or AA.

^{1}H NMR, ^{13}C NMR, and 2D-^{1}H NOESY measurements were carried out on an ARX300 or an ARX500 spectrometer, respectively (Bruker, Karlsruhe, Germany).

2.2. Synthesis and characterization of N-(1-adamantyl)acrylamide

N-(1-adamantyl)acrylamide (Fig. 1) was synthesized according to [27]. The amount of 0.15 mol acryloyl chloride was dissolved in dried toluene, to which 0.20 mol potassium carbonate was added at 0 °C. 0.078 mol of 1-adamantylamine dissolved in 150 mL dried toluene was added dropwise. The mixture was stirred for 2.5 h at 0 °C. After completion of the reaction 400 mL of distilled water was added. The precipitate was filtered off, rinsed successively with 100 mL hydrochloric acid solution (0.1 M), 100 mL sodium hydroxide solution (0.1 M), and distilled water and finally dried *in vacuo*. The crude product was purified by recrystallization in water/methanol (50/50, v/v). The organic layer which remains after filtration of the precipitate was separated from the aqueous phase. The organic solvent was gently evaporated under reduced pressure. The produced solid material was purified in the same way as the filtrated precipitate. A white crystalline powder (yield about

72%) was obtained. Characterization was done using ^{1}H NMR, ^{13}C NMR, determination of the melting point, and elemental analysis.

^{1}H NMR (300 MHz, $CDCl_3$): δ = 5.49 (dd, $^{3}J_{cis,vic}$ = 10.1 Hz, $^{2}J_{gem}$ = 1.6 Hz, 1H, H_a), 6.15 (dd, $^{3}J_{trans,vic}$ = 16.9 Hz, $^{2}J_{gem}$ = 1.6 Hz, 1H, H_b), 5.94 (dd, $^{3}J_{trans,vic}$ = 16.9 Hz, $^{3}J_{cis,vic}$ = 10.1 Hz, 1H, H_c), 5.17 (bs, 1H, NH), 2.02–1.95 (m, 9H, H-2,3), 1.68 (bs, 6H, H-4). – ^{13}C NMR (300 MHz, $CDCl_3$): (= 164.7 (CO-1′), 132.9 (CH_2-3′), 125.9 (CH-2′), 52.1 (C_q-1), 41.3, (CH_2-2), 36.2 (CH_2-4), 29.4 (CH-3). Anal calcd (average of two measurements) for $C_{18}H_{19}NO$: N, 6.83; C, 76.1; H, 9.2. Found: N, 6.73; C, 75.52; H, 9.34. Melting point: 150–152 °C. s: singlet, bs: broad singlet, dd: doublet of doublet, and q: quartet.

2.3. Synthesis of stationary phases

In order to ensure the covalent attachment of the monolith to the inner capillary wall, the fused silica capillaries were first pretreated with 3-(trimethoxysilyl) propylmethacrylate (bind silane) in order to introduce vinylic anchoring groups on the inner wall of the fused silica capillary. Capillaries were pre-treated using the method described by Hjerten [28]. The capillaries were first flushed for in each case 15 min with acetone, hydrochloric acid solution (0.1 M), sodium hydroxide solution (0.1 M), water, and finally with acetone. They are subsequently rinsed for 30 min with a 30% (v/v) solution of 3-(trimethoxysilyl) propylmethacrylate (bind silane) in acetone and left overnight filled with this solution. Finally, the capillaries are washed out with acetone and water for each 15 min.

For polymerization reaction, the hydrophobic monomer N-(1-adamantyl)acrylamide was solubilized in aqueous phosphate buffer (100 mM, pH 7.0) with Me-β-CD. After solubilization, methacrylamide (MA), piperazinediacrylamide (PDA), vinylsulfonic acid 25% (w/v) (VSA) solution, and ammonium sulfate (AS) were added successively to the solution. Filling the capillary with the polymerization mixture was done with an in-house manufactured capillary-filling apparatus. At the beginning the polymerization mixture was degassed for 10–15 min using a membrane vacuum pump. Then the apparatus is refilled with argon. After that 10 μL of 10% (w/v) ammonium persulfate (APS) and 10 μL of 10% (v/v) N,N,N′,N′-tetramethylethylendiamine (TEMED) solution were added and the solution was mixed using a spatula for 3–5 s. Subsequently, the capillary was dipped into the reaction mixture, and with help of an argon overpressure (ca. 1–2 bar) the reaction mixture was passed into the capillary. This process was continued until the first drop of the polymerization mixture became visible at the opposite end of the capillary. Both ends of the capillary were then sealed with silicone grease and the polymerization process was allowed to proceed overnight at room temperature. Afterwards, the resulting monolith was rinsed with distilled water for about 2–3 h with the help of an HPLC pump (50–100 bar) and a flow splitter. The detection window was created in the capillary during the rinsing process by burning off 1–2 mm of the outer polyimide coating and pyrolyzing and removing the monolith inside by a stream of water. Before installing the capillary in the CEC instrument, a few mm (ca. 10 mm) of the outer polyimide coating were removed at the inlet end of the monolithic capillary using a sharp blade. Finally, the capillary was installed in the CEC apparatus and rinsed and equilibrated with mobile phase.

2.4. Chromatographic system

The CEC apparatus was already described in [16] and consists of a FUG HCN 35-35000 high voltage generator (F.U.G. Elektronic GmbH, Rosenheim, Germany) with an in-house manufactured electronic steering unit for controlled electrokinetic injection, a spectra 100 UV-VIS detector (Thermo Separation Product, San Jose, CA, USA) with detection cell for in-capillary detection, and a Shimadzu (Kyoto, Japan) LC-10 AD HPLC pump for conditioning and equilibrating the monolithic capillary with new mobile phase using 50–100 bar. Data treatment and recording was done with EZ-Chrom 6.6 (Scientific Software, San Roman. CA, USA). For the CEC experiments, sample solutions (250–300 mg L^{-1}) were prepared in the mobile phase. Sample injection was performed electrokinetically (6 kV for 6 s). UV detection was at a wavelength of 230 nm (214 nm for CD-modified-CEC experiment). DMF was used as non-retained EOF marker.

MEKC experiments were carried out on a Crystal 300 series CE systems (ATI Unicam, Cambridge, UK) with Spectra 100 variable UV/VIS detector (Thermo Separation Product). Fused silica capillaries (50 μm I.D. × 360 μm O.D.) were from Polymicro Technologies (Phoenix, USA). Sodium dodecyl sulfate (SDS) was used as micelle-forming surfactant, thiourea was used as marker of the hold-up time, and quinine hydrochloride was used as marker of the migration time of the micelles. Sodium borate buffer (10 mM, pH 9.0) with 100 mM SDS containing different concentrations of cyclodextrin was used as separation buffer. The sample solution (150 mg L^{-1}) of N-(1-adamantyl)acrylamide was prepared in the separation buffer without CD. Sample injection was performed hydrodynamically (30 mbar for 0.30 min). UV detection was at a wavelength of 214 nm. The effective length of the capillary was 49.0 cm, which corresponds to a total length of 63.6 cm.

Water/methanol mobile phases buffered with triethylamine/acetic acid (pH* = 6.8–7.0, electric conductivity 120–150 μS/cm) were used for CEC separations in the RP mode. For normal phase separations, methanol (100%) or methanol/acetonitrile mobile phases buffered with triethylamine/acetic acid (pH* = 6.5–6.9, electric conductivity 110–140 μs/cm) were used.

Different classes of analytes were studied: alkylphenones (acetophenone, propiophenone, butyrophenone, valerophenone, and hexanophenone) as hydrophobic analytes and phenolic compounds (3-methoxybenzaldehyde, 4-hydroxy-3-methoxybenzaldehyde, 4-hydroxybenzaldehyde, 3,4-dihydroxybenzaldehyde, and resorcinol) as hydrophilic analytes.

3. Results and discussion

3.1. Solubilization of hydrophobic monomer by host–guest complexation

Acrylamide-based monolithic stationary phases prepared from water-soluble monomers are hydrophilic and not suitable for RP-CEC. In order to increase the hydrophobicity of the synthesized monolithic stationary phases more hydrophobic structure units are required, which have to be introduced by incorporating hydrophobic monomers into the polymerization mixture. To this end, N-(1-adamantyl)acrylamide was selected as highly hydrophobic monomer. N-(1-adamantyl)acrylamide can be dissolved in aqueous solution after its solubilization via complexation with a water-soluble CD. A high binding constant *e.g.* with Me-β-CD [14,29] due to good size matching between the size of the adamantyl group and the cavity of β-CD allows the solubilization of this monomer with a low concentration of CD. N-(1-adamantyl)acrylamide was solubilized in water using different types of cyclodextrin (Me-β-CD, dimethyl-β-CD, 2-HP-γ-CD, α-CD, and γ-CD). As a first step, the molar ratio CD/monomer which was needed for the complete solubilization of N-(1-adamantyl)acrylamide was determined. Different molar ratios were needed for the complete solubilization of this monomer. For example, 128 mg of Me-β-CD, 384 mg of

Table 1
Cyclodextrin-modified MEKC, observed retention factors k_{ob} for N-(1-adamantyl)acrylamide dependent on the concentration of selected cyclodextrins in the separation buffer (100 mmol L^{-1} SDS, 10 mmol L^{-1} $Na_2B_4O_7$, pH = 9.0), capillary (50 μm I.D., 49.0 cm effective length, 63.6 cm total length); marker of hold-up time: thiourea, marker of the migration time of the micelles: quinine hydrochloride. Data shown are the average of triplicate measurements (standard deviation in brackets).

Ligand	Concentration (mM)	k_{ob}
Me-β-CD	0.00	17.52 (±0.367)
	10.0	11.20 (±0.173)
	25.0	3.81 (±0.046)
	35.0	1.99 (±0.151)
2-HP-γ-CD	10.0	6.72 (±0.045)
	25.0	2.12 (±0.015)
	35.0	1.11 (±0.005)
α-CD	10.0	14.56 (±0.151)
	25.0	14.68 (±0.864)
	35.0	12.01 (±0.301)
Dimethyl-β-CD	10.0	14.05 (±0.050)
	25.0	6.79 (±0.017)
	35.0	3.45 (±0.025)

2-HP-γ-CD, and 166.0 mg of dimethyl-β-CD were needed to solubilize 20 mg of N-(1-adamantyl)acrylamide in 500 μL water. This corresponds to a 1.0, 2.50, and 1.28 CD/monomer molar ratio. γ-CD and α-CD did not solubilize the monomer completely at any molar ratio investigated. Differences in the required molar ratios can be attributed to differences in the complex formation constants of the formed monomer/CD complexes.

3.2. CD-modified MEKC

The observed retention factor k_{obs} of a neutral analyte in CD-MEKC is given by the following equation [30,31]:

$$k_{obs} = \frac{t_{mig} - t_0}{t_0(1 - (t_{mig}/t_{mc}))} \quad (1)$$

where t_{mig} = migration time of the solute, t_0 = migration time of the EOF marker ($K_{dis} \rightarrow 0$), t_{mc} = migration time of a hydrophobic marker (quinine hydrochloride, $K_{dis} \rightarrow \infty$). It was assumed that the micelle marker does not interact with the CD.

As expected, the observed retention factor for N-(1-adamantyl)acrylamide was decreased by the addition of CD to the separation buffer (Table 1). Without addition of CD to the separation buffer the retention factor for N-(1-adamantyl)acrylamide corresponds to the retention factor of a hydrophobic solute. Addition of Me-β-CD or 2-HP-γ-CD decreases the retention factor significantly, while addition of dimethyl-β-CD decreases the observed retention factor to a much lower extent. In addition, the observed retention factor of N-(1-adamantyl)acrylamide was only affected very little by addition of native α-CD. These findings indicate that Me-β-CD and 2-HP-γ-CD form stronger complexes with N-(1-adamantyl)acrylamide than dimethyl-β-CD or α-CD. This explains, why they are better solubilizing agents for N-(1-adamantyl)acrylamide. This observation can be explained in part by size matching of the adamantyl group with the cavity of these cyclodextrins. However, different size matching does not explain the strong effect of 2-HP-γ-CD. Terabe et al. [32] have explained this phenomenon by co-inclusion of the monomeric surfactant molecule together with the analyte molecule. In further studies, we selected Me-β-CD as solubilizing agent because of its ability to solubilize N-(1-adamantyl)acrylamide at a 1:1 molar ratio, its high solubility in water and its availability at low price.

3.3. CD-modified CEC

Cyclodextrin-modified CEC was employed as a method to study the inclusion complex of Me-β-CD with N-(1-adamantyl) acrylamide and to determine its complex formation constant [14]. In case of complexation with cyclodextrin, the observed retention factor k^* of a solute is defined as,

$$k^* = \varphi K^* \quad (2)$$

where $\varphi = V_s/V_m$ is the phase ratio (V(stationary phase)/V(mobile phase)) within the column, and K^* is the apparent partitioning coefficient which is defined as:

$$K^* = \frac{c_s}{c_{aq} + c_{com}} \quad (3)$$

where c_s is the molar concentration of free solute in the stationary phase, c_{aq} is the molar concentration of free solute in the mobile phase, and c_{com} is the molar concentration of complexed solute in the mobile phase. If the molar concentration of free cyclodextrin is assumed to be identical to the total concentration of cyclodextrin [CD], the complex formation constant B is defined by the following equation:

$$B = \frac{c_{com}}{c_{aq}[CD]} \quad (4)$$

Substitution of c_{com} in Eq. (3) by Eq. (4), followed by substitution of K^* in Eq. (3) by Eq. (2), gives,

$$k^* = \frac{\varphi c_s}{(c_{aq} + B c_{aq}[CD])} \quad (5)$$

which is equal to

$$k^* = k\frac{1}{1 + B[CD]} \quad (6)$$

where k is the retention factor in the absence of cyclodextrin. Rearrangement of Eq. (6) gives [33],

$$\frac{1}{k^*} = \frac{1}{k} + \frac{B}{k}[CD] \quad (7)$$

By plotting $1/k^*$ against the concentration of cyclodextrin in the mobile phase (y-reciprocal plot), the complex formation constant B can be determined (B = slope/y-intercept).

For this purpose, a highly polar stationary phase was prepared by using N-isopropylacrylamide as monomer in the polymerization mixture in order to avoid the interaction of cyclodextrin in the mobile phase with the hydrophobic groups of the stationary phase (Table 2, Monolith 7). In a first step, acetophenone was used to test the validity of Eq. (7). The plot of $1/k^*$ versus concentration of cyclodextrin in the mobile phase is linear with positive y-intercept (Fig. S2, see Supporting material).

For N-(1-adamantyl)acrylamide, the observed retention factor was also decreased with increasing concentration of Me-β-CD in the mobile phase. The y-reciprocal plot (Fig. 2) shows a linear dependence of $1/k^*$ on the concentration of cyclodextrin in the mobile phase, indicating the formation of a host-guest complex with 1:1 stoichiometry [34]. A stoichiometry of 1:1 can also be deduced from NMR data (Job's method, see Supporting material, Fig. S1).

Complex formation constants were calculated for acetophenone and N-(1-adamantyl)acrylamide (mobile phase: methanol/water, 30/70, v/v, buffered with triethylamine/acetic acid, pH* = 7.0, electric conductivity = 120 μS/cm). The standard error of the complex formation constant ΔB was calculated from the standard deviation

Table 2
Composition of polymerization mixtures with varied molar fraction of the hydrophobic monomer N-(1-adamantyl)acrylamide (in 100 mM phosphate buffer, pH = 7.0).

Monolith	Volume (mL)	N-(1-adamantyl)acrylamide (mg)	Me-β-CD (mg)	PDA (mg)	VSA (μL)	MA (mg)
1	0.7	10	65	65	15	40
2	0.7	20	128	65	15	30
3	0.7	30	191	65	15	20
4	0.7	40	255	65	15	10
5	0.7	50	320	65	15	0.0
6	0.7	30	191	65	35	20
7	0.6	N-isopropyl-acrylamide: 50	(No addition)	35	10	0.0

Monoliths 1–6: %*T* = 16.4 (w/v); %*C* = 56.6 (w/w); APS (10%, w/v): 10 μL, TEMED (10%, v/v): 10.0 μL.
Monolith 7: %*T* = 14.2 (w/v); %*C* = 41.2 (w/w); APS (2.5%, w/v): 10 μL, TEMED (2.5%, v/v): 10.0 μL.
Ammonium sulfate: Monoliths 1–3: 50 mg/mL; Monoliths 4 and 5: 11.40 mg/mL; Monolith 6: 17.1 mg/mL; Monolith 7: 50.0 mg/mL.

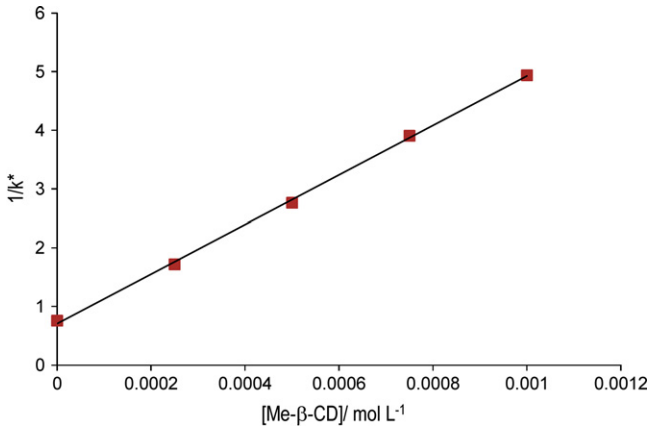

Fig. 2. Cyclodextrin–modified CEC, 1/k* for N-(1-adamantyl)acrylamide *vs.* concentration of statistically methylated β-CD present in the mobile phase (methanol/water, 30/70, v/v) buffered with triethylamine/acetic acid, pH* = 7.0, electric conductivity = 120 μs/cm. Each data point is the average of triplicate measurements, standard deviation represented as error bar.

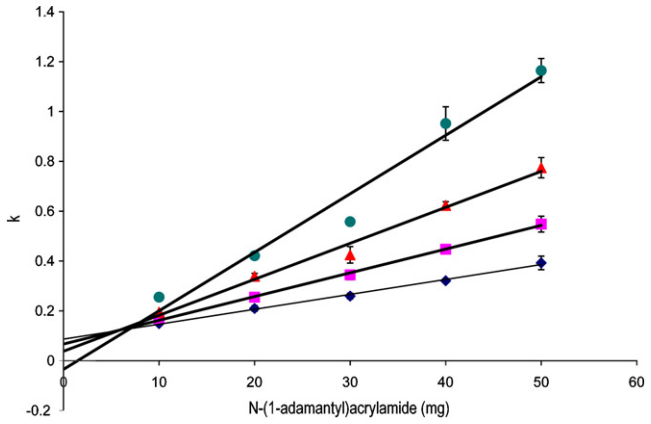

Fig. 3. Retention factors for alkylphenones *vs.* mass of N-(1-adamantyl)acrylamide present in the polymerization mixture. Mobile phase: methanol/water (50:50, v/v) buffered with triethylamine/acetic acid, pH* = 7.0, electric conductivity = 125 μS/cm.

of the slope s_b and of the *y*-intercept s_a according to the error propagation law:

$$\Delta B = B\sqrt{\left(\frac{s_b}{b}\right)^2 + \left(\frac{s_a}{a}\right)^2},$$

where *b* and *a* are the slope and intercept.

Following complex formation constants were obtained: *B*(acetophenone) = 45 ± 2.80; *B*(N-(1-adamantyl)acrylamide) = 5896 ± 247. The high value of the formation constant for N-(1-adamantyl)acrylamide reflects the well-known size matching of the adamantyl group with the cavity size of Me-β-CD [26].

3.4. 2D-^{1}H NOESY

The 2D-^{1}H NOESY spectrum for a solution of 0.125 mol L^{-1} (1:1 molar ratio) of Me-β-CD/N-(1-adamantyl)acrylamide in 1 mL D_2O is shown in Fig. S3 (see Supporting material). The 2D-^{1}H NOESY spectrum displays clear NOE cross-peaks between the protons of the cyclodextrin cavity (3.5–4.0 ppm) and the protons of the adamantyl group. This spectrum also shows no cross peaks between the acrylamide group protons (H_a, H_b, and H_c) and the protons of the adamantyl group. These findings support strongly our assumption that only the hydrophobic part of the guest monomer (the adamantyl group) is embedded into the cavity of the CD. Therefore, the acrylamide group can be regarded not to be shielded by the host so that it is accessible during the polymerization process.

3.5. Variation of the content of hydrophobic monomer

Highly cross-linked macroporous amphiphilic monolithic stationary phases were synthesized for CEC by host–guest complexation of N-(1-adamantyl)acrylamide with Me-β-CD and *in situ* free radical copolymerization of MA, cyclodextrin-solubilized N-(1-adamantyl)acrylamide, PDA, and VSA in aqueous medium in 100 μm I.D. pre-treated fused-silica capillaries. The total monomer concentration (%*T*) and the cross-linking degree (%*C*) nomenclature introduced by Hjerten [35] in 1962 is used throughout, the contribution of the constant amount of VSA in the reaction mixture was not taken into account for the calculations.

In first investigations different concentrations of the hydrophobic monomer N-(1-adamantyl)acrylamide were incorporated into the polymerization mixture with the aim to investigate the chromatographic properties (retention mechanism) of the resulting monoliths when using a buffered water/methanol mobile phase. The hydrophilic methacrylamide monomer was replaced gradually by the hydrophobic monomer so that the total monomer concentration (%*T*) and the percentage of crosslinker (%*C*) remained constant (Table 2, Monoliths 1–5).

Table 3
Methylene selectivity α_{meth} (±confidence range) dependent on the content of N-(1-adamantyl)acrylamide in the polymerization mixture. Mobile phase: methanol/water (50:50, v/v) buffered with triethylamine/acetic acid, pH* = 7.00, electric conductivity = 125 μ/cm (see also Table 2).

Monolith	N-(1-adamantyl)acrylamide (mg)	α_{meth} (±confidence range)
1	10.0	0.076 (±0.050)
2	20.0	0.103 (±0.020)
3	30.0	0.107 (±0.020)
4	40.0	0.156 (±0.030)
5	50.0	0.157 (±0.020)

With constant composition of the mobile phase the retention factors for a homologues series of alkylphenones increase linearly with increasing content of the hydrophobic monomer in the polymerization mixture (see Fig. 3). The methylene selectivity α_{meth} [36] is calculated from the slope of the regression line when plotting $\log k$ *versus* n_{CH_2} of the alkylphenones studied (n_{CH_2} = 1–4 for acetophenone, propiophenone, butyrophenone, and valerophenone) (see Table 3). Confidence limits were calculated by multiplying the standard deviation of the slope s_b with t (95%, f = 2).

The increase of the concentration of hydrophobic monomer in the polymerization mixture results in an increase in the hydrophobicity quantified by α_{meth}, resulting also in an increase in the retention factors of the alkylphenones (in the reversed-phase mode). These findings reveal the contribution of the hydrophobic monomer in the retention mechanism. In addition, it can be concluded that the composition of the resulting polymer reflects the composition of the polymerization mixture.

3.6. Variation of total monomer concentration

In a second step we studied the influence of the total monomer concentration (%T) on the retention factors of a homologues series of alkylphenones, on the specific permeability K°, on the electroosmotic mobility μ_{eo}, and on the methylene selectivity α_{meth}. Five different monoliths with varied total monomer concentrations were prepared (see Table 4).

Changing %T results in a change of the volume ratio (V(stationary phase)/V(mobile phase)) in the resulting monolithic capillaries. The volume fraction of the stationary phase increases with increasing %T, which in turn will increase the retention factors of the analytes in agreement with the definition of the retention factor: $k = K\varphi$. With constant composition of the mobile phase the retention factors for several alkylphenones increase linearly with increasing %T (see Fig. 4). However, as expected, the methylene selectivity α_{meth} was not affected by the variation of %T (see Table 4).

The hydrodynamic permeability K_p of a monolith is defined according to Darcy's law as the linear velocity u of a liquid streaming through the pore network normalized on the length of the chromatographic bed L, and on the pressure difference between both ends Δp. The specific permeability K° is the permeability K_p normalized on the viscosity of the liquid η and the total porosity ε of the filled capillary. The specific permeability is given by:

$$K^\circ = K_p \eta \varepsilon \quad (8)$$

The total porosity ε is accessible by using the relationship between the linear velocity u and the volume flow rate F.

$$u = \frac{F}{\pi \varepsilon r^2} \quad (9)$$

Substitution of ε and $K_p = uL/\Delta p$ into K° gives:

$$K^\circ = \frac{LF\eta}{\pi \Delta p r^2} \quad (10)$$

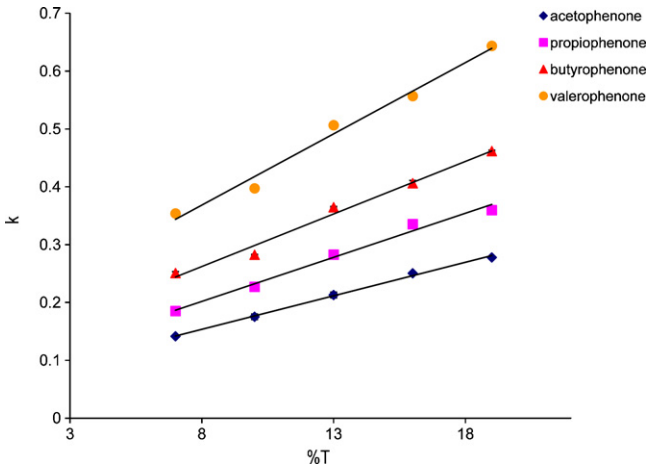

Fig. 4. Retention factors for several alkylphenones *vs.* %T (composition of polymerization mixture see Table 4). Mobile phase: methanol/water (50:50, v/v) buffered with triethylamine/acetic acid, pH* = 7.0, electric conductivity = 125 μS/cm.

K° was determined for monoliths with different %T by determining the volume flow rate using an HPLC pump with flow splitter and employing water as liquid phase ($\eta = 10^{-3}$ Pa s at 20 °C) (Table 4). The specific permeability decreases with increasing %T, which can be explained by a decrease in the mean diameter of the flow-through pores in the monolithic skeleton [37]. Electroosomotic mobilities μ_{eo} for monoliths with different %T were also calculated (Table 4). With the first three monoliths (Monoliths 8–10) the electroosmotic mobility is not significantly affected, while for monoliths with higher %T (Monoliths 10 and 11) μ_{eo} is slightly decreased. These results can be explained by assuming that with the first three monoliths the thickness of the electrical double layer is much smaller than the mean channel diameter of the flow-through pores, while for the last two monoliths the mean channel diameters decrease to an extent that the double layers start to overlap, which in turn decreases the electroosmotic mobility.

In order to verify the assumption that the mean channel diameter (size of flow-through pores) decreases as %T increases, SEM photographs were taken and analyzed for the domain size (mean globule size + mean channel diameter) [38] for three monoliths (Fig. 5). The SEM photographs demonstrate that by increasing %T the degree of globule-stacking of the resulting polymer is increased and the mean diameter of the flow-through pores is decreased accordingly.

3.7. Chromatographic properties

Acrylamide-based monoliths co-polymerized from water-soluble monomers and water-insoluble monomers have an amphiphilic character and can be used for the separation of analytes

Table 4
Composition of the polymerization mixtures of the monoliths with varied %T, specific permeability K° (±standard deviation), electroosmotic mobility μ_{eo}, and methylene selectivity α_{meth} (±confidence range). Mobile phase: methanol/water (50:50, v/v) buffered with triethylamine/acetic acid, pH* = 7.0, electric conductivity = 125 μS/cm.

Monolith	%T (w/v)	V (mL)	K° (m^2)	α_{meth}	μ_{eo} (cm^2 kV^{-1} min^{-1})
8	7.2	1.60	3.2×10^{-12} ($\pm 0.12 \times 10^{-12}$)	0.128 (±0.02)	9.83 (±0.105)
9	10.5	1.10	4.7×10^{-13} ($\pm 0.46 \times 10^{-13}$)	0.123 (±0.03)	9.88 (±0.103)
10	13.5	0.85	3.1×10^{-13} ($\pm 0.43 \times 10^{-13}$)	0.127 (±0.02)	9.84 (±0.352)
11	16.4	0.70	6.0×10^{-14} ($\pm 0.06 \times 10^{-14}$)	0.118 (±0.02)	8.43 (±0.105)
12	19.2	0.60	Not determined	0.120 (±0.03)	7.86 (±0.208)

N-(1-adamantyl)acrylamide: 30 mg, Me-β-CD: 191 mg.
PDA: 65.0 mg, MA: 20 mg, %C = 56.6 (w/w).
APS (10%, w/v): 10.0 μL, TEMED (10%, v/v): 10.0 μL.
Ammonium sulfate: 50.0 mg/mL, VSA: 15 μL.

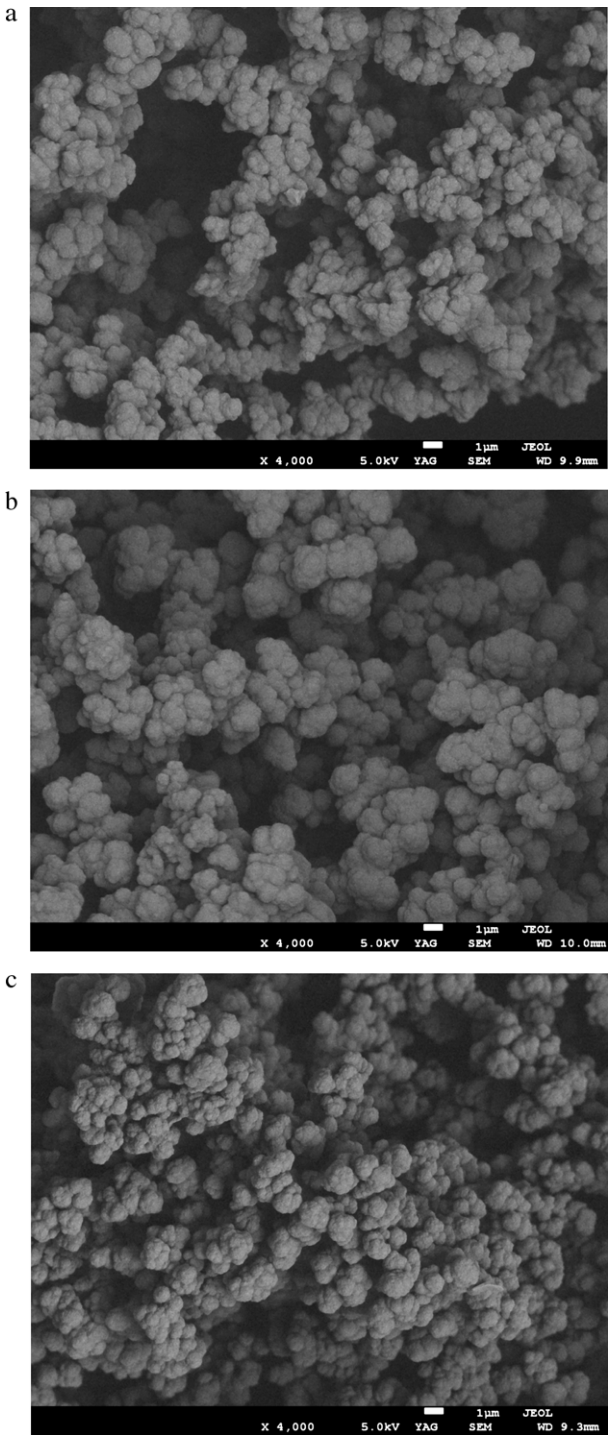

Fig. 5. SEM photographs for Monoliths 8, 9, and 10 with identical magnification (4000×). (a) Monolith 8, 7.2%T, (b) Monolith 9, 10.5%T, (c) Monolith 10, 13.5%T.

in the reversed- and in the normal-phase elution mode [3]. In Fig. 6 a model of the synthesized cross-linked polymer is shown which illustrates the presence of hydrophobic, hydrophilic and charged moieties. If this model is correct (based on the assumption that the composition of the polymer reflects the composition of the polymerization mixture and that all monomers present in the polymerization mixture react with similar reaction rates) then these hydrophobic, hydrophilic and charged moieties will all contribute to the chromatographic properties of the synthesized monolith. Hydrophobic interactions will prevail for hydrophobic solutes and

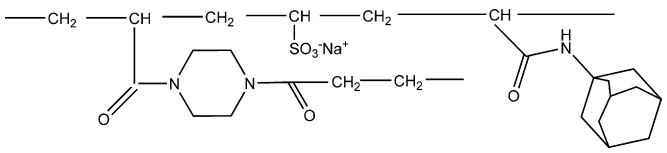

Fig. 6. Schematic representation of a model of the synthesized monolith.

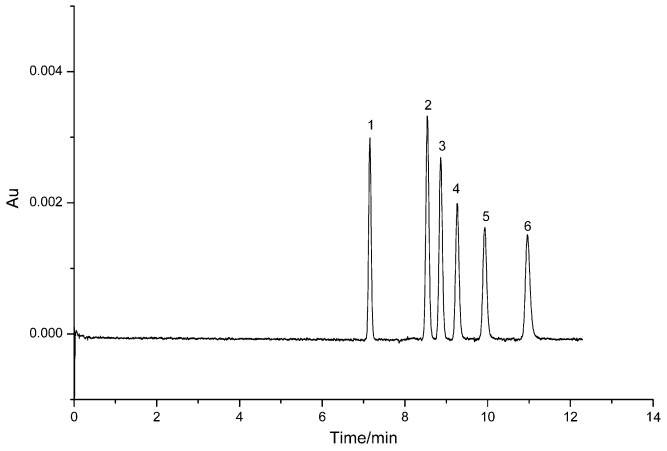

Fig. 7. Reversed-phase separation of alkylphenones on Monolith 6 (see Table 2). Analytes: (1) DMF (2) acetophenone (3) propiophenone (4) butyrophenone (5) valerophenone (6) hexanophenone. Mobile phase: methanol/water (50:50, v/v) buffered with triethylamine/acetic acid, pH* = 7.0, electric conductivity = 125 μS/cm; capillary dimensions 317 mm (245 mm) × 100 μm; UV detection at 230 nm; electrokinetic injection: 1.5 kV for 3 s; separation voltage: 22.5 kV.

aqueous mobile phase, while polar interactions will prevail for polar solutes and nonpolar mobile phase.

Based on these assumptions, the elution order for a series of alkylphenones was investigated (see Fig. 7). The elution order observed (increasing retention factor with increasing alkyl chain length) indicates a (pure) reversed-phase elution mode for hydrophobic solutes when using a buffered aqueous mobile phase. As expected for the reversed phase elution mode, the logarithmic retention factors are decreased linearly with increase in the volume fraction of methanol in the mobile phase (see Fig. 8).

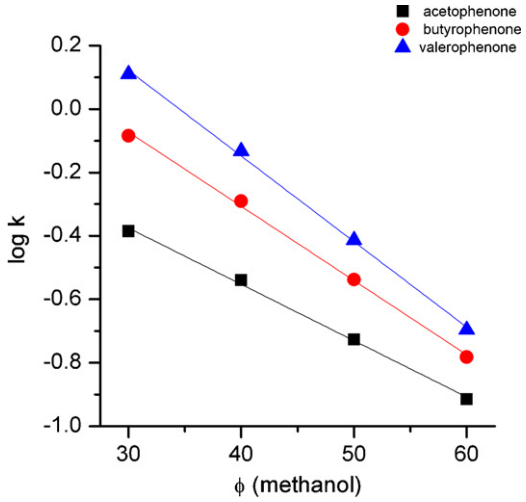

Fig. 8. Log *k* of alkylphenones versus volume fraction of methanol (in %) in the mobile phase. Mobile phase: methanol/water, buffered with triethylamine/acetic acid, pH* = 7.0, electric conductivity = 120 μS/cm.

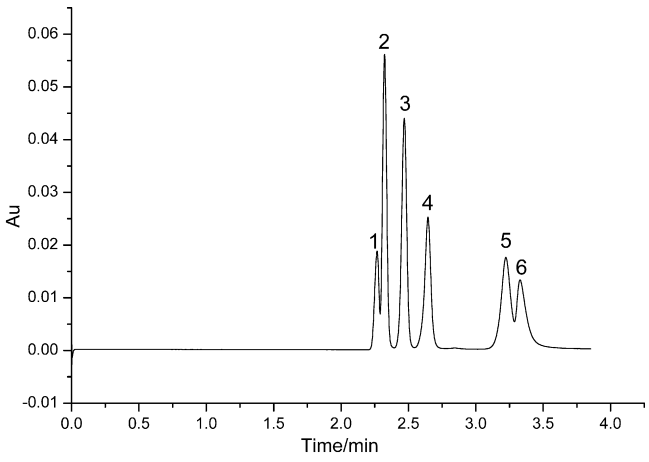

Fig. 9. Normal-phase separation of phenolic analytes on Monolith 6 (see Table 2). Analytes: (1) DMF (2) 3-methoxybenzaldehyde (3) 4-hydroxy-3-methoxybenzaldehyde (4) 4-hydroxybenzaldehyde (5) 3,4-dihydroxybenzaldehyde (6) resorcinol. Mobile phase: methanol/ACN (50:50, v/v) buffered with triethylamine/acetic acid, pH* = 6.40, electric conductivity = 100 μS/cm; capillary dimensions 247 mm (175 mm) × 100 μm; UV detection at 230 nm; electrokinetic injection: 6 kV for 3 s; separation voltage: 22 kV.

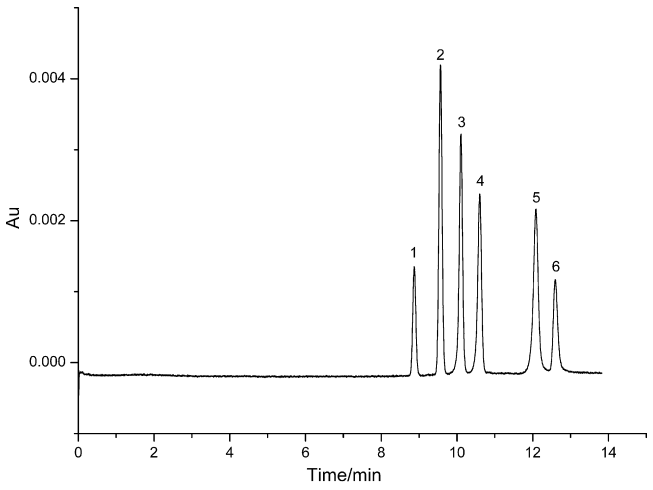

Fig. 11. Mixed-mode separation of phenolic analytes on Monolith 6. Analytes: (1) DMF (2) 3-methoxybenzaldehyde (3) 4-hydroxy-3-methoxybenzaldehyde (4) 4-hydroxybenzaldehyde (5) 3,4-dihydroxybenzaldehyde (6) resorcinol. Mobile phase: methanol/water (80:20, v/v) buffered with triethylamine/acetic acid, pH* = 6.86, electric conductivity = 105 μS/cm; capillary dimensions 317 mm (245 mm) × 100 μm; UV detection at 230 nm; electrokinetic injection: 1.5 kV for 3 s; separation voltage: 20 kV.

We also investigated the selectivity with more hydrophilic (neutral) polar phenolic solutes (resorcinol, 3,4-dihydroxybenzaldehyde, 4-hydroxybenzaldehyde, 4-hydroxy-3-methoxybenzaldehyde, and 3-methoxybenzaldehyde) in the normal-phase elution mode using different methanol/acetonitrile mobile phases buffered with triethylamine/acetic acid (see Fig. 9). Under these conditions, the polar phenolic solutes elute according to what would be expected in the normal-phase mode, *i.e.*, they are eluted according to an increase in the polarity. Retention factors increase with increasing volume fraction of acetonitrile in the mobile phase (see Fig. 10).

However, when using a buffered aqueous mobile phase, the retention behavior of these solutes can neither be described as a reversed- nor as a normal-phase retention behavior (see Fig. 11). It has to be described as a mixed-mode retention behavior. While the elution order follows what would be expected in the normal-phase mode, *i.e.*, the solutes are eluted in the order of increasing polarity, the retention factors are decreased with increasing volume fraction of methanol in the mobile phase as in the reversed-phase mode.

Plotting of the logarithm of the retention factor against the volume fraction of methanol in the mobile phase (see Fig. 10) reveals that there is a transition from a normal-phase elution regime (with non-aqueous mobile phase), in which hydrophobic interactions (with the adamantyl groups) are suppressed, to a mixed-mode elution regime (with aqueous mobile phase), in which hydrophobic and hydrophilic interactions contribute both to the observed retention.

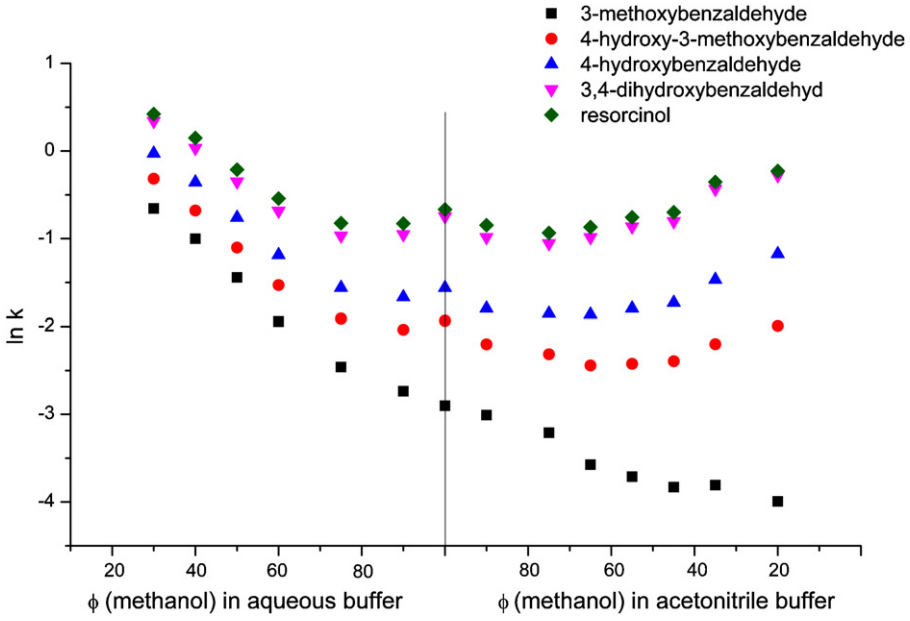

Fig. 10. Logarithmic retention factor for phenolic analytes *vs.* volume fraction of MeOH (in %) in the mobile phase; Monolith 6. Mobile phase: MeOH/aqueous buffer or buffered MeOH/ACN pH* = 6.30 ± 0.4, electric conductivity 110 ± 15 μs/cm. EOF marker DMF; capillary dimensions 247 mm (175 mm) × 100 μm; UV detection at 230 nm; electrokinetic injection: 6 kV for 3 s.

4. Conclusions

A new synthesis procedure for amphiphilic polyacrylamide-based monolithic stationary phases was developed. Host–guest complexation of highly hydrophobic analytes with water soluble cyclodextrins is shown to be an interesting alternative to the synthesis in non-aqueous medium for the synthesis of adamantyl-group containing acrylamide-based monolithic stationary phases for CEC. Due to the amphiphilic nature of the synthesized continuous beds, polar and non-polar neutral analytes can be separated employing different retention modes depending on the type of the mobile phase and the properties of the solute.

Acknowledgements

A.A. Al-Massaedh thanks Al al-Bayt University (Mafraq, Jordan) for financial support. We also thank Mr. M. Hellwig (Electron Microscopy and Microanalysis Laboratory, University of Marburg, Marburg, Germany) for carrying out the SEM measurements.

Appendix A. Supplementary data

Supplementary data associated with this article can be found, in the online version, at http://dx.doi.org/10.1016/j.chroma.2013.02.046.

References

[1] F. Al-Rimawi, U. Pyell, J. Sep. Sci. 29 (2006) 2816.
[2] K. Ohyama, D. Horiguchi, N. Kishikawa, N. Kuroda, J. Sep. Sci. 34 (2011) 2279.
[3] A. Wahl, F. Al-Rimawi, I. Schnell, O. Kornysova, A. Maruska, U. Pyell, J. Sep. Sci. 31 (2008) 1519.
[4] R. Ludewig, S. Nietzsche, G.K.E. Scriba, J. Sep. Sci. 34 (2011) 64.
[5] D. Hoegger, R. Freitag, J. Chromatogr. A 914 (2001) 211.
[6] D. Hoegger, R. Freitag, Electrophoresis 24 (2003) 2958.
[7] V. Ratautaite, A. Maruska, M. Erickson, O. Kornysova, J. Sep. Sci. 32 (2009) 2582.
[8] K. Ohyama, Y. Fukahori, K. Nakashima, T. Sueyoshi, N. Kishikawa, N. Kuroda, J. Chromatogr. A 1217 (2010) 1501.
[9] C. Ericson, S. Hjerten, Anal. Chem. 71 (1999) 1621.
[10] J.L. Liao, N. Chen, C. Ericson, S. Hjerten, Anal. Chem. 68 (1996) 3468.
[11] I. Gusev, X. Huang, C. Horvath, J. Chromatogr. A 855 (1999) 273.
[12] S. Xie, F. Svec, J.M.J. Frechet, J. Chromatogr. A 775 (1997) 65.
[13] A. Palm, M.V. Novotny, Anal. Chem. 69 (1997) 4499.
[14] F. Al-Rimawi, U. Pyell, J. Sep. Sci. 30 (2007) 761.
[15] F. Al-Rimawi, U. Pyell, J. Chromatogr. A 1160 (2007) 326.
[16] A. Wahl, I. Schnell, U. Pyell, J. Chromatogr. A 1044 (2004) 211.
[17] C. Steffens, O. Kretschmann, H. Ritter, Macromol. Rapid Commun. 28 (2007) 623.
[18] O. Kretschmann, C. Steffens, H. Ritter, Angew. Chem. Int. Ed. 46 (2007) 2708.
[19] C. Aydogan, A. Tuncel, A. Denizli, J. Sep. Sci. 35 (2012) 1010.
[20] Q.Z. Wu, J.F. He, J.M. Ou, Chin. Chem. Lett. 23 (2012) 474.
[21] C.W. Huck, R. Bakry, G.K. Bonn, Eng. Life Sci. 5 (2005) 431.
[22] J.L. Liao, Y.M. Li, S. Hjerten, Anal. Biochem. 234 (1996) 27.
[23] C. Fujimoto, Anal. Chem. 67 (1995) 2050.
[24] D. Hoegger, R. Freitag, J. Chromatogr. A 1004 (2003) 195.
[25] S. Hjerten, J.L. Liao, R. Zhang, J. Chromatogr. 473 (1989) 273.
[26] F. van de Manakker, T. Vermonden, C.F. van Nostrum, W.E. Hennink, Biomacromolecules 10 (2009) 3157.
[27] W.A. Skinner, J.H. Lange, T.E. Shellenberger, W.T. Colwell, J. Med. Chem. 10 (1967) 949.
[28] S. Hjerten, J. Chromatogr. 347 (1985) 191.
[29] Y. Liu, Y.L. Zhao, H.Y. Zhang, Z. Fan, G.D. Wen, F. Ding, J. Phys. Chem. B 108 (2004) 8836.
[30] S. Terabe, K. Otsuka, K. Ichikawa, A. Tsuchiya, T. Ando, Anal. Chem. 56 (1984) 111.
[31] S. Terabe, Y. Miyashita, O. Shibata, E.R. Barnhart, L.R. Alexander, D.G. Patterson, B.L. Karger, K. Hosoya, N. Tanaka, J. Chromatogr. 516 (1990) 23.
[32] S. Terabe, Y. Miyashita, Y. Ishihama, O. Shibata, J. Chromatogr. 636 (1993) 47.
[33] K. Fujimura, T. Ueda, M. Kitagawa, H. Takayanagi, T. Ando, Anal. Chem. 58 (1986) 2668.
[34] J. Lipkowski, O.I. Kalchenko, J. Slowikowska, V.I. Kalchenko, O.V. Lukin, L.N. Markovsky, R. Nowakowski, J. Phys. Org. Chem. 11 (1998) 426.
[35] S. Hjerten, Arch. Biochem. Biophys. Suppl. 1 (1962) 147.
[36] A.M. Krstulovic, H. Colin, A. Tchapla, G. Guiochon, Chromatographia 17 (1983) 228.
[37] O. Kornysova, E. Machtejevas, V. Kudirkaite, U. Pyell, A. Maruska, J. Biochem. Biophys. Methods 50 (2002) 217.
[38] P. Aggarwal, H.D. Tolley, M.L. Lee, Anal. Chem. 84 (2012) 247.

Adamantyl-group containing mixed-mode acrylamide-based continuous beds for capillary electrochromatography. Part I: Study of a synthesis procedure including solubilization of N-adamantyl-acrylamide via complex formation with a water-soluble cyclodextrin

"Ayat Allah" Al-Massaedh, Ute Pyell*

University of Marburg, Department of Chemistry, Hans-Meerwein-Straße, D-35032 Marburg, Germany

Supporting Material

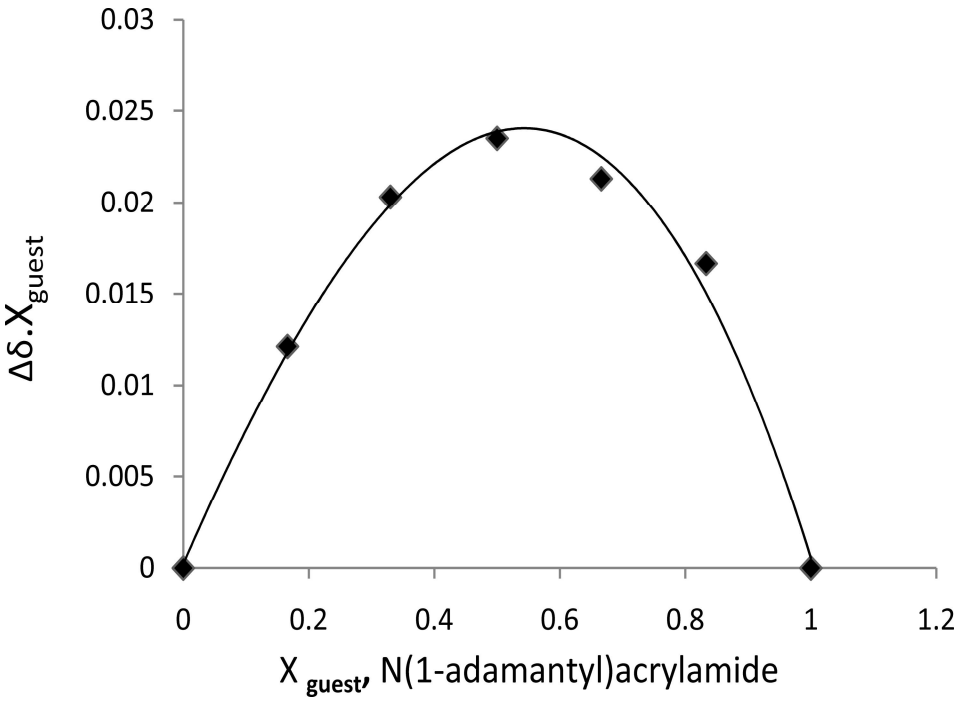

Figure S1. Job plot for N-(1-adamantyl)acrylamide/ statistically methylated-β-CD (Proton 2, see Fig. 1).

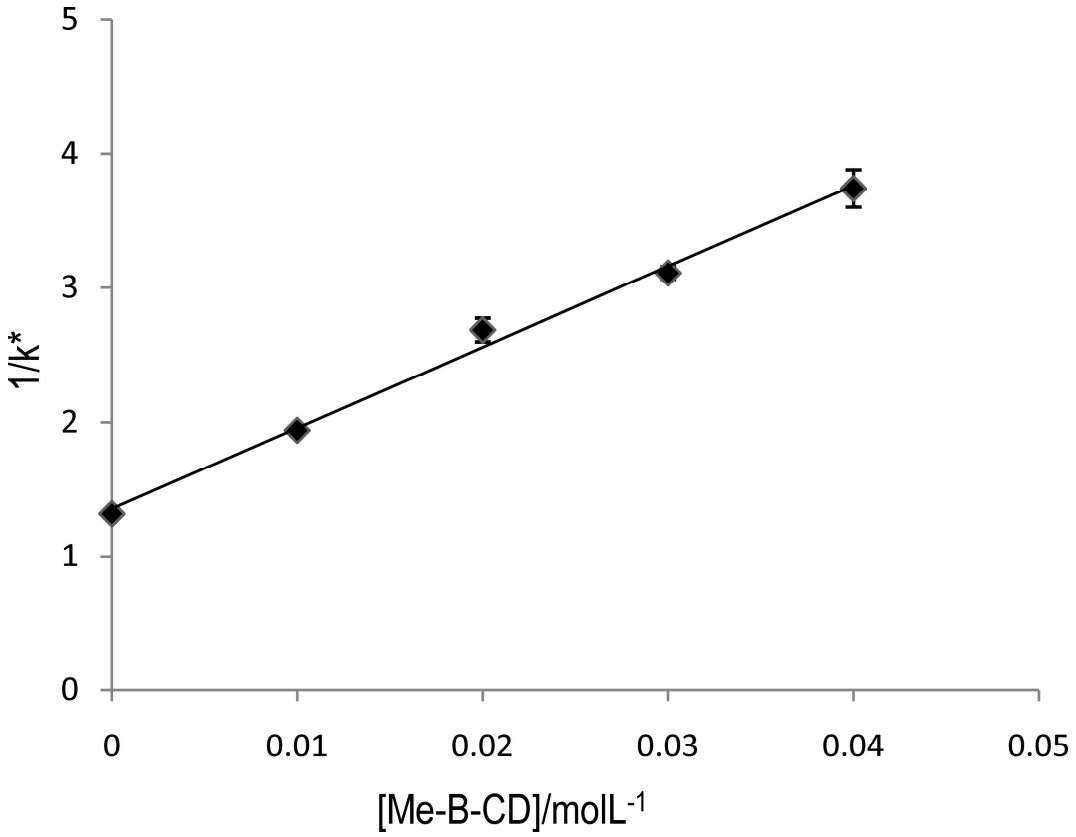

Figure S2. Cyclodextrin–modified CEC, 1/k* for acetophenone *versus* concentration of statistically methylated β-CD present in the mobile phase (methanol/water, 30/70, v/v) buffered with triethylamine/acetic acid, pH* = 7.0, electric conductivity = 120 µs/cm. Each data point is the average of triplicate measurements, standard deviation represented as error bar.

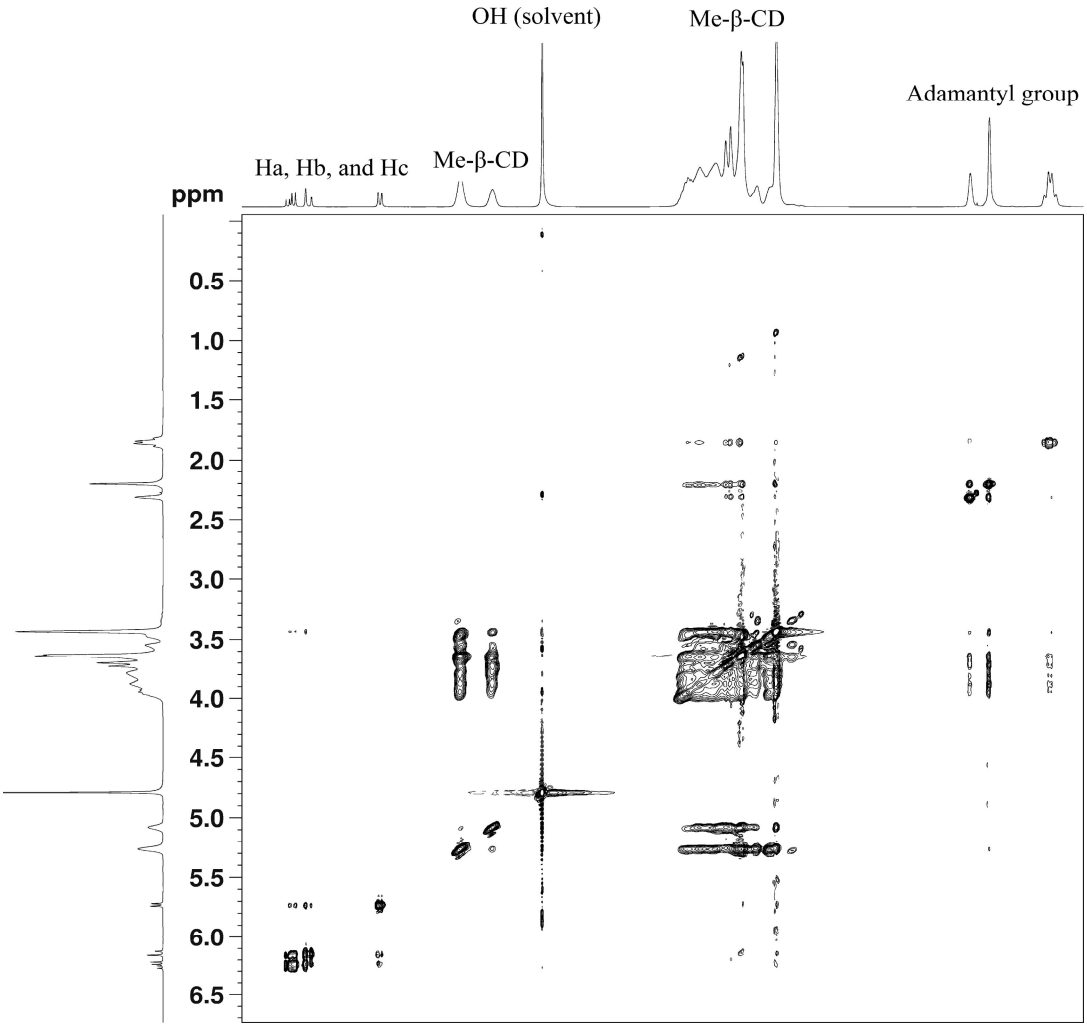

Figure S3. 2D ^{1}H NOESY spectrum of N-(1-adamantyl)acrylamide/methylated-β-CD complex in D_2O (mixing time 500 ms, 500 MHz).

ELSEVIER LICENSE
TERMS AND CONDITIONS

Apr 07, 2014

This is a License Agreement between "Ayat Allah" Al-Massaedh ("You") and Elsevier ("Elsevier") provided by Copyright Clearance Center ("CCC"). The license consists of your order details, the terms and conditions provided by Elsevier, and the payment terms and conditions.

All payments must be made in full to CCC. For payment instructions, please see information listed at the bottom of this form.

Supplier	Elsevier Limited The Boulevard,Langford Lane Kidlington,Oxford,OX5 1GB,UK
Registered Company Number	1982084
Customer name	"Ayat Allah" Al-Massaedh
Customer address	University of Marburg, 35032 Marburg, Germany.
License number	3363830312374
License date	Apr 07, 2014
Licensed content publisher	Elsevier
Licensed content publication	Journal of Chromatography A
Licensed content title	Adamantyl-group containing mixed-mode acrylamide-based continuous beds for capillary electrochromatography. Part I: Study of a synthesis procedure including solubilization of N-adamantyl-acrylamide via complex formation with a water-soluble cyclodextrin
Licensed content author	“Ayat Allah” Al-Massaedh, Ute Pyell
Licensed content date	19 April 2013
Licensed content volume number	1286
Licensed content issue number	
Number of pages	9
Start Page	183
End Page	191
Type of Use	reuse in a thesis/dissertation
Portion	full article
Format	both print and electronic
Are you the author of this Elsevier	Yes
Will you be translating?	No
Title of your thesis/dissertation	Adamantyl-Group Containing Mixed-Mode Acrylamide-Based Continuous Beds for Capillary Electrochromatography: Synthesis, Characterization, Optimization and Investigation of the Chromatographic Efficiency
Expected completion date	May 2014

5.2. Publication II

Adamantyl-group containing mixed-mode acrylamide-based continuous beds for capillary electrochromatography. Part II. Characterization of the synthesized monoliths by inverse size exclusion chromatography and scanning electron microscopy

"Ayat Allah" Al-Massaedh, Ute Pyell

Journal of Chromatography A, 1325 (2014) 247–255

doi: 10.1016/j.chroma.2013.12.026

5.2.1. Summary and discussion

In this publication, the impact of the concentration of the lyotropic salt ammonium sulfate in the polymerization mixture on the morphology, the pore size distribution, and the fractional volume of mesopores and macropores is studied by scanning electron microscopy (SEM) and inverse size exclusion chromatography (ISEC). For doing this, a series of amphiphilic macroporous N-adamantyl-group containing mixed-mode acrylamide-based monolithic stationary phases were synthesized under variation of the concentration of ammonium sulfate in the polymerization mixture. SEM photographs taken at different points along the same monolithic capillary demonstrate the homogeneity and uniformity of the formed monolith over the length of the capillary and the covalent attachment of the formed polymer to the confining wall. Additionally, SEM photographs demonstrate that the morphology of the synthesized monoliths is strongly dependent on the concentration of AS in the polymerization mixture, so that there is a clear increase in the domain size (average size of globules + average flow through pore diameter) with increasing concentration of AS in the polymerization mixture. For those monoliths which are synthesized with lower concentration of AS in the polymerization mixture, the morphology is composed of fine, small, and uniformly sized compact spherical microglobules, whereas, for those synthesized with higher concentration of AS, the size of the formed microglobules becomes larger and the formed microglobules are interconnected to each other forming a three dimensional inert-adherence heterogeneous morphology.

The pore size distribution of the synthesized monoliths is determined with inverse size exclusion chromatography (ISEC) using the retention data of a series of polystyrene standards with narrow molecular size distribution and known average molecular mass. ISEC data corroborate the results obtained by SEM studies and show a strong dependence of the pore size distribution on the concentration of AS in the polymerization mixture. ISEC data were used to create SEC calibration curves for the synthesized monolithic capillaries. For each monolithic capillary the SEC curves demonstrate the presence of two different types of pores: (i) pores located inside the microglobules (internal pores) and (ii) pores which are located between the microglobules (external pores). The dependence of the pore size distribution of the monolithic capillary on the concentration of AS in the polymerization mixture is reflected by the pore size distribution histograms constructed for the synthesized capillaries. These histograms demonstrate the presence of a trimodal pore size distribution for those monoliths which are synthesized with lower concentration of AS in the polymerization mixture, and a bimodal pore size distribution for those synthesized with higher content of AS in the

polymerization mixture. Furthermore, the ISEC histograms demonstrate that all synthesized monolithic capillaries are mesoporous with varied volume fraction of mesopores depending on the concentration of AS in the polymerization mixture.

An excellent capillary-to-capillary, day-to-day, and run-to-run reproducibility reached for the electroosmotic mobility and the retention factor determined with alkylphenones in the reversed-phase mode confirms that the synthesis procedures employed in this work are well controlled. Mixed-mode monolithic stationary phases show a high chemical stability against organic solvents like MeOH, ACN, or THF. This was confirmed by testing selected separation parameters and taking SEM micrographs before and after rinsing and equilibrating the capillary >24 h with THF.

5.2.2. Author contribution

The design of ISEC and SEM experiments and all the experimental part of this study were carried out by me. For SEM photographs, Mr. M. Hellwig (Electron Microscopy and Microanalysis Laboratory, University of Marburg, Marburg, Germany) provided the technical assistance needed in this regard. The draft of the manuscript was written by me and corrected by Prof. Dr. Ute Pyell. The final revision of the manuscript was conducted by me and Prof. Pyell before submission to the journal. Prof. Dr. Ute Pyell was responsible for the supervision of this work.

Journal of Chromatography A, 1325 (2014) 247–255

Contents lists available at ScienceDirect

Journal of Chromatography A

journal homepage: www.elsevier.com/locate/chroma

Adamantyl-group containing mixed-mode acrylamide-based continuous beds for capillary electrochromatography. Part II. Characterization of the synthesized monoliths by inverse size exclusion chromatography and scanning electron microscopy

"Ayat Allah" Al-Massaedh, Ute Pyell *

University of Marburg, Department of Chemistry, Hans-Meerwein-Straße, D-35032 Marburg, Germany

ARTICLE INFO

Article history:
Received 28 August 2013
Received in revised form
29 November 2013
Accepted 7 December 2013
Available online 16 December 2013

Keywords:
Acrylamide-based continuous beds
Monolithic stationary phase
Morphology
Pore size distribution
Inverse size exclusion chromatography
Scanning electron microscopy

ABSTRACT

In our previous article we have described the synthesis of a new amphiphilic monolithic stationary phase by in situ free radical copolymerization of cyclodextrin-solubilized N-adamantyl acrylamide, piperazinediacrylamide, methacrylamide and vinylsulfonic acid in aqueous medium in pre-treated fused silica capillaries of 100 μm I.D. In the present work, we study the morphology of different monolithic stationary phases synthesized under variation of the concentration of ammonium sulfate in the polymerization mixture. The pore size distribution is determined with inverse size exclusion chromatography (ISEC) using the retention data of a series of polystyrene standards with narrow molecular size distribution and known average molar mass ranging from 1560 to 2 010 000 g mol^{-1}. The impact of the concentration of the lyotropic salt ammonium sulfate in the polymerization mixture on the formed morphology, the pore size distribution, and the fractional volume of mesopores and macropores is determined. The homogeneity and uniformity of the formed monolith over the length of the capillary and the covalent attachment to the confining walls are confirmed. Repetition of the synthesis procedure shows that these morphology parameters are well controlled as there is an excellent capillary-to-capillary, day-to-day, and run-to-run reproducibility reached for the electroosmotic mobility and the retention factor determined with alkylphenones in the reversed-phase mode.

1. Introduction

In recent years, the development of polymer-based monolithic stationary phases has attracted great interest because of the advantages they offer over columns packed with particulate material like the possibility to fine–tune the chemical composition and the retention properties by variation of the types of monomer used in the polymerization mixture, the ease of their preparation by an in situ free radical copolymerization process, and chemical stability within a broad pH range [1–11]. The possibility of tailoring the chemical composition and adjusting the porous properties of polymer-based monoliths is one of the most important advantages of this type of stationary phase. The characterization of the porous properties of polymer-based monoliths has attracted much attention in the last years [1,3,8,12–16]. If polymer-based monolithic stationary phases are synthesized by an in situ free radical copolymerization process, the porous properties of the resulting monolith are set spontaneously during its synthesis depending on the composition of the polymerization mixture and on the reaction conditions [17–19]. Selection of the concentration and nature of the porogens used in the synthesis of the monolith is the main tool used for tailoring the porous properties without changing the chemical structure of the final monolith. As result of the phase separation process occurring during the polymerization, two main types of pores build up in the monolithic scaffold: mesopores and macropores (flow-through pores). According to the IUPAC classification, mesopores are pores with a diameter between 2 and 50 nm, and macropores are those with a diameter larger than 50 nm [14]. Mesopores are filled with a "stagnant" mobile phase, in which solute molecules are transported by diffusion [15]. Their presence in the monolithic scaffold results in a larger surface area and a higher sample capacity when compared to a material without mesopores, whereas, macropores are essential for providing an adequate permeability and access of the mesopores in the monolithic scaffold.

Because chromatographic properties of polymer-based monoliths are strongly influenced by their morphology (pore size distribution, domain size, and pore volume), several attempts have been made to optimize their porous properties for obtaining a better separation efficiency. These attempts include the optimization of following synthesis parameters (concerning the

* Corresponding author. Fax: +49 6421 2822124.
E-mail address: pyellu@staff.uni-marburg.de (U. Pyell).

0021-9673/$ – see front matter © 2013 Elsevier B.V. All rights reserved.
http://dx.doi.org/10.1016/j.chroma.2013.12.026

composition of the polymerization mixture and the reaction conditions): (i) types and molar fractions of monomers, (ii) type and molar fraction of crosslinker (*C*%), (iii) total monomer concentration (*T*%), (iv) types and concentrations of porogens, (v) type, concentration and activation of initiator, (vi) reaction time, and (vii) reaction temperature, and (viii) post-polymerization modifications including hyper-crosslinking [4,7,11–13,17,20–24].

In this context, different methods have been used for the characterization of monolithic stationary phases: scanning electron microscopy (SEM) [10,25–27], transition electron microscopy (TEM) [28], X-ray scattering [29], atomic force microscopy (AFM) [2,30], nitrogen adsorption isotherms (BET) [13,31,32], mercury intrusion porosimetry (MIP) [14,27], and inverse size exclusion chromatography (ISEC) [3,14,15,31,33,34]. Among the numerous techniques which are used for the determination of the porosities, the pore size distribution, and the pore volumes, inverse size exclusion chromatography (ISEC), which was introduced originally by Halasz and Martin in 1978 [33], is the only technique that can be conventionally used to characterize the porosity of the packing material in the wet state. Additionally, the dependence of the formed morphology of the macroporous monolith synthesized in a capillary on the diameter and the shape of the channel (confinement effect [35]) makes ISEC to the method of choice as it can be performed with the same monolithic capillary which is employed in separation. In ISEC, the investigated material is used as stationary phase in a chromatographic column under conditions in which the elution behavior of known molar mass polymer standards is governed by steric effects only. Under these conditions, interactions between the investigated material and the polymer standards are eliminated via selecting an appropriate mobile phase and a suitable type of polymer standards. Pore dimensions are determined with a set of polymer standards with well-defined size. The correlation between the retention data of these standards and the so-called "exclusion pore diameter" is used to gain information about accessible pore volumes and hence the pore size distribution [33]. Different types of monolithic stationary phases were characterized by using ISEC: polymethacrylate-based [14], polystyrene-divinylbenzene-based [3,36], silica-based [15,37], and polyacrylamide-based monoliths [12].

A few years ago, Urban et al. [14] determined the pore size distribution of polymethacrylate-based monolithic stationary phases synthesized in 250-μm I.D. fused silica capillaries by copolymerization of butyl methacrylate and ethylene dimethacrylate in the presence of a varied concentration of a mixture of porogens (1-propanol and 1,4-butanediol) using inverse size-exclusion chromatography (ISEC) and mercury-intrusion porosimetry (MIP). The authors observed that the porous properties of the synthesized monolithic stationary phases (pore size distribution, porosities, pore volumes, surface area, and hydrodynamic permeability) are strongly affected by the composition of the polymerization mixture, and that the concentration of the porogens in the polymerization mixture has a significant influence on the total and flow-through porosities.

In our previous publication [6], we have developed an amphiphilic monolith which is prepared by in situ free radical copolymerization of N-adamantyl acrylamide solubilized via complex formation with statistically methylated β-CD, piperazine-diacrylamide, methacrylamide and vinylsulfonic acid in aqueous medium in pre-treated fused silica capillaries of 100 μm I.D. In the current study, a series of amphiphilic macroporous N-adamantyl-group containing mixed-mode acrylamide-based continuous beds is synthesized under variation of the concentration of ammonium sulfate in the polymerization mixture according to the procedure described in our previous publication [6]. These monoliths are characterized by scanning electron microscopy (SEM) and inverse size exclusion chromatography (ISEC) to study the impact of this varied synthesis parameter on the morphology (e.g. the domain size), the pore size distribution (including internal and external "mesopores"), and the fractional volumes of different types of pores. SEM is also used to confirm the homogeneity and uniformity of the monolith filling procedure over the length of the capillary including the efficient covalent attachment of the formed polymeric monolith to the confining walls. We also investigate whether these morphology parameters are well controlled under the selected synthesis conditions by repetition of the synthesis procedure and estimation of the capillary-to-capillary, the day-to-day, and the run-to-run repeatability for several chromatographic parameters taking the separation of alkylphenones in RP-CEC as an example.

2. Theoretical considerations

In a polymer-based monolith, the flow-through pores take over the function of the interstitial pores of a particulate chromatographic bed. The total geometrical volume V_G of a monolithic separation capillary is the sum of the volume of the solid stationary phase (polymer, monolith) V_M, and the total volume V_P of the pores, which are accessible to the mobile phase (comprising the volume of the flow-through pores V_F and the volume V_I, which includes the small-size inter-globular pores and the intra-globular pores, ignoring the volume of the permanently closed pores) [$V_G = V_M + V_P = V_M + (V_F + V_I)$]. In other words: when comparing a monolith to a packed bed, the volume of the flow-through pores V_F is regarded to be equivalent to the volume of the interstitial pores, whereas the sum of the volumes of the small-size inter-globular pores and the intra-globular pores V_I is regarded to be equivalent to the volume of the pores within the particles. The distinction between pores belonging to V_F or to V_I can be made on the basis of the type of mass transport within these pores.

Generally, either the elution volume or the elution time (corresponding to each polymer standard) are possible magnitudes for the evaluation of the results of ISEC experiments [15]. However, the flow rates in a monolithic capillary are very small so that their precise measurement is challenging and prone to systematic errors. An alternative is the use of the relative elution time τ, which is defined here to be the elution time of a standard normalized on the elution time of a non-excluded (and non-retained) solute (e.g. toluene): $\tau = t_S/t_T = V_S/V_T$ (t_S and V_S are the elution time and the elution volume of a polymer standard (polystyrene standard), t_T and V_T are the elution time and the elution volume of the marker (e.g. toluene) with $\tau = 1$) [38,39].

The method of Halasz and Martin [33] allows in a very simple way the direct calculation of pore size distribution curves from elution data and has therefore been used by several workers in the characterization of monolithic capillary columns [14,15]. The method is based on a calibration curve which was obtained by the comparison of pore size distribution data obtained with ISEC for several silica gels having narrow pore size distributions to those obtained with the "classical" methods: mercury intrusion porosimetry and evaluation of nitrogen adsorption isotherms. According to the definition given by Halasz and Martin the magnitude ϕ_n is the smallest pore diameter into which a standard with the average molar mass $\overline{M}_{w,n}$ can diffuse "unhindered" (further details are given in the Supplementary data). Therefore ϕ_n is the exclusion limit (with regard to pore dimension) which is assigned to a standard. From plotting $lg(\overline{M}_{w,n}/g\ mol^{-1})$ against $lg(\phi_n/0.1\ nm)$ they obtained a straight line which can be described by the function:

$$\overline{M}_{w,n} = 2.25 \left(\frac{\phi_n}{0.1\ \ nm}\right)^{1.7}\ \ g\ \ mol^{-1} \qquad (1)$$

The fact that this function resembles that obtained for the coil diameters d_c of polystyrene standards dissolved in THF [40] ($\overline{M}_{w,n} = 10.87\,(d_c/0.1\ \text{nm})^{1.7}\ \text{g mol}^{-1}$) gives some evidence for the validity of this approach. Rearrangement of Eq. (1) now permits calculating the exclusion limit ϕ_n for each standard with known $\overline{M}_{w,n}$:

$$\frac{\phi_n}{0.1\ \text{nm}} = 0.62\left(\frac{\overline{M}_{w,n}}{\text{g mol}^{-1}}\right)^{0.59} \quad (2)$$

According to this approach, two polystyrene standards with the weight-averaged mean molar masses $\overline{M}_{w,n}$ and $\overline{M}_{w_{n+1}}$ ($\overline{M}_{w_{n+1}} > \overline{M}_{w_n}$) correspond to the exclusion limits ϕ_n and ϕ_{n+1}, respectively. V_n is then the fractional volume (a fraction of the total pore volume) of those pores that have a size equal to or larger than ϕ_n and V_{n+1} is the fractional volume of those pores that have a size equal to or larger than ϕ_{n+1} (where $\phi_{n+1} > \phi_n$). This means that the fractional volume of the pores inside the monolithic capillary that have a pore diameter larger than ϕ_n and smaller than ϕ_{n+1} is given by the following equation:

$$\Delta V_{n+1,n} = V_{n+1} - V_n = (t_{n+1} - t_n)F \quad (3)$$

where $\Delta V_{n+1,n}$ can be obtained directly from the ISEC data [14,15,31,33] provided that F can be precisely estimated. This is, however, often not the case, when ISEC is performed with monolithic capillaries. In this case the pore size distribution can be deduced directly from the normalized elution times as $\Delta V_{n+1,n}/V_T$ is equivalent to $\Delta\tau = (\tau_{n+1} - \tau_n)$ [14,15,31].

3. Experimental

3.1. Materials and equipments

All chemicals were used without further purification. N,N,N′,N′-tetramethylethylenediamine (TEMED), 3-(trimethoxysilyl) propyl methacrylate (bind silane), di-sodium hydrogen phosphate dihydrate, N,N-dimethylformamide (DMF), ammonium sulfate (AS), and hydrochloric acid were from Fluka (Buchs, Switzerland). Propiophenone, butyrophenone, valerophenone, and hexanophenone, were from Sigma Aldrich (Steinheim, Germany). Vinylsulfonic acid (VSA) (25%, w/v in aqueous solution) was from Sigma Aldrich (Milwaukee, USA). Ammonium persulfate (APS) was from Sigma Aldrich. Methacrylamide, acetic acid, and sodium dihydrogen phosphate monohydrate were from Merck (Darmstadt, Germany). Acetophenone is from Riedel-de Haen (Seelze, Germany). Triethylamine is from KMF Laborchemie (Lohmar, Germany). 1,4-Diacryloylpiperazine (PDA) was either from Alfa-Aesar (Karlsruhe, Germany) or from Molekula (Dorset, UK). Statistically methylated β-CD was either from ABCR (Karlsruhe, Germany) or from Sigma Aldrich (Louis, USA). 1-Adamantanamine was either from Alfa-Aesar (Karlsruhe, Germany) or from ICN Biochemicals (Cleveland, Ohio). N-(1-adamantyl)acrylamide was synthesized according to [6]. Polystyrene standards with narrow molar mass distributions (polydispersity index < 1.1) and average molar masses of 1560, 3460, 10 300, 19 100, 34 000, 65 000, 96 000, 243 000, 335 000, 546 000, 803 000, 944 000, and 2 010 000 g mol^{-1} were from Polymer Standards Service GmbH (Mainz, Germany). Fused silica capillaries (100 μm I.D. × 360 μm O.D.) were from Polymicro Technologies (Phoenix, USA).

With all mobile phases, the electric conductivity κ and the pH* value were controlled. The pH* value is the pH in the presence of an organic solvent with a pH meter calibrated with aqueous buffer. The pH* was determined for the mobile phases after addition of the organic solvent to the aqueous buffer. The pH meter Inolab pH 720, and the conductometer LF 191 (WTW, Weinheim, Germany) were used to measure the pH* and κ of the prepared mobile phases.

Table 1
Composition of the polymerization mixture of the monoliths synthesized with varied content of ammonium sulfate (AS) and varied molar fraction of vinylsulfonic acid (VSA) in the polymerization mixture (in 0.70 mL 100 mM phosphate buffer, pH = 7.0).

Monolith	AS/mg	VSA (25%, w/v)/μL
A	8	15
B	12	15
C	32	15
D	42	15
E	64	15
F	12	35

Total monomer concentration (*T*%): 16.4 (w/v), crosslinker concentration (*C*%): 56.60 (w/w), N-(1-adamantyl)acrylamide: 30 mg, statistically methylated-β-CD: 191 mg, PDA: 65 mg, MA: 20 mg, APS (10%, w/v): 10 μL, TEMED (10%, v/v): 10.0 μL.

Mobile phases and the mixed-mode monolithic stationary phases used in CEC and ISEC measurements were prepared/synthesized according to the procedures described in our previous publication [6]. For monoliths with varied content of ammonium sulfate, all experimental parameters were fixed with exception of the mass of ammonium sulfate (8, 12, 32, 42, and 64 mg) added to the polymerization mixture (Table 1, Monoliths A–E).

3.2. Chromatographic system

The CEC apparatus is already described in [41] and consists of a FUG HCN 35-35000 high voltage generator (F.U.G. Elektronik GmbH, Rosenheim, Germany) with an in-house manufactured electronic steering unit for controlled electrokinetic injection, a spectra 100 UV-VIS detector (Thermo Separation Product, San Jose, CA, USA) with detection cell for in-capillary detection, and a Shimadzu (Kyoto, Japan) LC-10 AD HPLC pump for conditioning and equilibrating the monolithic capillary with new mobile phase using 50–100 bar. Data treatment and recording was done with EZ-Chrom 6.6 (Scientific Software, San Roman, CA, USA).

For the CEC experiments, sample solutions (c = 250–300 mg L^{-1}) were prepared in the mobile phase. Sample injection was performed electrokinetically (injection parameters: 3 kV for 3 s). UV detection was at a wavelength of 230 nm. N,N-dimethylformamide (DMF) was used as non-retained EOF marker. Different water/methanol mobile phases buffered with triethylamine/acetic acid (pH* = 6.8–7.0, κ = 120–150 μS cm^{-1}) were used for separations in the reversed-phase mode. Alkylphenones (acetophenone, propiophenone, butyrophenone, and valerophenone) were employed as neutral test solutes.

3.3. Inverse size exclusion chromatography

As in-house-built ISEC instrument we employed the modified CEC instrumentation described above. Propulsion of mobile phase was with the Shimadzu LC-10 AD HPLC pump. The spectra 100 UV-VIS detector with detection cell for in-capillary detection was operated at 254 nm. Injection was performed with a Rheodyne Model 7752i (Cotati, CA, USA) with a loop volume of 5 μL. A stainless steel T-piece placed after the injector acts as flow splitter. The inlet side of the monolithic capillary is connected to one side of the flow splitter and the outlet side is connected to another auxiliary monolithic capillary used for reducing the flow rate of the mobile phase inside the main monolithic capillary. Another side of the flow splitter is connected to an open-tube restrictory capillary with 25 μm I.D. used for controlling the flow rate inside the main monolithic capillary. The polystyrene standard solutions were prepared in THF (1 g L^{-1} each) employing toluene as t_0 marker. THF was used as mobile phase. Experiments were performed at a constant flow rate of the mobile phase. Toluene is added to each polystyrene standard solution. Each injection was repeated three times.

3.4. SEM experiments

Five different monolithic capillaries freshly prepared under variation of the concentration of ammonium sulfate in the polymerization mixture were rinsed with distilled water for 2–3 h (Monoliths A–E, see Table 1). Each monolithic capillary was cut into six segments at different points along the monolithic capillary. For preparation of the SEM micrographs, these segments were glued vertically onto SEM stubs with help of an electrically conductive adhesive (N650, Plano, Wetzlar, Germany). The capillaries were then sputter-coated with platinum (sputtering time 1.5–2.0 min, thickness approx. 10 mm) to prevent surface charging. Finally the samples were investigated with a field emission scanning electron microscope JEOL JSM-7500F at an electron energy of 5.0 kV using a BSE Detector (Autrata type TS6114, Brno, Czech Republic).

4. Results and discussion

4.1. Scanning electron microscopy

Scanning electron microscopy (SEM) is widely used for the qualitative characterization of the morphology of polymer-based monoliths in the dry state. It is used mainly for analyzing the domain size (average size of globules + average flow through pore diameter) [25].

For a detailed investigation of the impact of the concentration of ammonium sulfate in the polymerization mixture on the formed morphology of the polymer-filled capillary, and consequently, on the chromatographic performance of the produced monoliths, five monoliths were synthesized with varied concentration of ammonium sulfate in the polymerization mixture (Table 1, Monoliths A–E).

In order to study the homogeneity and uniformity of the monolith filling procedure over the length of a 100 μm I.D. capillary, SEM micrographs were taken at different points along the monolithic capillaries and analyzed at different magnifications. As an example, Fig. 1a–c shows for Monolith B three SEM micrographs for three segments of the same monolithic capillary at a fixed magnification of 4000× (further SEM micrographs taken for Monoliths A–E at 4000× and 10 000×, see Figs. S1–S9, Supplementary data). These SEM micrographs show a high degree of similarity and consistency in the magnitudes of the domain size for six segments of the same monolithic capillary, which indicates that the polymeric monoliths synthesized are homogenously and uniformly prepared over the length of a 100 μm I.D. capillary. In addition, the polymer was shown to be tightly bonded to the inner wall of the capillary (Fig. S10a, Supplementary data). A close inspection of the confining wall region revealed the formation of an apparently denser (less macroporous) layer of the formed polymer (Fig. S10b, Supplementary data). This layer originates from the incorporation of pendent methacrylate vinyl groups (bind silane, bonded covalently to the confining wall) into the polymerization reaction, reflecting the efficiency of the capillary pre-treatment step. We conclude that the formed polymeric monolith is effectively covalently attached to the inner capillary wall, and consequently, shrinking can be avoided.

The SEM micrographs were also analyzed for their domain size (average size of globules + average diameter of flow through pores) [25]. The SEM micrographs shown in Fig. 2a–d and Fig. 1 (for further SEM micrographs at different magnifications see Figs. S1–S9, Supplementary data) clearly demonstrate that the morphology of the synthesized monoliths is strongly dependent on the concentration of the lyotropic salt ammonium sulfate in the polymerization mixture. For monoliths synthesized with lower concentration of ammonium sulfate, the formed morphology (Figs. 1 and 2a) is composed of fine, small, and uniformly sized compact spherical microglobules, resulting in apparently small flow-through pores, which corresponds to a small domain size monolith. For monoliths synthesized with higher concentration of ammonium sulfate (Fig. 2b–d) the size of the formed microglobules becomes larger and the microglobules are interconnected to each other forming three dimensional inter-adherence globules (via globule stacking) with irregular size, resulting in an apparently larger volume fraction of the flow-through channels in the monolithic scaffold.

There is a clear increase in the domain size with increasing concentration of ammonium sulfate in the polymerization mixture. It was reported that the separation efficiency of polymer-based monolithic stationary phases varies directly with their domain size [25], so that monoliths with a smaller domain size and a narrower average flow-through pore size are characterized by an improved efficiency. As will be shown in the third paper of this series, these induced variations in the morphology (the domain size) of the synthesized monolithic stationary phases induce characteristic variations in the efficiency determined by CEC with neutral hydrophobic solutes in the RP mode [11].

4.2. Inverse size exclusion chromatography

4.2.1. Chemical stability

Prerequisite of inverse size exclusion chromatography (ISEC) with THF as mobile phase is the chemical stability of the stationary phase against THF. This stability was confirmed by testing selected separation parameters (the electroosmotic mobility and the retention factors for alkylphenones) before and after rinsing and equilibrating the capillary >24 h with a tetrahydrofuran (THF) rich mobile phase (further details are given in the Supplementary data). The results were further confirmed by SEM micrographs taken from the same capillary (cut into two pieces) without and after rinsing with THF (see Figs. S11 and S12, Supplementary data).

4.2.2. Estimation of the exclusion pore size

According to the method suggested by Al-Bokari et al. [15], for each monolithic capillary the logarithm of the normalized average molar mass $\overline{M}_w$ of the polystyrene standard was plotted versus its relative elution time τ (Fig. 3a–d). In each case, the plot obtained (which corresponds to a SEC calibration curve [14]) has a segmented (two slopes) profile, whereas each segment is approximately linear. The existence of a segmented profile in the SEC calibration curve is commonly explained by the presence of two different types of pores [15,31,38,39]. In accordance with Al-Bokari et al. [15], we ascribe the appearance of a segmented (two slopes) profile in the SEC calibration curves to the existence of two different types of pores: (i) pores located inside the (micro)globules (internal pores, intra-globular pores) and (ii) pores which are located between the (micro)globules (external pores, inter-globular pores). From Eq. (2) the value of the exclusion pore size ϕ_e is directly accessible from the intersection point of the two straight lines representing the two segments. We assume that all the pores inside the monolithic capillary having a size equal to or larger than ϕ_e belong to the external pores, while the pores having a size smaller than ϕ_e belong to the internal pores.

In comparing the curves obtained for the different monoliths (Fig. 3a–d), it is observed that the value of the exclusion pore size ϕ_e obtained for each monolith is dependent on the concentration of ammonium sulfate in the polymerization mixture. The value of ϕ_e is shifted to higher values with increasing concentration of ammonium sulfate. For Monolith A (8 mg AS) ϕ_e is around 29.2 nm, for Monolith B (12 mg AS) ϕ_e is 42.8 nm, while for Monoliths C and E (32 and 64 mg AS) ϕ_e is around 53.9 nm. This shift in ϕ_e from 29.2 to 53.9 nm must be ascribed to alterations in the morphology of the synthesized monoliths, which are also documented by the SEM micrographs. Moreover, the slopes of the SEC calibration plots are

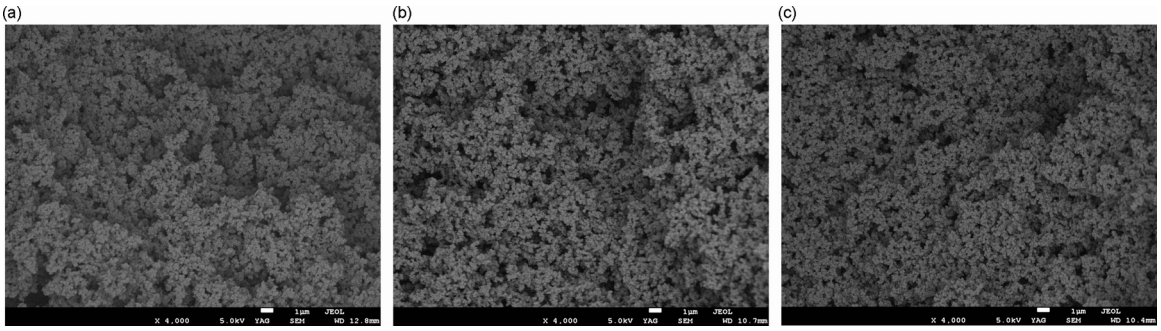

Fig. 1. SEM micrographs of different segments of Monolith B with identical magnification (4000×).

also dependent on the concentration of ammonium sulfate in the polymerization mixture. There is a decrease in the slope of the first part of the curve (internal pores) when comparing Monolith A with B, whereas with Monolith C and E this slope remains approximately constant, while there is a characteristic shift in the starting point. At the same time there is an increase in the slope of the second part of the curve (external pores) going from Monolith A and B to Monolith C and E. This increase is accompanied by a disappearance of the coelution of the standards with high $\overline{M}_w$. As will be shown in the next section, these changes can be fully explained by a shift of the pore size distribution.

4.2.3. Estimation of pore size distributions

Due to experimental restrictions of this work, the pore size distribution inside the monolithic capillaries is expressed as the fractional volume $\Delta V_{n+1,n}$ (i.e. the fractional volume occupied by pores with a larger diameter than ϕ_n and a smaller diameter than ϕ_{n+1}) normalized on the total pore volume V_T. As shown in Section 2 this volume ratio is equivalent to $\Delta\tau$ (Eq. (3)). The data of the pore size distribution obtained for the synthesized monolithic capillaries via the method described in Section 2 are shown in Table 2 and Fig. 4a–d. According to the histograms depicted in Fig. 4a–d the pore size distributions for the four monoliths investigated differ considerably. For Monoliths A and B, the histograms depicted in Fig. 4a–d reveal the presence of a trimodal pore size distribution (three maxima), which implies the presence of three different types of pores, which we ascribe to following types of pores: (i) internal mesopores with a diameter lower than ϕ_e located inside the microglobules, (ii) external mesopores with a diameter between ϕ_e and 325 nm located outside the microglobules in clusters of microglobules, and (iii) external macropores with a diameter larger than 325 nm which are located between the clusters of microglobules (although this definition is not in accordance with the IUPAC definition of mesopores and macropores [14]). This assumption of a trimodal pore size distribution (in accord with the assumption of a hierarchically structured material) is supported by the fact that with this

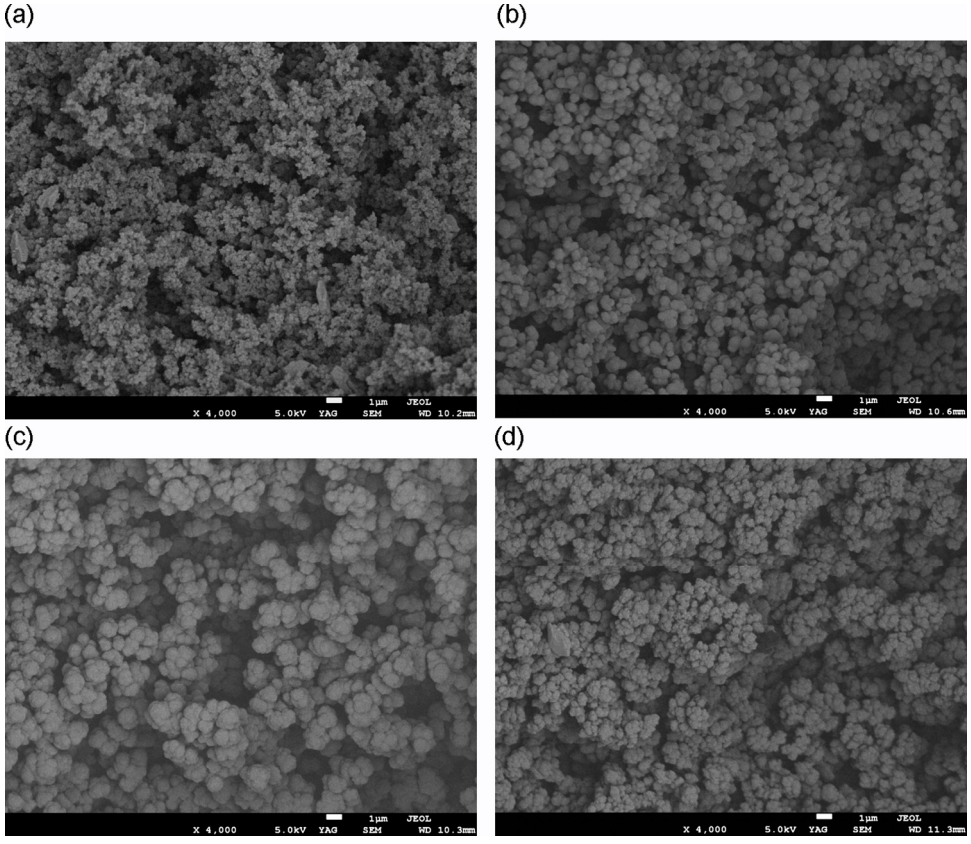

Fig. 2. SEM micrographs for Monolith A, C, D, and E with identical magnification (4000×). (a) Monolith A, (b) Monolith C, (c) Monolith D, and (d) Monolith E. For polymerization mixture composition refer to Table 1.

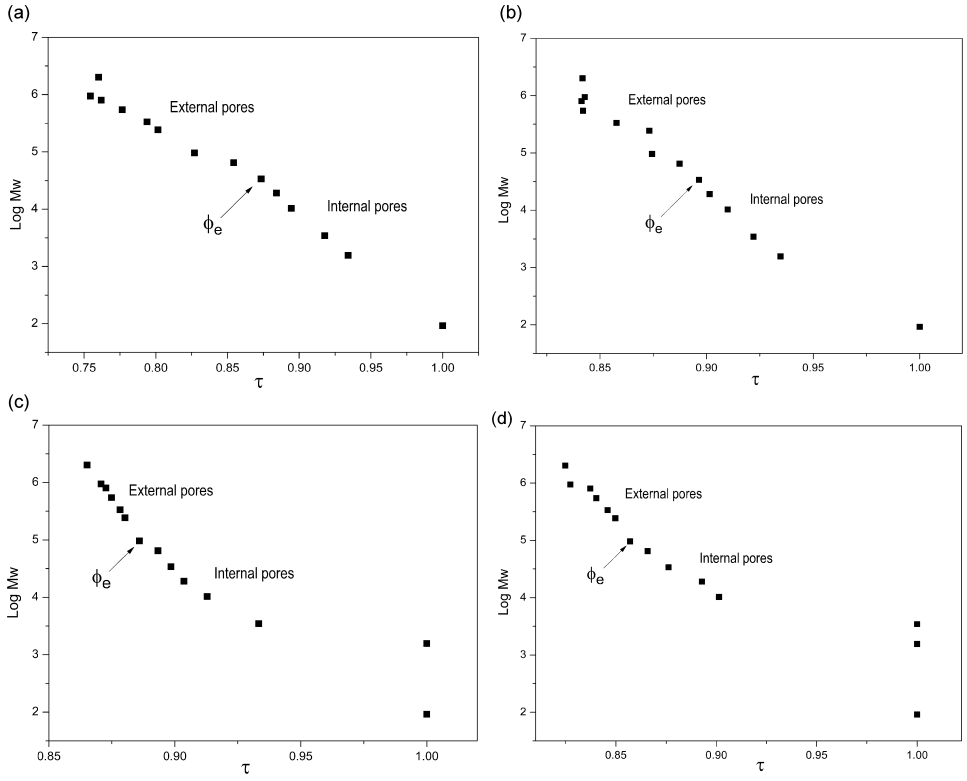

Fig. 3. SEC calibration curves for Monoliths A, B, C, and E. (a) Monolith A, (b) Monolith B, (c) Monolith C, and (d) Monolith E. Relative elution time τ = elution time of polystyrene standard divided by elution time of toluene. Mobile phase: THF, UV detection at 254 nm. Polystyrene standards dissolved in THF at $c = 1\ g\ L^{-1}$. For polymerization mixture composition refer to Table 1.

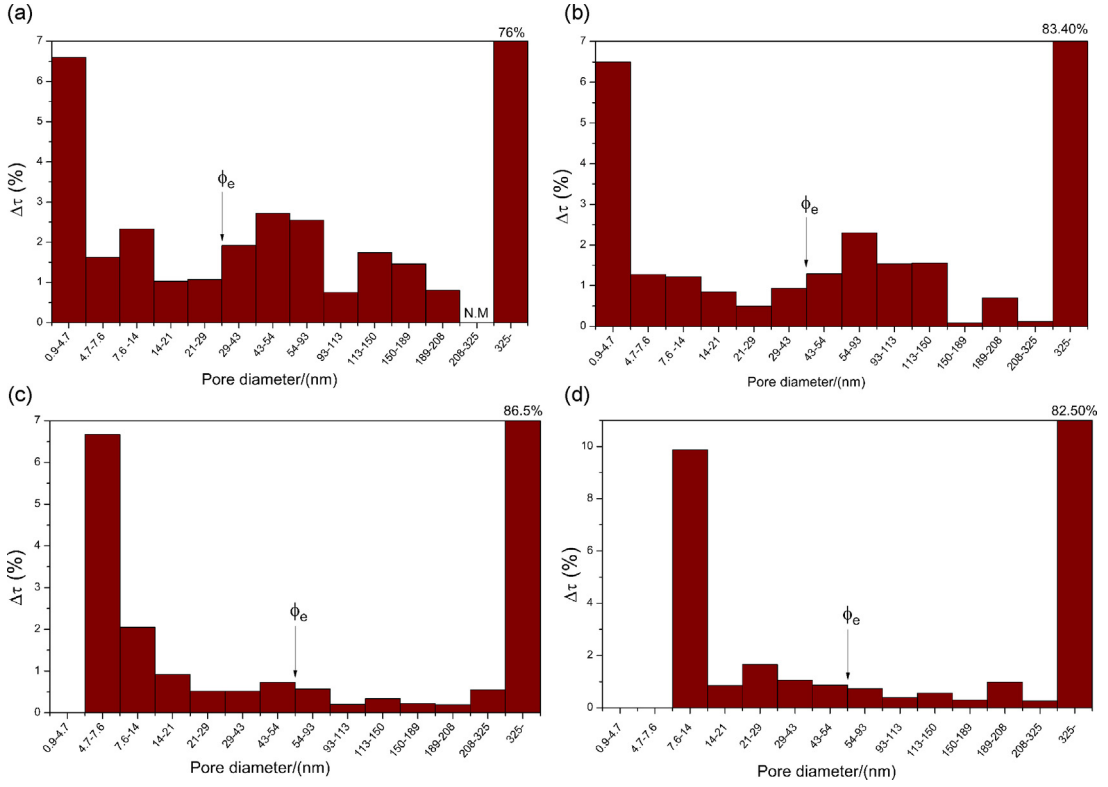

Fig. 4. Pore size distributions for Monoliths A, B, C, and E measured by ISEC. (a) Monolith A, (b) Monolith B, (c) Monolith C, and (d) Monolith E. Experimental conditions see Fig. 3. For polymerization mixture composition refer to Table 1.

Table 2
Exclusion pore diameters ϕ_n assigned for toluene and polystyrene standards, and associated fractional volume $\Delta V_{n+1,n}$ normalized on the total pore volume V_T expressed as $\Delta\tau$ % for Monolith A, B, C, and E (for polymerization composition refer to Table 1).

$\overline{M}_{w,n}$	ϕ_n (nm)	$\Delta\phi$ (nm)	$\Delta\tau$ (% for the Monoliths)			
			A	B	C	E
Toluene	0.9	0.9–4.7	6.60	6.55	0.00	0.00
1560	4.7	4.7–7.6	1.63	1.27	6.67	0.00
3460	7.6	7.6–14.4	2.33	1.21	2.05	9.87
10 300	14.4	14.4–20.8	1.03	0.82	0.92	0.85
19 100	20.8	20.8–29.2	1.07	0.50	0.52	1.66
34 000	29.2	29.2–42.8	1.92	0.90	0.52	1.05
65 000	42.8	42.8–53.9	2.72	1.30	0.73	0.86
96 000	53.9	53.9–93.3	2.55	0.14	0.57	0.73
243 000	93.3	93.3–113	0.75	1.55	0.21	0.39
335 000	113	113–150	1.74	1.56	0.34	0.55
546 000	150	150–189	1.46	0.08	0.20	0.30
803 000	189	189–208	0.80	0.70	0.20	0.99
944 000	208	208–325	N.M.	0.12	0.55	0.26
2 010 000	325	>325	76.0	83.30	86.52	82.50

type of monolith there is a coelution of the standards having highest $\overline{M}_w$, which is typical for chromatographic beds with interstitial pores. The volume fraction of the external mesopores can easily be determined by adding the values listed in Table 2 between ϕ_e and 325 nm. This value is 11.9% for Monolith A and 5.5% for Monolith B.

In contrast to this trimodal pore size distribution, with Monolith C and E there is only a bimodal pore size distribution defined by the presence of only two different types of pores: (i) internal pores with a diameter lower than ϕ_e located inside the microglobules, and (ii) external pores with a diameter larger than ϕ_e located outside the microglobules. In accordance with the large slope of the second part of the SEC calibration curve (external pores), the volume fraction of pores with diameters between ϕ_e and 325 nm is very low. For Monoliths C and E the pores, which we have denoted external mesopores, are no longer visible as a distinct type of pores.

In comparing the histograms obtained for the different monoliths (Fig. 4a–d), it is also observed that the percentage of the contribution of each type of pores to the total pore volume is affected by the concentration of ammonium sulfate in the polymerization mixture (Table 3). As a general trend, for Monoliths A–C the volume fraction of the internal pores (11.3–12.6%) is shown to be only slightly varied, while for Monolith E this magnitude is shifted to a higher value (14.30%). In Table 3 we have also listed the volume fractions of mesopores and macropores (according to IUPAC nomenclature). Here, for Monoliths A–C the volume fraction of mesopores decreases strongly from 17.3% to 11.4%, while with Monolith E a value of 14.3% was determined.

In order to explain the differences in the volume fractions of mesopores and macropores and internal and external porosities (see Table 3) for the different monoliths, a close inspection of their morphology is needed. As shown in Section 4.1(SEM micrographs), Monoliths A–C have a hierarchical structure consisting of microglobules, clusters of microglobules, and interconnected clusters of microglobules forming the monolithic scaffold, whereas for Monolith E there are no (spherical) microglobules visible and the morphology consists of interconnected highly branched structures. There is a clear change in the morphology going from Monolith C to Monolith E, which is obviously reflected by the values determined for Monolith E regarding both volume fraction of mesopores and internal porosity. These two values are not within the trend which is given by the values determined for Monoliths A–C. On the other hand, for Monoliths A–C there is a clear trend for the volume fraction of mesopores, while the internal porosity remains approximately constant. This trend can be explained by a shift of the pore size distribution of the internal pores to higher values when increasing the concentration of ammonium sulfate in the polymerization mixture. This assumption is corroborated by the observation of an increase in the size of the microglobules with increasing concentration of ammonium sulfate in the polymerization mixture (see Fig. 2). This trend is followed by the volume fraction of the external mesopores: 11.9% for Monolith A, 5.5% for Monolith B, and not identifiable for Monolith C.

Another interesting observation visible in Figs. 3 and 4 is the coelution of the smallest size polystyrene standard (1560 g mol^{-1}) with toluene obtained for Monolith C and the coelution of the two smallest size polystyrene standards (1560 and 3460 g mol^{-1}) with toluene obtained for Monolith E. From this observation follows that for Monolith C the volume fraction of the internal pores with a diameter $\leq$4.7 nm is negligible while this is the case for Monolith E with internal pores having a diameter $\leq$7.6 nm. This observation is consistent with the described shift of the pore size distribution of the internal pores to higher values induced by increasing the concentration of ammonium sulfate in the polymerization mixture.

In order to explain the apparent absence of very small mesopores in monoliths synthesized with higher concentration of ammonium sulfate in the polymerization mixture (Monoliths C and E), another phenomenon occurring during the ISEC experiments has to be taken into consideration. It was observed that the ISEC experiments started with constant elution volumes for those monoliths synthesized with a lower concentration of ammonium sulfate in the polymerization mixture (Monoliths A and B) whereas for monoliths synthesized with a higher concentration of ammonium sulfate in the polymerization mixture (Monoliths C and E), the results indicated that equilibration had not been reached. After that, Monoliths C and E were rinsed with THF for 5–6 h without sample injection, and subsequently the monolithic capillaries were left overnight under THF conditions. After this procedure the ISEC experiments were started again with constant elution volumes.

This phenomenon is explained by us with the swelling of those parts of the monolith that are in contact with the organic solvent THF and the development of a layer having a gel porosity. Gel pores are formed as a result of the solvation and swelling of those polymer

Table 3
Pore volume fractions determined from ISEC data for internal pores, external pores, mesopores, and macropores.

Monolith	Internal pores (%)	External pores (%)	Mesopores (%)	Macropores (%)
A	12.66	87.34	17.30	82.70
B	11.24	88.76	12.55	87.45
C	11.41	88.59	11.41	88.59
E	14.30	85.70	14.29	85.71

Table 4
Capillary-to-capillary, day-to-day, and run-to-run reproducibility of Monolith B; overall relative standard deviation for electroosmotic mobility μ_{eo}, retention factors of acetophenone and butyrophenone.

RSD (%)	μ_{eo} (cm^2 kV^{-1} min^{-1})	k (acetophenone)	k (butyrophenone)
Capillary to capillary N = 15 (5 capillaries, each 3 runs)	15.15	2.35	3.30
Day to day N = 36 (4 days, each 9 runs)	0.73	1.00	1.01
Run to run N = 19	0.43	0.75	0.84

Mobile phase: methanol/water (50:50, v/v) buffered with triethylamine/acetic acid, pH* = 7.0, electric conductivity = 125 μS cm^{-1}.

Table 5
Between groups variance s_B^2, within groups variance s_W^2, and ratio of variances S_B^2/S_W^2 for electroosmotic mobility μ_{eo} and retention factors for acetophenone and butyrophenone determined as capillary-to-capillary and as day-to-day repeatability on Monolith B. For other experimental conditions see Table 4.

	Capillary-to-capillary				Day-to-day			
	s_B^2	s_W^2	S_B^2/S_W^2	$F_{4,10,95}$ crit.	s_B^2	s_W^2	S_B^2/S_W^2	$F_{3,32,95}$ crit.
μ_{eo} ($cm^2\ kV^{-1}\ min^{-1}$)	2.04449	0.000574	3563	3.478	0.0082	0.00087	9.373	2.901
k (acetophenone)	0.000107	0.0000037	28.45	3.478	0.00003	0.000002	13.24	2.901
k (butyrophenone)	0.000616	0.0000076	81.24	3.478	0.00007	0.000008	9.466	2.901

chains, which are only slightly cross-linked. According to the definition given by Heitz and Kern [42] gel porosity is characterized to be present in swollen statistically crosslinked polymers. These polymers do not show any porosity in the unswollen state. This type of porosity has to be distinguished from the porosity which is found with highly crosslinked materials which are produced by a polymerization process involving a phase separation. These materials are porous also in the unswollen state.

As described in a further paper of this series [11], Monoliths C and D deviate in their chromatographic properties significantly from Monoliths A and B: Whereas for Monoliths A and B the minimum plate height H_{min} for alkylphenones separated by CEC in the RP mode (determined as the lowest point in the corresponding Van Deemter plot) is quasi-independent of the retention factor ($k < 0.4$), for Monoliths C and D the minimum plate height H_{min} (for the same solutes) is significantly higher and strongly dependent on the retention factor. Obviously, there is a transition in the material (porous) properties when comparing Monoliths A + B with Monoliths C–E. Those properties observed with the monoliths with larger domain size can be ascribed (in part) to the development of a gel porosity, which is apparently absent or less pronounced for monoliths with smaller domain size.

The concept of gel porosity was introduced into the discussion on macroporous polymers by Nischang and Brueggemann [10] and Nischang et al. [16]. They reported that slightly crosslinked polymer chains are generated in the advanced stage of the polymerization process as a result of the different reaction rates exhibited by mono- and divinyl monomers used in the copolymerization reaction. These soft layers swell in contact with a hydroorganic solvent, resulting in a non-uniform gel (non-uniform with respect to crosslinking degree and pore-size distribution after swelling), which is containing (small-size) micropores and mesopores. Nischang [3] reported that the development of this type of porosity is strongly dependent on the globule (domain) size (more pronounced in monoliths with larger globule size), the degree of crosslinking, and the type and volume fraction of the organic modifier in the mobile phase.

4.3. Repeatability of the synthesis procedure

In order to investigate whether the CEC instrument employed in these investigations and the synthesis procedure developed by us can be used for routine analysis, the capillary-to-capillary, the day-to-day, and the run-to-run repeatabilities were measured for Monolith B (see Table 1) using a test mixture of acetophenone and butyrophenone (Table 4). Five monolithic capillaries are prepared from the same polymerization mixture and tested for the separation of acetophenone and butyrophenone under identical conditions (capillary-to-capillary RSD). For each capillary, three runs were performed by measuring the electroosmotic mobility μ_{eo} and the retention factors for the alkylphenones. In another study, the day-to-day repeatability was investigated by calculating the RSD for the same parameters for 36 runs (4 days, each 9 runs). In the same regard, the run-to-run repeatability was investigated by calculating the RSD for these parameters for nineteen runs performed within one day with one Monolith B. All these values are listed in Table 4. These results show that the synthesis procedure can be regarded to be well controlled (capillary-to-capillary RSD for the retention factor = 2.3–3.3%, whereas capillary-to-capillary RSD for the electroosmotic mobility = 15%). In contrast to these values the run-to-run RSD is much lower with 0.43% for the electroosmotic mobility and 0.75–0.84% for the determined retention factors confirming the precision and the reliability of the CEC instrument used.

We were interested to investigate, whether the fact that the temperature cannot be controlled has a significant impact on the variance measured. To this end, analysis of variance (ANOVA) [43] was used to assess whether there is a significant difference between the values obtained for μ_{eo} and k within four days for one capillary (day-to-day repeatability) or for five capillaries (capillary-to-capillary repeatability). The variances between the groups s_B^2 (five capillaries or four days) and within the groups s_W^2 (within one day or within one capillary) were calculated. The ratio of the variances s_B^2/s_W^2 are compared to the tabulated F-values (see Table 5). In all cases the between groups variance is significantly higher than the within groups variance ($F_{calculated} > F_{tabulated}$). This means that testing one capillary at different days introduces a source of variance which is seen by us to be the uncontrolled temperature. Variation in the temperature of the separation capillary has an impact on the electroosmotic mobility via change in the viscosity of the mobile phase, and an impact on the retention factor via change in the distribution coefficient.

However, ANOVA also shows that the source of variance introduced by testing different capillaries is much higher, so that in the present case the precision of those data gained with different capillaries at different days is not biased by the uncontrolled temperature. Major sources of variance expected for the capillary-to-capillary repeatability are differences in the monoliths tested with regard to phase ratio, morphology, chemical composition of the copolymer (hydrophobicity), and zeta potential at the liquid/solid-interface [44].

5. Conclusions

Morphology and porous properties of the synthesized polyacrylamide-based continuous beds can be studied by a combination of inverse size exclusion chromatography (ISEC) and scanning electron microscopy (SEM). The pore size distribution estimated via the method of Halasz and Martin [33] reveals characteristic differences between the monolithic capillaries studied. Whereas in two cases there are trimodal pore size distributions, in other cases there are only bimodal size distributions. ISEC clearly demonstrates that a considerable fraction of the pore volume must be assigned to pores with a diameter $\leq$200 nm. In all cases there is an internal porosity, which we ascribe to pores inside the microglobules. In all cases the material is clearly mesoporous (volume fraction of mesopores varies between 17.3% and 11.4%). The pore size distributions determined by ISEC are highly dependent on the concentration of ammonium sulfate in the polymerization mixture. SEM micrographs of the monoliths inside the capillaries confirm homogeneity and uniformity of the formed monoliths including the efficient covalent attachment of

the produced polymeric monolith onto the inner capillary wall. The SEM micrographs corroborate the results obtained by ISEC and show a strong dependence of the formed morphology on the concentration of ammonium sulfate in the polymerization mixture. Monoliths synthesized in this work show a high chemical stability against organic solvents by testing selected separation parameters and taking SEM micrographs before and after rinsing and equilibrating the capillary >24 h with THF. There is an excellent capillary-to-capillary, day-to-day, and run-to-run reproducibility reached for the electroosmotic mobility and the retention factors determined with alkylphenones in the reversed-phase mode.

Acknowledgements

A.A. Al-Massaedh thanks Al Albayt University (Mafraq, Jordan) for financial support. We also thank Mr. M. Hellwig (Electron Microscopy and Microanalysis Laboratory, University of Marburg, Marburg, Germany) for carrying out the SEM measurements. We are very grateful to Prof. Dr. S. Agarwal (University of Bayreuth, Germany) for giving us samples of the polystyrene standards.

Appendix A. Supplementary data

Supplementary data associated with this article can be found, in the online version, at http://dx.doi.org/10.1016/j.chroma.2013.12.026.

References

[1] I. Nischang, J. Chromatogr. A 1287 (2013) 39.
[2] M. Laher, T.J. Causon, W. Buchberger, S. Hild, I. Nischang, Anal. Chem. 85 (2013) 5645.
[3] I. Nischang, J. Chromatogr. A 1236 (2012) 152.
[4] I. Nischang, I. Teasdale, O. Brueggemann, Anal. Bioanal. Chem. 400 (2011) 2289.
[5] J. Urban, P. Jandera, Anal. Bioanal. Chem. 405 (2013) 2123.
[6] A.A. Al-Massaedh, U. Pyell, J. Chromatogr. A 1286 (2013) 183.
[7] T. Muellner, A. Zankel, C. Mayrhofer, H. Reingruber, A. Hoeltzel, Y. Lv, F. Svec, U. Tallarek, Langmuir 28 (2012) 16733.
[8] P.G. Wang (Ed.), Monolithic Chromatography and its Modern Applications, ILM Publications, St. Albans, UK, 2010.
[9] G. Guiochon, J. Chromatogr. A 1168 (2007) 101.
[10] I. Nischang, O. Brueggemann, J. Chromatogr. A 1217 (2010) 5389.
[11] A.A. Al-Massaedh, U. Pyell, J. Chromatogr. A (2013), http://dx.doi.org/10.1016/j.chroma.2013.11.003.
[12] V. Ratautaite, A. Maruska, M. Erickson, O. Kornysova, J. Sep. Sci. 32 (2009) 2582.
[13] T. Jiang, J. Jiskra, H.A. Claessens, C.A. Cramers, J. Chromatogr. A 923 (2001) 215.
[14] J. Urban, S. Eeltink, P. Jandera, P.J. Schoenmakers, J. Chromatogr. A 1182 (2008) 161.
[15] M. Al-Bokari, D. Cherrak, G. Guiochon, J. Chromatogr. A 975 (2002) 275.
[16] I. Nischang, I. Teasdale, O. Brueggemann, J. Chromatogr. A 1217 (2010) 7514.
[17] F. Svec, J. Chromatogr. A 1217 (2010) 902.
[18] E.C. Peters, F. Svec, J.M.J. Frechet, Adv. Mater. 11 (1999) 1169.
[19] C. Viklund, F. Svec, J.M.J. Frechet, K. Irgum, Chem. Mater. 8 (1996) 744.
[20] F. Svec, J.M.J. Frechet, Chem. Mater. 7 (1995) 707.
[21] D. Hoegger, R. Freitag, Electrophoresis 24 (2003) 2958.
[22] S. Xie, F. Svec, J.M.J. Frechet, J. Polym. Sci. A: Polym. Chem. 35 (1997) 1013.
[23] S. Eeltink, L. Geiser, F. Svec, J.M.J. Frechet, J. Sep. Sci. 30 (2007) 2814.
[24] S. Eeltink, J.M. Herrero-Martinez, G.P. Rozing, P.J. Schoenmakers, W.T. Kok, Anal. Chem. 77 (2005) 7342.
[25] P. Aggarwal, H.D. Tolley, M.L. Lee, Anal. Chem. 84 (2012) 247.
[26] R. Ludewig, S. Nietzsche, G.K.E. Scriba, J. Sep. Sci. 34 (2011) 64.
[27] T.A.E. Jakschitz, C.W. Huck, S. Lubbad, G.K. Bonn, J. Chromatogr. A 1147 (2007) 53.
[28] J. Courtois, M. Szumski, F. Georgsson, K. Irgum, Anal. Chem. 79 (2007) 335.
[29] J. Crawshaw, R.E. Cameron, Polymer 41 (2000) 4691.
[30] J.L. Cabral, D. Bandilla, C.D. Skinner, J. Chromatogr. A 1108 (2006) 83.
[31] H. Guan, G. Guiochon, J. Chromatogr. A 731 (1996) 27.
[32] S. Brunauer, P.H. Emmett, E. Teller, J. Am. Chem. Soc. 60 (1938) 309.
[33] I. Halasz, K. Martin, Angew. Chem. Int. Ed. Engl. 17 (1978) 901.
[34] J.H. Knox, H.P. Scott, J. Chromatogr. 316 (1984) 311.
[35] I. Nischang, F. Svec, J.M.J. Frechet, J. Chromatogr. A 1216 (2009) 2355.
[36] R. Fuessler, H. Schaefer, A. Seubert, Anal. Bioanal. Chem. 372 (2002) 705.
[37] B.A. Grimes, R. Skudas, K.K. Unger, D. Lubda, J. Chromatogr. A 1144 (2007) 14.
[38] A. Korolev, E. Victorova, T. Ibragimov, A. Kanatyeva, A. Kurganov, J. Sep. Sci. 35 (2012) 957.
[39] E.N. Viktorova, A.A. Korolev, T.R. Ibragimov, A.A. Kurganov, Polym. Sci. Ser. A 53 (2011) 899.
[40] M.E. Van Kreveld, N. Van Den Hoed, J. Chromatogr. 83 (1973) 111.
[41] A. Wahl, I. Schnell, U. Pyell, J. Chromatogr. A 1044 (2004) 211.
[42] W. Heitz, W. Kern, Angew. Makromol. Chem. 1 (1967) 150.
[43] J.N. Miller, J.C. Miller, Statistics for Analytical Chemistry, Ellis Horwood Limited, London, 1993.
[44] F. Al-Rimawi, U. Pyell, J. Sep. Sci. 29 (2006) 2816.

Adamantyl-group containing mixed-mode acrylamide-based continuous beds for capillary electrochromatography. Part II. Characterization of the synthesized monoliths by inverse size exclusion chromatography and scanning electron microscopy

"Ayat Allah" Al-Massaedh, Ute Pyell*

University of Marburg, Department of Chemistry, Hans-Meerwein-Straße, D-35032 Marburg, Germany

* corresponding author

Supplementary data

Figure S1-S9: SEM micrographs for Monoliths A, B, C, D, and E at magnifications 4000x and 10000x (for polymerization composition see Tab. 1).

Figure S10: SEM micrograph for Monoliths F and C showing the covalent attachment of the polymeric monolith to the inner capillary wall (Fig. S10 a) and the formation a of less macroporous layer at the inner capillary wall (Fig. S10 b) as result of a successful capillary pre-treatment step.

Table S1-S3: Run-to-run, day-to-day, and capillary-to-capillary repeatability data for the retention factor of acetophenone, the retention factor of butyrophenone, and the electroosmotic mobility on Monolith B (see Tab. 1).

Section S1: Comment on the applicability of the method of Halasz and Martin.

Section S2: Investigation of the chemical stability of the synthesized monolith under ISEC conditions.

Table S4: Electroosmotic mobility, retention factors, and plate heights determined for the separation of alkylphenones before and after rinsing Monolith F with THF.

Figures S11+S12: SEM micrographs for Monolith F without and after rinsing with THF.

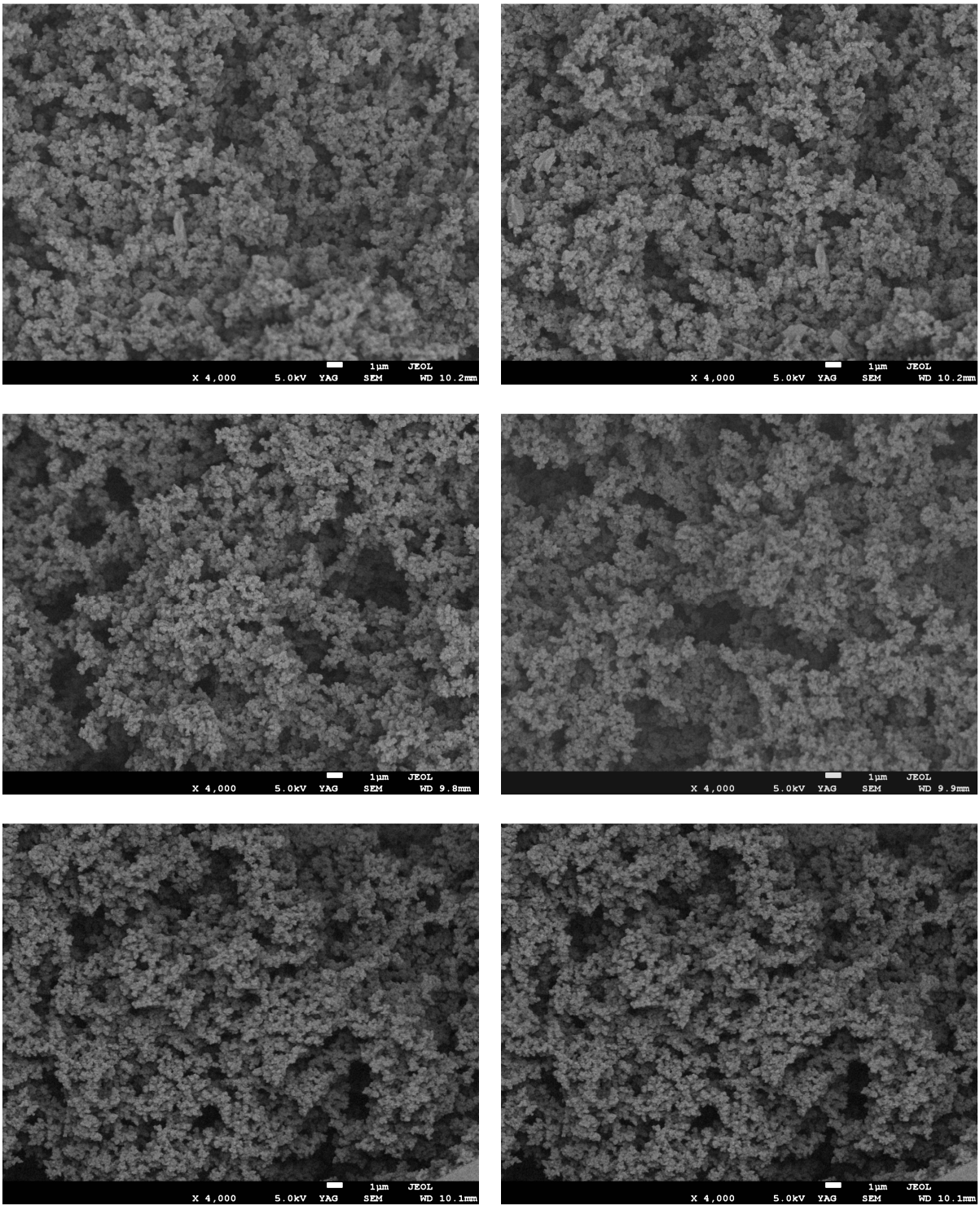

Figure S1. SEM micrographs for Monolith A with identical magnifications (4000 x).

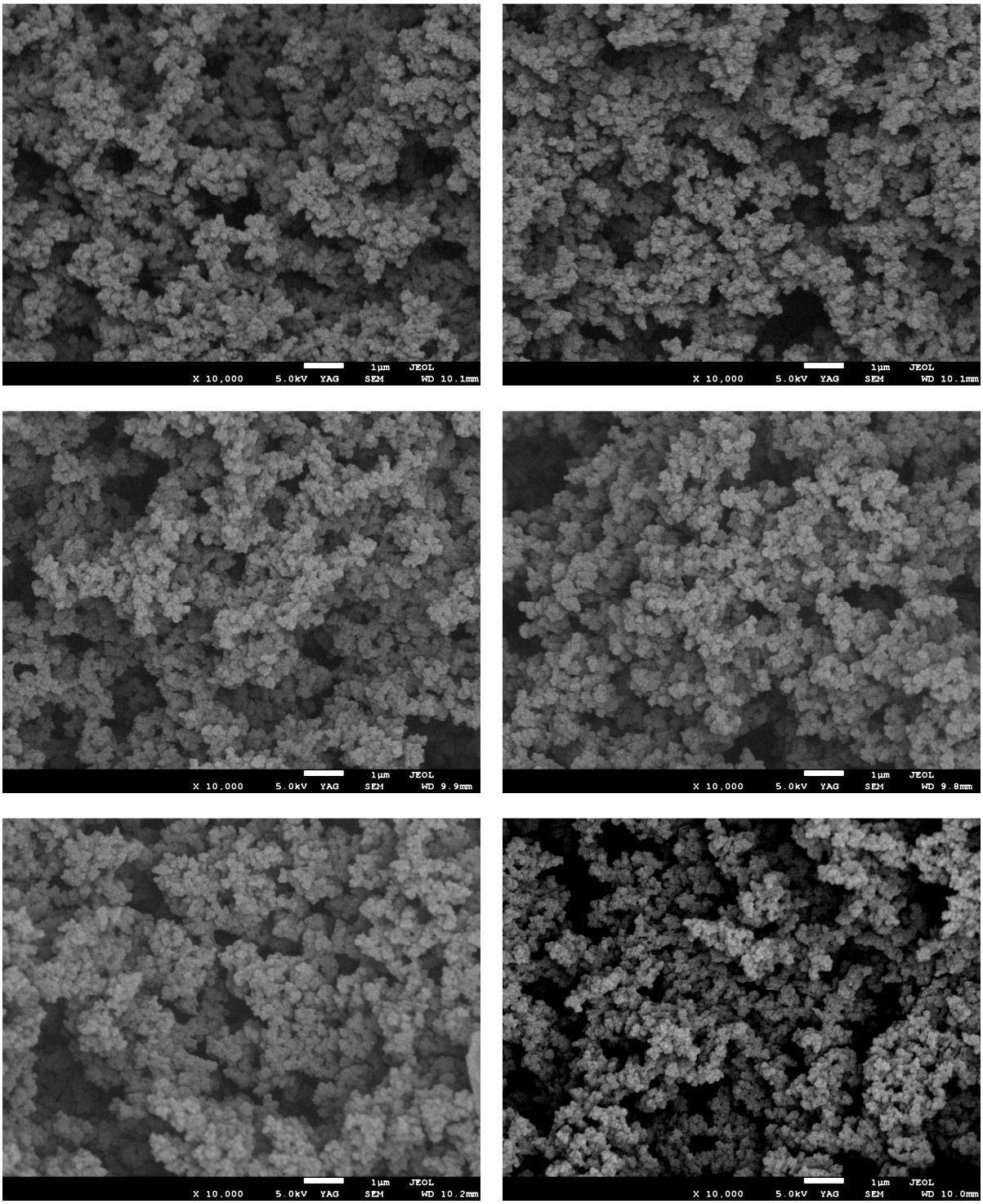

Figure S2. SEM micrographs for Monolith A with identical magnifications (10000x).

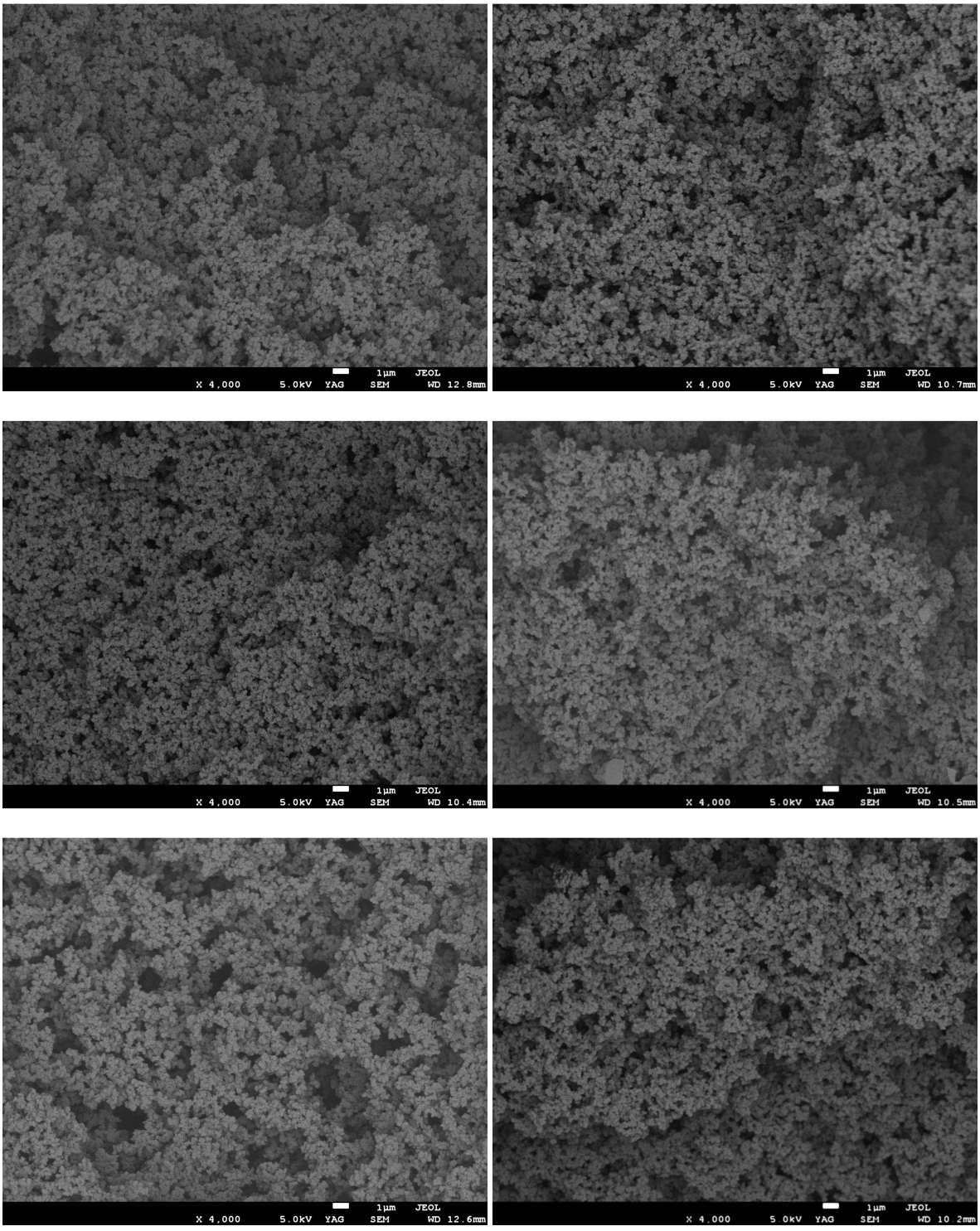

Figure S3. SEM micrographs for Monolith B with identical magnifications (4000x).

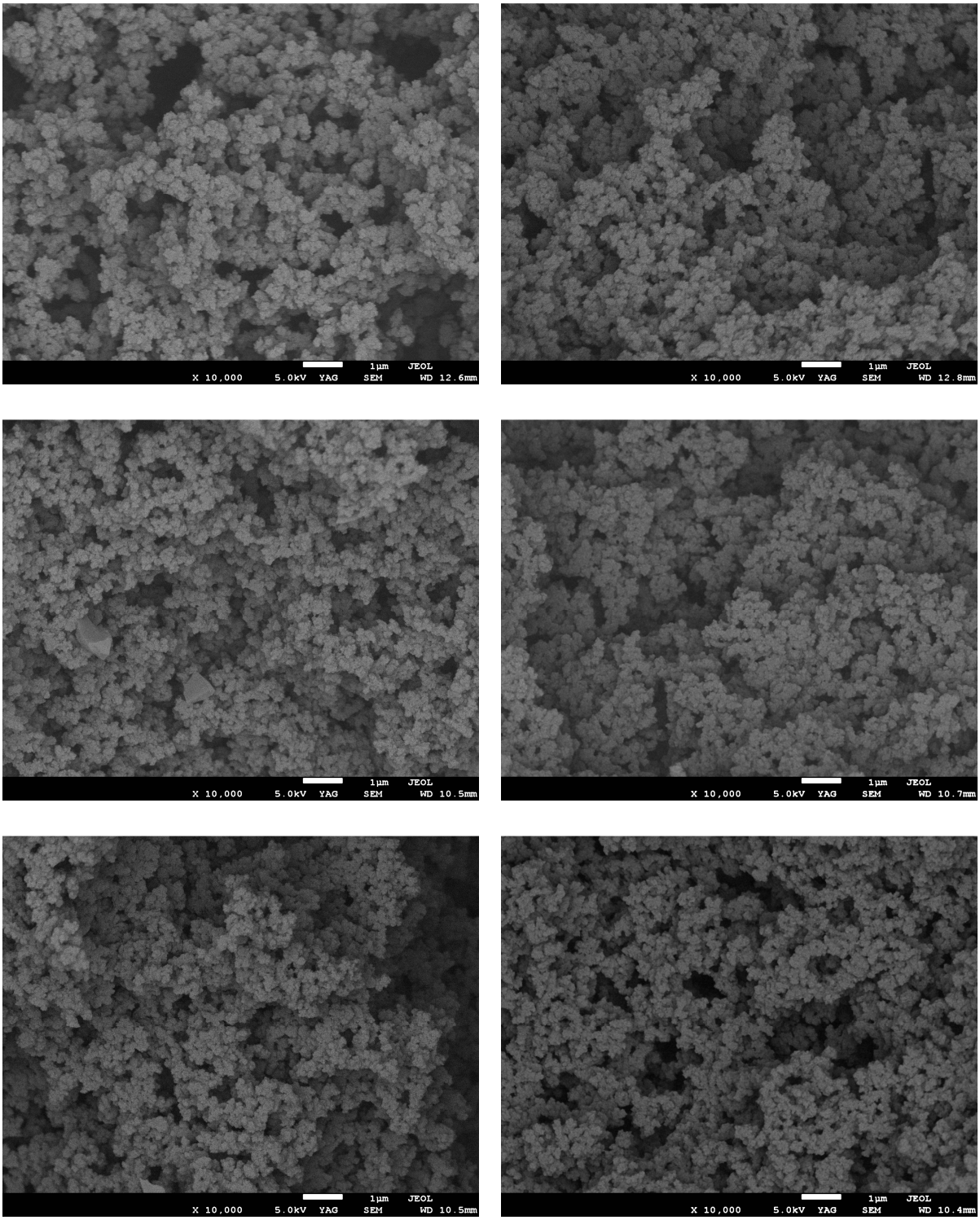

Figure S4. SEM micrographs for Monolith B with identical magnifications (10000x).

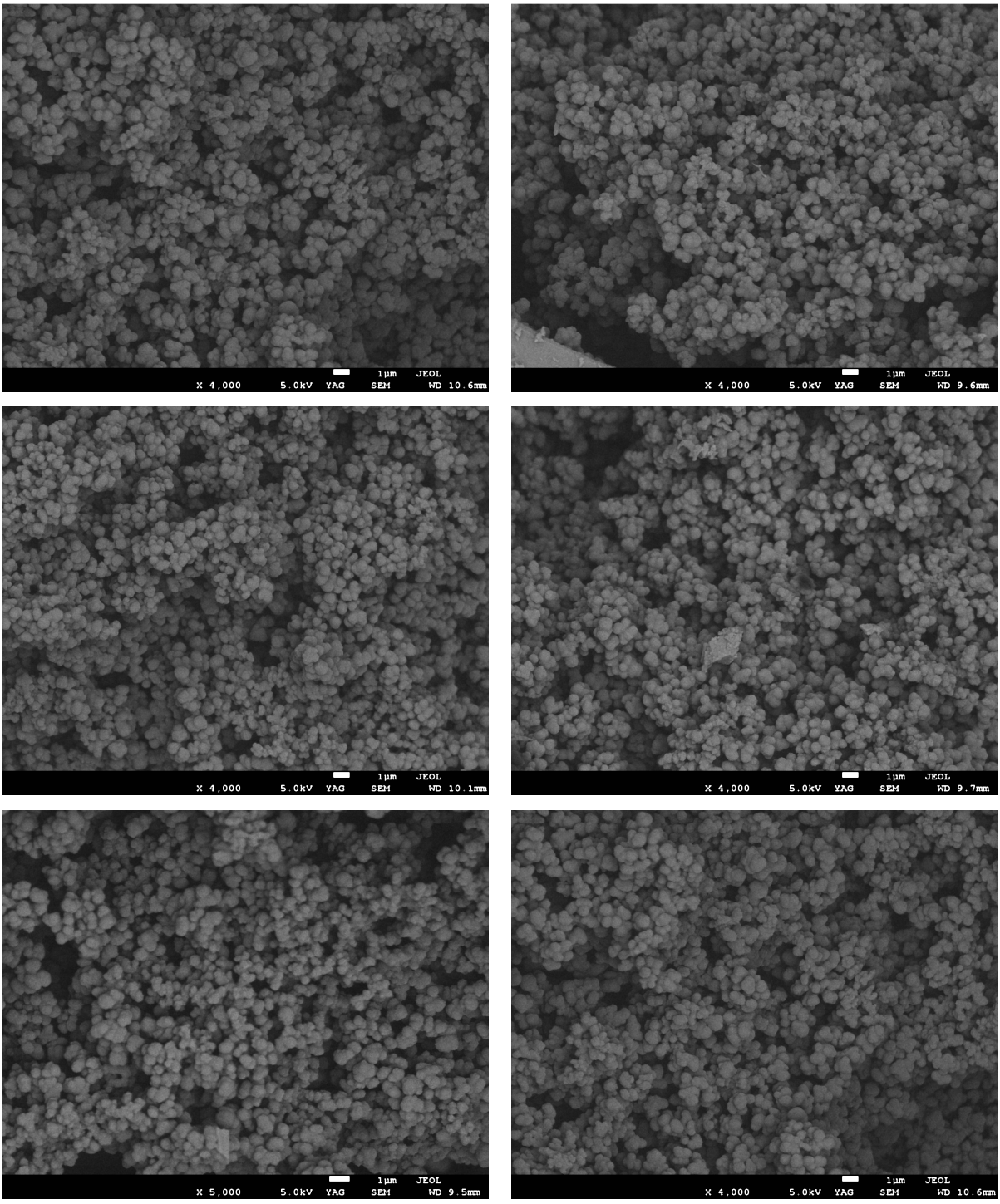

Figure S5. SEM micrographs for Monolith C with identical magnifications (4000x).

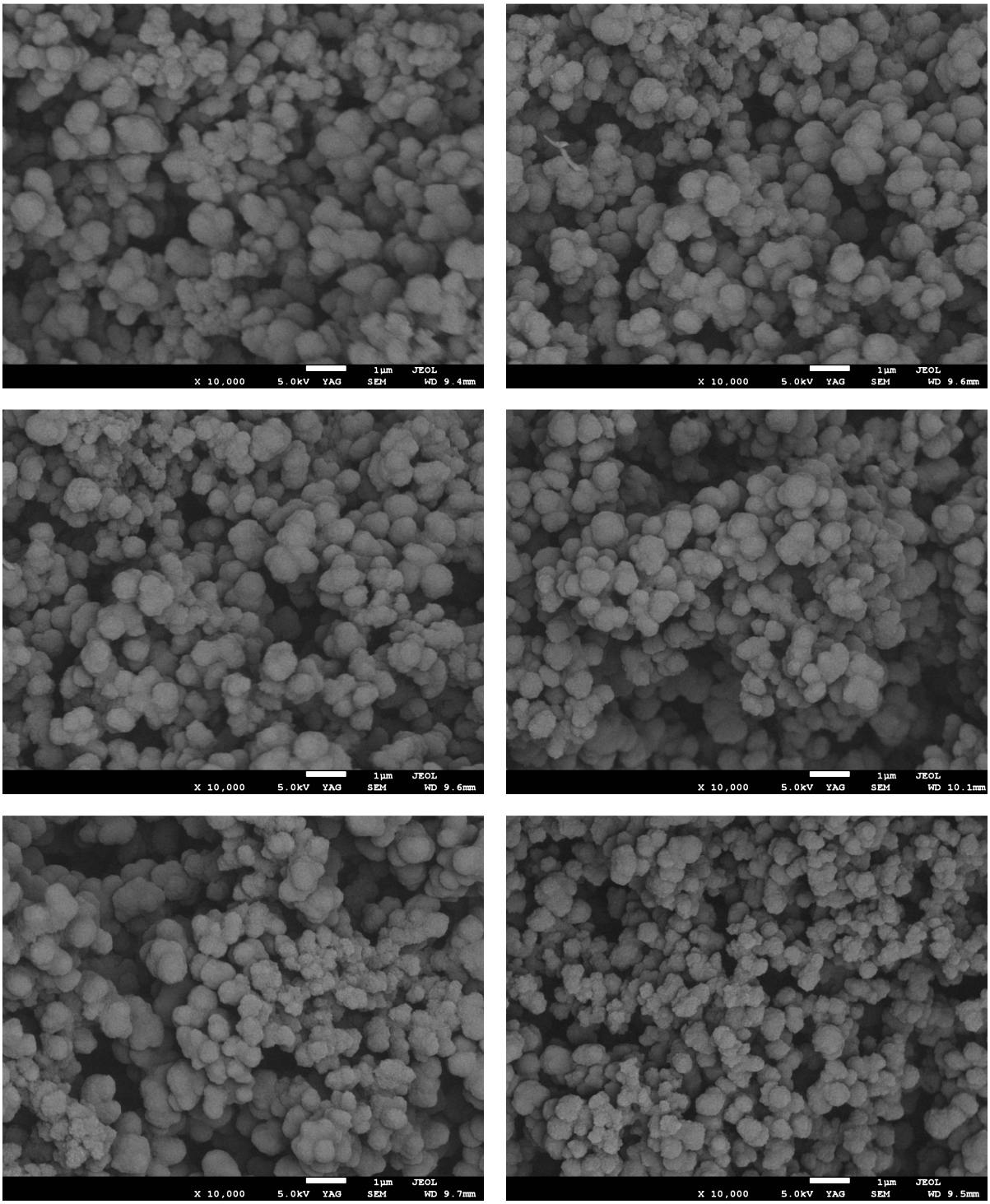

Figure S6. SEM micrographs for Monolith C with identical magnifications (10000x).

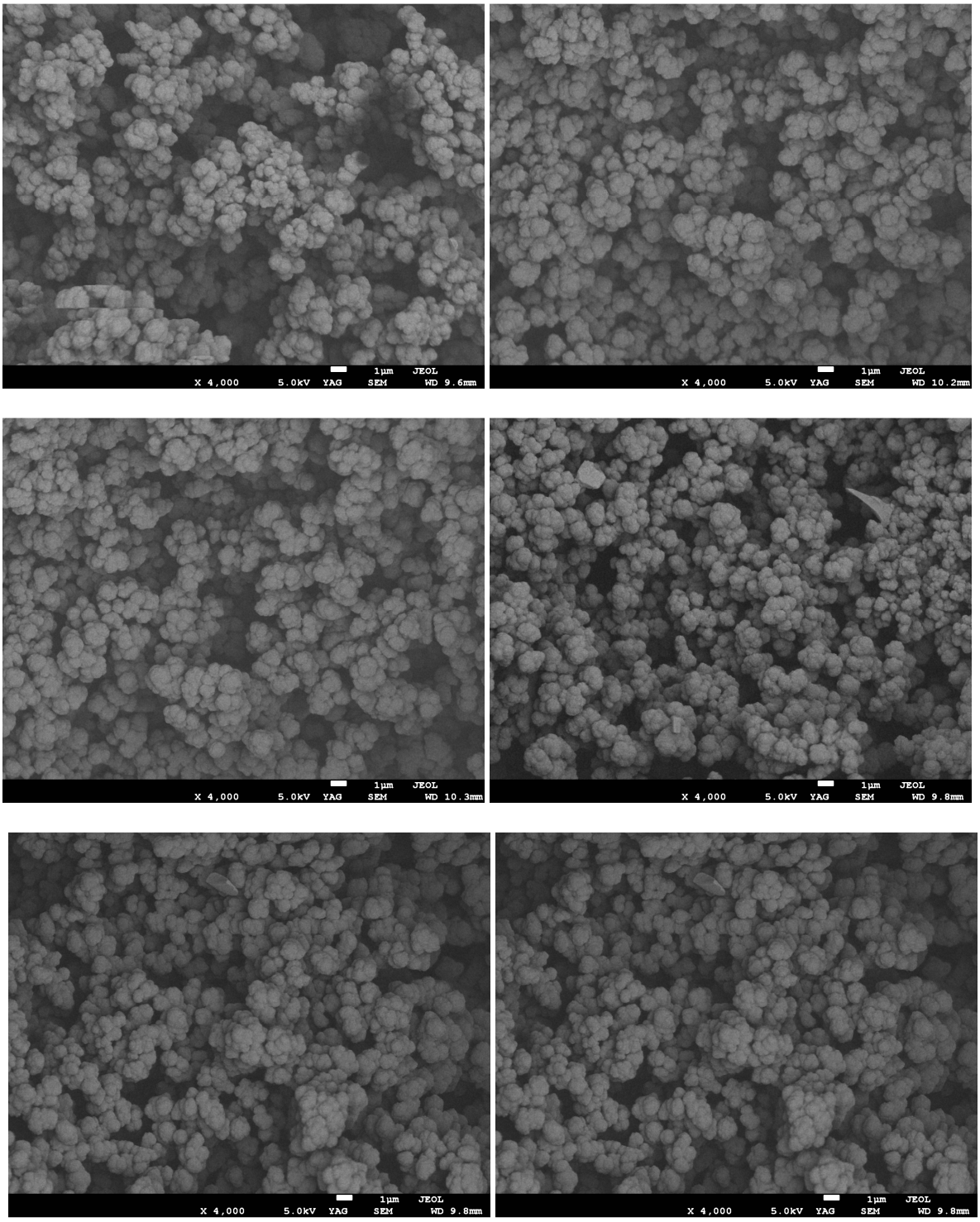

Figure S7. SEM micrographs for Monolith D with identical magnifications (4000x).

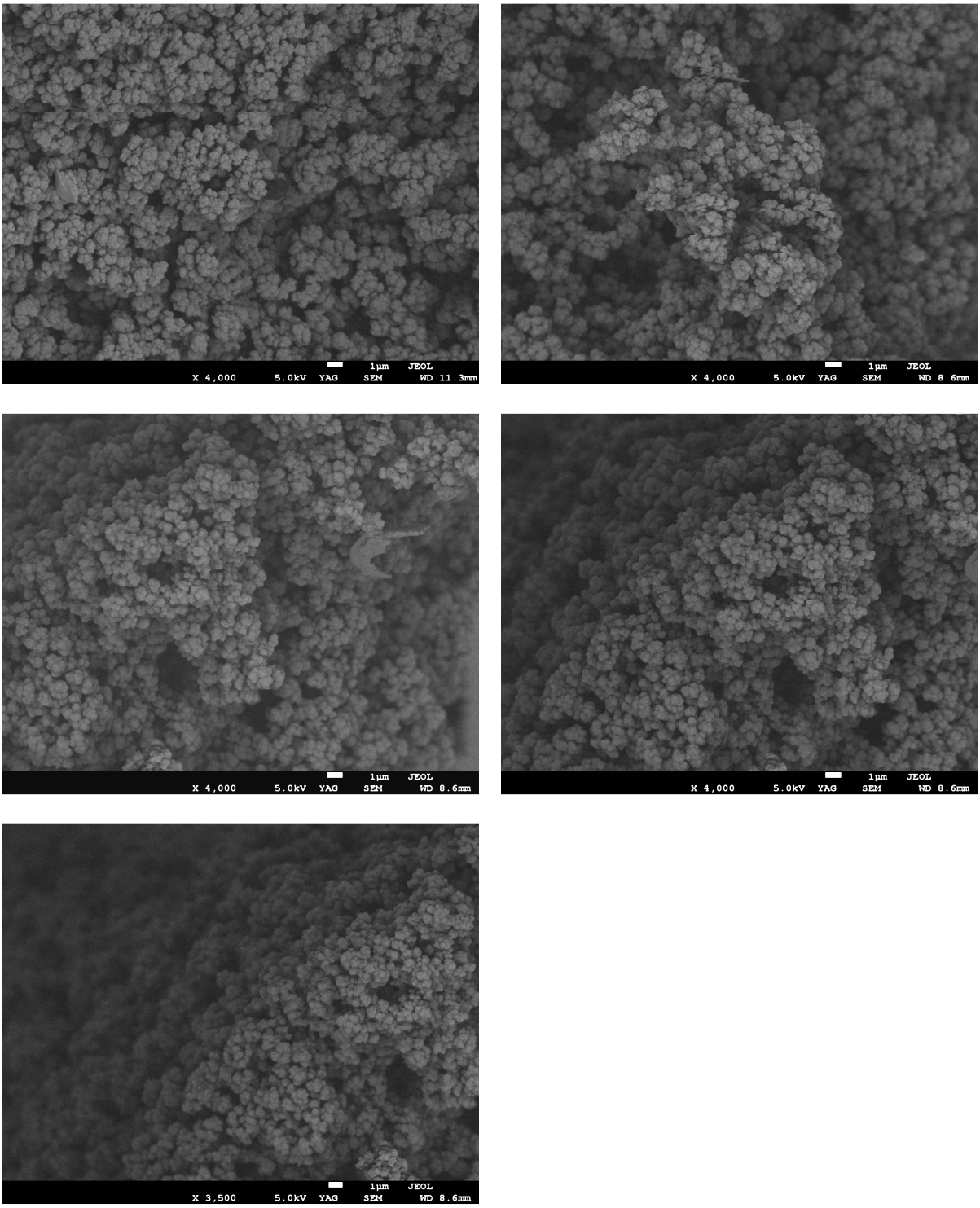

Figure S8. SEM micrographs for Monolith E with identical magnifications (4000x).

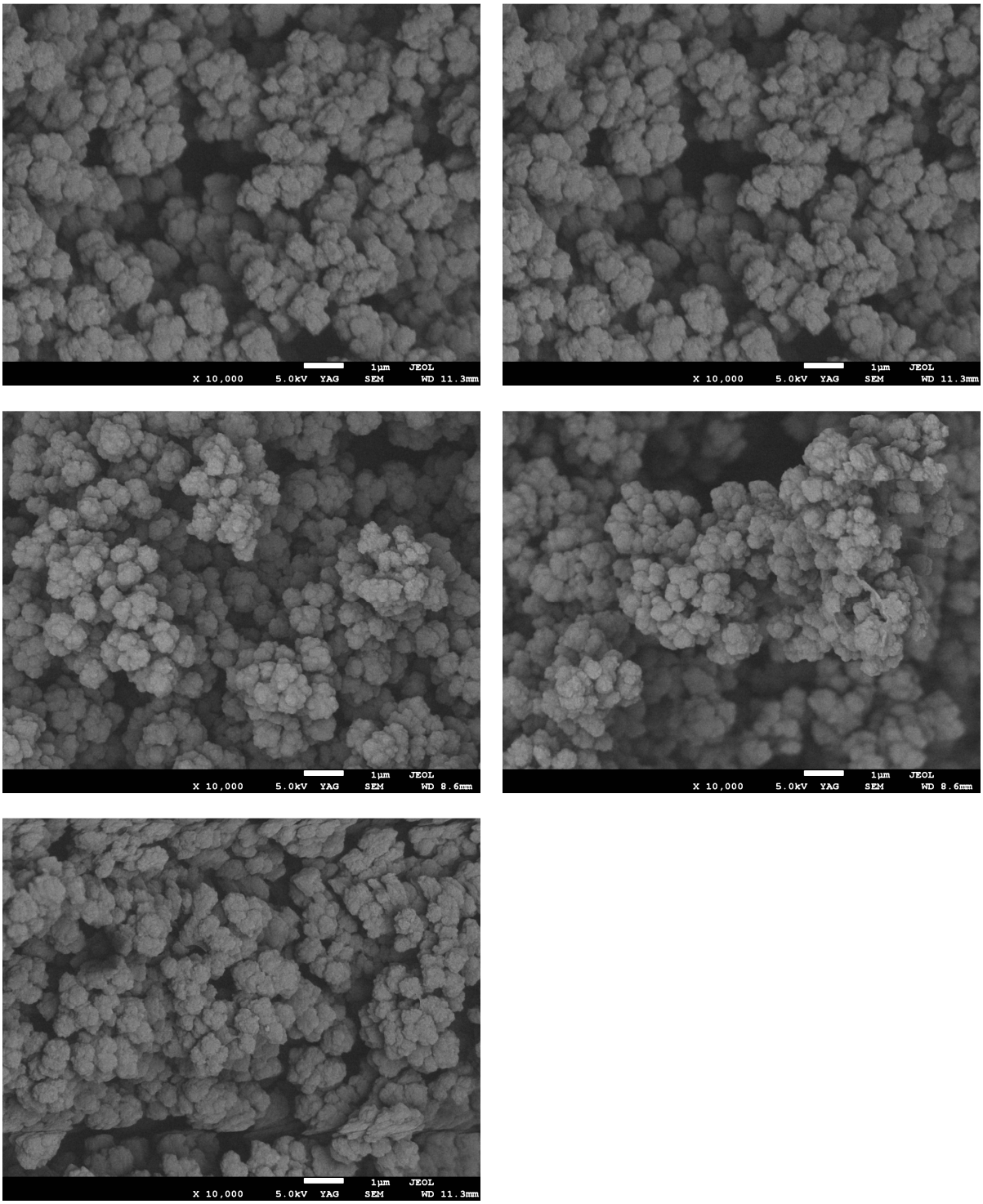

Figure S9. SEM micrographs for Monolith E with identical magnifications (10000 x).

(a) (b)

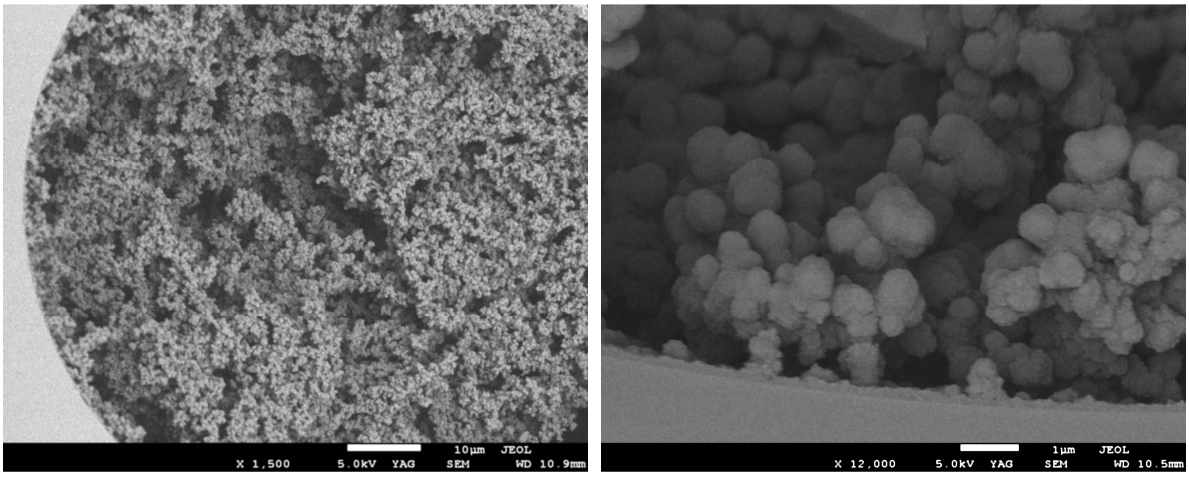

Figure S10. (a) SEM micrograph for Monolith F at 2000 x showing the covalent attachment of the polymeric monolith to the inner capillary wall. (b) SEM micrograph for Monolith C at 12000 x showing the formation of a less macroporous layer at the inner capillary wall as a result of the successful capillary pre-treatment step.

Table S1. Run-to-run repeatability data for the retention factor of acetophenone, the retention factor of butyrophenone, and the electroosmotic mobility on Monolith B (see Tab. 1). Mobile phase: methanol/water (50:50, v/v) buffered with triethylamine/acetic acid, pH* = 7.0, electric conductivity = 125 µS cm^{-1}. Capillary dimensions 206 mm (275 mm) x 100 µm; UV detection at 230 nm; electrokinetic injection: 6 kV for 3 s, separation voltage: 20.6 kV.

Number of runs	t_0/min	t_r/min acetophenone	t_r/min butyrophenone	k acetophenone	k butyrophenone	μ_{eo}/($cm^2kV^{-1}min^{-1}$)
1	5.297	6.485	7.267	0.224	0.372	5.191
2	5.275	6.485	7.235	0.229	0.371	5.213
3	5.287	6.472	7.25	0.224	0.371	5.201
4	5.280	6.462	7.24	0.223	0.371	5.208
5	5.283	6.475	7.255	0.225	0.373	5.205
6	5.267	6.455	7.238	0.225	0.374	5.221
7	5.258	6.445	7.228	0.225	0.374	5.230
8	5.267	6.462	7.248	0.226	0.376	5.221
9	5.255	6.440	7.222	0.225	0.374	5.233
10	5.252	6.43	7.21	0.224	0.372	5.236
11	5.247	6.428	7.208	0.225	0.373	5.241
12	5.223	6.397	7.177	0.224	0.374	5.265
13	5.222	6.402	7.183	0.226	0.375	5.266
14	5.233	6.415	7.203	0.225	0.376	5.255
15	5.230	6.410	7.193	0.225	0.375	5.258
16	5.222	6.407	7.197	0.227	0.378	5.266
17	5.260	6.460	7.260	0.228	0.380	5.228
18	5.263	6.473	7.275	0.229	0.382	5.225
19	5.272	6.470	7.275	0.227	0.379	5.216

Table S2. Day-to-day repeatability data, for the retention factor of acetophenone, the retention factor of butyrophenone, and the electroosmotic mobility on Monolith B (see Tab. 1). For other experimental conditions see Table S1.

	Number of runs	t_0/min	t_r/min acetophenone	t_r/min butyrophenone	k acetophenone	k butyrophenone	μ_{eo}/(cm^{2}kV^{-1}min^{-1})
Day 1	1	5.273	6.438	7.197	0.221	0.364	5.215
	2	5.187	6.335	7.085	0.221	0.365	5.301
	3	5.260	6.412	7.167	0.219	0.362	5.228
	4	5.227	6.378	7.137	0.220	0.365	5.261
	5	5.212	6.353	7.103	0.218	0.362	5.276
	6	5.203	6.365	7.123	0.223	0.369	5.285
	7	5.237	6.408	7.188	0.223	0.372	5.251
	8	5.295	6.495	7.298	0.226	0.378	5.193
	9	5.167	6.308	7.055	0.221	0.365	5.322
Day 2	1	5.227	6.387	7.147	0.222	0.367	5.261
	2	5.233	6.398	7.160	0.222	0.368	5.255
	3	5.217	6.373	7.132	0.221	0.367	5.271
	4	5.210	6.367	7.125	0.222	0.367	5.278
	5	5.190	6.345	7.103	0.222	0.368	5.298
	6	5.180	6.330	7.087	0.222	0.368	5.308
	7	5.182	6.335	7.095	0.222	0.369	5.306
	8	5.183	6.343	7.105	0.223	0.370	5.305
	9	5.190	6.352	7.118	0.223	0.371	5.298
Day 3	1	5.297	6.485	7.267	0.224	0.371	5.191
	2	5.275	6.485	7.235	0.229	0.371	5.213
	3	5.287	6.472	7.250	0.224	0.371	5.201
	4	5.280	6.462	7.240	0.223	0.371	5.208
	5	5.283	6.475	7.255	0.225	0.373	5.205
	6	5.267	6.455	7.238	0.225	0.374	5.221
	7	5.258	6.445	7.228	0.225	0.374	5.230
	8	5.267	6.462	7.248	0.226	0.376	5.221
	9	5.255	6.440	7.222	0.225	0.374	5.233
Day 4	1	5.222	6.400	7.178	0.225	0.374	5.266
	2	5.218	6.393	7.170	0.225	0.374	5.270
	3	5.203	6.372	7.138	0.224	0.371	5.285
	4	5.205	6.375	7.150	0.224	0.373	5.283
	5	5.237	6.415	7.187	0.224	0.372	5.251
	6	5.205	6.373	7.142	0.224	0.372	5.283
	7	5.287	6.478	7.260	0.225	0.373	5.201
	8	5.248	6.425	7.198	0.224	0.371	5.240
	9	5.288	6.478	7.260	0.225	0.372	5.200

Table S3. Capillary-to-capillary repeatability data for the retention factor of acetophenone, the retention factor of butyrophenone, and the electroosmotic mobility on Monolith B (see Tab. 1). For other experimental conditions see Table S1.

	Number of runs	t_0/(min)	t_r/(min) acetophenone	t_r/(min) butyrophenone	k, acetophenone	k, butyrophenone	μ_{eo}/($cm^2kV^{-1}min^{-1}$)
Capillary 1	1	6.690	8.313	9.430	0.242	0.409	4.755
	2	6.642	8.285	9.402	0.247	0.415	4.790
	3	6.690	8.308	9.407	0.242	0.410	4.755
Capillary 2	1	7.443	9.248	10.582	0.242	0.422	4.130
	2	7.467	9.265	10.578	0.241	0.416	4.116
	3	7.500	9.348	10.673	0.246	0.423	4.100
Capillary 3	1	4.995	6.217	7.062	0.244	0.413	6.382
	2	5.010	6.237	7.083	0.244	0.413	6.363
	3	5.007	6.235	7.080	0.245	0.414	6.366
Capillary 4	1	6.158	7.653	8.652	0.242	0.405	5.114
	2	6.257	7.777	8.787	0.242	0.404	5.033
	3	6.172	7.658	8.650	0.241	0.401	5.103
Capillary 5	1	5.625	6.920	7.778	0.230	0.383	4.890
	2	5.605	6.898	7.755	0.230	0.383	4.906
	3	5.638	6.937	7.797	0.230	0.383	4.880

Capillary 1: L_{eff} = 228 mm, L_{Total} = 300 mm; separation voltage: 21.5 kV

Capillary 2: L_{eff} = 224 mm, L_{Total} = 295 mm; separation voltage: 21.5 kV

Capillary 3: L_{eff} = 230mm, L_{Total} = 298 mm; separation voltage: 21.5 kV

Capillary 4: L_{eff} = 228 mm, L_{Total} = 297 mm; separation voltage: 21.5 kV

Capillary 5: L_{eff} = 206 mm, L_{Total} = 275 mm; separation voltage: 20.6 kV

S1. Comment on the applicability of the method of Halasz and Martin

Conventional size exclusion chromatography (SEC) regards the characterization and separation of macromolecules with a column packed with a stationary phase whose pore size distribution is well known [1]. The primary factor controlling the elution volume in SEC is the size of the solute, so that populations with larger molecules are excluded from a larger fraction of the pores than those with smaller molecules, therefore they are eluted earlier. The prerequisite of this method is that polymer standards with a known molar mass (synthesized from a well characterized monomer) are available for calibration, and that the solute molecules (to be characterized) are not adsorbed on the surface of the stationary phase. The method is calibrated by a plot of the logarithm of the normalized average molar mass $\overline{M}_{w,n}$ of the polymer standard versus its elution volume.

Conversely, inverse size exclusion chromatography (ISEC) uses well-defined polymer standards to gain information about the porosities and the dimensions of the pores (the pore size distribution) in a material which is to be characterized. With a particulate material, total, external, and internal porosities can be determined via injection of a solution containing a series of polymer standards having a narrow molar mass distribution and a low polydispersity, whereas the material to be studied is packed into a chromatographic column. The mobile phase is selected so as to minimize any interactions between the stationary phase and the standards. The retention data obtained for polymer standards can then be converted into a pore size distribution of the packed material, if there is an equation that correlates the average molar mass of the standard $\overline{M}_{w,n}$ to the so-called exclusion limit of the pores ϕ_n (see Section 2).

Since a polymer-based monolith is made of a large single piece of a highly porous material that fills the entire length and width of the capillary, its porous structure is different from that of a packed bed and characterized by the presence of two different types of pores: intra-globular pores and inter-globular pores (including flow-through pores). In a polymer-based monolith, the flow-through pores take over the function of the interstitial pores of a particulate chromatographic bed. The total geometrical volume V_G of a monolithic separation capillary is the sum of the volume of the solid stationary phase (polymer, monolith) V_M, and the total volume V_P of the pores which are accessible to the mobile phase (comprising the volume of the flow-through pores V_F and the volume V_I, which includes the small-size inter-globular pores and the intra-globular pores, ignoring the volume of the permanently closed pores). In other words: when comparing a monolith to a packed bed, the volume of the

flow-through pores V_F is regarded to be equivalent to the volume of the interstitial pores, whereas the sum of the volumes of the small-size inter-globular pores and the intra-globular pores V_I is regarded to be equivalent to the volume of the pores within the particles:

$$V_G = V_M + V_P = V_M + (V_F + V_I) \quad \text{(S1)}$$

The distinction between pores belonging to V_F or to V_I can be made on the basis of the type of mass transport within these pores. The geometrical volume V_G is readily determined from the capillary geometry:

$$V_G = \pi r^2 L \quad \text{(S2)}$$

where r is the inner radius of the capillary and L is the capillary length.

Because of its small molecular volume (having the smallest molar mass $M_{w,min}$), a small molecular standard, e.g. toluene, can penetrate into all accessible pores. Therefore, its elution volume V_{max} which is equal to its elution time t_{max} multiplied by the flow rate F corresponds to the total accessible pore volume V_P.

$$V_P = V_{max} = t_{max} F \quad \text{(S3)}$$

If chosen properly, the largest molar mass polymer standard $\overline{M}_{w,max}$ is too large to enter the intra-globular and the small-size inter-globular pores. Its elution volume V_{min} which is equal to its elution time t_{min} multiplied by the flow rate F corresponds to a volume V_F, which will include only flow-through pores:

$$V_F = V_{min} = t_{min} F \quad \text{(S4)}$$

Based on Eqs. S3 and S4, the volume V_I is then given by:

$$V_I = V_{max} - V_{min} = (t_{max} - t_{min}) F \quad \text{(S5)}$$

From these data, ISEC allows the determination of the total porosity ε_P, the flow-through porosity ε_F, and the small-size porosity ε_I of the monolithic material. These three porosities are defined as follows [2,3]:

$$\varepsilon_P = \frac{V_{max}}{V_G} \quad \text{(S6)}$$

$$\varepsilon_F = \frac{V_{min}}{V_G} \quad \text{(S7)}$$

$$\varepsilon_I = \varepsilon_P - \varepsilon_F = \frac{(V_{max} - V_{min})}{V_G} \quad \text{(S8)}$$

Moreover, ISEC provides insight into the pore size distribution of the investigated material. In the most simplified approach, the pores are assumed to be cylindrical and open at both ends, so that their dimensions can be quantified with one parameter, the pore diameter d_p. With the assumption that there is no retention by adsorption of the polystyrene standards or any other interaction of the standards with the stationary phase, a decrease in the relative elution time τ of the standard (see Section 2) reflects a decrease in the accessible fraction of the pore volume V_P. If we assume now that the distribution coefficient K_D (defined as the ratio of the concentration of the solute in the accessible pore liquid to the concentration of the solute in the external liquid) for each solute equals one – independent of the pore size (for the inaccessible pores $K_D = 0$) – the simplified approach of Halasz and Martin [4] is applicable. Halasz and Martin have emphasized that the assignment of exclusion limits ϕ_n (see Section 2) to calibration standards was done by "trial and error" in such a way "that the maxima of the pore size distribution curves measured by ISEC agreed with those values obtained by the classical methods" [4].

This approach ignores that in a confined environment K_D is smaller than 1 and a function of the pore diameter d_p. E.g. for spherical molecules of diameter d_m the distribution coefficient K_D equals $[1 - (d_m/d_p)]^2$ [5,6]. This fundamental error of the approach of Halasz and Martin has been addressed in 1984 by Knox and Scott [7] who showed that the correct calculation of pore size distributions from size-exclusion chromatographic data is possible, if the dependence of K_D on the pore dimension is taken into account. The curves obtained with the refined theory fit well with those obtained by mercury intrusion porosimetry, while those obtained with the approach of Halasz and Martin showed a considerable bias, which is mitigated by the introduced experimental correction factor. This comparison, however, overlooks another fundamental problem, which arises from the fact that the pores of a monolithic scaffold are neither ideally cylindric nor of any other regular shape so that in all cases the pore dimensions obtained by ISEC and by mercury intrusion porosimetry will be biased and have to be used within the constraints given by the method of determination [8].

S2. Investigation of the chemical stability of the synthesized monolith under ISEC conditions

In order to evaluate the chemical stability of the synthesized monoliths, we tested several performance parameters depending on the contact time with a THF rich mobile phase. This investigation is especially important with respect to a discussion on the validity of the results obtained by ISEC. Monolith F (for polymerization composition see Tab. 1) was selected for this study. In the first step, Monolith F was employed for the CEC separation of alkylphenones in the reversed-phase mode using a water/methanol (50/50, v/v) mobile phase buffered with triethylamine/acetic acid and DMF as non-retained marker. Separation parameters such as retention factors and electroosmotic mobility were determined. Additionally, SEM micrographs were taken at different magnifications. In the next step, a new synthesized monolithic capillary (Monolith F) was rinsed with THF for 6 hours continuously using a HPLC pump and, subsequently, was left overnight filled with THF. At the next day, the same capillary was again employed for the CEC separation of alkylphenones in the reversed-phase mode under the same experimental conditions as described before. In addition SEM micrographs were determined after having completed this study. A comparison of the results obtained with the fresh capillary and obtained with the capillary after rinsing overnight with THF shows that there is no significant alteration in the retention factors, the electroosmotic mobility, and the separation efficiency (Tab. S4, next page). Moreover, the SEM micrographs (Figures S11 and S12, see following pages) reveal that the morphology of the monolith remains unchanged. These findings confirm that monoliths synthesized in this work exhibit a high chemical stability against organic solvents such as MeOH, ACN, or THF. We therefore conclude that ISEC with THF as mobile phase is not biased by the degradation of the investigated material and can provide reliable data regarding internal and external porosities as well as pore size distributions.

Table S4. Electroosmotic mobility, retention factors, and plate heights determined from chromatograms for the separation of alkylphenones. Mobile phase: methanol/water (50:50, v/v) buffered with triethylamine/acetic acid, pH* = 7.0, electric conductivity = 125 µS/cm. Monolith F (see Tab. 1). The presented data are mean values for three consecutive measurements (standard deviations in brackets).

	With THF/ 24 hours		Without THF	
μ_{eo}/(cm^2 kV^{-1} min^{-1})	6.05 (± 0.09)		4.65 (± 0.02)	
Analyte	k	H/µm	k	H/µm
DMF	0	4.28 (± 0.15)	0	4.21 (± 0.34)
Acetophenone	0.19 (± 0.002)	5.52 (± 0.33)	0.19 (± 0.000)	4.33 (± 0.16)
Propiophenone	0.23 (± 0.004)	5.48 (± 0.15)	0.24 (± 0.000)	4.47 (± 0.32)
Butyrophenone	0.29 (± 0.005)	5.55 (± 0.32)	0.30 (± 0.000)	4.60 (± 0.30)
Valerophenone	0.39 (± 0.008)	5.43 (± 0.26)	0.40 (± 0.000)	4.80 (± 0.41)

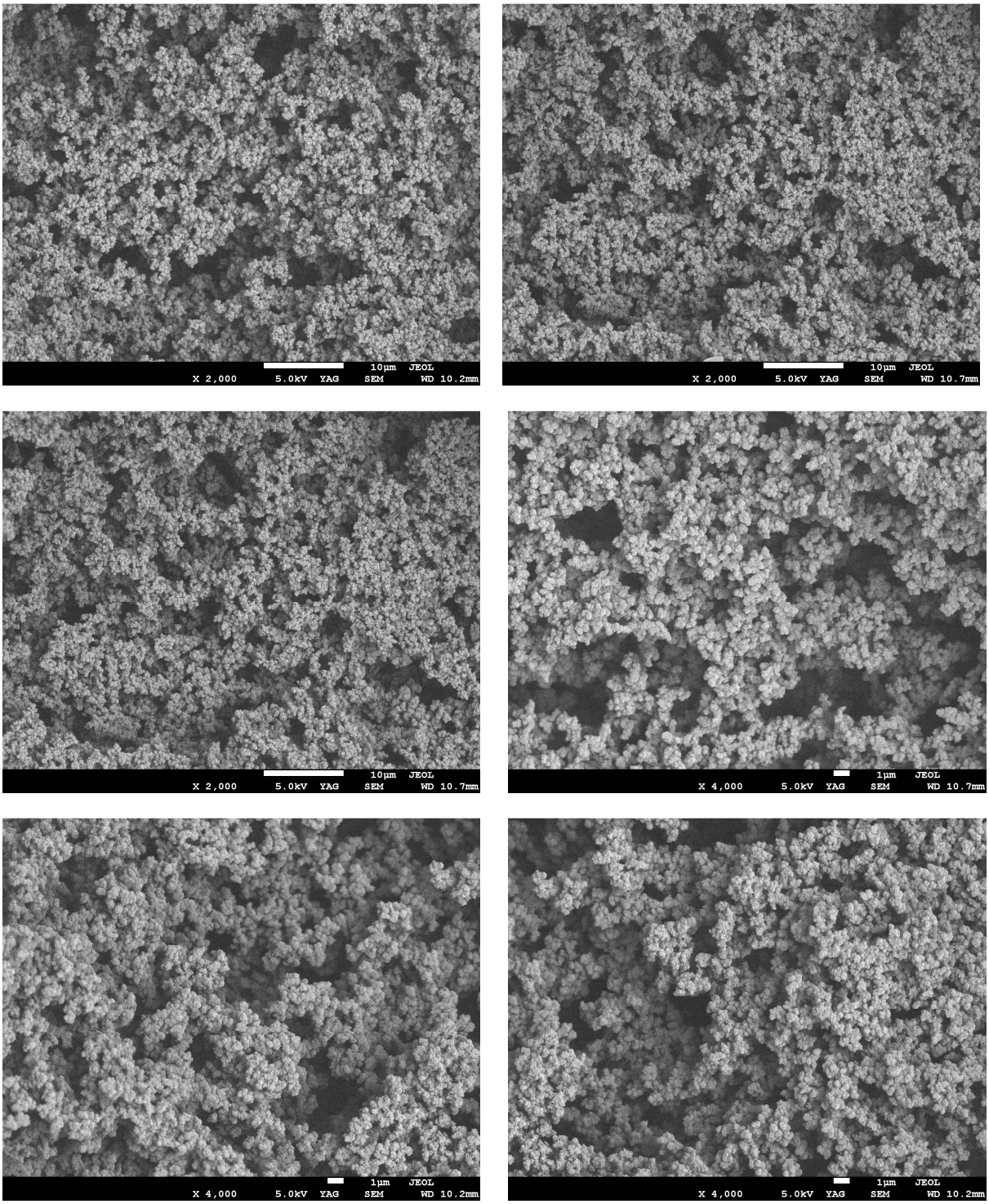

Figure S11. SEM micrographs for Monolith F without rinsing with THF, magnifications 2000 and 4000x.

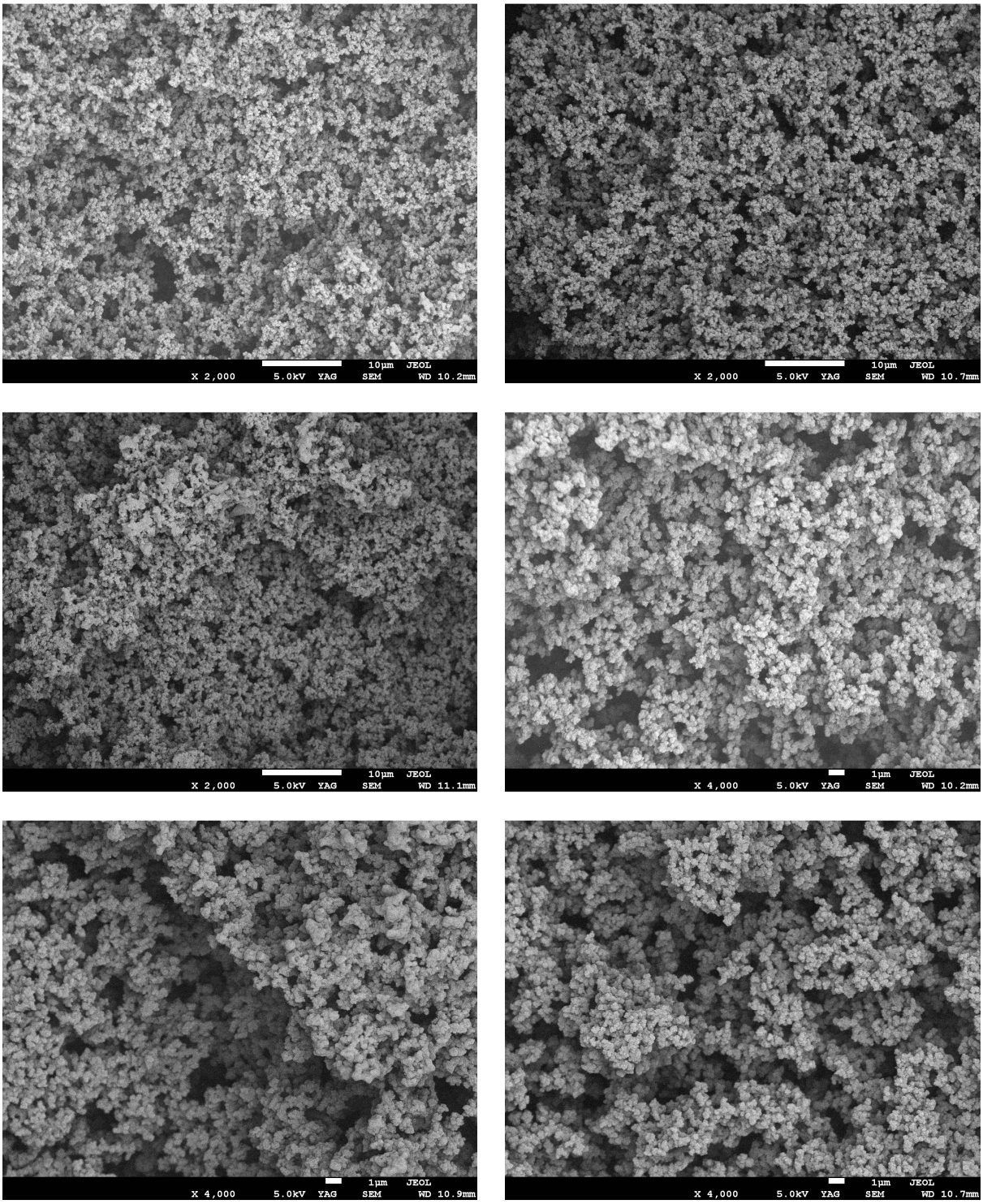

Figure S12. SEM micrographs for Monolith F after rinsing with THF, magnifications: 2000 and 4000x.

References

[1] H. Guan, G. Guiochon, J. Chromatogr. A 731 (1996) 27.

[2] M. Al-Bokari, D. Cherrak, G. Guiochon, J. Chromatogr. A 975 (2002) 275.

[3] J. Urban, S. Eeltink, P. Jandera, P.J. Schoenmakers, J. Chromatogr. A 1182 (2008) 161.

[4] I. Halasz, K. Martin, Angew. Chem. Inter. Ed. (Engl.) 17 (1978) 901.

[5] J.C. Giddings, E. Kucera, C.P. Russell, M.N. Myers, J. Phys. Chem. 72 (1968) 4397.

[6] K. Jerabek, Anal. Chem. 57 (1985) 1595.

[7] J.H. Knox, H.P. Scott, J. Chromatogr. 316 (1984) 311.

[8] P. DePhillips, A.M. Lenhoff, J. Chromatogr. A 883 (2000) 39.

ELSEVIER LICENSE
TERMS AND CONDITIONS

Apr 08, 2014

This is a License Agreement between "Ayat Allah" Al-Massaedh ("You") and Elsevier ("Elsevier") provided by Copyright Clearance Center ("CCC"). The license consists of your order details, the terms and conditions provided by Elsevier, and the payment terms and conditions.

All payments must be made in full to CCC. For payment instructions, please see information listed at the bottom of this form.

Supplier	Elsevier Limited The Boulevard, Langford Lane Kidlington, Oxford, OX5 1GB, UK
Registered Company Number	1982084
Customer name	"Ayat Allah" Al-Massaedh
Customer address	University of Marburg, 35032 Marburg, Germany.
License number	3364101452752
License date	Apr 08, 2014
Licensed content publisher	Elsevier
Licensed content publication	Journal of Chromatography A
Licensed content title	Adamantyl-group containing mixed-mode acrylamide-based continuous beds for capillary electrochromatography. Part II. Characterization of the synthesized monoliths by inverse size exclusion chromatography and scanning electron microscopy
Licensed content author	“Ayat Allah” Al-Massaedh, Ute Pyell
Licensed content date	17 January 2014
Licensed content volume number	1325
Licensed content issue number	
Number of pages	9
Start Page	247
End Page	255
Type of Use	reuse in a thesis/dissertation
Portion	full article
Format	both print and electronic
Are you the author of this Elsevier	Yes
Will you be translating?	No
Title of your thesis/dissertation	Adamantyl-Group Containing Mixed-Mode Acrylamide-Based Continuous Beds for Capillary Electrochromatography: Synthesis, Characterization, Optimization and Investigation of the Chromatographic Efficiency
Expected completion date	May 2014

5.3. Publication III

Adamantyl-group containing mixed-mode acrylamide-based continuous beds for capillary electrochromatography. Part III. Optimization of the chromatographic efficiency

"Ayat Allah" Al-Massaedh, Ute Pyell

Journal of Chromatography A, 1325 (2014) 186–194

doi: 10.1016/j.chroma.2013.11.003

5.3.1. Summary and discussion

In this publication, efficiency data are gained for a series of amphiphilic macroporous N-adamantyl-group containing mixed-mode acrylamide-based monolithic stationary phases synthesized under variation of different synthesis parameters. The studied synthesis parameters are (i) concentration of ammonium sulfate, (ii) concentration of the initiator ammonium persulfate, and (iii) concentration of the negatively charged monomer vinylsulfonic acid (VSA) in the polymerization mixture. The optimization of different synthesis parameters with regard to the chromatographic efficiency is studied under isocratic conditions for alkylphenones in the reversed-phase mode via CEC. The absence of a significant influence by heating (Joule heating) and via extra-column band broadening effects on the determined efficiency is confirmed. In this context, it is found that the removal of the polyimide coating from the inlet side of the separation capillary is necessary to avoid a characteristic distortion of the recorded peak, which in turn leads to significant extra-column band broadening and loss in column efficiency.

The influence of the different synthesis parameters on the chromatographic efficiency of the synthesized monoliths was clarified by constructing the Van Deemter curves for the nonretained analyte DMF and several alkylphenones. The observed overall flatness of these curves for retained analytes indicates that very high velocities can be applied without reduction in efficiency. The major conclusion is that with varied concentration of AS or varied concentration of ammonium persulfate in the polymerization mixture, a strong impact on the chromatographic efficiency is observed, while there is only a minor influence when varying the molar fraction of VSA. This is because the concentration of AS and APS in the polymerization mixture has a strong impact on the morphology (domain size) of the formed monolith, and consequently, on its chromatographic efficiency. As a general trend, the efficiency increases with decreasing domain size of the monolith. The varying dependence of the minimum plate height H_{min} and the peak asymmetry AF on the retention factor k for different monoliths synthesized under variation of the lyotropic salt AS in the polymerization mixture is discussed. The results obtained show that the dependence of H_{min} on k increases with increasing domain size of the monolith, so that monoliths with larger domain size exhibit this dependence, while those with smaller domain size do not. This dependence was explained by us based on the fact that monoliths synthesized with higher concentration of AS in the polymerization mixture exhibit a large domain size globular structure. Monoliths with such morphology are susceptible to the formation gel pores (micropores and small mesopores) when they are in contact with a hydroorganic solvent, resulting in the (sterically) hindered diffusion of retarded solutes resulting in an increase in the resistance to mass transfer and decrease in the column efficiency.

5.3.2. Author contribution

All the experimental part of this study was performed by me. Some of the CEC experiments were performed by B. Sc. D. Urban under my supervision. The draft of the manuscript was written by me and corrected by Prof. Dr. Ute Pyell. The final revision of the manuscript was conducted by me and Prof. Dr. Ute Pyell before submission to the journal. Prof. Dr. Ute Pyell was responsible for the supervision of this work.

Journal of Chromatography A, 1325 (2014) 186–194

Contents lists available at ScienceDirect

Journal of Chromatography A

journal homepage: www.elsevier.com/locate/chroma

Adamantyl-group containing mixed-mode acrylamide-based continuous beds for capillary electrochromatography. Part III. Optimization of the chromatographic efficiency

"Ayat Allah" Al-Massaedh, Ute Pyell *

University of Marburg, Department of Chemistry, Hans-Meerwein-Straße, D-35032 Marburg, Germany

ARTICLE INFO

Article history:
Received 30 August 2013
Received in revised form 29 October 2013
Accepted 1 November 2013
Available online 9 November 2013

Keywords:
Capillary electrochromatography
Monolithic stationary phase
Continuous bed
Cyclodextrin
Height equivalent to a theoretical plate

ABSTRACT

In a previous article we described the synthesis of amphiphilic monolithic stationary phases by in situ free radical copolymerization of cyclodextrin-solubilized N-adamantyl acrylamide, piperazinediacrylamide, methacrylamide and vinylsulfonic acid in aqueous medium in pre-treated fused silica capillaries of 100 μ.m I.D. In this work, a series of N-adamantyl-group containing acrylamide-based continuous beds is synthesized under variation of different synthesis parameters. The studied synthesis parameters are (i) concentration of the lyotropic salt ammonium sulfate, (ii) concentration of the initiator ammonium persulfate, and (iii) concentration of the negatively charged monomer vinylsulfonic acid in the polymerization mixture. The influence of the synthesis parameters on the chromatographic efficiency is studied under isocratic conditions for a homologues series of alkylphenones in the reversed-phase mode at constant composition of the mobile phase via capillary electrochromatography with varied electric field strength. With varied concentration of the lyotropic salt ammonium sulfate or varied concentration of the initiator ammonium persulfate in the polymerization mixture, a strong impact on the chromatographic efficiency is observed, while there is only a minor influence when varying the molar fraction of the charged monomer VSA. The absence of a significant influence of extra-column band broadening effects on the determined efficiency is confirmed. There is a good repeatability (with respect to capillary-to-capillary variation and run-to-run variation) reached for the theoretical plate heights obtained for DMF and selected alkylphenones in the reversed-phase mode.

1. Introduction

In capillary electrochromatography (CEC) polyacrylamide-based organic monolithic stationary phases synthesized in situ in fused-silica capillaries are an alternative to capillaries packed with particulate material [1–4]. Monolithic materials as stationary phases in chromatography have attracted a widespread interest during the last two decades which is documented in a large number of review articles [5–12]. In the last years the optimization of organic monoliths for the separation of small molecules has come into the focus of intense research activities [6,7,13–20].

The interest in polymer-based monolithic stationary phases stems from their chemical resistance toward a broad range of possible mobile phase compositions including pH, the possibility to fine-tune the chemical composition and the retention properties by variation of the mass fractions and the type(s) of monomer used in the polymerization mixture, and the ease of their preparation by an in situ free radical polymerization process. However, the actual situation must be characterized as follows: the separation efficiency observed for small molecules is often relatively poor (in comparison to particulate modified silica gel) and largely dependent on retention factors (and mobile phase composition) and even reported to be solute-specific [17,21,22]. The reason why the chromatographic performance shows these dependencies is far from being fully understood. The situation is also characterized by the observation that polymer-based monolithic stationary phases show a much better chromatographic efficiency when they are employed in CEC in comparison to the efficiency observed in capillary liquid chromatography (CLC) [23].

If the preparation of the organic monolith is performed by free radical copolymerization, the morphology of the macroporous polymer is formed spontaneously depending on the composition of the polymerization mixture and on the reaction conditions [10]. The morphological properties (such as average pore size and average microglobule size) of the produced organic monolith are usually controlled by following synthesis parameters: (i) type(s) and molar fraction(s) of monomer(s), (ii) type and molar fraction of crosslinker (%*C*), (iii) total monomer concentration (%*T*), (iv) type(s)

* Corresponding author. Tel.: +49 6421 2822192; fax: +49 6421 2822124.
E-mail address: pyellu@staff.uni-marburg.de (U. Pyell).

0021-9673/$ – see front matter © 2013 Elsevier B.V. All rights reserved.
http://dx.doi.org/10.1016/j.chroma.2013.11.003

and concentration(s) of porogen(s), (v) type, concentration and activation of initiator, (vi) reaction time, and (vii) reaction temperature [1–3,10,24–29]. There is a large number of investigations on the influence of these synthetic parameters on characteristics of the formed monolith. The mechanical and chemical stability, the permeability, and the domain size of the formed monolith defined as the combination of the mean flow-through pore size and the mean globule size [30] are influenced by the total monomer concentration (%*T*) [2–4,31] and the mass fraction of crosslinker (%*C*) [1,2,31]. The hydrodynamic permeability and the pore size distribution of the produced monolith are also affected by the concentration of the free radical initiator in the polymerization mixture [25].

Hoegger and Freitag [1] investigated the influence of various factors affecting the morphology and the chromatographic properties of hydrophilic polyacrylamide-based continuous beds polymerized form the water soluble co-monomers N,N-dimethylacrylamide (DMAA), piperazinediacrylamide (PDA), and vinylsulfonic acid (VSA). They observed that the mass fraction of crosslinker (%*C*), the type and the concentration of the pore forming agent, the type of solvent, and the type and molar fraction of the monomers in the polymerization mixture have a significant influence on the morphology and the chromatographic properties of the produced monolith. In a similar study, Ratautaite et al. [3] investigated the effect of buffer concentration and pH (buffer used as polymerization medium), and the total monomer concentration (%*T*) on the morphology and the chromatographic properties of amphiphilic polyacrylamide-based monoliths polymerized from the water soluble co-monomers methacrylamide (MA), piperazinediacrylamide (PDA), N-isopropylacrylamide (IPA), and vinylsulfonic acid (VSA). The authors confirmed that the hydrodynamic permeability is dependent on the ionic strength of the buffer. There is an increase in the volume fraction of flow-through pores in the monolithic scaffold with increasing buffer concentration.

In a previous publication [4], we reported the synthesis of a monolith which is based on the solubilization of N-adamantyl acrylamide in aqueous solution via a 1:1 complex formed with statistically methylated β-CD. Monoliths are prepared by in situ free radical copolymerization of this complex with PDA, MA and VSA in aqueous medium in pre-treated fused silica capillaries (100 μ.m I.D.). In the second paper of this series [32], we performed detailed investigations of these continuous beds (synthesized under variation of the concentration of the lyotropic salt ammonium sulfate in the polymerization mixture) regarding their morphology and porous properties by inverse size exclusion chromatography (ISEC) and scanning electron microscopy (SEM). In the present paper, we investigate the chromatographic efficiency of a series of N-adamantyl-group containing amphiphilic acrylamide-based continuous beds synthesized under variation of several synthetic parameters, which can be regarded to be decisive for the morphology (and chromatographic efficiency) of the produced macroporous polymer: (i) the concentration of the lyotropic salt ammonium sulfate in the polymerization mixture, (ii) the composition of the mixture of monomers (variation of the concentration of the charge-bearing monomer vinylsulfonic acid) and (iii) the concentration of the initiator. The impact of these varied parameters on the chromatographic efficiency obtained for a homologues series of alkylphenones is investigated by CEC in the reversed-phase mode at constant composition of the mobile phase under variation of the separation voltage. Special emphasis is placed on the confirmation of the absence of a significant influence of extra-column band broadening effects. The repeatability of the synthesis procedure is confirmed by comparison of data obtained for several capillaries regarding the plate heights reached for DMF and selected alkylphenones in the reversed-phase mode.

2. Experimental

2.1. Chemicals and instruments

All chemicals were used without further purification. *N*,*N*,*N*′,*N*′-Tetramethylethylendiamine (TEMED), 3-(trimethoxysilyl) propyl methacrylate (bind silane), di-sodium hydrogenphosphate dihydrate, N,N-dimethylformamide (DMF), ammonium sulfate (AS), and hydrochloric acid (37%, v/v) were from Fluka (Buchs, Switzerland). Propiophenone, butyrophenone, valerophenone, vinylsulfonic acid (VSA, 25%, w/v in aqueous solution), and ammonium persulfate (APS) were from Sigma Aldrich (Steinheim, Germany). Methacrylamide, acetic acid (AA), and sodium dihydrogen phosphate monohydrate were from Merck (Darmstadt, Germany). Acetophenone was from Riedel-de Haen (Seelze, Germany). Triethylamine (TEA) was from KMF Laborchemie (Lohmar, Germany). 1,4-Diacryloylpiperazine (PDA) was either from Alfa-Aesar (Karlsruhe, Germany) or from Molekula (Dorset, UK). Statistically methylated β-cyclodextrin (Me-β-CD) was either from ABCR (Karlsruhe, Germany) or from Sigma Aldrich (Louis, USA). N-(1-adamantyl)acrylamide was synthesized according to [33] (synthesis procedure and product characterization see [4]). Fused silica capillaries (100 μm I.D. × 360 μm O.D.) were from Polymicro Technologies (Phoenix, USA).

With all mobile phases the electric conductivity and the pH* value were controlled. The pH* value is the pH in the presence of organic solvent determined with a pH meter calibrated with an aqueous buffer. The pH* was determined with the mobile phase after addition of the organic solvent to the aqueous buffer. The pH meter Inolab pH 720 (WTW instruments, Weinheim, Germany), and the conductometer LF 191 (WTW, Weinheim, Germany) were used to measure the pH* and the electric conductivity of the prepared mobile phases. Mobile phases were prepared by buffering 100 mL of distilled water with 2–3 mL of a mixture of 0.2 mol L^{-1} TEA with 0.2 mol L^{-1} AA (1:1, v/v). Subsequently, the required volume of this solution is taken and mixed with the corresponding volume of organic solvent. The pH* and the electric conductivity of the final mixture were adjusted with 0.20 mol L^{-1} TEA or AA.

The mixed-mode monolithic stationary phases used in CEC measurements were synthesized as described in Ref. [4] by copolymerization of a mixture of N-(1-adamantyl)acrylamide (solubilized via 1:1 complex formation with Me-β-CD), methacrylamide (MA) as hydrophilic monomer, piperazinediacrylamide (PDA) as crosslinker, ammonium sulfate (AS) as lyotropic salt, vinylsulfonic acid (VSA) as charge-bearing monomer, ammonium persulfate (APS) as free radical polymerization initiator, and *N*,*N*,*N*′,*N*′-tetramethylethylendiamine (TEMED) as catalyst (accelerator) in the redox initiator system in aqueous phosphate buffer (100 mM, pH 7.0) inside a 100 μm I.D. fused-silica capillary, which had been pre-treated with 3-(trimethoxysilyl)propyl methacrylate (bind silane). For monoliths prepared under varied concentration of ammonium sulfate (addition of 8, 12, 32, or 42 mg AS to a fixed volume of solution), all synthesis parameters were kept constant with exception of the concentration of ammonium sulfate present in the polymerization mixture (Table 1 – Monoliths A, B, C, and D). For monoliths with varied molar fraction of vinylsulfonic acid, different volumes of vinylsulfonic acid (7.5, 15, 25, and 35 μL, 25%, w/v) were added to the polymerization mixture (Table 1 – Monoliths E, F, G, and H). For monoliths prepared with varied concentration of the redox initiator, the synthesis procedure was altered by variation of the mass of ammonium persulfate (10 μL of 3.5, 7, 10, and 15%, w/v) present in the polymerization mixture (Table 1 – Monoliths I, J, K, and L).

Table 1
Composition of the polymerization mixtures of the monoliths with different content of ammonium sulfate (AS), molar fraction of vinylsulfonic acid (VSA), and concentration of ammonium persulfate (APS) (in 0.70 mL 100 mM phosphate buffer, pH = 7.0).

Monolith	AS (mg)	VSA (25%, w/v) (μL)	APS % (w/v), 10 μL
A	8	15	10
B	12	15	10
C	32	15	10
D	42	15	10
E	12	7.5	10
F	12	15	10
G	12	25	10
H	12	35	10
I	12	15	3.5
J	12	15	7
K	12	15	10
L	12	15	15

Total monomer concentration (%*T*): 16.4 (w/v), crosslinker concentration (%*C*), N-(1-adamantyl)acrylamide: 30 mg, statistically methylated-β-CD: 191 mg, PDA: 65 mg, MA: 20 mg, TEMED (10% v/v): 10.0 μL.

2.2. Chromatographic system

The CEC apparatus is described in Ref. [31] and consists of a FUG HCN 35-35000 high voltage generator (FUG Elektronic GmbH, Rosenheim, Germany) with an in-house manufactured electronic steering unit for controlled electrokinetic injection, a spectra 100 UV-VIS detector (Thermo Separation Product, San Jose, CA, USA) with detection cell for in-capillary detection, and a Shimadzu (Kyoto, Japan) LC-10 AD HPLC pump in combination with a flow splitter for conditioning and equilibrating the monolithic capillary with new mobile phase using 50–100 bar. Data treatment and recording was done with EZ-Chrom 6.6 (Scientific Software, San Roman, CA, USA). For the CEC experiments, sample solutions with an analyte concentration of 250–300 mg L^{-1} were prepared in the mobile phase. Sample injection was performed electrokinetically. If not otherwise indicated, the injection parameters are 3 kV for 3 s. UV detection was at a wavelength of 230 nm. *N*,*N*-Dimethylformamide (DMF) was used as a neutral non-retained EOF marker. Water/methanol mobile phases buffered with triethylamine/acetic acid (pH* = 6.8–7.0, electric conductivity 120–150 μS/cm) were used for separations in the reversed-phase mode. In this work, triethylamine/acetic acid was mainly used as buffer system since it has a lower electric conductivity than other buffers, e.g. phosphate, acetate, or borate buffer. Alkylphenones were taken as test solutes (hydrophobic analytes).

Retention time and peak width (peak width at base) are determined with the software employed for recording and data treatment (EZ-Chrom 6.6). The peak width is obtained from applying the tangent method. The asymmetry factor (AF) is calculated at 5% of the maximum peak height. It corresponds to the distance from the leading edge to the tailing edge of the peak divided by twice the distance from the center line of the peak to the leading edge. All efficiency data are mean values (N = 2–3).

3. Results and discussion

3.1. Extra-column band broadening

In a first step we have confirmed the absence of a significant influence of extra-column band broadening processes. In total, the variance of a recorded peak σ^2 is given by the variance due to the separation process σ^2_{sep} and the variances due to injection σ^2_I and detection σ^2_D:

$$\sigma^2 = \sigma^2_{sep} + \sigma^2_I + \sigma^2_D \quad (1)$$

With instrumentation designed for CEC, band broadening due to the detection volume can be assumed to be negligible because detection is performed directly in a segment of the separation capillary being filled or void of stationary phase [34]. With the optical arrangement of the detector used (radiation focused inside the capillary with help of a ball lens) the length of the "effective detection cell" can be assumed to be less than 500 μm. The data acquisition sampling frequency was set to 10 Hz and the rise time of the UV/VIS detector was adjusted to 0.3 s. We estimated the peak width at half height of the recorded peaks to have a minimum value of 4 s (data not shown). We deduce from this comparison that the temporal and spatial resolution of the detector will not contribute significantly to the observed efficiency.

The sample is injected directly onto the first segment of the separation capillary via controlled application of voltage and time (electrokinetic injection). In all experimental studies, we have verified the absence of volume overload by variation of the injection parameters. If the determined efficiency data are independent of the injection volume, the absence of volume overload is confirmed. We have also verified the absence of a concentration overload by variation of the concentration of analyte in the sample solution (concentration range 100–700 mg L^{-1}, data not shown).

However, we have noticed that the removal of the polyimide coating from the inlet side of the monolithic capillary is necessary to avoid characteristic distortions of the recorded peaks [35]. Fig. 1 shows electropherograms, which were obtained for alkylphenones before and after removal of the polyimide coating from the inlet side of the monolithic capillary with help of a sharp blade. It is clearly seen that the removal of the polyimide coating (ca. 10 mm at the capillary end) from the inlet side of the monolithic capillary results in a drastic improvement of the peak symmetry and a complete elimination of the peak distortion.

3.2. Influence of Joule heating effects

In capillary electrochromatography Joule heating resulting from the application of voltage accompanies the propulsion of the mobile phase. In order to evaluate the impact of Joule heating on chromatographic parameters, the separation of alkylphenones in the reversed-phase mode with Monolith H (see Table 1) was taken as an example. Two parameters were investigated as a function of the applied voltage (12–25 kV): (i) electroosmotic flow velocity and (ii) retention factor.

Fig. 2 shows the electroosmotic flow velocity plotted against the applied voltage. There is a linear dependency of the electroosmotic flow velocity u_{eo} on the applied voltage U (x-axis intercept = 2.44 kV, $R^2 = 0.9994$). The linearity of the function $u_{eo} = f(U)$ demonstrates that heating effects can be neglected. An increase in temperature would result in a significant deviation from linearity [34]. In addition, the small positive x-intercept indicates that the electroosmotic pressure generated inside the organic monolith balances the inversely directed hydrostatic pressure (due to the geometry of the apparatus) at very low applied voltage. For the same monolith, it is shown that the retention factors for selected alkylphenones are not affected significantly by a variation of the separation voltage confirming the conclusion that effects due to Joule heating can be neglected (see Fig. S1, Supplementary data).

3.3. Variation of the concentration of ammonium sulfate

In the first part of this series [4], we have investigated the influence of the concentration of the hydrophobic monomer N-adamantyl acrylamide in the polymerization mixture on the retention factors measured for alkylphenones in the reversed-phase mode with mobile phases containing methanol and aqueous buffer. Similar measurements were done with capillaries

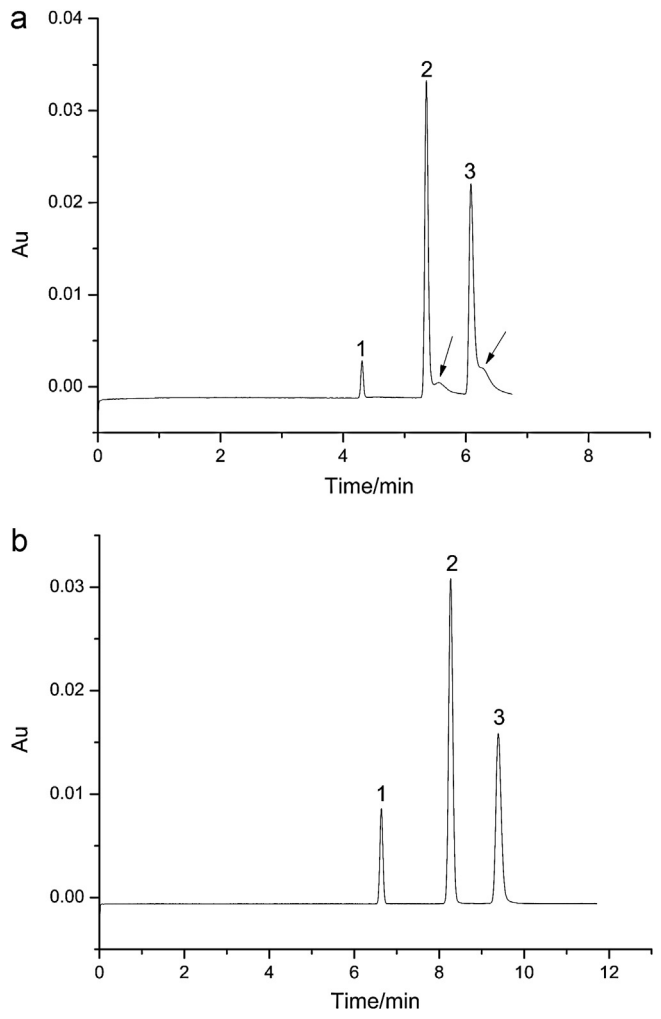

Fig. 1. Electropherograms of alkylphenones on Monolith B (Table 1), (a) separation before removal of polyimide coating, separation voltage 24 kV, and (b) separation after removal of polyimide coating, separation voltage 21.5 kV. Analytes: (1) DMF, (2) acetophenone, and (3) butyrophenone. Mobile phase: methanol/water (50:50, v/v) buffered with triethylamine/acetic acid, pH* = 7.0, electric conductivity = 125 μS/cm; capillary dimensions 230 mm (298 mm) × 100 μm; UV detection at 230 nm; electrokinetic injection: 6 kV for 3 s.

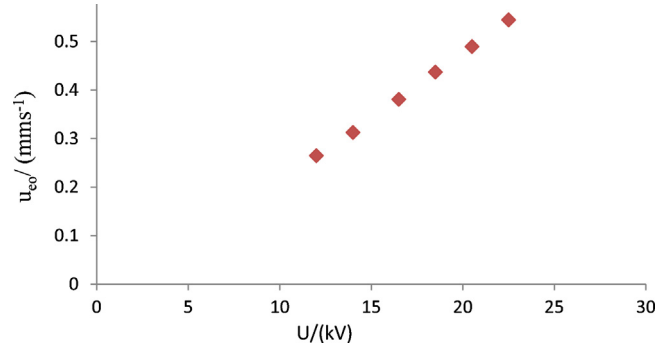

Fig. 2. Dependency of the electroosmotic flow velocity u_{eo} on the applied voltage. Monolith H. Mobile phase: methanol/water (50:50, v/v) buffered with triethylamine/acetic acid, pH* = 7.00, electric conductivity = 125 μS/cm. Capillary dimensions 245 mm (317 mm) × 100 μm; UV detection at 230 nm; electrokinetic injection: 3 kV for 3 s.

Table 2
Electroosmotic mobility, retention factors k for acetophenone and butyrophenone, optimum mobile phase velocity u_{opt}, and minimum plate height H_{min} obtained for monoliths prepared with different mass fraction of ammonium sulfate (AS) in the polymerization mixture (Table 1 – Monoliths A, B, C, and D). Data shown are the average of triplicate runs (standard deviations in brackets).

Monolith	A	B	C	D
DMF				
AS/mg	8	12	32	42
μ_{eo}/(cm^2 kV^{-1} min^{-1})	3.19 (±0.012)	5.70 (±0.007)	9.13 (±0.007)	8.56 (±0.009)
u_{opt}/(mm s^{-1})[a]	0.42	0.55	1.09	1.64
H_{min}/μm[a]	9.1	4.6	4.2	6.5
Acetophenone				
k	0.281 (±0.005)	0.245 (±0.001)	0.201 (±0.003)	0.176 (±0.001)
u_{opt}/(mm s^{-1})[a]	0.42	0.45	1.20	1.64
H_{min}/μm[a]	8.3	4.8	5.7	10.0
Butyrophenone				
k	0.473 (±0.010)	0.413 (±0.002)	0.316 (±0.003)	0.278 (±0.001)
u_{opt}/(mm s^{-1})[a]	0.42	0.38	1.20	1.05
H_{min}/μm[a]	8.7	4.5	7.00	12.7

[a] Determined as the lowest point in the corresponding Van Deemter plot.

synthesized under variation of %*T*. In this third part of the series, we are interested in optimizing with respect to the obtainable efficiency the synthesis parameters for a separation capillary prepared with a fixed composition (and fixed total concentration) of the monomers N-adamantyl acrylamide, piperazinediacrylamide, and methacrylamide in the polymerization mixture. To this end, the separation of alkylphenones with different alkyl chain length in the reversed-phase mode at constant composition of the mobile phase under variation of the applied voltage (10–26 kV) was selected as test system (mobile phase: methanol/water (50:50, v/v) buffered with triethylamine/acetic acid, pH* = 7.0, electric conductivity = 125 μS/cm).

The first synthesis parameter, which was studied, was the concentration of ammonium sulfate (AS) in the polymerization mixture, which is known for acrylamide-based macroporous polymers to influence largely the domain size of the formed monolith [1,2,29]. All authors have reported an increasing domain size with increasing AS concentration, which is attributed to the influence of AS on the phase separation process.

We synthesized different monoliths with varied concentration of AS in the polymerization mixture (11.7–60 g/L) (see Table 1; Monoliths A–D). The same monoliths had been investigated in the second paper of this series [32] by SEM and ISEC. Whereas the pore size distributions determined by ISEC are highly dependent on the concentration of AS, the SEM photographs corroborate the results obtained by ISEC and show a strong dependence of the formed morphology on the concentration of AS (increase in domain size with increasing concentration of AS). Electroosmotic mobilities and retention factors obtained with these monoliths are listed in Table 2l. At higher concentration of AS, there is no dependence of μ_{eo} on the synthesis parameters, while at lower concentration of AS, μ_{eo} is reduced with decreasing concentration of AS. This behavior can be attributed to the dependence of the domain size on the AS concentration and to the occurrence of double layer overlap in the smaller flow-through pores. The dependence of k on the AS concentration is unexpected. One possible explanation of this phenomenon might be that the AS concentration not only influences the morphology of the formed polymer (with regard to the domain size), it might also have an influence on the phase ratio *V*(polymer)/*V*(mobile phase).

Additionally, it was observed that the electroosmotic mobility increases with increasing separation voltage for those monoliths,

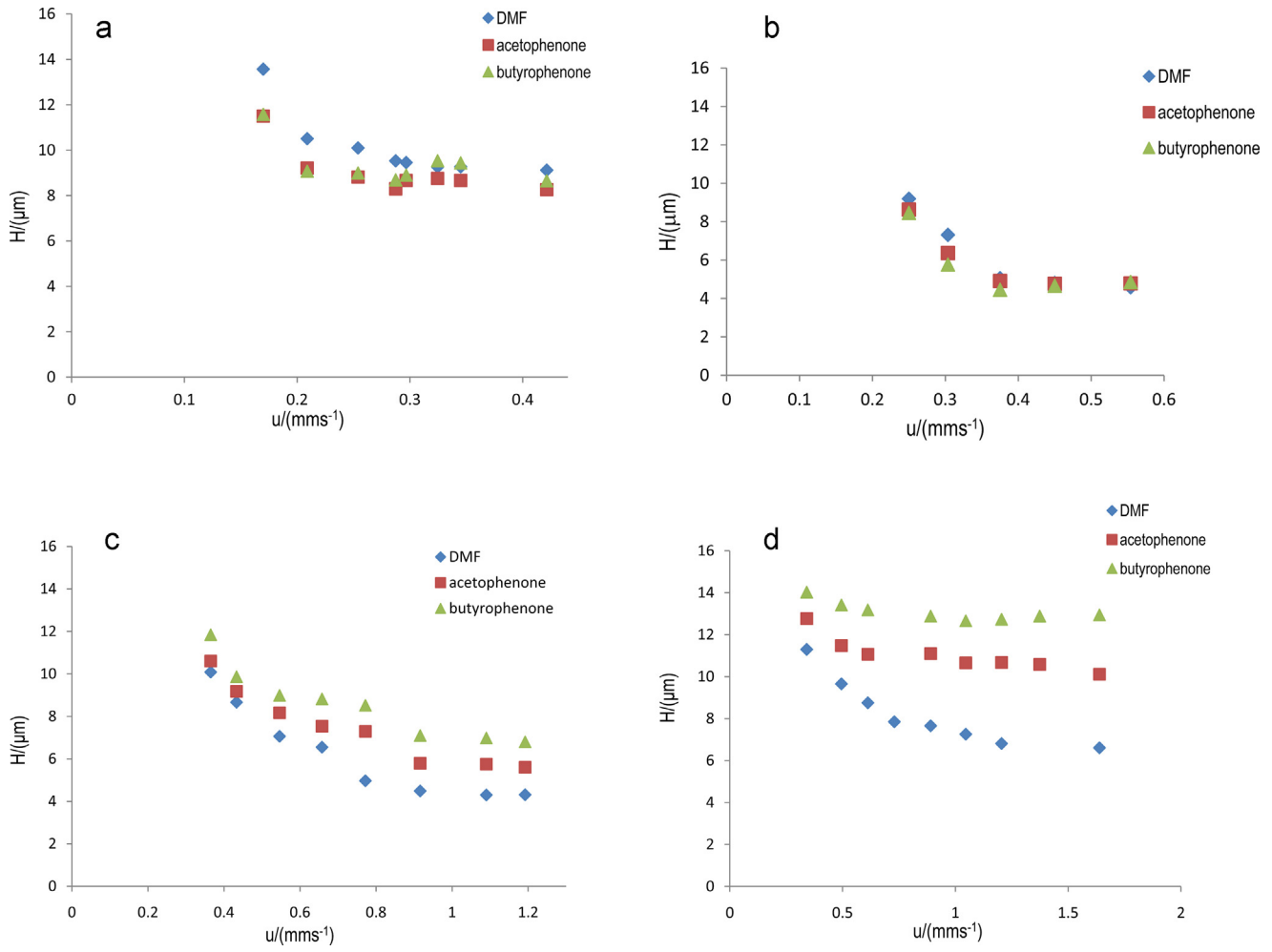

Fig. 3. Van Deemter plots for DMF, acetophenone, and butyrophenone on monoliths prepared with (a) 8 mg AS, (b) 12 mg AS, (c) 32 mg AS, and (d) 42 mg AS in the polymerization mixture (Table 1 – Monoliths A, B, C, and D). Mobile phase: methanol/water (50:50, v/v) buffered with triethylamine/acetic acid, pH* = 7.0, electric conductivity = 120 µS/cm. UV detection at 230 nm.

which were synthesized with a higher content of ammonium sulfate in the polymerization mixture (Monoliths B–D, see Supplementary data, Figure S2). Regarding the low conductivity of the mobile phase and the low electric current strength measured (few µA) and the fact that in all cases the same type of mobile phase was used, we exclude the presence of heating effects (see also Section 3.2). As we have shown in a previous paper [32] the polymeric material produced is mesoporous so that the observed dependence of μ_{eo} on U can be attributed to the presence of electroosmosis of the second kind, which has been reported by Nischang and Tallarek [36]. The dependence of μ_{eo} on U (with excluded heating effects) can be regarded as an indirect evidence for the mesoporosity determined in previous studies [32].

Fig. 3 shows the Van Deemter plots obtained for the nonretained analyte DMF ($k = 0$), and the retained analytes acetophenone and butyrophenone (for retention factors see Table 2). The velocity range investigated is determined by the experimental set-up used (limited voltage range and need to avoid detrimental counter flow at low voltage). All curves can be characterized to be very flat having a small C-term. There is a large impact of the AS concentration on the plate height reached at the minimum of the curve. As a general trend, the efficiency increases with decreasing domain size of the monolith (see SEM photographs presented in [32]). For Monoliths A–D, the minimum plate height H_{min} and the optimum linear mobile phase velocity u_{opt} for each analyte were determined as the lowest point in the corresponding Van Deemter plots (Table 2).

Results in Fig. 3 and Table 2 demonstrate that for Monoliths B–D monolithic capillaries with smaller domain size (lower content of AS) exhibit lower H_{min} values for all three analytes. When the domain size was decreased further (by decreasing the content of AS), again a decrease in efficiency was observed. Fig. 3 shows that Monolith B (12 mg AS) has the highest efficiency (lowest H_{min}) for all three analytes. For the nonretained analyte DMF the minimum plate height H_{min} decreases from about 9.1 µm for Monolith A (8 mg AS) to about 4.6 µm for Monolith B (12 mg AS) and increases again to about 6.5 µm for Monolith D (42 mg AS). The same trend was observed for the retained analytes acetophenone and butyrophenone. The minimum plate height H_{min} decreases from about 8.3 (8.7) µm for Monolith A (8 mg AS) to about 4.8 (4.5) µm for Monolith B (12 mg AS) and increases again with Monolith C (32 mg AS) and Monolith D (64 mg AS) to about 5.7 (7.0) and 10.0 (12.7) µm, respectively (Table 2).

If we take into account, that the domain size increases with increasing AS concentration (as was shown by SEM [32]), the conclusion must be drawn that the efficiency can be improved by decreasing the domain size. However, with very low AS concentration an additional reduction in efficiency with decreasing AS concentration is found. These results correspond to those of Eeltink et al. [27], Lin et al. [37], Peters et al. [38], and Bedair and El-Rassi [39], who observed with methacrylate-based monoliths synthesized with different pore size (by variation of the content of pore forming agent in the polymerization reaction), a similar decrease

Table 3
Retention factor k, minimum plate height H_{min} (determined as the lowest point in the corresponding Van Deemter plot), optimum mobile phase velocity u_{opt}, and peak asymmetry factor AF for acetophenone, and butyrophenone on Monoliths B, C, and D. Mobile phase: methanol/water (50:50, v/v) buffered with triethylamine/acetic acid, pH* = 7.0, electric conductivity = 125 μS/cm. Data shown are the average of triplicate runs (standard deviations in brackets).

Analyte	At optimum velocity				At highest velocity		
	u_{opt}/mm s^{-1}	k	H_{min}/μm	AF	u_{max}/mm s^{-1}	H/μm	AF
Monolith B							
Acetophenone	0.45	0.211 (±0.001)	4.8 (±0.06)	1.033 (±0.005)	0.55	4.8 (±0.26)	1.081 (±0.013)
Butyrophenone	0.38	0.360 (±0.005)	4.5 (±0.26)	1.161 (±0.035)	0.55	4.9 (±0.32)	1.125 (±0.02)
Monolith C							
Acetophenone	1.20	0.180 (±0.001)	5.7 (±0.02)	1.017 (±0.005)	1.20	5.7 (±0.02)	1.017 (±0.005)
Butyrophenone	1.20	0.270 (±0.001)	7.0 (±0.11)	1.063 (±0.008)	1.20	7.0 (±0.11)	1.063 (±0.008)
Monolith D							
Acetophenone	1.64	0.176 (±0.00)	10.0 (±0.19)	1.025 (±0.009)	1.64	10.0 (±0.19)	1.025 (±0.009)
Butyrophenone	1.05	0.278 (±0.001)	12.7 (±0.11)	1.027 (±0.016)	1.64	12.8 (±0.54)	1.056 (±0.15)

in efficiency for monoliths synthesized with a very low concentration of pore forming agent in the polymerization mixture. The authors explained this phenomenon by double-layer overlap in the small size flow-through pores. It is interesting to note that the optimum linear velocity u_{opt} ($u = L_D/t_0$; L_D = length of the capillary to the detector, t_0 = elution time of a nonretained neutral marker) increases with increasing the concentration of ammonium sulfate in the polymerization mixture. For the nonretained analyte DMF (for other analytes see Table 2) u_{opt} increases from about 0.4 mm s^{-1} for Monolith A to about 1.6 mm s^{-1} for Monolith D. In all cases, the resulting curve is very flat, so that it is difficult to estimate its minimum plate height.

The most characteristic difference between the curves obtained for different monoliths (shown in Fig. 3) is the varying dependence of H_{min} on the retention factor. For a detailed discussion of this dependency, the retention factor, the peak asymmetry factor, and H_{min} were determined for the tested analytes with Monoliths B, C, and D at the optimum mobile phase velocity and the highest mobile phase velocity (Table 3) (electropherograms of the tested analytes on Monoliths B, C, and D at highest mobile phase velocity are shown in the Supplementary data, Figure S3). According to Fig. 3 and the values listed in Table 3, Monoliths A and B do not exhibit a significant dependence of H_{min} on the retention factor, whereas for Monoliths C and D there is a strong increase in H_{min} with increasing the retention factor. It is also interesting to see that this dependence of H_{min} on k is increasing with increasing domain size, as Monolith D shows a stronger dependence of H_{min} on k than Monolith C.

SEM photographs for Monoliths C and D (as we have shown in a previous paper [32]) reveal that the structure of these monoliths is a large domain size globular structure with a heterogeneous globule size distribution. In recent publications, Nischang et al. [6,40] reported that polystyrene-DVB based monoliths with a large domain size and a heterogeneous globular structure similar to those of Monoliths C and D are susceptible to the development of a gel porosity when the stationary phase is in contact with an organic solvent. Macroporous polymers of this type have an outer layer of slightly crosslinked polymer chains that is readily swollen when immersed in a hydroorganic solvent forming very small gel pores (micropores and small mesopores).

Microporous materials are known to show the phenomenon of hindered diffusion [41]. The degree of reduction of the apparent diffusion coefficient (e.g. in membrane pores) is a function of the ratio of the solute radius to the pore radius. Beck and Schultz [41] report for microporous membranes with known pore geometry (straight through-pores) that when the ratio of the solute radius to the pore radius is 1/10, the apparent diffusion coefficient is about 40% lower than that estimated in bulk solution. Hindered diffusion can be described by the Renkin equation [42], which combines exclusion from pores based on geometrical considerations (steric hindrance at the entrance to the pores, see also [43,44]) with frictional resistance within the pores based on the additional hydrodynamic drag on the solute due to the proximity of the pore walls.

Another interesting observation shown in Table 3 is the dependence of the asymmetry factor AF on the retention factor. For all three monoliths investigated, there is an increase in AF with increasing k. The presented data, however, do not allow deciding whether also the mobile phase velocity has an influence on this parameter.

3.4. Concentration of initiator

Another variable that has an influence on the chromatographic performance of the synthesized monoliths via changing the overall rate of polymerization is the concentration of the free radical initiator. In general, an increase in the initiator concentration enhances the rate of polymerization, which results in a later phase separation and consequently the formation of small globules. Regarding the finally produced monolith, increasing the concentration of the initiator results in a decrease of the domain size, which in turn decreases its hydrodynamic permeability (via reduction of the mean flow-through pore size) and will also affect its efficiency [45].

In order to study the effect of the initiator concentration on the column performance, four monolithic columns were synthesized with increasing APS concentrations (Table 1 – Monoliths I, J, K, and L, corresponding to final concentration of 2.2×10^{-3} M, 4.4×10^{-3} M, 6.2×10^{-3} M, 9.4×10^{-3} M APS, respectively). Monolith L with 9.4×10^{-3} M APS showed a very bad permeability, which in turn prevented the formation of a detection window (no further CEC measurements). Monolith I with 2.2×10^{-3} M had a good permeability, but did not permit reproducible measurements due to frequent unavoidable current break down resulting from bubble formation inside the monolith. We explain this phenomenon with the occurrence of intersegmental pressure differences resulting from differences in the electroosmotically generated flow rate between adjacent segments. Monoliths J and K with $c(\mathrm{APS}) = 4.4 \times 10^{-3}$ M or 6.2×10^{-3} M, in contrast, allowed repeatable measurements without current breakdown. Van Deemter plots for the solutes DMF and acetophenone are shown in Fig. 4a and b. There is a small improvement in the column efficiency with higher initiator concentration, which can be attributed to a reduction in the domain size of the resulting monolith. There is no significant influence on the retention factor (data not shown).

3.5. Molar fraction of vinylsulfonic acid

As third synthesis parameter, the molar fraction of vinylsulfonic acid in the polymerization mixture was varied. Four

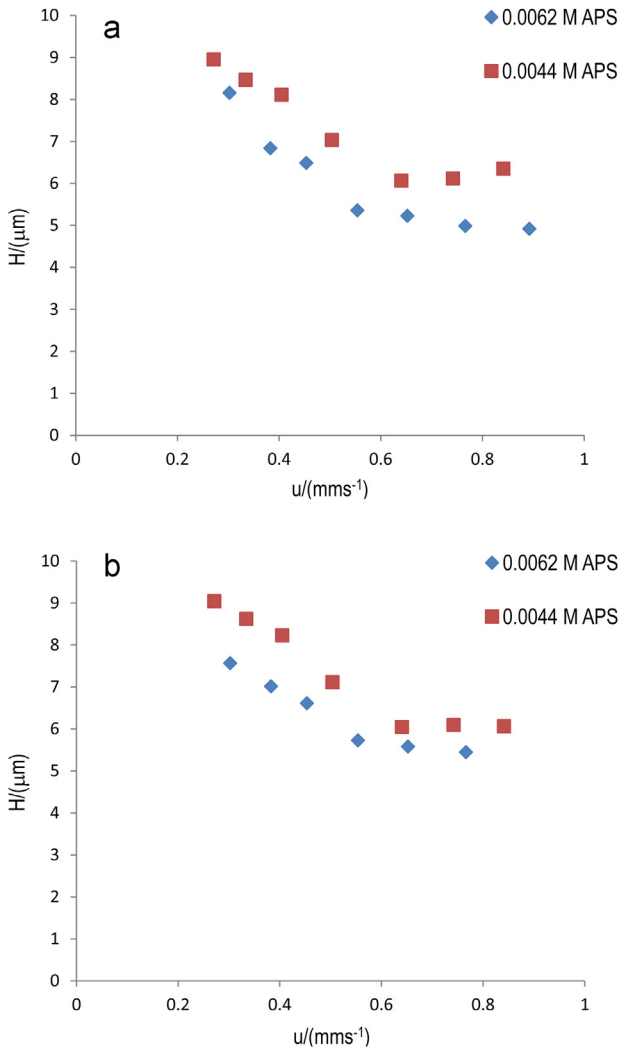

Fig. 4. Van Deemter plots for (a) DMF and (b) acetophenone on monoliths synthesized with 10 µL of 7% and 10% APS in 0.7 ml solution (Monoliths J and K). Mobile phase: methanol/water (50:50, v/v) buffered with triethylamine/acetic acid, pH* = 7.0, electrical conductivity = 120 µS/cm. UV detection at 230 nm.

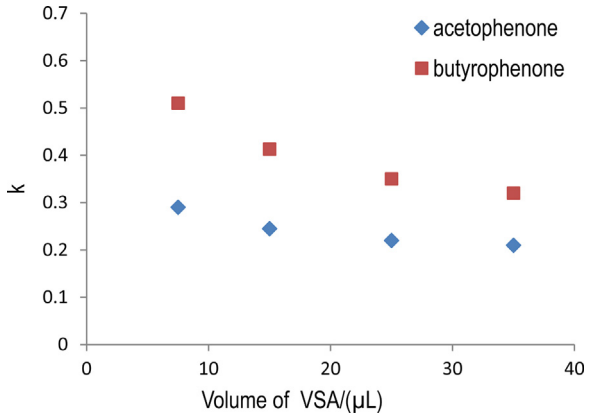

Fig. 5. Dependency of the retention factors of acetophenone and butyrophenone on the volume of VSA in the polymerization mixture (Monoliths E, F, G, and H, corresponding to 7.5, 15, 25, and 35 µL VSA). Mobile phase: methanol/water (50:50, v/v) buffered with triethylamine/acetic acid, pH* = 7.0, electric conductivity = 125 µS/cm.

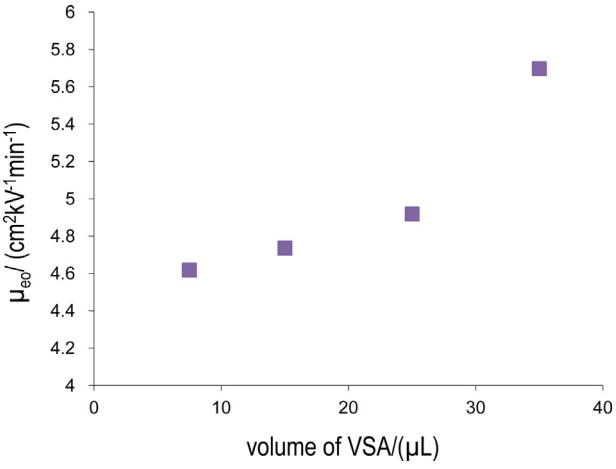

Fig. 6. Electroosmotic mobility versus volume of VSA present in the polymerization mixture (Monoliths E, F, G, and H, corresponding to 7.5, 15, 25, and 35 µL VSA, Table 1). Mobile phase: methanol/water (50:50, v/v) buffered with triethylamine/acetic acid, pH* = 7.0, electric conductivity = 125 µS/cm.

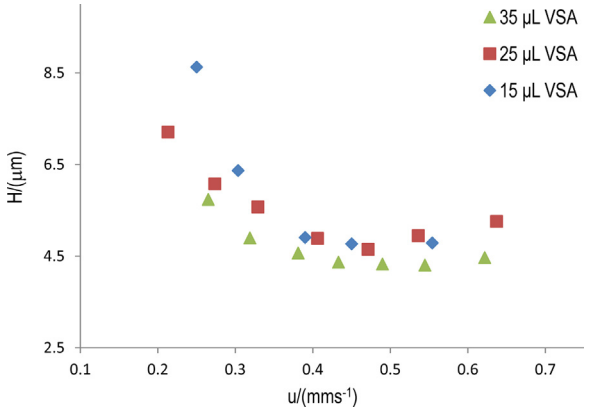

Fig. 7. Van Deemter plots for acetophenone on Monoliths F, G, and H (corresponding to 15, 25, and 35 µL VSA in the polymerization mixture). Mobile phase: methanol/water (50:50, v/v) buffered with triethylamine/acetic acid, pH* = 7.0, electric conductivity = 125 µS/cm.

monolithic capillaries were synthesized containing different volume fractions of VSA in the polymerization mixture (Table 1 – Monoliths E, F, G, and H, corresponding to 7.5, 15, 25, and 35 µL VSA (25%, w/v in aqueous solution) in 0.7 mL solution). VSA is hydrophilic; therefore an increase of its molar fraction in the polymerization mixture will decrease the hydrophobicity of the resulting monolithic stationary phase, which in turn decreases the retention factor for neutral analytes in the reversed-phase mode [46,47]. Indeed, the retention factors for acetophenone and butyrophenone were decreased with increasing the volume fraction of VSA in the polymerization mixture (mobile phase: methanol/water (50:50, v/v) buffered with triethylamine/acetic acid, pH* = 7.0, electric conductivity = 125 µS/cm) (Fig. 5).

There is an increase in the electroosmotic mobility with increasing content of VSA in the polymerization mixture (Fig. 6), which can be attributed to the increase in the surface charge density (number of charged groups per surface unit polymer) [47]. Van Deemter plots of these monoliths were measured for the retained analyte acetophenone (Fig. 7) (for the non-retained analyte DMF see Figure S4, Supplementary data). Results show no significant influence of the content of VSA in the polymerization mixture on the observed efficiency. With increasing the content of VSA in the polymerization mixture, only a slight shift to lower plate heights is achieved. This observation can be explained by the decrease in the retention factor for neutral analytes because of the reduced hydrophobicity of the monolithic stationary phase (see Fig. 5). We

Table 4
Between groups variance s_B^2, within groups variance s_W^2, ratio of variances s_B^2/s_W^2 and overall relative standard deviation for the theoretical plate heights for DMF and selected alkylphenones determined with three batches of Monolith B (see Table 1), three repeated runs with each capillary (see also Table S1, Supplementary data).

	s_B^2	s_W^2	s_B^2/s_W^2	$F_{2,6,95}$ crit.	RSD, % N = 9 (3 cap., each 3 runs)
H, DMF/(μm)	0.2765	0.0200	13.81	5.143	5.23
H, acetophenone/(μm)	0.4407	0.03172	13.89	5.143	5.98
H, butyrophenone/(μm)	0.1821	0.05673	3.21	5.143	2.88

Mobile phase: methanol/water (50:50, v/v) buffered with triethylamine/acetic acid, pH* = 7.0, electric conductivity = 125 μS/cm.
Further details regarding retention factors, electroosmotic mobilities, capillary dimensions, injection parameters, or applied voltages see Table S1, Supplementary data.

also observed a shift of u_{opt} to higher linear mobile phase velocity. In analogy to results obtained by Peters et al. [38] and Bedair and El-Rassi [39] with monoliths of different chemical composition operated in CEC, an impact of the VSA content on the morphology of the formed macroporous polymer might be expected. However, this expectation is not corroborated by our experimental results.

3.6. Repeatability of the synthesis procedure

In order to investigate whether the synthesis procedure employed is reproducible, three different monolithic capillaries (Monolith B, see Table 1) were prepared at three different days (different batches) with a fixed composition of the polymerization mixture and tested for the separation of acetophenone and butyrophenone under identical conditions (see Table S1, Supplementary data). For each capillary, three runs were performed by measuring the plate heights for the non-retained marker DMF and the two alkylphenones. The reached RSDs (3–6%, see Table 4) demonstrate that (regarding the chromatographic efficiency measured) the synthesis procedure employed is very well controlled. Data regarding the electroosmotic mobilities and the retention factors obtained for these three capillaries are listed in Table S1, Supplementary data. Also for these parameters there is only a small variation (RSD for the retention factors = 1–2%; RSD for the electroosmotic mobility = 9%).

The capillary-to-capillary variation of the theoretical plate height is significant (when compared to the run-to-run variation) for the first two solutes investigated, which was confirmed by analysis of variance (ANOVA) [48]. The variances between the groups s_B^2 (three capillaries) and within the groups s_W^2 (three repeated runs for each capillary) were calculated. The ratio of the variances s_B^2/s_W^2 is compared to the tabulated F-values (P = 95%, see Table 4). In the case of DMF and acetophenone the between groups variances are significantly higher than the within groups variances ($F_{calculated} > F_{tabulated}$), whereas in the case of butyrophenone there is no significant difference between these two variances ($F_{calculated} < F_{tabulated}$). These data confirm that the production of the capillaries introduces a (controlled) source of variance, which can be identified as a small variation in the phase ratio, the morphology (e.g. with respect to domain size and pore size distribution), the hydrophobicity (i.e. chemical composition of the co-polymer), or the zeta potential at the liquid/solid-interface [49].

4. Conclusions

Careful optimization of the parameters for the synthesis of N-adamantyl-group containing polyacrylamide-based continuous beds enables the preparation of continuous beds, which can be applied with high efficiency in reversed-phase capillary electrochromatography. The investigations show that (under the conditions of our experiments) the chromatographic efficiency is not only strongly dependent on the concentration of the lyotropic salt ammonium sulfate but also on the concentration of the initiator in the polymerization mixture, while the molar fraction of the charged monomer VSA only has a minor influence. When compared to data gained by SEM and ISEC [32], the observed differences can in part be explained by the influence of the varied parameters on the domain size of the formed monolith. There is a good capillary-to-capillary repeatability reached for the plate heights measured for DMF and selected alkylphenones in the reversed-phase mode confirming that the synthesis procedure employed in this work is well controlled.

Acknowledgement

A.A. Al-Massaedh thanks Al-Albayt University (Jordan) for financial support.

Appendix A. Supplementary data

Supplementary data associated with this article can be found, in the online version, at http://dx.doi.org/10.1016/j.chroma.2013.11.003.

References

[1] D. Hoegger, R. Freitag, Electrophoresis 24 (2003) 2958.
[2] D. Hoegger, R. Freitag, J. Chromatogr. A 914 (2001) 211.
[3] V. Ratautaite, A. Maruska, M. Erickson, O. Kornysova, J. Sep. Sci. 32 (2009) 2582.
[4] A.A. Al-Massaedh, U. Pyell, J. Chromatogr. A 1286 (2013) 183.
[5] I. Nischang, J. Chromatogr. A 1287 (2013) 39.
[6] I. Nischang, I. Teasdale, O. Brueggemann, Anal. Bioanal. Chem. 400 (2011) 2289.
[7] J. Urban, P. Jandera, Anal. Bioanal. Chem. 405 (2013) 2123.
[8] F. Svec, J. Chromatogr. A 1228 (2012) 250.
[9] I. Nischang, O. Brueggemann, F. Svec, Anal. Bioanal. Chem. 397 (2010) 953.
[10] F. Svec, J. Chromatogr. A 1217 (2010) 902.
[11] A. Nordborg, E.F. Hilder, Anal. Bioanal. Chem. 394 (2009) 71.
[12] G. Guiochon, J. Chromatogr. A 1168 (2007) 101.
[13] I. Nischang, O. Brueggemann, J. Chromatogr. A 1217 (2010) 5389.
[14] I. Nischang, I. Teasdale, O. Brueggemann, J. Chromatogr. A 1217 (2010) 7514.
[15] J. Urban, F. Svec, J.M.J. Frechet, J. Chromatogr. A 1217 (2010) 8212.
[16] K. Liu, H.D. Tolley, M.L. Lee, J. Chromatogr. A 1227 (2012) 96.
[17] T.J. Causon, E.F. Hilder, I. Nischang, J. Chromatogr. A 1263 (2012) 108.
[18] C. Puangpila, T. Nhujak, Z. El-Rassi, Electrophoresis 33 (2012) 1431.
[19] P. Jandera, M. Stankova, V. Skerikova, J. Urban, J. Chromatogr. A 1274 (2013) 97.
[20] M. Stankova, P. Jandera, V. Skerikova, J. Urban, J. Chromatogr. A 1289 (2013) 47.
[21] Y. Huo, P.J. Schoenmakers, W.T. Kok, J. Chromatogr. A 1175 (2007) 81.
[22] S. Eeltink, G.P. Rozing, P.J. Schoenmakers, W.T. Kok, J. Chromatogr. A 1109 (2006) 74.
[23] A.M. Siouffi, J. Chromatogr. A 1126 (2006) 86.
[24] F. Svec, J.M.J. Frechet, Chem. Mater. 7 (1995) 707.
[25] S. Xie, F. Svec, J.M.J. Frechet, J. Polym. Sci. Part A: Polym. Chem. 35 (1997) 1013.
[26] S. Eeltink, L. Geiser, F. Svec, J.M.J. Frechet, J. Sep. Sci. 30 (2007) 2814.
[27] S. Eeltink, J.M. Herrero-Martinez, G.P. Rozing, P.J. Schoenmakers, W.T. Kok, Anal. Chem. 77 (2005) 7342.
[28] T. Jiang, J. Jiskra, H.A. Claessens, C.A. Cramers, J. Chromatogr. A 923 (2001) 215.
[29] A. Maruska, O. Kornysova, J. Biochem. Biophys. Methods 59 (2004) 1.
[30] P. Aggarwal, H.D. Tolley, M.L. Lee, Anal. Chem. 84 (2012) 247.
[31] A. Wahl, I. Schnell, U. Pyell, J. Chromatogr. A 1044 (2004) 211.
[32] A.A. Al-Massaedh, U. Pyell, under review.
[33] W.A. Skinner, J.H. Lange, T.E. Shellenberger, W.T. Colwell, J. Med. Chem. 10 (1967) 949.
[34] H. Rebscher, U. Pyell, Chromatographia 38 (1994) 737.
[35] F. Baeuml, T. Welsch, J. Chromatogr. A 961 (2002) 35.
[36] I. Nischang, U. Tallarek, Electrophoresis 25 (2004) 2935.
[37] J. Lin, G. Huang, X. Lin, Z. Xie, Electrophoresis 29 (2008) 4055.
[38] E.C. Peters, M. Petro, F. Svec, J.M.J. Frechet, Anal. Chem. 70 (1998) 2288.
[39] M. Bedair, Z. El-Rassi, Electrophoresis 23 (2002) 2938.
[40] I. Nischang, J. Chromatogr. A 1236 (2012) 152.

[41] R.E. Beck, J.S. Schultz, Science 170 (1970) 1302.
[42] E.M. Renkin, J. Gen. Physiol. 38 (1954) 225.
[43] J.C. Giddings, E. Kucera, C.P. Russell, M.N. Myers, J. Phys. Chem. 72 (1968) 4397.
[44] K. Jerabek, Anal. Chem. 57 (1985) 1595.
[45] F. Svec, J.M.J. Frechet, Macromolecules 28 (1995) 7580.
[46] F. Al-Rimawi, U. Pyell, J. Chromatogr. A 1160 (2007) 326.
[47] M. Zhang, Z. El-Rassi, Electrophoresis 22 (2001) 2593.
[48] J.N. Miler, J.C. Miller, Statistics for Analytical Chemistry, Ellis Horwood Limited, London, 1993.
[49] F. Al-Rimawi, U. Pyell, J. Sep. Sci. 29 (2006) 2816.

Adamantyl-group containing mixed-mode acrylamide-based continuous beds for capillary electrochromatography. Part III. Optimization of the chromatographic efficiency

"Ayat Allah" Al-Massaedh, Ute Pyell*

University of Marburg, Department of Chemistry, Hans-Meerwein-Straße, D-35032 Marburg, Germany

* corresponding author

Supplementary data

Figure S1: Dependence of the retention factors for alkylphenones on the applied voltage. Monolith H.

Figure S2. Dependence of the electroosmotic mobility on the applied voltage for Monoliths A, B, C, and D.

Figure S3: Electropherograms obtained for the separation of alkylphenones on monoliths synthesized with varied concentration of the lyotropic salt ammonium sulfate in the polymerization mixture at highest mobile phase linear velocity.

Figure S4: Van Deemter plot for DMF on monoliths synthesized with varied concentration of the negatively charged monomer vinylsulfonic acid in the polymerization mixture (Monoliths F, G, and H).

Table S1: Capillary-to-capillary reproducibility data for the retention factor, the electroosmotic mobility, the number of theoretical plates, and the plate height for DMF and selected alkylphenones determined with Monolith B.

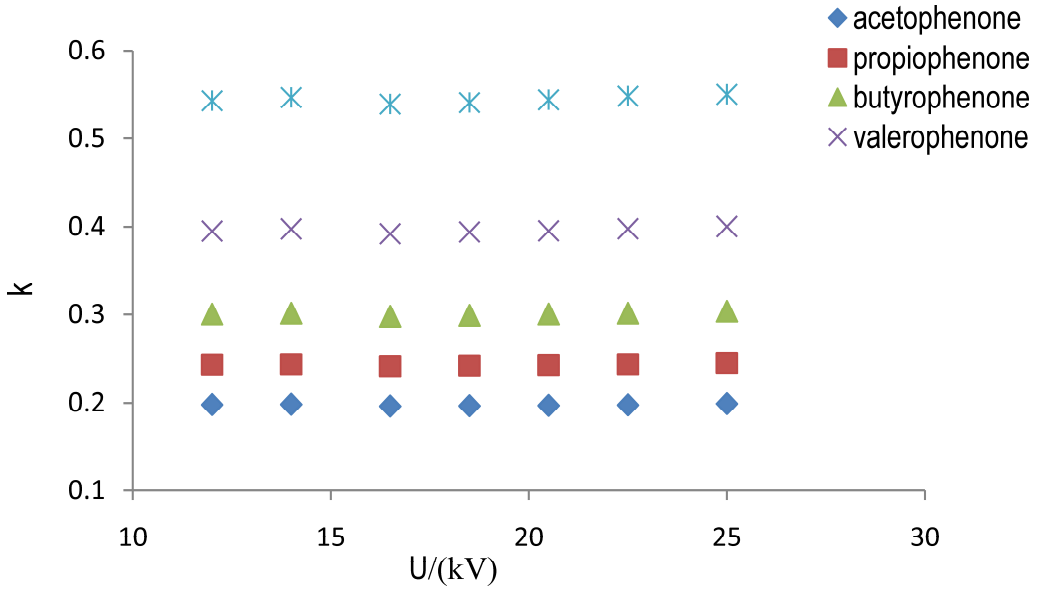

Figure S1. Dependence of the retention factors for alkylphenones on the applied voltage. Monolith H. Mobile phase: methanol/water (50:50, v/v) buffered with triethylamine/acetic acid, pH* = 7.0, electric conductivity = 125 μS/cm. Capillary dimensions 245 mm (317 mm) × 100 μm; UV detection at 230 nm; electrokinetic injection: 3 kV for 3 s.

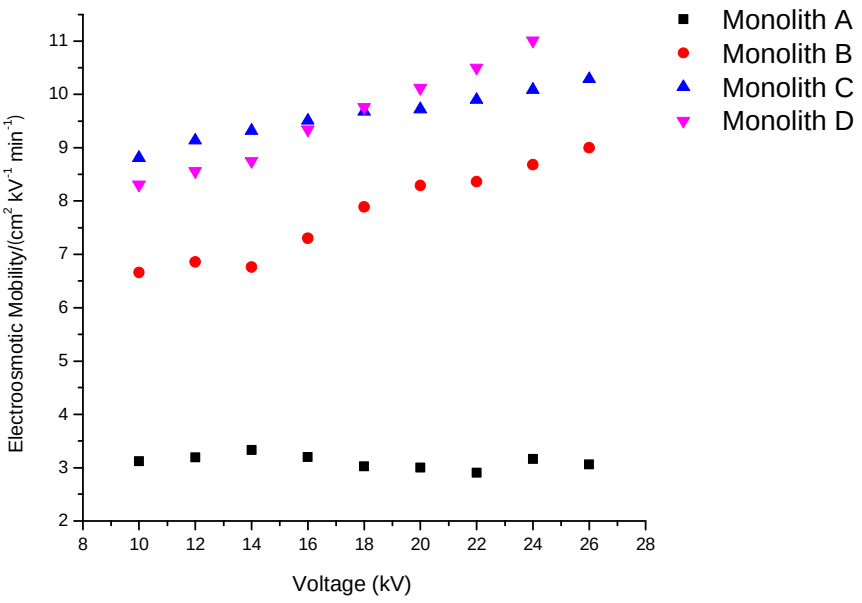

Figure S2. Dependence of the electroosmotic mobility μ_{eo} on the applied voltage for Monoliths A, B, C, and D

(a)-

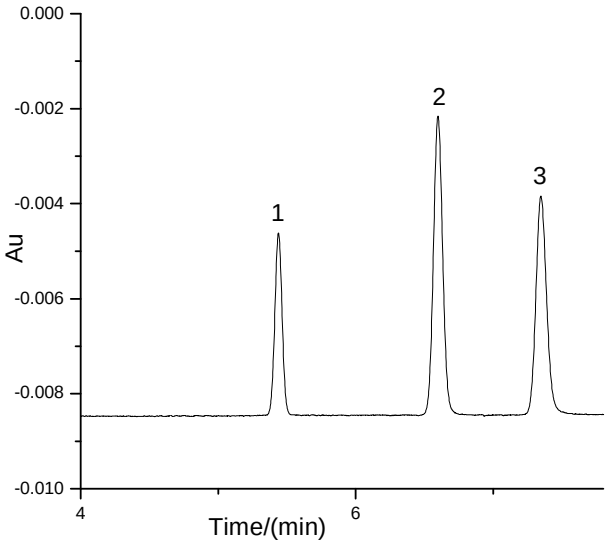

(b)-

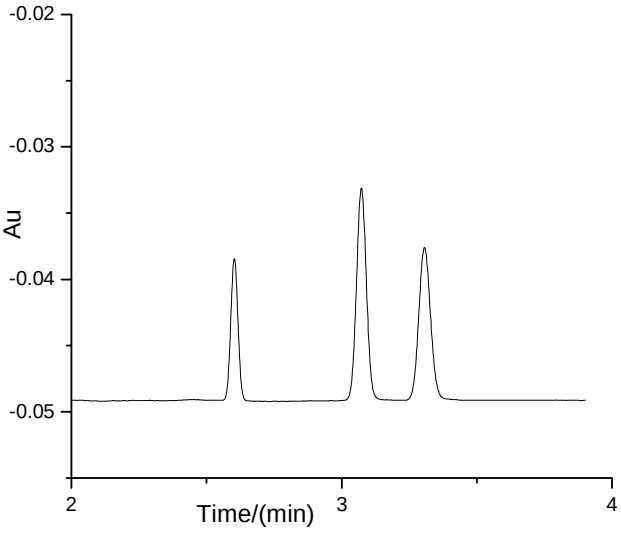

Figure S3 continued on next page.

(c)-

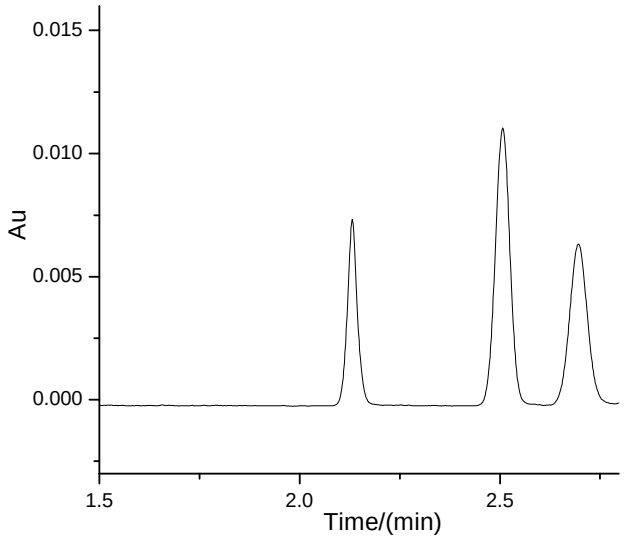

Figure S3. Separation of alkylphenones on Monoliths B, C, and D at highest mobile phase velocity (a) Monolith B, (b) Monolith C, and (c) Monolith D. Analytes: (1) DMF, (2) acetophenone, and (3) butyrophenone. Mobile phase: methanol/water (50:50, v/v) buffered with triethylamine/acetic acid, pH* = 7.0, electric conductivity = 125 µS/cm.

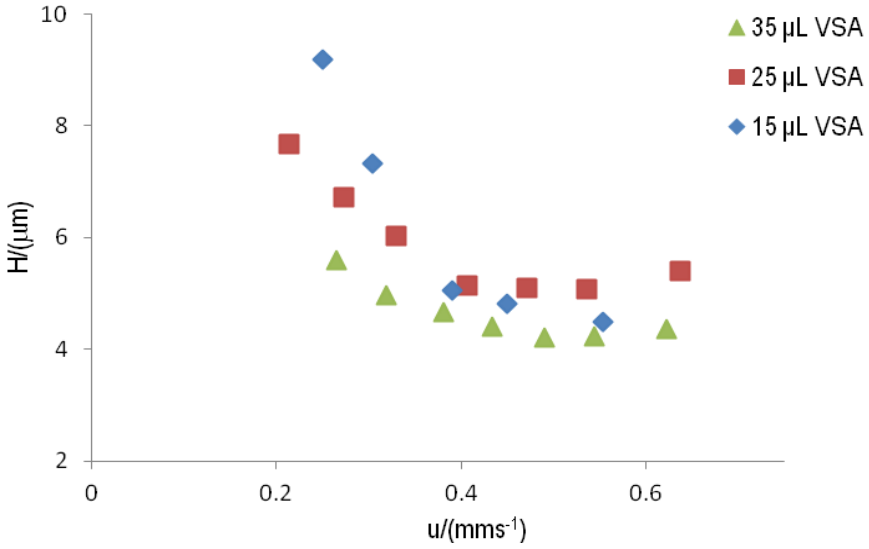

Figure S4. Van Deemter plot for DMF obtained with Monoliths F, G, and H (see Tab. 1). Mobile phase: methanol/water (50:50, v/v) buffered with triethylamine/acetic acid, pH* = 7.0, electric conductivity = 125 µ S/cm.

Table S1. Capillary-to-capillary repeatability data for the retention factor k, the electroosmotic mobility μ_{eo}, the number of theoretical plates N, and the theoretical plate height H for DMF and selected alkylphenones determined with Monolith B (see Tab. 1). Mobile phase: methanol/water (50:50, v/v) buffered with triethylamine/acetic acid, pH* = 7.0, electric conductivity = 125 µS/cm. UV detection at 230 nm.

	Run	t_0/min	t_r/min aceto-phenone	t_r/min butyro-phenone	k aceto-phenone	k butyro-phenone	μ_{eo}/ ($cm^2\,kV^{-1}\,min^{-1}$)	N DMF	N aceto-phenone	N butyro-phenone	H/µm DMF	H/µm aceto-phenone	H/µm butyro-phenone
Capillary 1	1	6.158	7.653	8.652	0.242	0.405	5.11	38300	35600	26800	5.96	6.41	8.51
	2	6.257	7.777	8.787	0.242	0.404	5.03	38500	34400	27100	5.93	6.63	8.42
	3	6.172	7.658	8.650	0.240	0.401	5.10	37700	34800	27000	6.04	6.56	8.44
Capillary 2	1	6.690	8.308	9.407	0.241	0.406	4.76	38200	33900	25500	5.96	6.73	8.96
	2	6.773	8.455	9.600	0.248	0.417	4.70	38600	33700	25800	5.91	6.77	8.85
	3	6.667	8.292	9.408	0.243	0.411	4.77	40100	35000	26700	5.68	6.51	8.55
Capillary 3	1	7.443	9.248	10.58	0.242	0.421	4.13	43200	35900	27200	5.19	6.23	8.23
	2	7.467	9.265	10.57	0.240	0.416	4.12	40600	38900	25800	5.52	5.75	8.68
	3	7.500	9.348	10.67	0.246	0.423	4.10	40800	38200	28000	5.49	5.86	7.99

Capillary 1: L_{eff} = 228 mm, L_{Total} = 297 mm; separation voltage: 21.5 kV; electrokinetic injection: 6 kV for 6 s.

Capillary 2: L_{eff} = 228 mm, L_{Total} = 300 mm; separation voltage: 21.5 kV; electrokinetic injection: 6 kV for 6 s.

Capillary 3: L_{eff} = 224 mm, L_{Total} = 295 mm; separation voltage: 21.5 kV; electrokinetic injection: 6 kV for 6 s.

ELSEVIER LICENSE
TERMS AND CONDITIONS

Apr 08, 2014

This is a License Agreement between "Ayat Allah" Al-Massaedh ("You") and Elsevier ("Elsevier") provided by Copyright Clearance Center ("CCC"). The license consists of your order details, the terms and conditions provided by Elsevier, and the payment terms and conditions.

All payments must be made in full to CCC. For payment instructions, please see information listed at the bottom of this form.

Supplier	Elsevier Limited The Boulevard, Langford Lane Kidlington, Oxford, OX5 1GB, UK
Registered Company Number	1982084
Customer name	"Ayat Allah" Al-Massaedh
Customer address	University of Marburg, 35032 Marburg, Germany.
License number	3364111338753
License date	Apr 08, 2014
Licensed content publisher	Elsevier
Licensed content publication	Journal of Chromatography A
Licensed content title	Adamantyl-group containing mixed-mode acrylamide-based continuous beds for capillary electrochromatography. Part III. Optimization of the chromatographic efficiency
Licensed content author	“Ayat Allah” Al-Massaedh, Ute Pyell
Licensed content date	17 January 2014
Licensed content volume number	1325
Licensed content issue number	
Number of pages	9
Start Page	186
End Page	194
Type of Use	reuse in a thesis/dissertation
Portion	full article
Format	both print and electronic
Are you the author of this Elsevier	Yes
Will you be translating?	No
Title of your thesis/dissertation	Adamantyl-Group Containing Mixed-Mode Acrylamide-Based Continuous Beds for Capillary Electrochromatography: Synthesis, Characterization, Optimization and Investigation of the Chromatographic Efficiency
Expected completion date	May 2014

5.4. Publication IV

Adamantyl-group containing mixed-mode acrylamide-based continuous beds for capillary electrochromatography. Part IV: Investigation of the chromatographic efficiency dependent on the retention mode

"Ayat Allah" Al-Massaedh, Ute Pyell

Journal of Chromatography A, 1349 (2014) 80-89

doi: 10.1016/j.chroma.2014.05.002

5.4.1. Summary and discussion

In this publication, we study with different classes of neutral analytes (with varied hydrophobicity) the impact of the type of retention mode (influenced by the type of analyte and the mobile phase composition) and the impact of the analyte functionality on the chromatographic efficiency and peak symmetry with a monolith synthesized under optimized synthesis parameters. With this monolithic capillary high separation efficiencies (up to ca. 220,000 m^{-1}) are obtained for the separation of different analyte classes (alkylphenones, nitrotoluenes, and phenolic compounds with k = 0.2-0.55) in the reversed-phase mode, in the normal-phase mode, and in the mixed mode. For neutral alkylanilines (k < 0.25) plate numbers of about 300,000 m^{-1} can be routinely reached in the reversed-phase elution mode. For phenolic analytes, it is shown that the analyte functionality and the mobile phase composition have a strong influence on peak symmetry and chromatographic efficiency. For explaining the effective separation of low molecular weight compounds exhibited by the synthesized monolithic capillaries, a mechanism of the formation of their morphology (phase-separation process) in the presence of Me-β-CD as solubilizing agent is suggested. This is mechanism based on the idea that due to the high complex stability constant of the adamantyl group with methylated-β-CD in aqueous phase the outside of the formed precipitated nuclei is enriched by complexed adamantyl groups forming a hydrophilic outer surface shielding layer. Consequently, the growth of the swollen nuclei takes place in a diffusion controlled manner during polymerization, which results in a decrease in the rate of growth of the swollen nuclei. This leads to a retardation of the phase separation process and to the formation of a monolith of small domain size with reduced microheterogeneity.

The potential of the synthesized mixed-mode monolithic stationary phases for the separation of protonated alkylanilines in the ion-exchange mode is confirmed showing peak compression, which is typical for a stationary phase with a bimodal pore size distribution. With increased mass fraction of the polar monomer methacrylamide in the polymerization mixture the spectrum of retention modes can even be extended to the separations of very polar solutes (nucleosides) in the HILIC mode.

In this publication, we suggest a simplified two-parameter plate height equation $H = B/u + C\,u$ to fit experimental efficiency data obtained by CEC with an organic monolith.

With increasing efficiency of the monolithic capillary it is observed that longitudinal diffusion becomes the dominant mechanism of peak broadening. This was confirmed by comparing the values of plate height for propiophenone obtained via fitting the experimental data to the simplified two parameter plate height equation with that value which is obtained by modelling the peak broadening with molecular diffusion in an open tube.

5.4.2. Author contribution

All the experimental part of this study was carried out by me. The section of theoretical considerations was written by Prof. Dr. Ute Pyell. The draft of the manuscript was written by me and corrected by Prof. Dr. Ute Pyell. The final revision of the manuscript was conducted by me and Prof. Dr. Ute Pyell before submission to the journal. Prof. Ute Pyell was responsible for the supervision of this work.

Journal of Chromatography A, 1349 (2014) 80–89

Contents lists available at ScienceDirect

Journal of Chromatography A

journal homepage: www.elsevier.com/locate/chroma

Adamantyl-group containing mixed-mode acrylamide-based continuous beds for capillary electrochromatography. Part IV: Investigation of the chromatographic efficiency dependent on the retention mode

"Ayat Allah" Al-Massaedh, Ute Pyell*

University of Marburg, Department of Chemistry, Hans-Meerwein-Straße, D-35032 Marburg, Germany

ARTICLE INFO

Article history:
Received 25 January 2014
Received in revised form 26 April 2014
Accepted 1 May 2014
Available online 9 May 2014

Keywords:
Capillary electrochromatography
Monolithic stationary phase
Band broadening
Cyclodextrin
Axial diffusion
Efficiency

ABSTRACT

In our previous work we have described the synthesis, characterization, and optimization of the chromatographic efficiency of a highly crosslinked macroporous mixed-mode acrylamide-based monolithic stationary phase synthesized by in situ free radical copolymerization of cyclodextrin-solubilized N-adamantyl acrylamide, piperazinediacrylamide, methacrylamide and vinylsulfonic acid in aqueous medium in pre-treated fused silica capillaries of 100 μm I.D. In the present work, we study with different classes of neutral analytes (with varied hydrophobicity) the impact of the type of retention mode (influenced by the type of analyte and the mobile phase composition) and the impact of the solute functionality on the chromatographic efficiency and peak symmetry with a monolith synthesized under optimized synthesis parameters. With this monolithic capillary high separation efficiencies (up to ca. 220,000 m^{-1}) are obtained for the separation of different analyte classes (alkylphenones, nitrotoluenes, and phenolic compounds with $k = 0.2–0.55$) in the reversed-phase mode, in the normal-phase mode, and in the mixed mode. For neutral alkylanilines ($k < 0.25$) plate numbers of about 300,000 m^{-1} are routinely reached in the reversed-phase elution mode. For phenolic solutes separated in a mixed mode there is a solute-specific influence on peak symmetry and chromatographic efficiency. With increasing efficiency of the monolith, axial diffusion becomes an important mechanism of band broadening. For those peaks, which do not show a significant asymmetry (asymmetry factor ≤1.05), it is confirmed that plate heights gained via the tangent method are equivalent to those gained via moment analysis.

1. Introduction

In the last years, there is growing interest in organic polymer monoliths for CEC and LC. Their ease of preparation in the confines of different separation channels and the availability of a wide variety of suitable monomers make them an attractive alternative to columns packed with particulate material [1–10]. Typically, organic polymer monoliths are prepared by an *in situ* free radical copolymerization of a mixture of monomers dissolved in a porogenic solvent in the presence of an initiator (system) inside a pre-treated fused silica capillary or inside the channel of a microfluidic chip, whereas inorganic silica-based monoliths are prepared via a sol–gel process from inorganic precursors such as alkoxides in the presence of a water-soluble porogen such as poly(ethylene glycol) (PEG) [11,12]. Differences in the synthesis procedure affect the morphology, the porous properties, and the chromatographic performance of the resulting monolith. The main characteristic structural differences between these two types of monoliths are the type of pore size distribution and, consequently, the volume fraction of mesopores (pores with a diameter between 2 and 50 nm). These differences make silica-based monoliths to an excellent material for the separation of low molecular weight compounds [1,12,13], while organic polymer monoliths have been mainly used for the separation of larger molecules like proteins, peptides, or DNA fragments [1]. Against this background, in the last years the optimization of polymer-based monoliths for the separation of small molecules has come into the focus of intense research activities [4,6,7,10,14–23].

Generally, adjusting the porous properties of polymer-based monoliths, which have a strong influence on their chromatographic performance, is always carried out via optimization of the synthesis parameters concerning the composition of the polymerization mixture and the reaction conditions [2,10,22,24–32]. In analogy

* Corresponding author. Tel.: +49 6421 2822192; fax: +49 6421 2822124.
E-mail address: pyellu@staff.uni-marburg.de (U. Pyell).

http://dx.doi.org/10.1016/j.chroma.2014.05.002
0021-9673/

to chromatographic beds packed with particulate material, a large effort has been put into the synthesis of monoliths with homogeneous morphology. One parameter to describe the morphology of a polymeric monolith is the domain size defined as the combination of the mean flow-through pore size and the mean globule size [33]. Efficiencies of monolithic columns have been reported to be correlated with the domain size [33,34]. Other parameters characterizing the monolith structure are the pore size distribution, the external and internal porosity and the globule size distribution.

The separation efficiency observed for small molecules with an organic polymer monolith is often relatively poor and largely dependent on the retention factor and the chromatographic conditions and even reported to be solute-specific [18,35,36]. Largely differing efficiencies have been obtained for the separation of small molecules by CEC with organic polymer monoliths. Efficient separations of small molecules could be achieved by CEC with acrylamide-based monoliths. Hoegger and Freitag [26] obtained minimum plate heights H_{min} of 10–15 μm for the unretained marker dimethylformamide (DMF) and the analyte phenanthrene, when they studied an acrylamide-based monolith prepared from N,N-dimethylacrylamide (DMAA), hexylacrylate (HeA) piperazindiacrylamide (PDA), and vinylsulfonic acid (VSA) employing a purely organic (methanol/acetonitrile) mobile phase. Better efficiencies (H_{min} = 5–10 μm for DMF) were obtained with a hydro-organic mobile phase and a more hydrophilic acrylamide-based monolith synthesized from DMAA, PDA, and VSA [28]. In a similar approach Palm and Novotny [37] and Zhang and El Rassi [38] synthesized acrylamide-based monoliths for CEC from acrylamide (partly replaced by butyl, hexyl or lauryl acrylate and acrylic acid or VSA) and bisacrylamide in the presence of poly(oxyethylene) as porogenic polymer in formamide or N-methylformamide/aqueous buffer. For this type of stationary phase efficiencies up to ca. 400,000 plates m^{-1} were reported (e.g. for phenones k = 0.1–0.4; H_{min} = 3 μm). High efficiencies (N = 220,000–260,000 m^{-1}) were also reached for phenolic solutes (k = 0.2–0.8) separated by mixed-mode CEC on a monolith which was synthesized in the presence of ammonium sulfate in aqueous medium from N-IPA, PDA, VSA and N,N′-ethylenedianilinediacrylamide solubilized by formation of a complex with statistically methylated β-CD [39]. Enlund et al. [40] obtained efficiencies up to ca. 200,000 plates m^{-1} for the CEC separation of hydrophobic amines (tricyclic antidepressants) using a hydro-organic mobile phase with an acrylamide-based monolith synthesized from N-isopropylacrylamide (N-IPA), methacrylamide (MA), piperazinediacrylamide (PDA), and vinylsulfonic acid (VSA).

In our previous publication [8], we reported the synthesis of a monolith which is based on the solubilization of N-adamantyl acrylamide in aqueous solution via a 1:1 complex formed with statistically methylated β-CD. Monoliths were prepared by in situ free radical copolymerization of this complex with PDA, MA and VSA in aqueous medium in pre-treated fused silica capillaries (100 μm I.D.). In following publications [9,10], we studied the influence of the composition of the polymerization mixture and morphology and porous properties on efficiency characteristics of the resulting monoliths. In the present paper, we investigate with different types of solutes (with varied hydrophobicity) the impact of the type of interaction between the solute and the stationary phase on peak symmetry and reached efficiency with a monolith synthesized under optimized synthesis parameters. We compare results obtained with different solute classes (alkylphenones, alkylanilines, nitrotoluenes, and phenolic compounds) in the reversed-phase mode, in the normal-phase mode, and in a mixed retention mode, taking into consideration that a change in the retention mode can be reached via alteration of the mobile phase composition. It is shown for very polar solutes (nucleosides) that separations in the HILIC mode can be achieved with a monolith synthesized with a higher molar fraction of polar monomers. Separations in the ion-exchange mode are investigated for protonated alkylanilines showing the phenomenon of peak compression, which confirms the (meso)porosity data obtained in our previous work [9]. Special emphasis is placed on the confirmation of the validity of the mathematical procedure employed for the evaluation of plate heights from recorded chromatograms. We investigate whether with increasing efficiency axial diffusion becomes the dominant band broadening mechanism.

2. Influence of Me-β-CD on the phase separation process

The role of CDs in polymer synthesis was extensively studied by Ritter and coworkers [41–48]. These authors investigated the procedure of solubilization of hydrophobic monomers by complex formation with water-soluble cyclodextrins and subsequent reaction of the formed host-guest complex by free radical polymerization or copolymerization in aqueous solution. They used different classes of hydrophobic monomers to obtain homopolymers and copolymers by using cyclodextrin in polymer synthesis.

In the present work, to explain the effective separation of small molecules exhibited by monoliths synthesized by us [8–10], the formation of their morphology has to be discussed. We assume following mechanism of pore formation in the presence of Me-β-CD as solubilizing agent. The free radical initiator ammonium persulfate (APS) is added to the polymerization mixture in the presence of *N,N,N′,N′*-tetramethylethylenediamine (TEMED) as accelerator to produce alkylaminomethyl ($(CH_3)_2NCH_2CH_2(CH_3)NC^{\bullet}H_2$) and sulfate free radicals ($HO_3SO^{\bullet}$) [49]. The formed radicals initiate the vinyl copolymerization of the monomers N-adamantyl acrylamide (solubilized by complexation with a cyclodextrin), methacrylamide (MA), vinylsulfonic acid (VSA), and crosslinker piperazinediacrylamide (PDA) in aqueous solution forming crosslinked polymer chains (oligomers). In order to achieve a prolongation of the growing polymer chains, the cyclodextrin host has to slip off from the solubilized monomer and thus remains dissolved in the aqueous phase [47,48]. The growing polymer chains start to precipitate (phase-separation) in the reaction medium as soon as their concentration in the reaction medium exceeds a critical limit (nucleation stage). We further assume that because of the high complex stability constant of the adamantyl group with Me-β-CD in aqueous phase [50], the outside of the formed nuclei (globules) is enriched by complexed adamantyl groups forming a hydrophilic outer surface shielding layer. As the polymerization proceeds, the formed insoluble polymeric nuclei covered with a hydrophilic CD outer surface layer continue to grow as a result of the phase transfer of monomers and oligomers from the reaction medium into the swollen nuclei. Additionally, we assume that in the presence of a hydrophilic CD outer surface shielding layer the phase transfer of the monomers and oligomers into the swollen nuclei takes place in a diffusion controlled manner, which means that the rate of the growing of the swollen nuclei becomes dependent on the mass transfer rate with which the monomers, crosslinker, and oligomers diffuse from the surrounding solution into the swollen nuclei through the CD shielding layer. This model includes the assumption that the presence of a hydrophilic CD outer surface shielding layer results in a sterically hindered phase transfer process, resulting in a decrease in the rate of growth of the swollen nuclei, while the polymerization in solution is preferred. The subsequently produced polymer chains formed in solution at an advanced state of the polymerization will react to a very low extent with the shielded pendant vinylic groups of the globules and, consequently, polymerization at the globule surface is effectively suppressed. This would lead to a decrease in the (local) variation of the degree of cross-linking density within the formed globules (decrease of radial globule heterogeneity) avoiding largely the formation of a layer of

low crosslinking density. In addition, this would also lead to the retardation of the phase separation process and, consequently, to the formation of a monolith of small domain size, which we have already confirmed by SEM studies [9].

Since phase separation is occurring continuously, the polymerization takes place in solution as well as within the swollen precipitated nuclei. As the polymerization proceeds, the precipitated polymeric nuclei (globules) react with other globules forming aggregated clusters. These clusters remain dispersed in the liquid phase and continue to grow until their increase in size enables their mutual contact, building up a polymeric scaffold [51]. Summarizing these considerations, we expect that the synthesis conditions of this type of monolith (including the complexation of water-insoluble monomers by water-soluble cyclodextrins) will have a large impact on the morphology and the chromatographic efficiency of the formed monoliths, when compared to those organic monoliths synthesized in the presence of organic solvent in the polymerization mixture.

3. Experimental

3.1. Chemicals and instruments

All chemicals were used without further purification. *N,N,N′,N′*-Tetramethylethylendiamine (TEMED), 3-(trimethoxysilyl) propyl methacrylate (bind silane), di-sodium hydrogen phosphate dihydrate, N,N-dimethylformamide (DMF), ammonium sulfate (AS), hydrochloric acid (37%, v/v), uracil, and thymine were from Fluka (Buchs, Switzerland). Propiophenone, butyrophenone, valerophenone, hexanophenone, 4-ethylaniline, 4-butylaniline, 4-pentylaniline, 4-hexylaniline, vinylsulfonic acid (VSA) (25%, w/v, in aqueous solution), ammonium persulfate (APS), sodium tetraborate-10-hydrate, uridine, and inosine were from Sigma–Aldrich (Steinheim, Germany). 5-Methyluridine was from Sigma–Aldrich (St. Louis, USA). Methacrylamide (MA), acetic acid (AA), sodium dihydrogen phosphate monohydrate, methyl benzoate, ethyl benzoate, propyl benzoate, butyl benzoate, 3-methoxybenzaldehyde, 3-methoxy-4-hydroxybenzaldehyde, 4-hydroxybenzaldehyde, and 3,4-dihydroxybenzaldehyde were from Merck (Darmstadt, Germany). 4-Propylaniline was from Alfa-Aesar (Karlsruhe, Germany). Acetophenone was from Riedel-de Haen (Seelze, Germany). Triethylamine (TEA) was from KMF Laborchemie (Lohmar, Germany). 1,4-Diacryloylpiperazine (PDA) was either from Alfa-Aesar (Karlsruhe, Germany) or from Molekula (Dorset, UK). Statistically methylated β-CD (Me-β-CD) was either from ABCR (Karlsruhe, Germany) or from Sigma–Aldrich (Louis, USA). N-(1-Adamantyl) acrylamide was synthesized according to [52] (synthesis procedure and characterization see [8]). Fused silica capillaries (100 μm i.d. × 360 μm o.d.) were from Polymicro Technologies (Phoenix, USA). Nitrotoluenes, resorcinol, and toluene were available at the Department of Chemistry, University of Marburg.

With all mobile phases the electric conductivity and the pH* value were controlled. The pH* value is the pH in the presence of organic solvent determined with a pH meter calibrated with an aqueous buffer. The pH* was determined with the mobile phase after addition of the organic solvent to the aqueous buffer. The pH meter Inolab pH 720 (WTW instruments, Weinheim, Germany), and the conductometer LF 191 (WTW, Weinheim, Germany) were used to measure the pH* and the electric conductivity of the prepared mobile phases. Mobile phases were prepared by buffering 100 mL distilled water with 2–3 mL of a mixture of 0.2 mol L^{-1} TEA with 0.2 mol L^{-1} AA (1:1, v/v). Subsequently, the required volume of this solution is taken and mixed with the corresponding volume of organic solvent. The pH* and the electric conductivity of the final mixture were adjusted with 0.20 mol L^{-1} TEA or AA.

The mixed-mode monolithic stationary phases were synthesized as described in [8] by copolymerization of a mixture of N-(1-adamantyl)acrylamide solubilized via 1:1 complex formation with statistically methylated β-CD, methacrylamide (MA) as hydrophilic monomer, piperazinediacrylamide (PDA) as crosslinker, ammonium sulfate (AS) as lyotropic salt, vinylsulfonic acid (VSA) as charge-bearing monomer, ammonium persulfate (APS) as free radical polymerization initiator, and *N,N,N′,N′*-tetramethylethylendiamine (TEMED) as part of the redox initiator system dissolved in aqueous phosphate buffer (100 mM, pH 7.0) inside a 100 μm I.D. fused-silica capillary, which had been pretreated with 3-(trimethoxysilyl)propyl methacrylate (bind silane).

3.2. Chromatographic system

The CEC apparatus is described in [53] and consists of a FUG HCN 35-35000 high voltage generator (FUG Elektronic GmbH, Rosenheim, Germany) with an in-house manufactured electronic steering unit for controlled electrokinetic injection, a spectra 100 UV–vis detector (Thermo Separation Products, San Jose, CA, USA) with detection cell for in-capillary detection, and a Shimadzu (Kyoto, Japan) LC-10 AD HPLC pump in combination with a flow splitter for conditioning and equilibrating the monolithic capillary with new mobile phase using 50–100 bar. Data treatment and recording was done with EZ-Chrom 6.6 (Scientific Software, San Roman. CA, USA). For the CEC experiments, sample solutions with an analyte concentration of 250–300 mg L^{-1} were prepared in the mobile phase (for nucleosides 400–500 mg L^{-1}). Sample injection was performed electrokinetically. If not otherwise indicated, the injection parameters are 3 kV for 3 s. UV detection was at a wavelength of 230 nm (for nucleosides 254 nm). *N,N*-Dimethylformamide (DMF) was used as a neutral non-retained EOF marker. Different water/methanol mobile phases buffered with triethylamine/acetic acid (pH* = 6.8–7.0, electric conductivity 120–150 μS cm^{-1}) were used for separations in the reversed-phase mode or in a mixed mode. Water/acetonitrile mobile phase buffered with triethylamine/acetic acid (pH* = 7.04, electric conductivity 140 μS cm^{-1}) was used for the separation of the nucleosides in the HILIC mode. Aqueous borate buffer containing 40% (v/v) acetonitrile was used as mobile phase for the separation of alkylanilines in the reversed-phase mode. Aqueous phosphate buffer containing 70% acetonitrile mobile phase (pH* = 3.1, electric conductivity 220 μS cm^{-1}) was used for separations in the ion-exchange mode. In this work, triethylamine/acetic acid was mainly used as buffer system since it has a lower electric conductivity than other buffers, e.g. phosphate, acetate, or borate buffer.

Different classes of solutes were tested: alkylphenones and alkyl benzoates as examples of very hydrophobic solutes, alkylanilines and nitrotoluenes as less hydrophobic neutral solutes and phenolic compounds as more polar (hydrophilic) solutes. Nucleosides were taken as an example of very polar neutral solutes for CEC separations in the HILIC mode. Protonated alkylanilines were also tested as positively charged solutes.

4. Results and discussion

4.1. Calculation of efficiency data

According to the detailed discussion outlined in Section S1 (Supplementary data), the number of theoretical plates N and the height equivalent to a theoretical plate H were calculated using retention time and peak width determined by the software employed for recording and data treatment (EZ-Chrom 6.6). Alternatively, efficiency data are (more correctly) determined by moment analysis (see Section S1; Supplementary data). In Table 1 efficiency

Table 1
Retention factor k, peak asymmetry factor AF, number of theoretical plates per meter calculated using tangent method $N_{Tangent}$ m^{-1}, number of theoretical plates per meter calculated using moment analysis N_{Moment} m^{-1}, and ratio of $N_{Tangent}/N_{Moment}$. Mobile phase: methanol/water (50:50, v/v) buffered with triethylamine/acetic acid, pH* = 7.0, electric conductivity = 125 μS cm^{-1}. Stationary phase: Monolith A, capillary dimensions 210(282) mm × 100 μm. Data shown are the average of triplicate measurements, corresponding electropherograms are shown in Fig. S1.

Analyte	k	AF (±s.d.)	$N_{Tangent}$ m^{-1} (±s.d.)	N_{Moment} m^{-1} (±s.d.)	$N_{Tangent}/N_{Moment}$ (±s.d.)
DMF	0.00	1.012 (±0.008)	225,000 (±900)	278,000 (±20,000)	0.814 (±0.053)
Acetophenone	0.207	1.026 (±0.004)	237,000 (±17,000)	272,000 (±7500)	0.871 (±0.063)
Propiophenone	0.257	1.054 (±0.020)	220,000 (±700)	226,000 (±13,000)	0.976 (±0.563)
Butyrophenone	0.322	1.122 (±0.017)	216,000 (±6500)	188,000 (±6300)	1.150 (±0.010)
Valerophenone	0.432	1.430 (±0.174)	197,000 (±(8500)	129,000 (±20,000)	1.570 (±0.271)

data calculated applying the tangent method are compared to those determined via moment analysis. It is obvious that the results gained via the tangent method or via moment analysis are equivalent for those peaks, which do not show a significant asymmetry. For DMF and acetophenone the plate numbers calculated via moment analysis are even higher than those calculated by assuming a Gaussian peak shape. Possibly, this is an indication of the presence of a small volume overload (resulting in a peak with negative excess (curtosis)). In case of propiophenone (AF = 1.05) there is no significant deviation in the results obtained via the two methods. However, for butyrophenone with AF = 1.12 and valerophenone with AF = 1.43 the plate numbers calculated via moment analysis are significantly lower than those estimated from application of the tangent method (see Table 1).

This deviation is because peak distortions in low peak height areas have a large impact on the second moment about the mean while these distortions are completely ignored by the tangent method. However, from the data presented in Table 1 it can be also deduced that efficiency data gained via moment analysis must be checked very carefully. Very small deviations in drawing the baseline result in large differences in the resulting value for the second moment about the mean (visible as a large standard deviation for those data calculated via moment analysis). Reproducible data were only produced via moment analysis by checking each drawn baseline carefully manually with a graphical procedure.

From the data compared in Table 1 we conclude that the tangent method provides equivalent efficiency data if AF ≤1.05. It has the advantage over moment analysis that it is more robust and that it can be automated with a suitable algorithm also in the case of S/N < 200. For 1.05 ≤ AF ≤ 1.10 the resulting bias for those data being obtained by the tangent method is relatively low taking into account that even in the case of S/N ≥ 200 the accuracy of efficiency data obtained by moment analysis can have a bias of several percent due to the imprecision of the determination of the second central moment [54]. If the tangent method is applied for peaks with AF ≥ 1.10 then the asymmetry factor should be given when comparing the results.

4.2. Plate height curve

For a detailed investigation of the impact of the retention factor on the obtained efficiency and peak asymmetry, we synthesized a monolith with optimized synthesis parameters under optimized conditions Monolith A (with polymerization composition: N-adamantyl acrylamide: 30 mg; Me-β-CD: 191 mg; MA: 20 mg; AS: 12 mg; VSA (25%, w/v): 35 μL; PDA: 65 mg; APS (10%, w/v): 10 μL; TEMED (10%, v/v): 10 μL (in 0.70 mL 100 mM phosphate buffer, pH = 7.0); %T: 16.4, w/v; %C: 56.6, w/w, for abbreviations see Section 3.1). Fig. 1 shows the Van Deemter plots for this monolith determined in the reversed phase mode with DMF as non-retained marker (k = 0) and for a homologues series of alkylphenones (k = 0.2–0.5, for peak asymmetry factors and minimum plate heights at different mobile phase velocities see Tables S1 and S2 and Fig. S2, Supplementary data). High

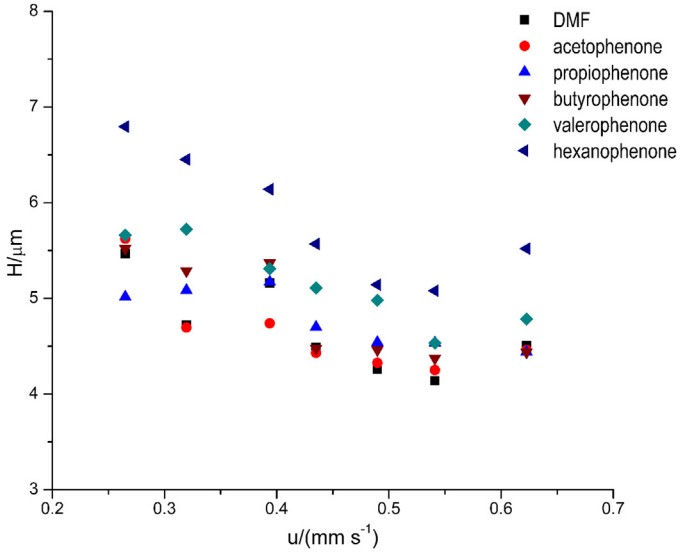

Fig. 1. Van Deemter plots for DMF, acetophenone (k = 0.198), propiophenone (k = 0.243), butyrophenone (k = 0.300), valerophenone (k = 0.395), and hexanophenone (k = 0.542) on Monolith A. Mobile phase: methanol/water (50:50, v/v) buffered with triethylamine/acetic acid, pH* = 7.0, electric conductivity = 125 μS cm^{-1}. Capillary dimensions 245 mm (317 mm) × 100 μm; UV detection at 230 nm; electrokinetic injection: 3 kV for 3 s. All data are listed in Tables S1 and S2. Dixon's Q-test (P = 95%) was applied to all extreme values. Identified outliers are removed from the data set. If the calculated Q-value is higher than 50% of the critical value, the median was taken instead of the mean (see also Table S2).

efficiencies were obtained not only for the EOF marker DMF but also for the retarded analytes using MeOH/H_2O (50:50, v/v) buffered with triethylamine/acetic acid, pH* = 7.0 (electric conductivity = 125 μS cm^{-1}) as mobile phase. The overall flatness of these curves indicates a small C-term contribution also for retarded analytes (the corresponding electropherograms are shown in Fig. S2).

As a general trend, the Van Deemter plots for the alkylphenones show a small dependence of H on the retention factor (see also Table S2, Supplementary data). At lower applied voltage (12–14 kV corresponding to 0.265–0.319 mm s^{-1}) there is a large run-to-run variation in the plate height, whereas at higher mobile phase velocity the run-to-run variation in H is reduced. At the highest mobile phase velocity (0.622 mm s^{-1}), there is (clearly visible for valerophenone and hexanophenone) a small increase in H and AF with increasing retention factor. Another interesting observation shown in Table S2 (Supplementary data) is the independence of AF on the mobile phase velocity.

4.3. Variation of the retention mode

With Monolith A, theoretical plate numbers, retention factors, and asymmetry factors were determined for different classes of analytes (Table 2). High plate numbers up to 220,000 m^{-1} were obtained for most of the tested analytes using different elution modes. However, plate numbers up to 300,000 m^{-1} were routinely

Table 2
Retention factors, efficiencies (per meter), and asymmetry factors for alkylphenones, alkyl benzoates, alkylanilines, nitrotoluenes, and phenolic analytes recorded with Monolith A, capillary dimensions 245(317) mm × 100 μm. Data shown are the average of triplicate runs (standard deviations in brackets).

Separation mode	Analytes	Retention factor ± s.d.	Efficiency (N/m)	Asymmetry factor ± s.d.
Reversed-phase mode[a]	DMF		239,000 (±1900)	1.092 (± 0.03)
(see Fig. S2 in Supplementary data)	Acetophenone	0.20 (±0.0000)	231,000 (±8800)	1.073 (±0.41)
μ_{eo} = 4.54 cm^2 kV^{-1} min^{-1} ± 0.015 cm^2 kV^{-1} min^{-1}	Propiophenone	0.24 (±0.0006)	224,000 (±16,000)	1.144 (±0.14)
(n = 3)	Butyrophenone	0.30 (±0.0008)	218,000 (±14,000)	1.129 (±0.08)
	Valerophenone	0.39 (±0.0008)	210,000 (±18,000)	1.224 (±0.03)
	Hexanophenone	0.53 (±0.0320)	202,000 (±12,000)	1.323 (±0.04)
Reversed-phase mode[a]	DMF		230,000 (±3500)	1.047 (±0.02)
(see Fig. S3 in Supplementary data)	Methyl benzoate	0.25 (±0.0007)	226,000 (±4900)	1.096 (±0.02)
μ_{eo} = 4.78 cm^2 kV^{-1} min^{-1} ± 0.004	Ethyl benzoate	0.29 (±0.0009)	218,000 (±6500)	1.092 (±0.01)
cm^2 kV^{-1} min^{-1} (n = 3)	Propyl benzoate	0.38 (±0.0014)	223,000 (±9000)	1.157 (±0.05)
	Butyl benzoate	0.52 (±0.0020)	184,000 (±4900)	1.219 (±0.04)
Reversed-phase mode[b]	DMF		287,000 (±1600)	1.069 (±0.04)
(see Fig. 2)	4-Ethylaniline	0.13 (±0.0018)	307,000 (±4300)	1.108 (±0.02)
μ_{eo} = 9.32 cm^2 kV^{-1} min^{-1} ± 0.065 cm^2 kV^{-1} min^{-1}	4-Propylaniline	0.16 (±0.0027)	316,000 (±11,000)	1.121 (±0.04)
(n = 3)	4-Butylaniline	0.20 (±0.0038)	305,000 (±9600)	1.185 (±0.02)
	4-Pentylaniline	0.25 (±0.0050)	294,000 (±26,000)	1.163 (±0.04)
	4-Hexylaniline	0.32 (±0.0065)	254,000 (±18,000)	1.325 (±0.11)
Mixed-mode[c]	DMF		215,000 (±19,000)	1.033 (±0.03)
(see Fig. S5 in Supplementary data)	4-Nitrotoluene	0.11 (±0.0002)	220,000 (±15,000)	1.089 (±0.06)
μ_{eo} = 4.48 cm^2 kV^{-1} min^{-1} ± 0.009 cm^2 kV^{-1} min^{-1}	2,4,6-Trinitrotoluene	0.23 (±0.0009)	223,000 (±14,000)	1.221 (±0.12)
(n = 3)				
Mixed-mode[c]	DMF		216,000 (±10,000)	1.063 (±0.03)
(see Fig. 11 in [8])	3-Methoxybenzaldehyde	0.07 (±0.0002)	226,000 (±1900)	1.017 (±0.02)
μ_{eo} = 4.37 cm^2 kV^{-1} min^{-1} ± 0.006 cm^2 kV^{-1} min^{-1}	4-Hydroxy-3-methoxybenzaldehyde	0.13 (±0.0004)	237,000 (±6900)	0.854 (±0.02)
(n = 3)	4-Hydroxybenzaldehyde	0.19 (±0.0062)	206,000 (±14,000)	0.834 (±0.03)
	3,4-Dihydroxybenzaldehyde	0.36 (±0.0010)	175,000 (±20,000)	1.001 (±0.03)
	Resorcinol	0.40 (±0.0297)	221,000 (±23,000)	1.341 (±0.02)
Normal-phase mode[d]	DMF		201,000 (±15,000)	0.916 (±0.03)
(see Fig. 9 in [8])	4-Hydroxy-3-methoxybenzaldehyde	0.09 (±0.0001)	192,000 (±11,000)	1.120 (±0.02)
μ_{eo} = 10.63 cm^2 kV^{-1} min^{-1} ± 0.068 cm^2 kV^{-1} min^{-1}	4-Hydroxybenzaldehyde	0.16 (±0.0003)	184,000 (±11,000)	1.067 (±0.02)
(n = 3)	Resorcinol	0.42 (±0.0002)	96,000 (±3000)	1.756 (±0.02)

[a] Mobile phase: methanol/water (50:50, v/v) buffered with triethylamine/acetic acid, pH* = 7.0, electric conductivity = 125 μS cm^{-1}.
[b] Mobile phase: 5.0 mM $Na_2B_4O_7 \cdot 10H_2O$ containing 40% ACN, pH* = 10.65, electric conductivity = 310 μS cm^{-1}.
[c] Mobile phase: methanol/water (80:20, v/v) buffered with triethylamine/acetic acid, pH* = 6.68, electric conductivity = 105 μS cm^{-1}.
[d] Mobile phase: methanol/ACN (60:40, v/v) buffered with triethylamine/acetic acid, pH* = 6.40, electric conductivity = 120 μS cm^{-1}.

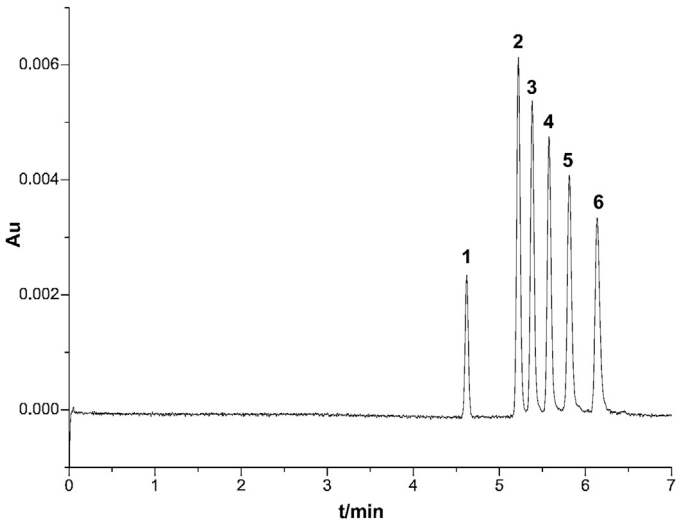

Fig. 2. Reversed phase separation of alkylanilines on Monolith A. Analytes: (1) DMF (2) 4-ethylaniline (3) 4-propylaniline (4) 4-butylaniline (5) 4-pentylaniline (6) 4-hexylaniline. Mobile phase: 5.0 mM $Na_2B_4O_7{\cdot}10H_2O$ contain 40% ACN, pH* = 10.65, electric conductivity = 310 μS cm^{-1}. Capillary dimensions 245 mm (317 mm) × 100 μm; UV detection at 230 nm; electrokinetic injection: 1.5 kV for 3 s; separation voltage: 18 kV.

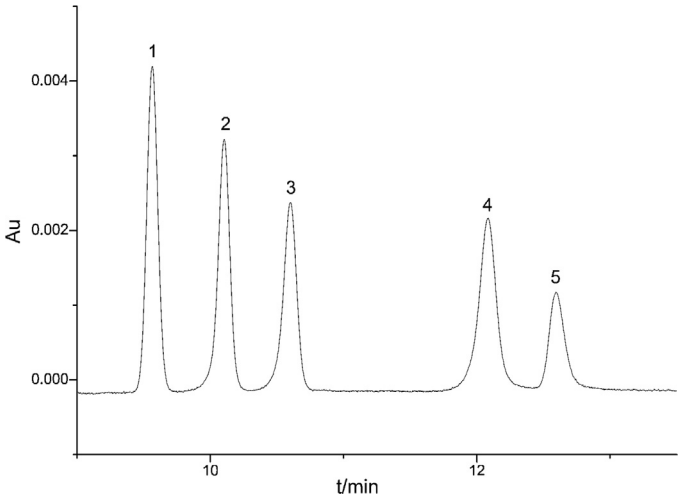

Fig. 3. Expanded view of electropherograms of phenolic solutes: (1) 3-methoxybenzaldehyde, (2) 4-hydroxy-3-methoxy benzaldehyde, (3) 4-hydroxybenzaldehyde, (4) 3,4-dihydroxybenzaldehyde, (5) resorcinol. For mobile phase composition see Table 2.

Reproduced from Ref. [8] with permission. Copyright 2013, Elsevier.

obtained only for alkylanilines using an aqueous borate buffer containing 40% (v/v) ACN. Different efficiencies (at optimum mobile phase velocity) were obtained for different types of analytes using different elution modes (Table 2). The results suggest that these differences stem from the differences in analyte functionality and/or mobile phase composition. For alkylphenones and alkyl benzoates, which were separated in the reversed-phase mode (using the same mobile phase composition), the values of efficiency and peak asymmetry are relatively close to each other. The alkylanilines were separated with the highest efficiency using a mobile phase containing 40% (v/v) ACN. Further studies are needed to evaluate whether better efficiencies can be obtained with acetonitrile-containing mobile phases than with methanol-containing mobile phases, possibly due to a lower viscosity of the former [55]. Another possible reason for the improved efficiency might be given by a mobile phase-dependent swelling of the stationary phase [35].

Separations in the reversed-phase mode were obtained for different solute classes: (i) alkylphenones (Fig. 7 in [8]) (ii) alkyl benzoates (Fig. S3, Supplementary data) and (iii) alkylanilines (Fig. 2). For these three different analyte classes a linear relationship was observed between the logarithmic retention factor and the number of methylene groups in the alkyl chain. From the slope of these straight lines the methylene selectivity α_{meth} was determined (Fig. S4, Supplementary data). As the methylene selectivity is a measure of the hydrophobicity of the stationary phase (relative to the hydrophobicity of the mobile phase), α_{meth} was not affected by changing the type of homologous series (Table S3, Supplementary data) (for mobile phases used refer to Table 2).

The retention of the investigated nitrotoluenes (4-nitrotoluene, 2,4,6-trinitrotoluene) follows neither a reversed-nor a normal-phase retention mode. It has to be described as a mixed-mode retention behavior (Fig. S5, Supplementary data). While the elution order follows what would be expected in the normal-phase mode, i.e., the solutes are eluted in the order of increasing polarity, the retention factors are decreased with increasing volume fraction of methanol in the mobile phase as in the reversed-phase mode (see Supplementary data, Fig. S6). The same phenomenon was observed with phenolic solutes as described in [8].

Another characteristic point depicted in Fig. 3 and in Table 2 is that phenolic solutes separated in a mixed retention mode employing a mobile phase containing 80% (v/v) MeOH exhibit a significant solute-specific peak asymmetry. A close inspection of the peaks shown in Fig. 3 reveals that Peak 2 and 3 (hydroxybenzaldehydes) have a characteristic fronting, while Peak 4 (dihydroxybenzaldehyde) has a solute-specific peak broadening ("fronting and tailing"), whereas Peak 5 (resorcinol) shows tailing. It has to be emphasized that these characteristic solute-specific peak distortions are highly reproducible from run-to-run and from column to column. The simultaneous occurrence of peak fronting, peak tailing and solute-specific peak broadening is also shown in Fig. 8 of [39]. It is obviously a phenomenon which is associated with a mixed-retention mode, as for the alkylphenones separated in the reversed-phase mode (see Fig. S7a, Supplementary data) and for the phenolic solutes separated in the normal-phase mode (see Fig. S7b, Supplementary data) there are peaks with very small asymmetry factor for low retention factors while there is an increasing tailing with increasing retention factor. In all cases in the reversed-phase mode and in the normal-phase mode the asymmetry factor is $\geq$1. Peaks with an asymmetry factor <1 are only observed in a mixed retention mode. Plate height differences due to a solute-specific efficiency are more pronounced, when the plate height is estimated by moment analysis than by the tangent method (see Table S4, Supplementary data).

One possible explanation for these observations might be the development of a gel porosity in the monolithic scaffold at higher methanol content in the mobile phase (80%, v/v, MeOH), which results in a significant impact on peak asymmetry and efficiency. Nischang and co-workers [7,14,23] reported that the presence of a large volume fraction of organic modifier in the mobile phase leads to the formation of gel pores resulting in the (sterically) hindered diffusion of retarded analytes. In addition, the authors reported that the distribution of analytes between mobile phase and swollen stationary phase has a significant influence on band broadening of retarded analytes. The different accessibility of the swollen stationary phase for solutes of different shape might be responsible for the observed solute-specific phenomena.

It is interesting to note that those solute-specific peak distortions found with the phenolic solutes in a mixed retention mode are not present in the case of the mixed-mode separation of nitrotoluenes (see Fig. S5, Supplementary data). The phenomenon of a solute-specific efficiency has been reported also for methacrylate-based monolithic columns. For example, Eeltink et al. [36] studied

the separation of several polycyclic hydrocarbons by CEC employing a mobile phase containing 80% (v/v) acetonitrile. Although there is the general trend that H is increased with increasing retention factor, there is a specific increase in H for the solutes pyrene and benzo[a]pyrene, while H is lower for naphthalene, fluorene, anthracene and benz[a]anthracene. A similar observation was made by Huo et al. [35] who studied (by CEC with a methacrylate-based monolith) the peak shapes obtained for two pairs of solutes with similar retention factor but different structure: (i) butylbenzene and 1,2,4,5-tetramethyl benzene and (ii) biphenyl and naphthalene. They estimated via fitting of plate height curves to the "classical Van-Deemter equation" the C-term constants for three different compositions of the mobile phase. Whereas the C-term constants differ largely for Peak Pair 1 they are very similar for Peak Pair 2. First attempts to explain the experimental findings based on qualitative parameters like "flatness" or "flexibility" did not prove to be successful. They conclude that "apparently, other factors that are still unknown must play a role".

4.4. Ion-exchange mode

Adamantyl-group containing mixed mode acrylamide continuous beds co-polymerized from water soluble monomers (including the charged monomer vinylsulfonic acid (VSA)) and water-insoluble monomers have an amphiphilic and ionic character and can also be used in the ion-exchange mode [8]. Fig. 4 shows the CEC separation of protonated alkylanilines in the ion-exchange mode on Monolith A using a mobile phase composed of 30% (v/v) 10 mM aqueous solution of $NaH_2PO_4{\cdot}H_2O$ adjusted with phosphoric acid to pH 2.2 and 70% (v/v) acetonitrile. The final values are: ionic strength = 4.5 mM; pH* = 3.1, and electric field strength = 64 V mm^{-1}. Whereas, Peaks 4 and 5 show a large tailing (triangular peak shape), Peaks 2 and 3 are partly compressed so that they have an extremely small peak width at half height which would lead to extremely high efficiencies if it were taken for the calculation of the theoretical plate number.

An unexpected peak compression for charged analytes separated by CEC on an oppositely charged ion-exchanger has first been reported by Smith and Evans in 1994 [56]. More than one decade later Nischang and Tallarek succeeded in explaining this phenomenon by the presence of local electric field gradients and concentration polarization inside and between the particles. They were separating cationic analytes by CEC with fused silica capillaries packed with mesoporous particles of a strong cation-exchanger. Fronting, tailing and spiked peaks were observed as in the case reported here depending on the (average) electric field strength, the ionic strength of the mobile phase and the analyte retention factor.

Concentration polarization is related to an intra-particle pore space [57], which we equalize with the internal porosity of the monolith (which is, as shown before, to a large extent identical to the mesoporosity of the material). We therefore interpret the observation of the presence of an "inherent peak compression of charged analytes in CEC" [56,57] made with a polymeric monolith produced by us as an indirect evidence for the presence of an internal (meso)porosity of this material. This assumption is in agreement with the results obtained by using inverse size exclusion chromatography (ISEC) technique for the investigation of the porous properties of the synthesized monoliths [9]. These results confirm the mesoporosity of the synthesized monoliths. According to the best of our knowledge this is the first time that this special form of peak compression was described with a polymeric monolith.

4.5. Hydrophilic interaction liquid chromatography

We intended to investigate, whether adamantyl-group containing acrylamide-based continuous beds can also be employed in the HILIC mode. To this end, a highly polar monolithic capillary was synthesized by using a large concentration of the hydrophilic monomers methacrylamide (MA) and vinylsulfonic acid (VSA) in the polymerization mixture Monolith B (with polymerization composition: N-adamantyl acrylamide: 5.0 mg; Me-β-CD: 30 mg; MA: 45 mg; AS: 12 mg; VSA: 45 μL; PDA: 65 mg; APS (10%, w/v): 10 μL; TEMED (10%, v/v): 10 μL (in 0.70 mL 100 mM phosphate buffer, pH = 7.0); %T: 16.4, w/v; %C: 56.6, w/w, for abbreviations see Section 3.1). As test analytes we employed toluene as non-retained marker and very polar nucleosides (thymine, uracil, 5-methyl-uridine, uridine, and inosine) as retarded solutes. A chromatogram obtained in the HILIC mode is shown in Fig. 5. It must be emphasized that this type of monolith was not optimized regarding the obtainable

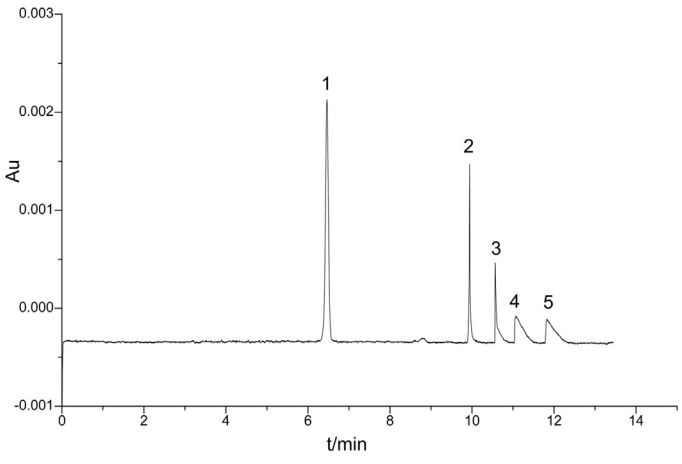

Fig. 4. Ion-exchange separation of alkylanilines on Monolith A. Analytes: (1) DMF (2) 4-ethylanilin (3) 4-butylaniline (4) 4-pentylaniline (5) 4-hexylaniline. Mobile phase: 30% (v/v) 10 mM aqueous solution of $NaH_2PO_4{\cdot}H_2O$ adjusted with phosphoric acid to pH 2.2 and 70% (v/v) acetonitrile. The final values are: ionic strength = 4.5 mM, pH* = 3.1, electric conductivity = 220 μS cm^{-1}. Capillary dimensions 315 mm (243 mm) × 100 μm; UV detection at 230 nm; electrokinetic injection: 1.5 kV for 3 s, separation voltage: 20 kV.

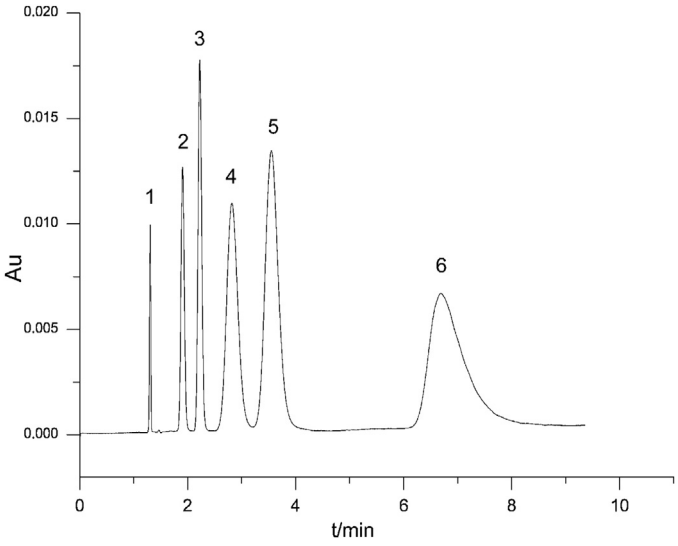

Fig. 5. Hydrophilic interaction mode (HILIC) separation of nucleosides on Monolith B. Analytes: (1) toluene (2) thymine (3) uracil (4) 5-methyl-uridine (5) uridine (6) inosine. Mobile phase: acetonitrile/water (90:10, v/v) buffered with triethylamine/acetic acid, pH* = 7.04, electric conductivity = 140 μS cm^{-1}. Capillary dimensions 223 mm (292 mm) × 100 μm; UV detection at 254 nm; electrokinetic injection: 3 kV for 3 s, separation voltage: 20 kV.

efficiency (in contrast to Monolith A). The elution order observed indicates that the analytes are separated according to an increase in their polarity while employing an aqueous/organic mobile phase ACN/H_2O (90:10, v/v) buffered with triethylamine/acetic acid, pH* = 7.04, electric conductivity = 140 μS cm^{-1}. In addition, the retention factors of nucleosides are decreased with decreasing volume fraction of ACN in the mobile phase as is typical of the HILIC mode (data not shown). The elution order observed is in agreement with the elution order obtained with a classical zwitterionic stationary phase in the HILIC mode [58].

4.6. Contribution of axial diffusion

According to the detailed discussion outlined in Section S2 (Supplementary data), the experimentally observable overall plate height equation is:

$$H = \frac{B}{u} + Cu \quad (1)$$

This equation deviates from those plate height equations commonly employed in liquid chromatography in the absence of a third term (the A-term), which is in a nonlinear fashion dependent on the linear mobile phase velocity and accounts for the coupling of interchannel flow inhomogeneities with radial molecular diffusion [59]. In addition, the significant contribution of extra-column band broadening effects will result in a constant third term. However, regarding the limited mobile phase linear velocity range accessible via capillary electrochromatography and the inherent imprecision of efficiency data obtained from peak analysis (Fig. 1), we propose to fit experimental data obtained by CEC with an organic monolith to the simplified two-parameter plate height equation Eq. (1). This fitting can easily be done by linear regression analysis.

This fitting will allow to estimate for an unretained marker and for retained solutes the minimum plate height H_{min}, the optimum linear mobile phase velocity u_{opt}, and the contribution of axial diffusion to the overall band broadening at optimum linear mobile phase velocity via the partial plate height $H_{B,opt} = B/u_{opt}$. The plausibility of the partial plate height $H_{B,opt}$ can be confirmed by comparison with data calculated from known diffusion coefficients in bulk solution. It should be noted that with the proposed simplified plate height equation $H_{min}/H_{B,opt} = 2$. In the case of H_B is equivalent to the partial plate height H_D resulting from axial diffusion (see Section S2), this ratio corresponds to a reduced plate height and represents the minimum plate height normalized on the band broadening due to unavoidable axial diffusion.

Preliminary experiments have shown that the fitting of efficiency data (see Fig. 3 in [10]) to the "classical Van-Deemter equation" will not result in a significant constant A-term. We ascribe this result to the restricted velocity range and to the absence of a significant influence of extra-column (instrumental) band broadening effects on the observed efficiency. In Section S2 (see Supplementary data) we have outlined why we suggest to fit experimental curves to a two-parameter plate height equation of the type $H = B/u + Cu$. Fig. 6 shows the fitting of data for propiophenone

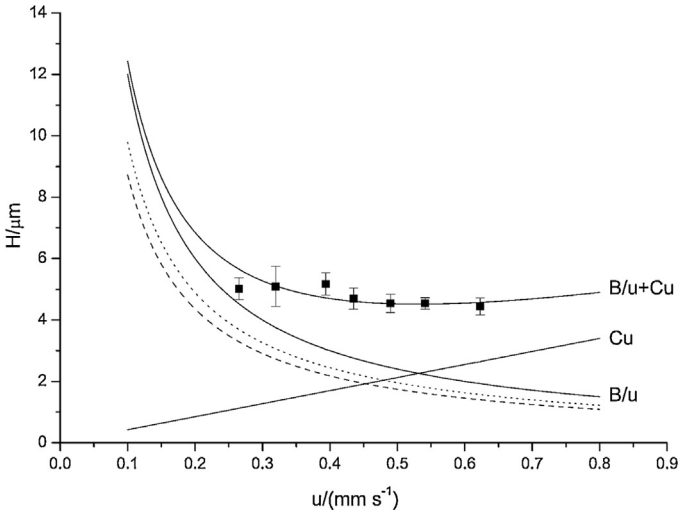

Fig. 6. Height equivalent of a theoretical plate and partial plate heights (solid lines generated from fitted data) versus linear mobile phase velocity compared to partial plate height curve modeled from known diffusion coefficient in bulk solution at 25 °C (dotted line) and 20 °C (dashed line). Measured mean (or median see Table S2) values are given as points with standard deviations as error bars. Solute: propiophenone, stationary phase: Monolith A, capillary dimensions: 245(317) mm × 100 μm, mobile phase: methanol/water (50:50, v/v) buffered with triethylamine/acetic acid, pH* = 7.0, electric conductivity = 125 μS cm^{-1}, UV detection at 230 nm, electrokinetic injection: 3 kV for 3 s.

taken from Fig. 1 (see also Tables S1 and S2, Supplementary data). This fit allows the estimation of the two constants for the B- and C-terms by linear regression and the calculation of these terms at different mobile phase velocities (for regression analysis see Table S5). Plotting of these data reveals that a plate height equation of the type $H = B/u + Cu$ is an adequate representation of the measured data. Values of the B-term constant, the C-term constant, the minimum plate height H_{min} ($= 2\sqrt{BC}$), the optimum linear mobile phase velocity u_{opt} ($= \sqrt{B/C}$), and the contribution of axial diffusion to the overall band broadening at optimum linear mobile phase velocity $H_{B,opt}$ ($= B/u_{opt}$) for all phenones investigated are given in Table 3. As $H_{min}/H_{B,opt}$ has in all cases a value of 2, neither resistance to mass transfer nor peak broadening due to flow inhomogeneities can be regarded to be the dominating peak broadening mechanism at optimum flow rate. The results given in Table 3 show that there is little influence of k on u_{opt}. There is a significant increase in H_{min} with k, which is to a very small extent reflected by an increase in B (which must be ascribed to the simplified data evaluation procedure) and to a much higher extent by an increase in C.

Our hypothesis that instrumental peak broadening and peak broadening because of a radial temperature gradient are insignificant is strongly supported. These data confirm that (as expected) with increasing efficiency of the monolith axial diffusion is becoming the dominating peak broadening mechanism. The ultimate limit of the efficiency must be given by the peak broadening which would be obtained exclusively by (free solution) molecular diffusion in an open tube.

Table 3
B-term and C-term constants, optimum mobile phase velocity u_{opt}, minimum plate height H_{min}, and plate height $H_{B,opt}$ corresponding to the contribution of the axial molecular diffusion to the overall band broadening at optimum linear mobile phase velocity. Stationary phase: Monolith A, capillary dimensions 245(317) mm × 100 μm. Mobile phase: methanol/water (50:50, v/v) buffered with triethylamine/acetic acid, pH* = 7.0, electric conductivity = 125 μS cm^{-1} (further statistical data see Table S5).

Analyte	k	B (μm^2 s^{-1})	C (ms)	u_{opt} (mm s^{-1})	H_{min} (μm)	$H_{B,opt}$ (μm)
DMF	0	1190	4.01	0.545	4.37	2.18
Acetophenone	0.198	1160	4.08	0.533	4.35	2.18
Propiophenone	0.243	1200	4.25	0.531	4.52	2.26
Butyrophenone	0.301	1300	3.76	0.588	4.42	2.21
Valerophenone	0.395	1350	4.22	0.566	4.78	2.38
Hexanophenone	0.543	1490	4.75	0.560	5.32	2.66

We were now interested in comparing H_B (obtained by fitting the experimental data to the plate height equation) to that value which is obtained by modeling the peak broadening with (free solution) molecular diffusion in an open tube. In CEC the residence time of a (neutral) solute in the mobile phase corresponds to the hold-up time t_0. The peak variance in length units σ_L^2 was calculated according to:

$$\sigma_L^2 = 2D_m t_0 \quad (2)$$

where D_m is the diffusion coefficient in the mobile phase and t_0 is the retention time of a nonretained marker. In this approach, the influence of the tortuosity of the chromatographic bed and diffusion within the stagnant mobile phase and within the stationary phase are neglected, assuming that both effects counterbalance each other.

We estimated D_m of propiophenone from D_m of butylbenzene (which has the same molar mass as propiophenone) in MeOH:H_2O (50:50, v/v) at 30 °C, which is 0.539×10^{-5} cm^2 s^{-1} [60]. This value has to be corrected with respect to the capillary temperature. As with the CEC apparatus employed the temperature is not controlled, we assumed the capillary temperature to be between 20 and 25 °C. Correct data were available for the viscosity ($\eta = 1.62 \times 10^{-3}$ Pa s for MeOH/H_2O (50/50, v/v) at 25 °C [61]). From these data D_m at 25 °C was calculated via the Stokes–Einstein equation to be 0.489×10^{-5} cm^2 s^{-1}.

With the known D_m the peak variance due to molecular diffusion (dependent on the mobile phase velocity) is now accessible via Eq. (2), which can be transformed into the partial plate height H_D (see Eq. S10, Supplementary data). A similar approach was made for the calculation of H_D at 20 °C ($\eta = 1.83 \times 10^{-3}$ Pa s for MeOH/H_2O (50/50, v/v) at 20 °C [61]). These modeled data for H_D at 20 and 25 °C are shown in Fig. 6 (dotted and dashed lines). The comparison with those data obtained by fitting of the experimental values to the plate height equation (solid lines) reveals that there is an excellent agreement of experimental and modeled data. This agreement strongly corroborates our assumption that a plate height equation of the type $H = B/u + Cu$ is an adequate representation of plate height data estimated for polymeric monolithic capillaries via CEC.

5. Conclusions

Analyte functionality and mobile phase composition (retention mode) have a strong influence on peak symmetry and chromatographic efficiency. High plate numbers up to 220,000 m^{-1} are obtained for most of the tested analytes employing different elution modes. For neutral alkylanilines ($k < 0.25$) plate numbers of about 300,000 m^{-1} can be routinely reached in the reversed-phase elution mode. For those peaks, which do not show a significant asymmetry (AF $\leq$ 1.05), plate heights gained via the tangent method or via moment analysis are equivalent. With increasing efficiency of the monolith, axial diffusion is becoming the dominating peak broadening mechanism at optimum mobile phase velocity. The influence of the analyte functionality and the mobile phase composition on the chromatographic efficiency needs further investigations. Separations in the ion-exchange mode show peak compression typical for a stationary phase with a very small size mesopores or micropores (i.e., the presence of a small pore space). With increased mass fraction of the polar monomer methacrylamide the spectrum of retention modes can even be extended to separations in the HILIC mode.

Conflict of interest

The authors declare they have no conflict of interest.

Acknowledgements

A.A. Al-Massaedh thanks Al-Albayt University (Jordan) for financial support.

Appendix A. Supplementary data

Supplementary data associated with this article can be found, in the online version, at http://dx.doi.org/10.1016/j.chroma.2014.05.002.

References

[1] G. Guiochon, J. Chromatogr. A 1168 (2007) 101.
[2] F. Svec, J. Chromatogr. A 1217 (2010) 902.
[3] I. Nischang, O. Brueggemann, F. Svec, Anal. Bioanal. Chem. 397 (2010) 953.
[4] I. Nischang, I. Teasdale, O. Brueggemann, Anal. Bioanal. Chem. 400 (2011) 2289.
[5] F. Svec, J. Chromatogr. A 1228 (2012) 250.
[6] J. Urban, P. Jandera, Anal. Bioanal. Chem. 405 (2013) 2123.
[7] I. Nischang, J. Chromatogr. A 1287 (2013) 39.
[8] A.A. Al-Massaedh, U. Pyell, J. Chromatogr. A 1286 (2013) 183.
[9] A.A. Al-Massaedh, U. Pyell, J. Chromatogr. A 1325 (2014) 247.
[10] A.A. Al-Massaedh, U. Pyell, J. Chromatogr. A 1325 (2014) 186.
[11] H. Minakuchi, K. Nakanishi, N. Soga, N. Ishizuka, N. Tanaka, Anal. Chem. 68 (1996) 3498.
[12] K. Nakanishi, H. Minakuchi, N. Soga, N. Tanaka, J. Sol–Gel Sci. Technol. 13 (1998) 163.
[13] N. Tanaka, H. Kobayashi, N. Ishizuka, H. Minakuchi, K. Nakanishi, K. Hosoya, T. Ikegami, J. Chromatogr. A 965 (2002) 35.
[14] I. Nischang, O. Brueggemann, J. Chromatogr. A 1217 (2010) 5389.
[15] I. Nischang, I. Teasdale, O. Brueggemann, J. Chromatogr. A 1217 (2010) 7514.
[16] J. Urban, F. Svec, J.M.J. Frechet, J. Chromatogr. A 1217 (2010) 8212.
[17] K. Liu, H.D. Tolley, M.L. Lee, J. Chromatogr. A 1227 (2012) 96.
[18] T.J. Causon, E.F. Hilder, I. Nischang, J. Chromatogr. A 1263 (2012) 108.
[19] C. Puangpila, T. Nhujak, R. El, Electrophoresis 33 (2012) 1431.
[20] P. Jandera, M. Stankova, V. Skerikova, J. Urban, J. Chromatogr. A 1274 (2013) 97.
[21] M. Stankova, P. Jandera, V. Skerikova, J. Urban, J. Chromatogr. A 1289 (2013) 47.
[22] A. Greiderer, L. Trojer, C.W. Huck, G.K. Bonn, J. Chromatogr. A 1216 (2009) 7747.
[23] I. Nischang, J. Chromatogr. A 1236 (2012) 152.
[24] F. Svec, J.M.J. Frechet, Chem. Mater. 7 (1995) 707.
[25] S. Xie, F. Svec, J.M.J. Frechet, J. Polym. Sci. A: Polym. Chem. 35 (1997) 1013.
[26] D. Hoegger, R. Freitag, J. Chromatogr. A 914 (2001) 211.
[27] T. Jiang, J. Jiskra, H.A. Claessens, C.A. Cramers, J. Chromatogr. A 923 (2001) 215.
[28] D. Hoegger, R. Freitag, Electrophoresis 24 (2003) 2958.
[29] A. Maruska, O. Kornysova, J. Biochem. Biophys. Methods 59 (2004) 1.
[30] S. Eeltink, J.M. Herrero-Martinez, G.P. Rozing, P.J. Schoenmakers, W.T. Kok, Anal. Chem. 77 (2005) 7342.
[31] S. Eeltink, L. Geiser, F. Svec, J.M.J. Frechet, J. Sep. Sci. 30 (2007) 2814.
[32] V. Ratautaite, A. Maruska, M. Erickson, O. Kornysova, J. Sep. Sci. 32 (2009) 2582.
[33] P. Aggarwal, H.D. Tolley, M.L. Lee, Anal. Chem. 84 (2012) 247.
[34] J. Lin, G. Huang, X. Lin, Z. Xie, Electrophoresis 29 (2008) 4055.
[35] Y. Huo, P.J. Schoenmakers, W.T. Kok, J. Chromatogr. A 1175 (2007) 81.
[36] S. Eeltink, G.P. Rozing, P.J. Schoenmakers, W.T. Kok, J. Chromatogr. A 1109 (2006) 74.
[37] A. Palm, M.V. Novotny, Anal. Chem. 69 (1997) 4499.
[38] M. Zhang, Z. El Rassi, Electrophoresis 22 (2001) 2593.
[39] A. Wahl, F. Al-Rimawi, I. Schnell, O. Kornysova, A. Maruska, U. Pyell, J. Sep. Sci. 31 (2008) 1519.
[40] A.M. Enlund, C. Ericson, S. Hjerten, D. Westerlund, Electrophoresis 22 (2001) 511.
[41] S. Bernhardt, P. Glockner, H. Ritter, Polym. Bull. 46 (2001) 153.
[42] P. Glockner, H. Ritter, Macromol. Rapid Commun. 20 (1999) 602.
[43] P. Casper, P. Gloeckner, H. Ritter, Macromolecules 33 (2000) 4361.
[44] J. Jeromin, H. Ritter, Macromol. Rapid Commun. 19 (1998) 377.
[45] S. Schwarz-Barac, H. Ritter, J. Macromol. Sci. Pure Appl. Chem. A40 (2003) 437.
[46] C. Steffens, O. Kretschmann, H. Ritter, Macromol. Rapid Commun. 28 (2007) 623.
[47] S. Bernhardt, P. Gloeckner, A. Theis, H. Ritter, Macromolecules 34 (2001) 1647.
[48] H. Ritter, M. Tabatabai, Prog. Polym. Sci. 27 (2002) 1713.
[49] X. Feng, X. Guo, K. Qiu, Makromol. Chem. 189 (1988) 77.
[50] M.V. Rekharsky, Y. Inoue, Chem. Rev. 98 (1998) 1875.
[51] P.G. Wang (Ed.), Monolithic Chromatography and its Modern Applications, ILM, Publications, St Albans, UK, 2010.
[52] W.A. Skinner, J.H. Lange, T.E. Shellenberger, W.T. Colwell, J. Med. Chem. 10 (1967) 949.
[53] A. Wahl, I. Schnell, U. Pyell, J. Chromatogr. A 1044 (2004) 211.

[54] P.G. Stevenson, H. Gao, F. Gritti, G. Guiochon, J. Sep. Sci. 36 (2013) 279.
[55] M. Motokawa, H. Kobayashi, N. Ishizuka, H. Minakuchi, K. Nakanishi, H. Jinnai, K. Hosoya, T. Ikegami, N. Tanaka, J. Chromatogr. A 961 (2002) 53.
[56] N.W. Smith, M.B. Evans, Chromatographia 38 (1994) 649.
[57] I. Nischang, U. Tallarek, J. Sep. Sci. 32 (2009) 3157.
[58] G. Marrubini, B.E.C. Mendoza, G. Massolini, J. Sep. Sci. 33 (2010) 803.
[59] G. Guiochon, J. Chromatogr. A 1126 (2006) 6.
[60] J. Li, P.W. Carr, Anal. Chem. 69 (1997) 2530.
[61] H. Colin, J.C. ez-Masa, G. Guiochon, T. Czajkowska, I. Miedziak, J. Chromatogr. 167 (1978) 41.

Adamantyl-group containing mixed-mode acrylamide-based continuous beds for capillary electrochromatography. Part IV: Investigation of the chromatographic efficiency dependent on the retention mode

"Ayat Allah" Al-Massaedh, Ute Pyell*

University of Marburg, Department of Chemistry, Hans-Meerwein-Straße, D-35032 Marburg, Germany

Supplementary data

Section S1: Calculation of efficiency data

Section S2: Band broadening processes

Table S1: Retention factor, asymmetry factor, and plate height H measured for repeated runs with Monolith A at different mobile phase velocities (single values).

Table S2: Retention factor k, asymmetry factor AF, and plate height H determined for DMF and alkylphenones as test solutes with Monolith A at different mobile phase velocities (mean values (or median) and s.d.).

Table S3: Methylene selectivity α_{meth} (± confidence range) for different classes of analytes separated on Monolith A.

Table S4: Efficiency data for different classes of analytes calculated via tangent method and moment analysis.

Table S5: Plate height equation constants B and C and correlation coefficient r determined from linear regression analysis.

Figure S1: Electropherograms of alkylphenones on Monolith A used for evaluation of the moment analysis method (see Section S1).

Figure S2: Electropherograms of alkylphenones on Monolith A at varied mobile phase linear velocity.

Figure S3: Reversed-phase separation of alkyl benzoates on Monolith A.

Figure S4: Plot of the logarithmic retention factor *versus* the number of methylene groups (n_{CH2}) in the alkyl chain of for alkyl benzoates, alkylanilines, and alkylphenones.

Figure S5: Mixed-mode separation of nitrotoluenes on Monolith A.

Figure S6: Log k of nitrotoluenes versus volume fraction of methanol in the mobile phase.

Figure S7: Expanded views of electropherograms of (a) alkylphenones eluted in the reversed-phase mode and (b) phenolic analytes eluted in the normal-phase mode on Monolith A.

S1. Calculation of efficiency data

Retention time and peak width (peak width at base) are determined with the software employed for recording and data treatment (EZ-Chrom 6.6). The peak width is obtained from applying the tangent method: straight lines are drawn tangent to the left and the right inflection point of the peak and the distance between the points where these lines intersect the base line is determined. With these data, the number of theoretical plates N and the height equivalent to a theoretical plate H are calculated via:

$$N = \left(\frac{t_R}{\sigma}\right)^2 = 16\left(\frac{t_R}{w}\right)^2 \qquad \text{(S1)}$$

$$H = \frac{L_{eff}}{N} \qquad \text{(S2)}$$

where t_R is the retention time, w is the peak width, and L_{eff} is the effective length of the column (inlet to detection). The asymmetry factor (AF) is calculated at 5% of the maximum peak height. It corresponds to the distance from the leading edge to the tailing edge of the peak divided by twice the distance from the centre line of the peak to the leading edge.

However, Eq. (S1) and application of the tangent method are only valid for peaks of Gaussian shape [1-3]. In the general case, the first and the second moment of the recorded peaks have to be calculated following the principles of moment analysis. Moment analysis is based on the so-called moment equations, which are principally valid for any distribution of a magnitude. In chromatography, of course, it is applied to the chromatographic peak, which is a distribution of the type S = f(t), where S = signal, t = time.

Following moments are defined for this type of distribution [2,4,5]:

$$m_n = \int_0^\infty S\, t^n\, dt \qquad (m_n = n^{th} \text{ moment}) \qquad \text{(S3)}$$

$$\mu_n = \frac{m_n}{m_0} = \frac{\int_0^\infty S\, t^n\, dt}{\int_0^\infty S\, dt} \qquad (\mu_n = n^{th} \text{ moment about the origin}) \qquad \text{(S4)}$$

$$\mu'_n = \frac{\int_0^\infty S\,(t-\mu_1)^n\, dt}{\int_0^\infty S\, dt} \qquad (\mu'_n = n^{th} \text{ moment about the mean}) \qquad \text{(S5)}$$

The zeroth moment m_0 is identical to the peak area. The first moment about the origin μ_1 corresponds to the retention time t_R, while the second moment about the mean μ'_2 corresponds to the variance of the peak in time units. According to the general definition of H it can be deduced:

$$H = \frac{\mu'_2 \, L_{eff}}{(\mu_1)^2} \qquad \text{(S6)}$$

These moments are easily accessible via numerical calculations, which have been performed by us for a selected data set from the raw data taking the reversed-phase separation of alkylphenones as an example (Figure S1). These runs have been selected because with this capillary very high asymmetry factors were obtained. Within these calculations, it was necessary to define exactly the baseline by regression analysis and to correct all data points with the defined baseline. It was also necessary to define start and end points by careful visual inspection. Following equations were employed:

$$\mu_1 = \frac{\sum_{i=1}^{N} S_{i,corr} \; t_i \; \Delta t}{\sum_{i=1}^{N} S_{i,corr} \; \Delta t} \qquad \text{(S7)}$$

$$\mu_2 = \frac{\sum_{i=1}^{N} S_{i,corr} \; (t_i)^2 \; \Delta t}{\sum_{i=1}^{N} S_{i,corr} \; \Delta t} \qquad \text{(S8)}$$

where N here is the number of data points, $S_{i,corr}$ = value of data point corrected for baseline, t_i = time of data point, Δt = time difference between data points (here 0.1 s). The second central moment about the mean was calculated via $\mu'_n = \mu_2 - (\mu_1)^2$ [4].

Moment analysis method is not advisable for chromatograms recorded with a low signal-to-noise ratio. This aspect of moment analysis was recently discussed by Stevenson *et al.* [6] in a paper on optimizing the location of peak boundaries for accurate moment calculations. The authors concluded that it is possible to perform moment analysis automatically if S/N exceeds 200.

S2. Band broadening processes

The parameter, which is employed for measuring the efficiency of a chromatographic system, is the height equivalent of a theoretical plate (HETP, H) which is defined as the peak variance in length units σ_L^2 normalized on (divided by) the migrated distance L_D ($H = \sigma_L^2/L_D$). In other words, it is the "rate at which the variance of the chromatographic band increases with increasing migration distance" [7,8].

Axial diffusion, flow inhomogeneities, temperature inhomogeneities, and mass-transfer resistances contribute simultaneously to the observed band dispersion. If these band broadening processes result in Gaussian band profiles, partial height equivalents of a theoretical plate (corresponding to partial normalized variances) can be defined which all contribute to the overall observed HETP:

$$H = H_D + H_F + H_R + H_T\ldots\ldots \quad \text{(S9)}$$

where H_D = plate height due to axial diffusion, H_F = plate height resulting from flow inhomogeneity (fluctuations of the local mobile phase velocity across the column [9]), H_R =plate height due to resistance to mass transfer (including diffusion in the stagnant mobile phase, diffusion in the stationary phase and sorption/desorption kinetics), H_T = plate height as result of a radial temperature gradient within the column. It can easily be verified by experiments with varied mobile phase flow rate (which corresponds to a varied mobile phase velocity) that the observed HETP is a function of the linear mobile phase velocity u (whereas u is commonly identified with the velocity with which an unretained marker is transported with the mobile phase along the column). The equation H = f(u) describing this dependence is the plate height equation.

If the processes listed in Eq. (S9) are independent from each other, partial plate height equations can be expressed. In the case of axial diffusion, the peak variance will increase linearly with time. Therefore H_D must be inversely proportional to the linear mobile phase velocity (B = const.):

$$H_D = B/u \quad \text{(S10)}$$

Resistance to mass transfer relates to the rate of equilibration between moving mobile phase, stagnant mobile phase and stationary phase. This equilibration rate depends on the diffusion coefficient of the solute in the stagnant mobile phase, the diffusion coefficient of the solute in the stationary phase, the morphology of the chromatographic bed (determining the diffusion distances and the extent to which diffusion is hindered [10]), and the sorption/desorption kinetics. There is no exact model of the equilibration processes taking place in an organic monolith. As has been shown in the second paper of this series [11], we have experimental evidence that the monolithic material investigated in this study is

considerably mesoporous. From this result we draw the conclusion that all processes named above will contribute to an overall resistance to mass transfer term proportional to the linear mobile phase velocity (C_R = const.) [12]:

$$H_R = C_R u \qquad \text{(S11)}$$

Flow inhomogeneities (within one channel, between channels of different geometry, and those related to a radial gradient of permeability [7-9]) are counteracted by molecular diffusion in radial direction. Regarding the (slow) propulsion of mobile phase by electroosmosis, the small domain size in the monolith [11], the small diameter of the capillary column (100 μm) and an effective length of the monolith of 150 to 250 mm, the long-time limit of validity of the Taylor-Aris model of dispersion can be expected to be reached [13,14]. In this case a flow inhomogeneity term proportional to the linear mobile phase velocity (C_F = const.) can be assumed, which would include effects due to a radial macroporosity gradient, which must result in an important trans-column flow inhomogeneity [15]:

$$H_F = C_F u \qquad \text{(S12)}$$

This assumption is corroborated by experiments made by Gritti and Guiochon [16] who have experimentally verified for HPLC columns of d = 4.6 mm that the trans-column eddy diffusion term and the relaxation of a radial concentration gradient in a packed bed depend on the flow rate of the mobile phase.

In a careful study, Gritti *et al.* [17] have discussed the validity of assuming a Taylor-Aris-type contribution for the plate height equation of columns packed with 1.5-3 μm particles operated under very high pressure (radial temperature gradient). They have shown that also in the case of a radial temperature gradient in a packed column, the Taylor-Aris theory of dispersion is valid. Consequently, we assume following partial plate height equation for band broadening by a radial temperature gradient:

$$H_T = C_T u \qquad \text{(S13)}$$

From these partial equations follows that the experimentally observable overall plate height equation will be:

$$H = B/u + C u \qquad \text{(S14)}$$

Table S1. Retention factor, asymmetry factor, and plate height H measured for repeated runs (single values) with Monolith A at different mobile phase velocities (for experimental conditions refer to Figure 1). Mobile phase: methanol/water (50:50, v/v) buffered with triethylamine/acetic acid, pH* = 7.0.

Analyte	U/kV	12			14			
	u/(mm s^{-1})	0.265 (± 0.005)			0.319 (± 0.004)			
DMF	k	0	0	0	0	0	0	0
	AF	1.089	1.125	1.144	1.08	1.134	1.064	1.170
	H/µm	6.22	5.47	5.10	4.72	4.73	5.57	4.09
Aceto-phenone	k	0.197	0.199	0.198	0.19	0.199	0.198	0.198
	AF	1.095	1.077	1.079	1.07	1.093	1.101	1.112
	H/µm	5.62	5.55	6.07	5.43	4.83	4.56	4.31
Propio-phenone	k	0.242	0.245	0.244	0.24	0.244	0.243	0.243
	AF	1.086	1.041	1.290	1.09	1.069	1.085	1.026
	H/µm	5.38	5.00	4.67	5.46	4.74	5.43	4.09
Butyro-phenone	k	0.299	0.302	0.301	0.30	0.302	0.301	0.301
	AF	1.076	1.055	1.061	1.11	1.189	1.121	1.191
	H/µm	5.90	5.47	5.21	5.42	5.34	5.18	5.22
Valero-phenone	k	0.393	0.397	0.396	0.39	0.399	0.397	0.398
	AF	1.200	1.222	-----[a]	1.19	1.167	1.158	1.363
	H/µm	5.66	6.32	5.35	5.79	5.66	5.24	7.30
Hexano-phenone	k	0.539	0.545	0.544	0.54	0.548	0.545	0.547
	AF	1.283	1.884	1.180	1.29	1.357	1.268	1.443
	H/µm	5.03	7.30	6.79	6.61	6.61	6.34	6.25

Analyte	U/(kV)	16.5						18.5					
	u/(mm s^{-1})	0.394 (± 0.014)						0.435 (± 0.005)					
DMF	k	0	0	0	0	0	0	0	0	0	0	0	
	AF	1.066	1.103	1.070	1.127	1.063	1.055	1.096	1.068	1.021	1.086	1.016	
	H/µm	4.39	5.09	4.56	5.54	5.54	5.84	4.76	4.28	4.36	4.71	4.34	
Aceto-phenone	k	0.195	0.197	0.197	0.199	0.198	0.197	0.196	0.197	0.196	0.197	0.201	
	AF	1.118	1.105	1.044	1.066	1.111	1.145	1.098	1.092	1.080	1.078	1.050	
	H/µm	4.72	4.66	4.35	6.01	5.38	4.77	4.42	4.37	4.34	4.05	4.96	
Propio-phenone.	k	0.241	0.242	0.241	0.245	0.244	0.243	0.241	0.243	0.242	0.243	0.247	
	AF	1.047	1.088	1.068	1.061	1.094	1.116	1.093	1.065	1.119	1.048	1.085	
	H/µm	5.07	4.83	4.69	5.50	5.49	5.45	4.35	4.53	5.19	4.92	4.51	
Butyro-phenone	k	0.297	0.299	0.298	0.303	0.302	0.301	0.297	0.300	0.298	0.299	0.308	
	AF	1.109	1.141	1.087	1.103	1.093	1.107	1.094	1.077	1.161	1.137	1.207	
	H/µm	4.94	5.36	4.45	5.59	6.10	5.77	4.68	4.42	4.48	5.16	4.35	
Valero-phenone	k	0.392	0.393	0.392	0.399	0.398	0.396	0.392	0.395	0.393	0.395	0.409	
	AF	1.234	1.291	1.189	1.292	1.280	1.219	1.186	1.212	1.168	1.164	1.252	
	H/µm	4.98	4.68	4.59	6.67	6.09	4.84	4.34	4.75	5.36	5.11	5.18	
Hexano-phenone	k	0.538	0.540	0.539	0.549	0.548	0.544	0.538	0.542	0.539	0.542	0.566	
	AF	1.287	1.265	1.243	1.336	1.340	1.481	1.393	1.360	1.276	1.238	1.280	
	H/µm	5.41	4.80	5.77	7.16	8.27	6.51	4.55	5.08	5.57	5.99	5.62	

Table S1 continued on next page

Analyte	U/kV	20.5				22.5				
	u/(mm s^{-1})	0.489 (± 0.002)				0.541 (± 0.008)				
DMF	k	0	0	0	0	0	0	0	0	0
	AF	1.089	1.127	1.061	1.028	0.978	1.041	1.086	0.996	1.071
	H/µm	4.57	4.16	3.89	4.36	4.25	4.08	4.34	3.82	4.14
Aceto-phenone	k	0.198	0.198	0.198	0.196	0.198	0.198	0.197	0.196	0.198
	AF	1.027	1.101	1.094	1.050	1.091	1.132	1.099	1.108	-----[a]
	H/µm	4.16	4.47	4.38	4.30	4.39	4.55	4.01	4.16	4.15
Propio-phenone	k	0.243	0.243	0.242	0.242	0.244	0.244	0.243	0.241	0.243
	AF	1.055	1.070	1.308	1.111	1.052	1.083	1.139	1.151	-----[a]
	H/µm	4.52	4.13	4.76	4.75	4.29	4.79	4.44	4.56	4.60
Butyro-phenone	k	0.301	0.301	0.300	0.299	0.301	0.303	0.301	0.299	0.301
	AF	1.072	1.060	1.207	1.086	1.123	1.151	1.148	1.095	1.983
	H/µm	4.35	4.93	4.52	4.05	4.38	4.25	4.28	4.37	4.59
Valero-phenone	k	0.396	0.396	0.395	0.394	0.397	0.399	0.398	0.394	0.396
	AF	1.253	1.226	1.194	1.209	1.098	1.300	1.196	1.178	1.295
	H/µm	4.74	4.41	5.24	5.62	4.86	4.25	4.83	4.54	4.18
Hexano-phenone	k	0.546	0.544	0.542	0.542	0.547	0.550	0.546	0.541	0.543
	AF	1.288	1.362	1.321	1.376	1.275	1.333	1.305	1.338	1.368
	H/µm	5.14	4.63	5.14	5.38	5.10	5.12	5.15	4.97	-----[a]

Analyte	U/kV	25					
	u/(mm s^{-1})	0.623 (± 0.012)					
DMF	k	0	0	0	0	0	0
	AF	1.109	1.073	1.027	1.128	1.032	1.060
	H/µm	4.30	4.89	4.02	4.43	4.82	4.57
Aceto-phenone	k	0.199	0.193	0.196	0.201	0.194	0.198
	AF	1.010	1.092	1.116	1.108	1.055	1.128
	H/µm	4.36	4.64	4.44	4.43	4.30	4.60
Propio-phenone	k	0.244	0.238	0.240	0.247	0.238	0.245
	AF	1.159	1.069	1.145	1.139	1.107	1.082
	H/µm	4.42	4.31	5.08	4.60	4.41	4.47
Butyro-phenone	k	0.302	0.293	0.297	0.305	0.294	0.304
	AF	1.173	1.072	1.129	1.121	1.038	1.091
	H/µm	4.55	4.33	5.06	4.65	4.26	4.30
Valero-phenone	k	0.399	0.385	0.391	0.401	0.386	0.401
	AF	1.232	1.126	1.248	1.243	1.121	1.046
	H/µm	5.86	4.72	4.60	4.86	5.25	4.64
Hexano-phenone	k	0.549	0.527	0.537	0.549	0.529	0.552
	AF	1.395	1.295	1.307	1.339	1.398	1.382
	H/µm	5.74	5.35	5.27	5.79	5.15	5.82

[a] outlier

Table S2. Retention factor k, asymmetry factor, and plate height H determined for DMF and alkylphenones as test solutes with Monolith A at different mobile phase velocities (for experimental conditions refer to Figure 1). Mean values (median values) and standard deviations (in brackets) are calculated from those values given in Table S1 (n = 3 at 12 kV, n = 4 at 14 and 20.5 kV, n = 5 at 18.5 and 22.5 kV, and n = 6 at 16.5 and 25 kV).

Analyte	Voltage/kV	12	14	16.5	18.5	20.5	22.5	25
	u/(mms^{-1})	0.265 (± 0.005)	0.319 (± 0.004)	0.394 (± 0.014)	0.435 (± 0.005)	0.489 (± 0.002)	0.541 (± 0.008)	0.623 (± 0.012)
DMF	k	0	0	0	0	0	0	0
	AF	1.119 (± 0.028)	1.113 (± 0.048)	1.081 (± 0.028)	1.057 (± 0.037)	1.076 (± 0.042)	1.034 (± 0.046)	1.071 (± 0.041)
	H/µm	5.47* (± 0.57)	4.72 * (± 0.61)	5.16 (± 0.59)	4.49 (± 0.23)	4.26* (± 0.29)	4.14* (± 0.20)	4.51 (± 0.33)
Aceto-phenone	k	0.198 (± 0.001)	0.198 (± 0.000)	0.197 (± 0.001)	0.197 (± 0.002)	0.197 (± 0.001)	0.197 (± 0.001)	0.197±(0.003)
	AF	1.084 (± 0.010)	1.096 (± 0.015)	1.098(± 0.037)	1.080 (± 0.018)	1.068(± 0.036)	1.108(± 0.018)	1.085(± 0.044)
	H/µm	5.62* (± 0.28)	4.69* (± 0.48)	4.74* (± 0.61)	4.43 (± 0.33)	4.33 (± 0.13)	4.25(± 0.22)	4.46(± 0.13)
Propio-phenone	k	0.243 (± 0.002)	0.244 (± 0.001)	0.243(± 0.002)	0.243 (± 0.003)	0.243 (± 0.001)	0.243 (± 0.001)	0.242 (± 0.004)
	AF	1.139 (± 0.133)	1.068 (± 0.029)	1.079(± 0.025)	1.082 (± 0.027)	1.136 (± 0.117)	1.106 (± 0.047)	1.117 (± 0.037)
	H/µm	5.02 (± 0.36)	5.09* (± 0.65)	5.17(± 0.36)	4.70(± 0.35)	4.54 (± 0.30)	4.54(± 0.19)	4.44* (± 0.28)
Butyro-phenone	k	0.301 (± 0.002)	0.301 (± 0.001)	0.300(± 0.002)	0.300(± 0.004)	0.300(± 0.001)	0.301 (± 0.002)	0.299 (± 0.005)
	AF	1.064 (± 0.011)	1.154 (± 0.042)	1.107(± 0.019)	1.135(± 0.052)	1.106(± 0.068)	1.300(± 0.383)	1.104 (± 0.047)
	H/µm	5.52 (± 0.35)	5.29 (± 0.11)	5.37(± 0.59)	4.48* (± 0.33)	4.46(± 0.37)	4.37(± 0.13)	4.44* (± 0.31)
Valero phenone	k	0.395 (± 0.002)	0.397 (± 0.002)	0.395(± 0.003)	0.397 (± 0.007)	0.395 (± 0.001)	0.397 (± 0.002)	0.394 (± 0.007)
	AF	1.211 (± 0.016)	1.220 (± 0.096)	1.251(± 0.043)	1.196 (± 0.037)	1.221(± 0.025)	1.213(± 0.085)	1.169 (± 0.084)
	H/µm	5.66* (± 0.49)	5.72* (± 0.90)	5.31(± 0.86)	5.11* (± 0.41)	4.99* (± 0.53)	4.53(± 0.32)	4.79* (± 0.49)
Hexano-phenone	k	0.543 (± 0.003)	0.546 (± 0.003)	0.543(± 0.005)	0.545 (± 0.012)	0.543 (± 0.002)	0.545(± 0.004)	0.540(± 0.011)
	AF	1.449 (± 0.380)	1.340(± 0.078)	1.325(± 0.085)	1.310 (± 0.064)	1.337 (± 0.040)	1.324(± 0.035)	1.353(± 0.046)
	H/µm	6.79* (± 1.20)	6.45(± 0.19)	6.14*(± 1.26)	5.57* (± 0.56)	5.14* (± 0.32)	5.08(± 0.08)	5.52(± 0.30)

* median value

Table S3. Methylene selectivity α_{meth} (± confidence range) for different classes of analytes (alkylphenones, alkyl benzoates, and alkylanilines), stationary phase: Monolith A, capillary dimensions 245(317) mm × 100 μm. For mobile phases refer to Table 2, regression lines see Figure S4.

Substance class	α_{meth} (± confidence range)
alkylphenones	0.106 (± 0.020)
alkyl benzoates	0.104 (± 0.030)
alkylanilines	0.100 (± 0.003)

Table S4. Plates per meter calculated via (i) tangent method performed by standard chromatography software and (ii) moment analysis using Origin 8.1. Analytes: alkyl benzoates, nitrotoluenes, and phenolic analytes. Stationary phase: Monolith A, capillary dimensions 245(317) mm × 100 μm. For mobile phase compositions refer to Table 2.

Analyte	N m^{-1} (Tangent method)	N m^{-1} (Moment analysis)	AF
DMF	242 000	257 000	1.030
methyl benzoate	235 000	221 000	1.064
ethyl benzoate	221 000	216 000	1.071
propyl benzoate	224 000	202 000	1.188
butyl benzoate	186 000	153 000	1.183
DMF	225 000	240 000	1.056
4-nitrotoluene	221 000	233 000	1.058
2,4,6-trinitrotoluene	218 000	172 000	1.147
DMF	229 000	215 000	1.092
3-methoxybenzaldehyde	225 000	220 000	1.006
4-hydroxy-3-methoxybenzaldehyde	238 000	147 000	0.836
4-hydroxybenzaldehyde	209 000	140 000	0.808
3,4-dihydroxybenzaldehyde	194 000	99 000	1.003
resorcinol	246 000	152 000	1.343

Table S5. Plate height equation constants B and C (Eq. 1) and correlation coefficient r determined from linear regression analysis (Hu plotted against u^2) for DMF and alkylphenones. Stationary phase: Monolith A, capillary dimensions 245(317) mm× 100 µm. Mobile phase: methanol/water (50:50, v/v) buffered with triethylamine/acetic acid, pH* = 7.0, electric conductivity = 125 µS cm^{-1}. The standard deviations for B and C given in brackets correspond to the standard deviations of the intercept and the slope of the regression line.

Analyte	B/(µm² s^{-1})± s.d	C/ms ± s.d	r
DMF	1190 (± 107)	4.01 (± 0.47)	0.968
Acetophenone	1160 (± 50.7)	4.08 (± 0.22)	0.993
Propiophenone	1200 (± 98.7)	4.25 (± 0.43)	0.975
Butyrophenone	1300 (± 99.6)	3.76 (± 0.43)	0.970
Valerophenone	1350 (± 93.6)	4.22 (± 0.41)	0.977
Hexanophenone	1490 (± 108)	4.75 (± 0.47)	0.960

(a)

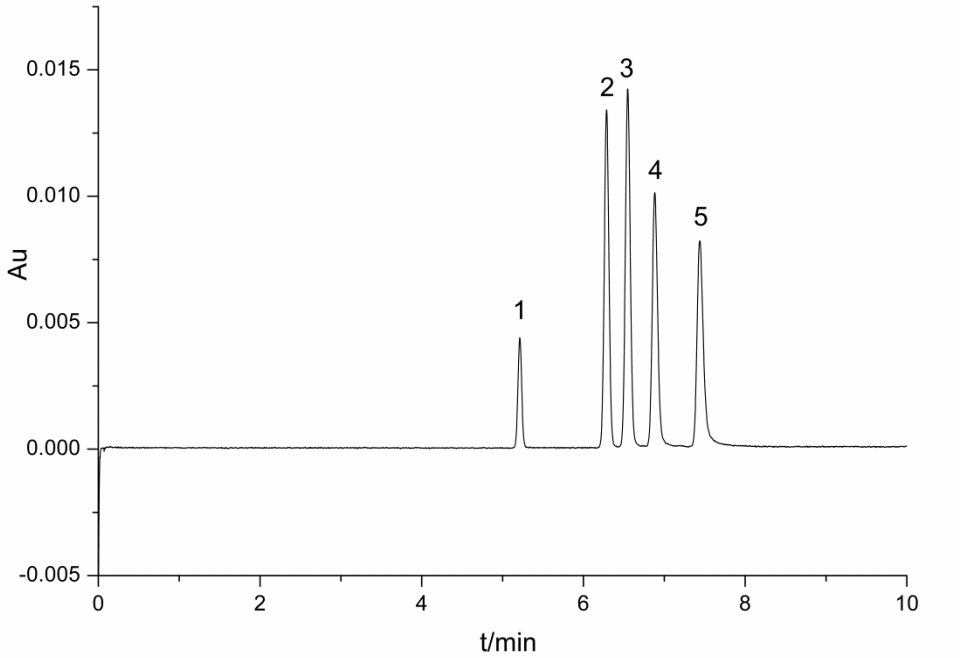

(b)

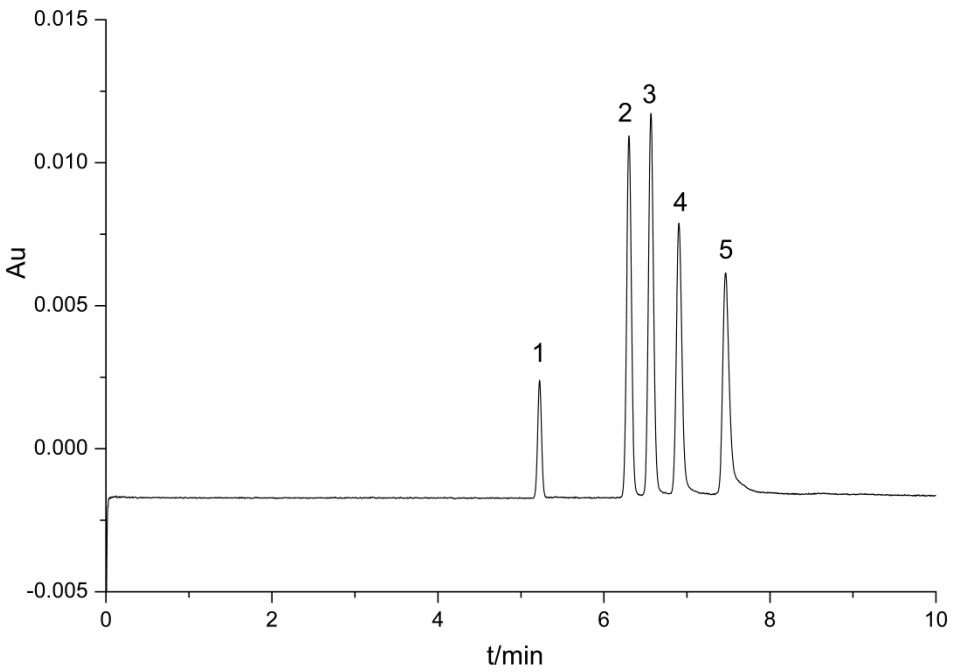

Figure S1 continued on next page

(c)

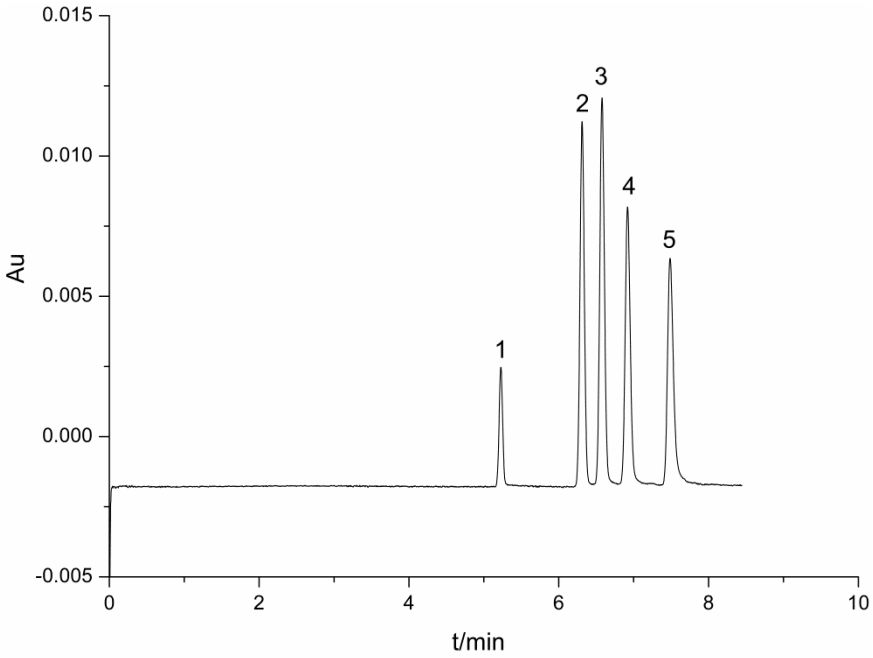

Figure S1. Electropherograms recorded for DMF and alkylphenones on Monolith A and evaluated via tangent method and moment analysis (see Table 1). (a) Run 1 (b) Run 2, (c) Run 3. Analytes: (1) DMF, (2) acetophenone, (3) propiophenone, (4) butyrophenone, and (5) valerophenone. Mobile phase: methanol/water (50:50, v/v) buffered with triethylamine/acetic acid, pH* = 7.0, electric conductivity = 125 μS cm^{-1}. Capillary dimensions 210(282) mm× 100 μm, UV detection at 230 nm; electrokinetic injection: 1.5 kV for 3 s; separation voltage: 20 kV.

(a)

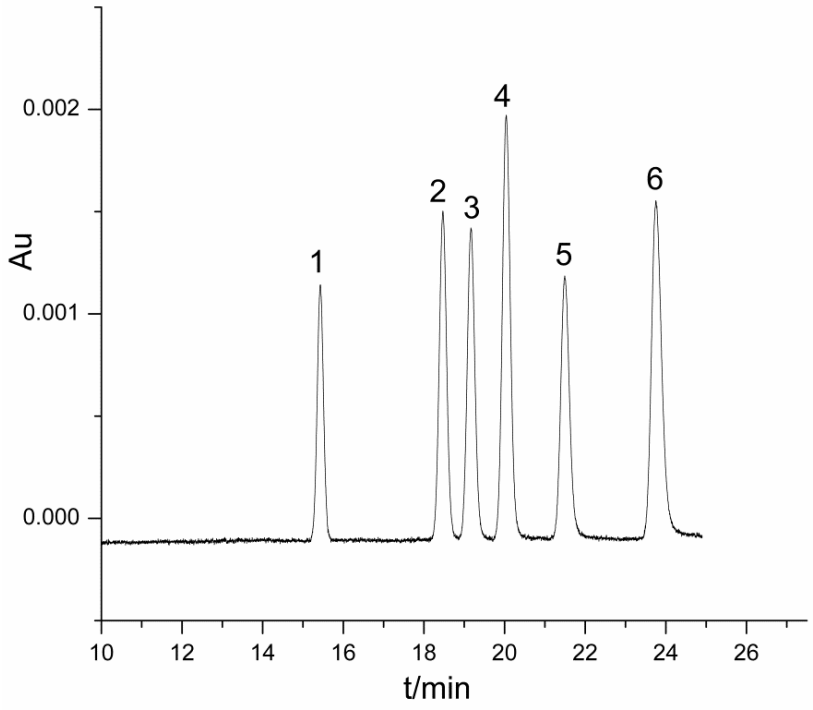

(b)

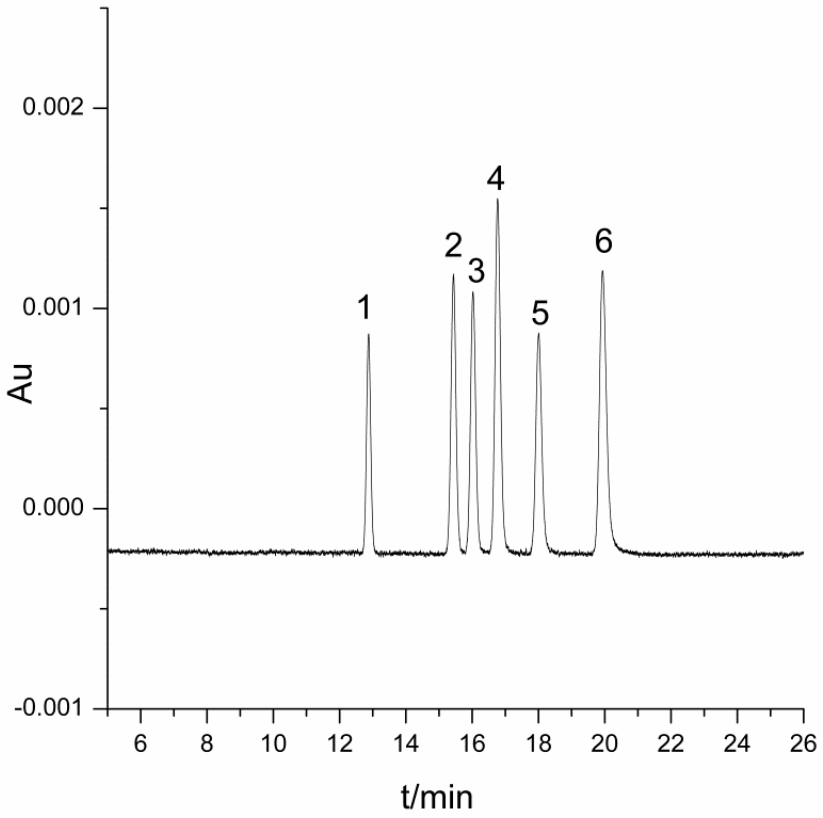

Figure S2 continued on next page

(c)

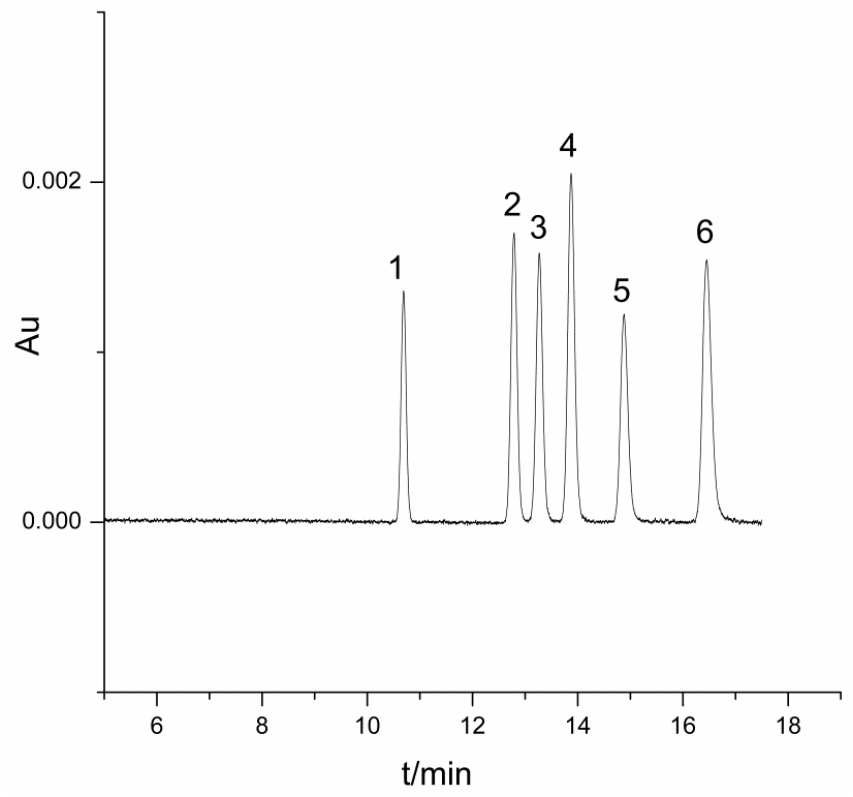

(d)

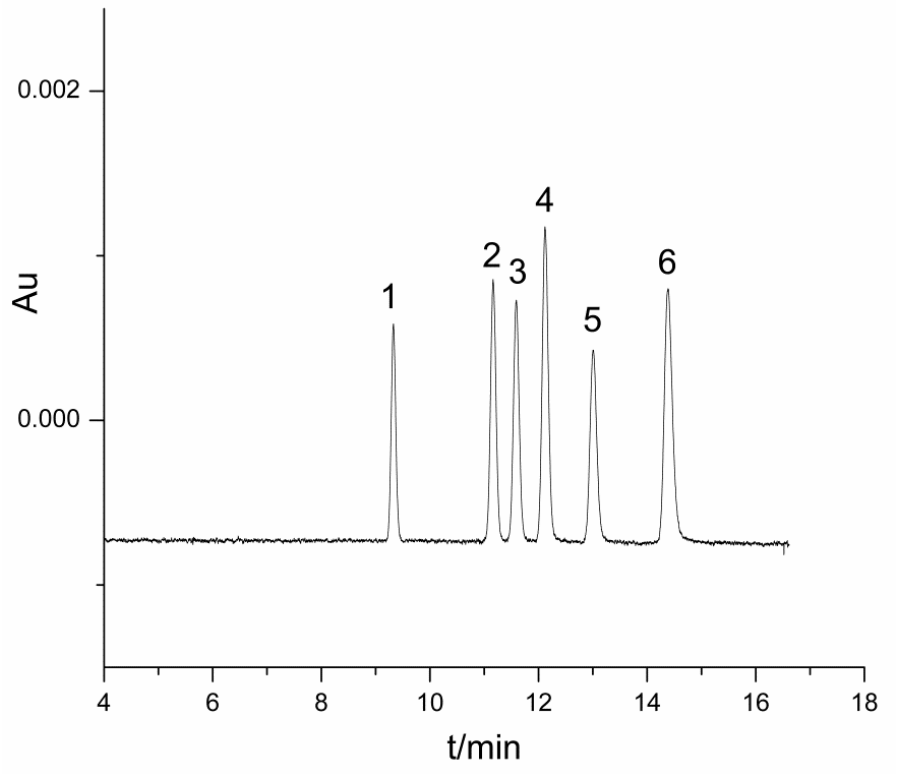

Figure S2 continued on next page

(e)

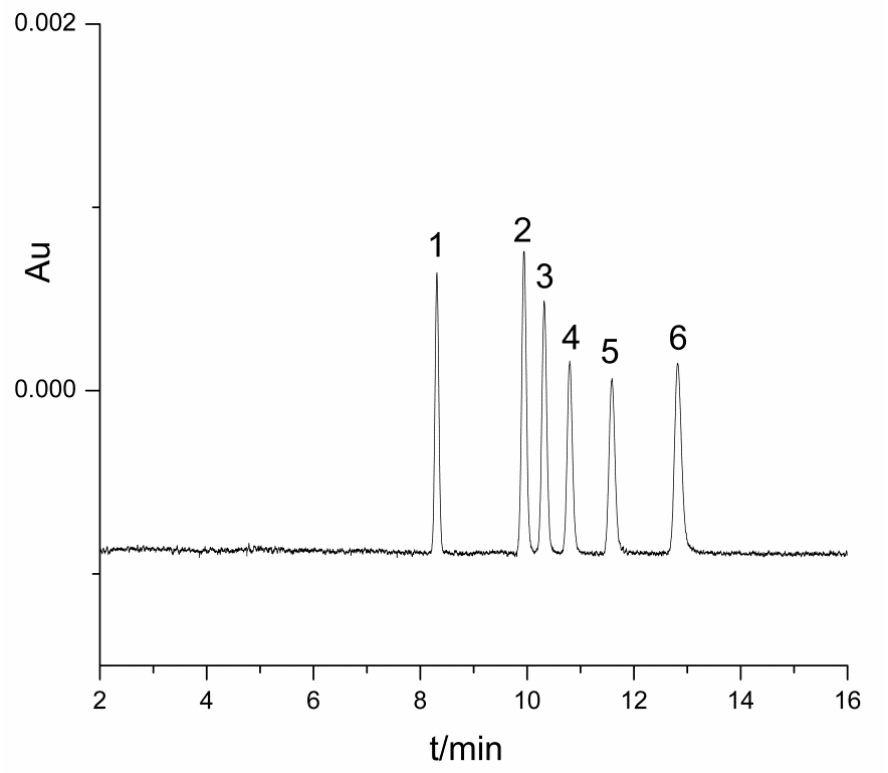

(f)

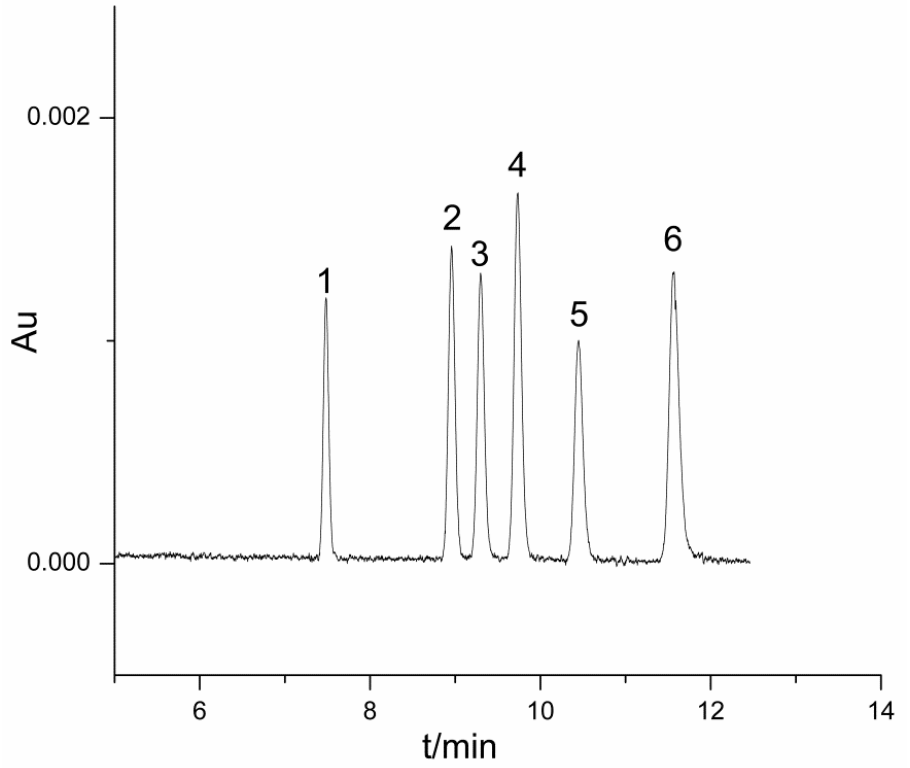

Figure S2 continued on next page

(g)

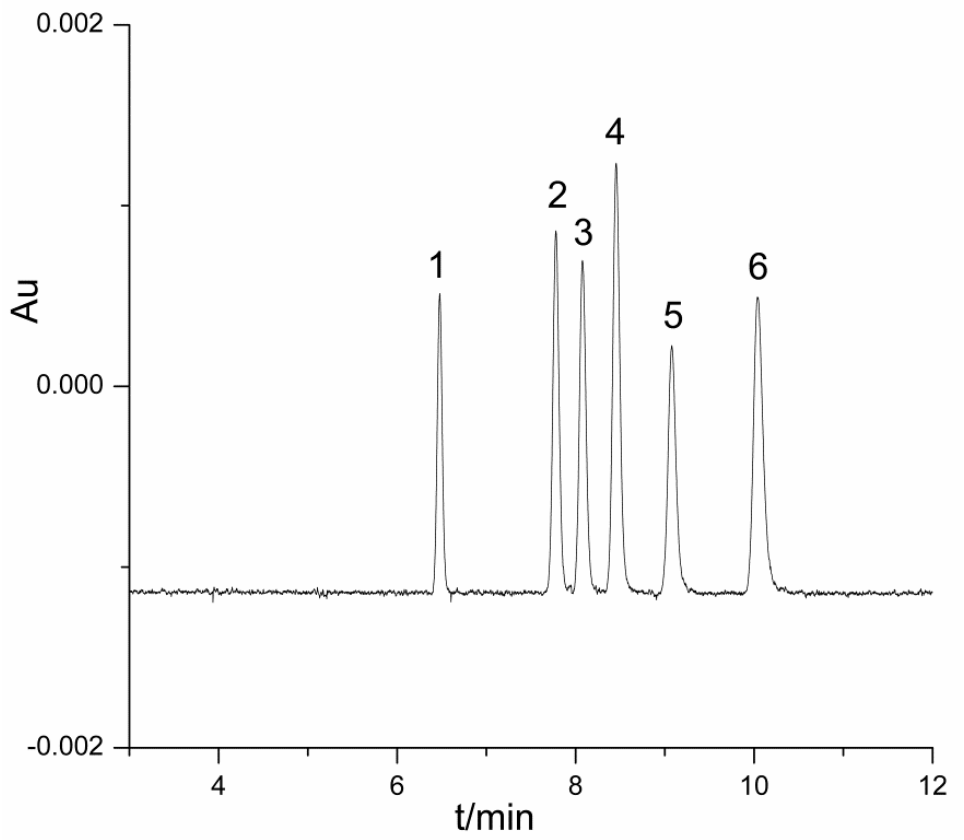

Figure S2: Electropherograms recorded for DMF and alkylphenones on Monolith A at different mobile phase velocities (see Figure 1). Mobile phase velocity: (a) 0.265 mms^{-1}, (b) 0.319 mms^{-1}, (c) 0.394 mm s^{-1}, (d) 0.435 mms^{-1}, (e) 0.489 mms^{-1}, (f) 0.541 mms^{-1}, and (g) 0.622 mms^{-1}. Analytes: (1) DMF, (2) acetophenone, (3) propiophenone, (4) butyrophenone, (5) valerophenone, and (6) hexanophenone. Mobile phase: methanol/water (50:50, v/v) buffered with triethylamine/acetic acid, pH* = 7.0, electric conductivity = 125 μS cm^{-1}. Capillary dimensions 245 mm (317 mm) x 100 μm; UV detection at 230 nm; electrokinetic injection: 3 kV for 3 s.

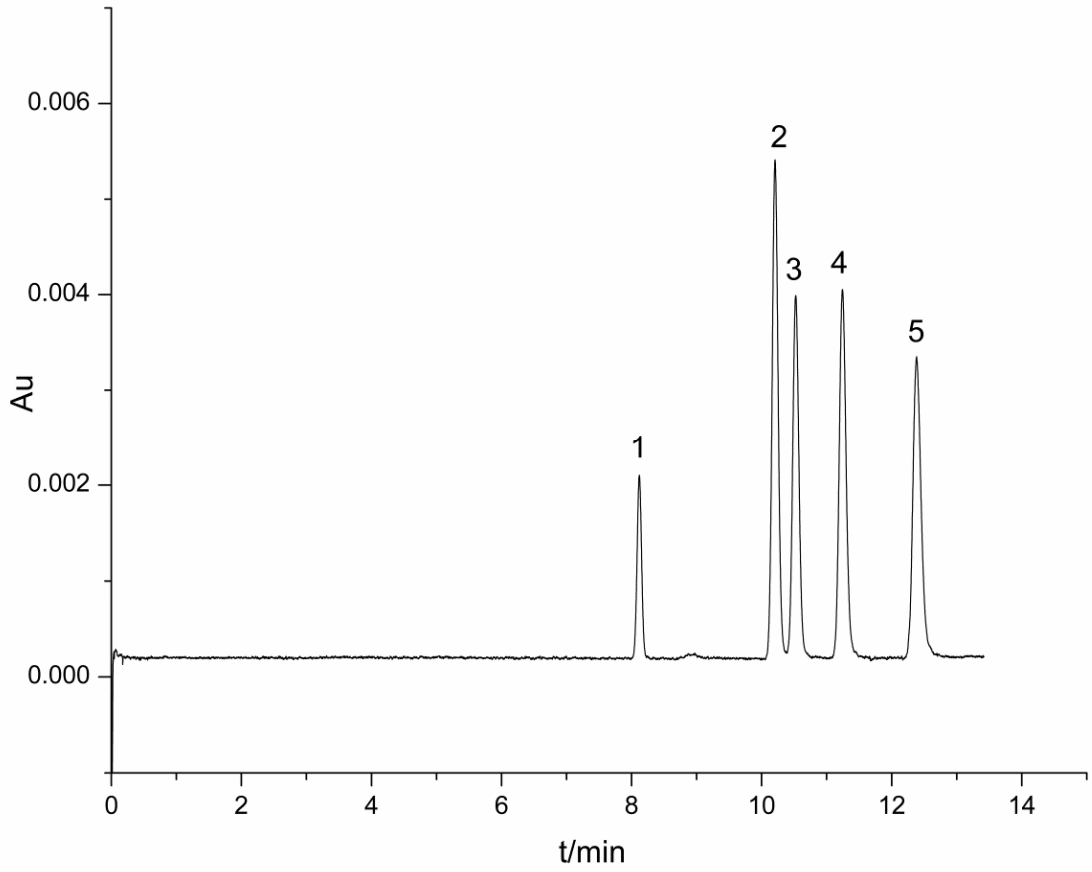

Figure S3. Reversed phase separation of alkyl benzoates on Monolith A. Analytes: (1) DMF (2) methyl benzoate (3) ethyl benzoate (4) propyl benzoate (5) butyl benzoate. Mobile phase: methanol/water (50:50, v/v) buffered with triethylamine/acetic acid, pH* = 7.0, electric conductivity = 125 μS cm^{-1}. Capillary dimensions 245 mm (317 mm) × 100 μm; UV detection at 230 nm; electrokinetic injection: 3 kV for 3 s, separation voltage: 20 kV.

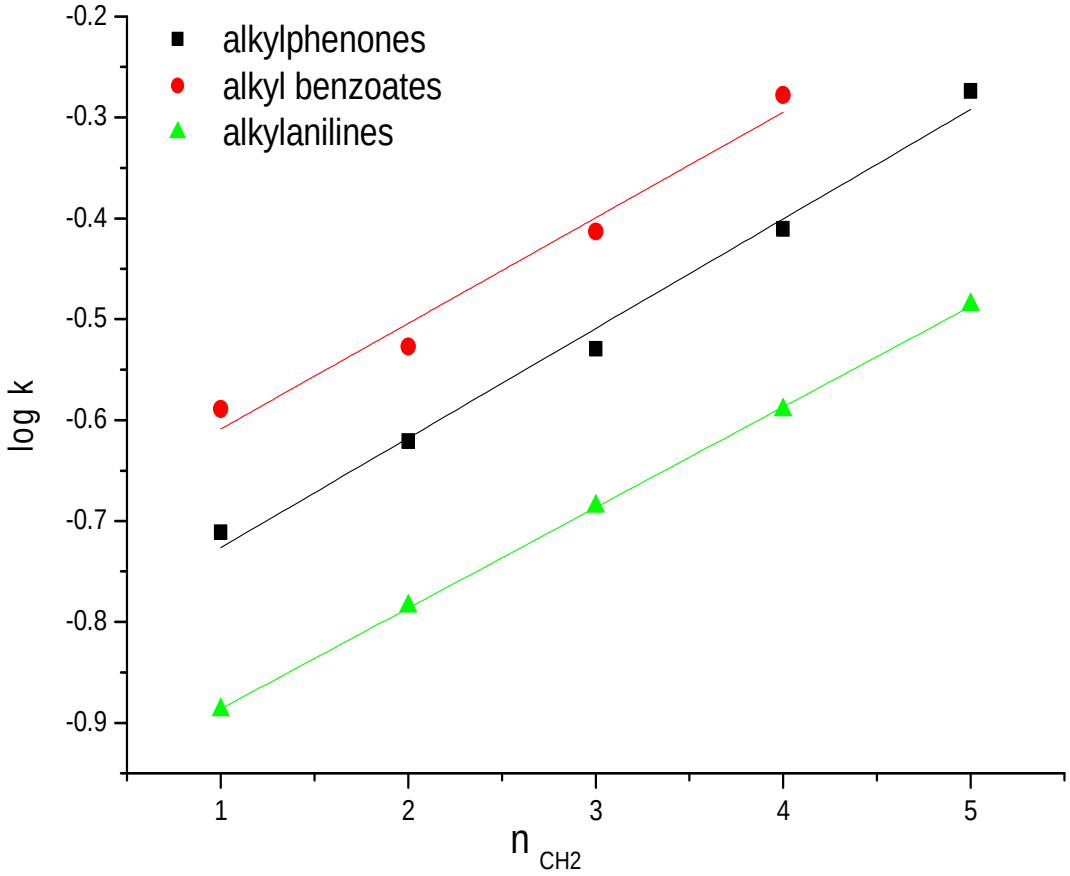

Figure S4. Plot of the logarithmic retention factors versus the number of methylene groups (n_{CH2}) in the alkyl chain for different classes of analytes. Stationary phase: Monolith A, capillary dimensions 245(317) mm× 100 µm. For mobile phases refer to Table 2.

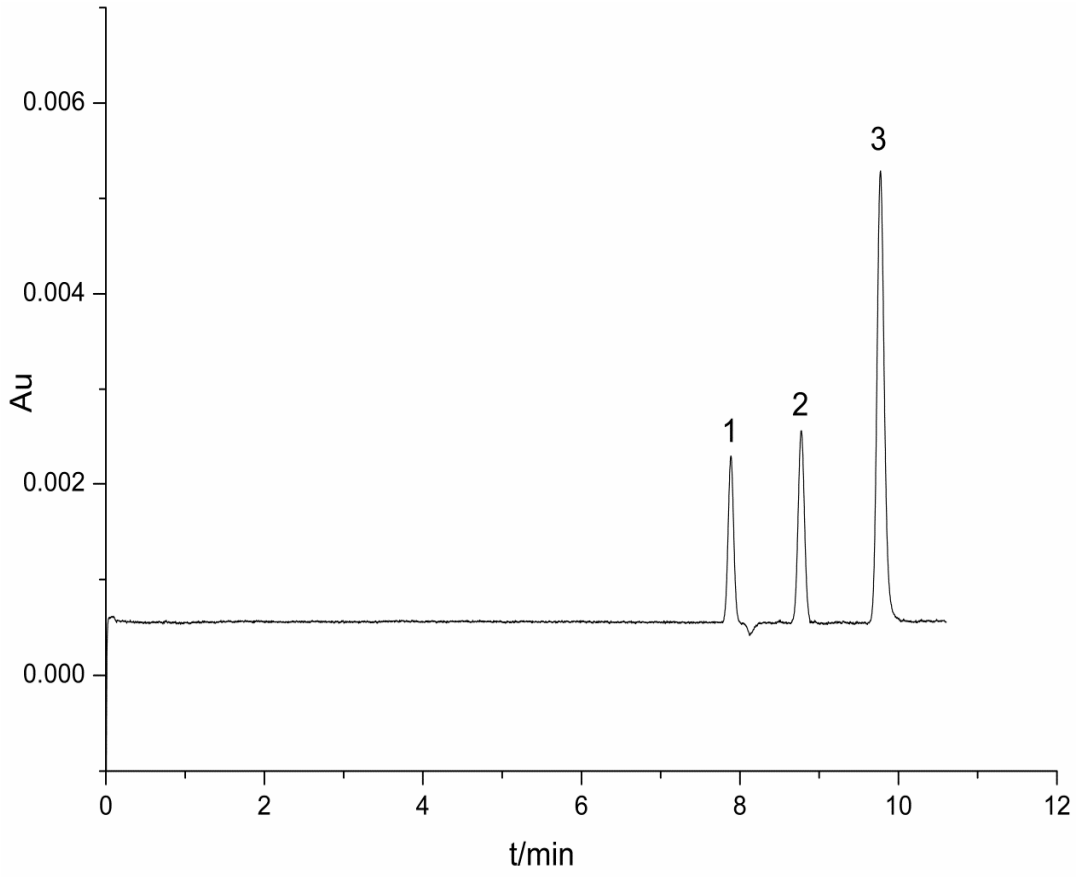

Figure S5. Mixed-mode phase separation of nitrotoluenes on Monolith A. Analytes: (1) DMF (2) 4-nitrotoluene (3) 2,4,6-trinitrotoluene. Mobile phase: methanol/water (80:20, v/v) buffered with triethylamine/acetic acid, pH* = 6.86, electric conductivity = 105 μS cm^{-1}. Capillary dimensions 245 mm (317 mm) × 100 μm; UV detection at 230 nm; electrokinetic injection: 1.5 kV for 3 s, separation voltage: 22 kV.

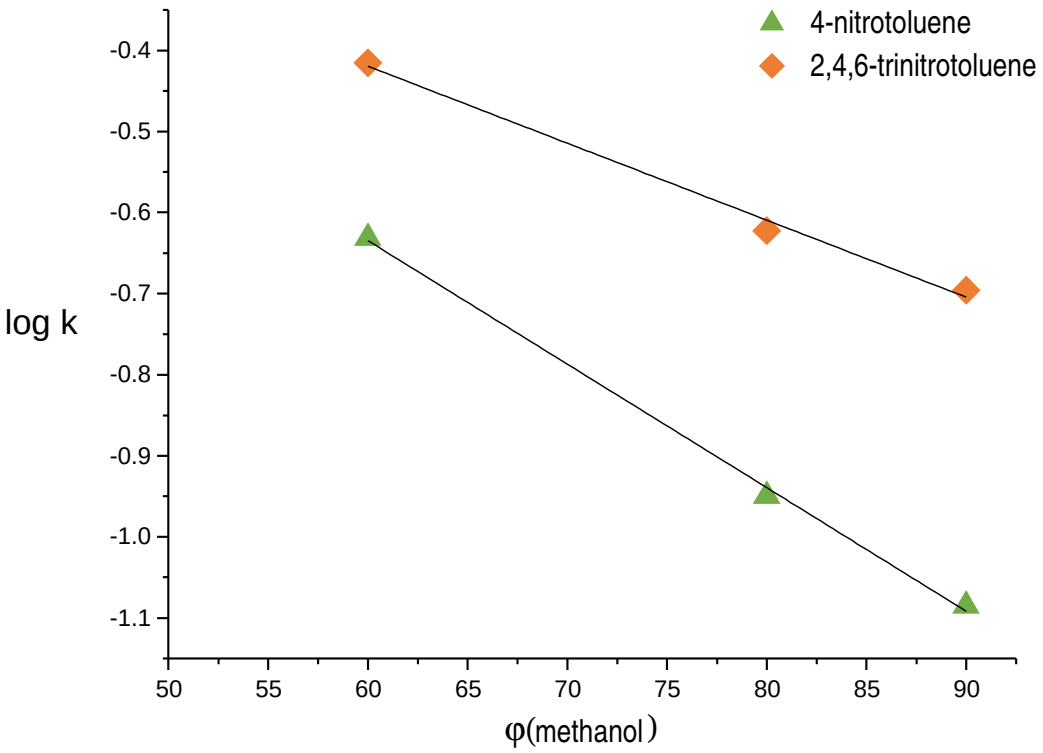

Figure S6. Log k of nitrotoluenes versus volume fraction of methanol in the mobile phase. Stationary phase: Monolith A, capillary dimensions 245(317) mm× 100 µm. Mobile phase methanol/water (80:20, v/v), buffered with triethylamine/acetic acid, pH* = 6.86, electric conductivity = 105 µScm^{-1}, UV detection at 230 nm, electrokinetic injection 1.5 kV for 3 s, separation voltage 22 kV.

(a)

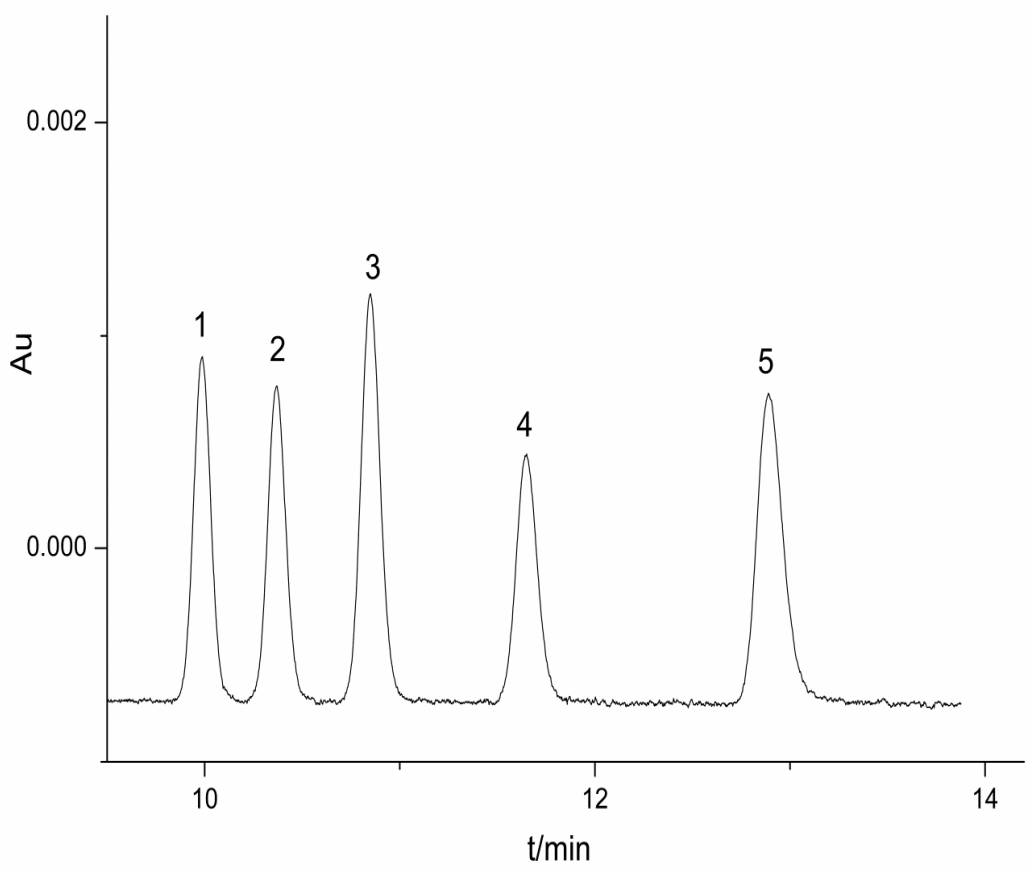

Figure S7 continued on next page

(b)

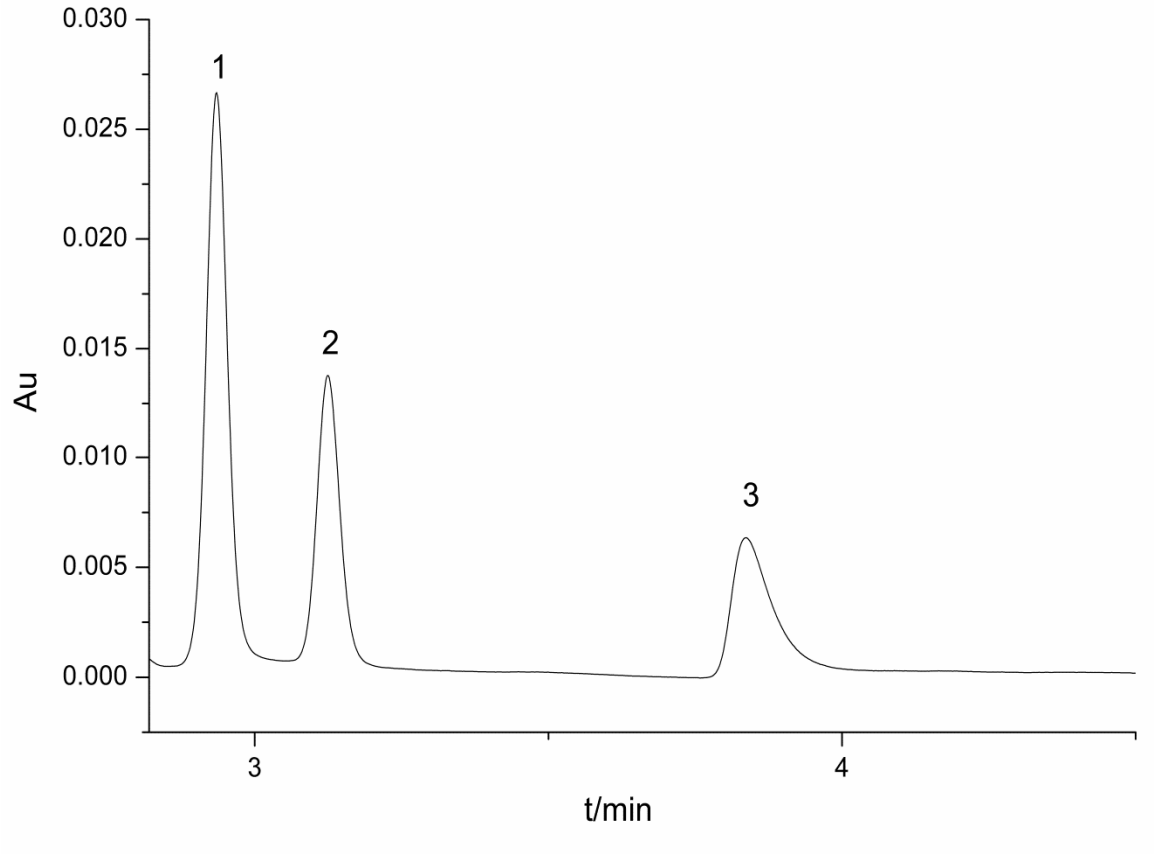

Figure S7. Expanded views of electropherograms of (a) alkylphenones eluted in the reversed-phase mode and (b) phenolic analytes eluted in the normal-phase mode on Monolith A. (a): (1) acetophenone, (2) propiophenone, (3) butyrophenone, (4) valerophenone, and (5) hexanophenone. (b): (1) 4-hydroxy-3-methoxy benzaldehyde, (2) 4-hydroxy benzaldehyde, and (3) resorcinol. For mobile phase composition see Table 2. Reproduced from Ref. [18] with permission. Copyright 2013, Elsevier.

References

[1] K. Miyabe, G. Guiochon, J. Phys. Chem. B 106 (2002) 8898.

[2] K. Miyabe, J. Sep. Sci. 32 (2009) 757.

[3] D.Y. Choi, K.H. Row, Biotechnol. Bioprocess Eng. 9 (2004) 495.

[4] S.A. Kevra, D.L. Bergman, J.T. Maloy, J. Chem. Educ. 71 (1994) 1023.

[5] Z. Liu, J. Roininen, I. Pulkkinen, P. Saari, T. Sainio, V. Alopaeus, Comput. Chem. Eng. 55 (2013) 50.

[6] P.G. Stevenson, H. Gao, F. Gritti, G. Guiochon, J. Sep. Sci. 36 (2013) 279.

[7] G. Guiochon, J. Chromatogr. A 1168 (2007) 101.

[8] J.Giddings, Dynamics of Chromatography, M. Dekker, New York, NY, 1965.

[9] U. Tallarek, E. Bayer, G. Guiochon, J. Am. Chem. Soc. 120 (1998) 1494.

[10] R.E. Beck, J.S. Schultz, Biochim. Biophys. Acta, Biomembr. 255 (1972) 273.

[11] A. A. Al-Massaedh, U. Pyell, J. Chromatogr. A 1325 (2014) 247.

[12] F. Gritti, G. Guiochon, J. Chromatogr. A 1221 (2012) 2.

[13] R. Aris, Proc. R. Soc. London, Ser. A 252 (1959) 538.

[14] R.Aris, Proc. R. Soc. London, Ser. A(1956) 67.

[15] T. Muellner, A. Zankel, C. Mayrhofer, H. Reingruber, A. Hoeltzel, Y. Lv, F. Svec, U. Tallarek, Langmuir 28 (2012) 16733.

[16] G. Guiochon, J. Chromatogr. A 1126 (2006) 6.

[17] F. Gritti, M. Martin, G. Guiochon, Anal. Chem. 81 (2009) 3365.

[18] A. A. Al-Massaedh, U. Pyell, J. Chromatogr. A 1286 (2013) 183.

ELSEVIER LICENSE
TERMS AND CONDITIONS

Jun 03, 2014

This is a License Agreement between "Ayat Allah" Al-Massaedh ("You") and Elsevier ("Elsevier") provided by Copyright Clearance Center ("CCC"). The license consists of your order details, the terms and conditions provided by Elsevier, and the payment terms and conditions.

All payments must be made in full to CCC. For payment instructions, please see information listed at the bottom of this form.

Supplier	Elsevier Limited The Boulevard,Langford Lane Kidlington,Oxford,OX5 1GB,UK
Registered Company Number	1982084
Customer name	“Ayat Allah” Al-Massaedh
Customer address	University of Marburg, 35032 Marburg, Germany.
License number	3401191182452
License date	Jun 03, 2014
Licensed content publisher	Elsevier
Licensed content publication	Journal of Chromatography A
Licensed content title	Adamantyl-group containing mixed-mode acrylamide-based continuous beds for capillary electrochromatography. Part IV: Investigation of the chromatographic efficiency dependent on the retention mode
Licensed content author	“Ayat Allah” Al-Massaedh, Ute Pyell
Licensed content date	4 July 2014
Licensed content volume number	1349
Licensed content issue number	None
Number of pages	10
Start Page	80
End Page	89
Type of Use	reuse in a thesis/dissertation
Portion	Full article
Format	both print and electronic
Are you the author of this Elsevier	Yes
Will you be translating?	No
Title of your thesis/dissertation	Adamantyl-Group Containing Mixed-Mode Acrylamide-Based Continuous Beds for Capillary Electrochromatography: Synthesis, Characterization, Optimization and Investigation of the Chromatographic Efficiency
Expected completion date	May 2014

6. CURRICULUM VITAE

"Ayat Allah" Al-Massaedh, M. Sc.

University of Marburg, Department of Chemistry
Hans-Meerwein-Straße, 35032 Marburg, Germany
Phone: +49 (0) 6421 2825411
E-mail: ayat1979@yahoo.com, almassaedh@aabu.edu.jo

Date of birth: 20 August 1979
Nationality: Jordanian

Education

2001-2003	**M.Sc.** Applied Chemistry, Jordan University of Science and Technology, Irbid, Jordan. Physical Chemistry. Thesis: "Adsorption and Hydrodechlorination of Freon 22 (CF_2ClH) over Pt/silica and Pt/ dimethylesiloxane silica".
1997-2001	**B.Sc.** Applied Chemistry, Jordan University of Science and Technology, Irbid, Jordan.

Employment

2005-2011	Lecturer of practical courses of analytical, instrumental, physical, general, and applied chemistry, Department of Chemistry, Al albayt University, Mafraq, Jordan.
2003-2005	Laboratory analyst (Quality Assurance Department) at VAPCO (Veterinary and Agricultural Product Company), Al Zarqa, Jordan.

Courses and Workshops

10/2011-3/2012	"Electromigration Separation Techniques" course by Prof. Dr. Ute Pyell, Department of Chemistry, University of Marburg, Marburg, Germany.

6/7/2012	"Current Issues of Instrumental Analysis" workshop, Agilent Technologies, Waldbronn, Germany.
4-6/7/2004	"Quality Control Charts in Chemical Analysis Lab" workshop, Royal Scientific Society, Amman, Jordan.

List of Publications

1	**A. A. Al-Massaedh**, U. Pyell, *J. Chromatogr. A* 1349 (**2014**) 80-89. "Adamantyl-group containing mixed-mode acrylamide-based continuous beds for capillary electrochromatography. Part IV: Investigation of the chromatographic efficiency dependent on the retention mode".
2	**A. A. Al-Massaedh**, U. Pyell, *J. Chromatogr. A* 1325 (**2014**) 186-194. "Adamantyl-group containing mixed-mode acrylamide-based continuous beds for capillary electrochromatography. Part III. Optimization of the chromatographic efficiency".
3	**A. A. Al-Massaedh**, U. Pyell, *J. Chromatogr. A* 1325 (**2014**) 247-255. "Adamantyl-group containing mixed-mode acrylamide-based continuous beds for capillary electrochromatography. Part II. Characterization of the synthesized monoliths by inverse size exclusion chromatography and scanning electron microscopy".
4	**A. A. Al-Massaedh**, U. Pyell, *J. Chromatogr. A* 1286 (**2013**) 183-191. "Adamantyl-group containing mixed-mode acrylamide-based continuous beds for capillary electrochromatography. Part I: Study of a synthesis procedure including solubilization of N-adamantyl-acrylamide via complex formation with a water-soluble cyclodextrin".
5	R. Hina, I. Arafa, **A. Masadeh**, *React. Kinet. Catal. Lett*. 87 (**2006**) 191-198. "Hydrogenation of $CHClF_2$ (CFC-22) over Pt-supported on silica-based polydimethylsiloxane composite matrices".

List of oral presentations

6/1/2013	"Synthesis, Characterization, and Chromatographic Applications of N-adamantyl-Functionalized Mixed-Mode Acrylamide-Based Continuous Beds for CEC", **23. Doktorandenseminar** des AK Separation Science, Hohenroda, Germany.
25/9/2012	"Preparation and Characterization of N-adamantyl-Functionalized Mixed-Mode Acrylamide-Based Continuous Beds for CEC", **CE Forum 2012** - Capillary Electromigration Separation Techniques, Aalen, Germany.
17/1/2012	"Preparation of Adamantyl-Functionalized Mixed-Mode Acrylamide-Based Continuous Beds for CEC" **weekly seminar** of the research groups of analytical chemistry in the Department of Chemistry, University of Marburg, Marburg, Germany.

List of poster presentations

16-17/9/2013	"Characterization of Adamantyl-Group Containing Mixed-Mode Acrylamide-Based Continuous Beds for Capillary Electrochromatography", **CE Forum 2013** - Capillary Electromigration Separation Techniques, Jena, Germany.
16-17/9/2013	"Adamantyl-Group Containing Mixed-Mode Acrylamide-Based Continuous Beds for Capillary Electrochromatography", **CE Forum 2013 -** Capillary Electromigration Separation Techniques, Jena, Germany.
16-20/6/2013	"Adamantyl-Group Containing Mixed-Mode Acrylamide-Based Continuous Beds for Capillary Electrochromatography", **HPLC 2013**- 39th International Symposium on High Performance Liquid Phase Separations and Related Techniques, Amsterdam, The Netherlands.
4-5/10/2011	"Preparation of Adamantyl-Functionalized Mixed-mode Acrylamide-Based Continuous Beds for CEC", **CE Forum 2011** - Capillary Electromigration Separation Techniques, Regensburg, Germany.

Membership

1	Member at German Chemical Society (GDCh)
2	Member in Marburg University Research Academy (MARA)

References

1	**Prof. Dr. Ute Pyell** Philipps-Universitaet Marburg / Department of Chemistry 35032 Marburg Germany Tel.: +49 6421 28 22192 E-mail: Pyellu@staff.uni-marburg.de
2	**Dr. Rateb Hina** Jordan University of Science and Technology/Department of Chemistry 22110 Irbid Jordan Tel.: +962-2-7201071 E-mail: rhhina@just.edu.jo